JEMS

JOURNAL OF ETA MARITIME SCIENCE

Volume: **12** Issue: **2**

June **2024**

E-ISSN: 2148-9386

www.jemsjournal.org

JEMS
JOURNAL OF ETA MARITIME SCIENCE
2024 / Volume • 12 - Issue • 2

Editorial Board

JEMS
JOURNAL OF ETA MARITIME SCIENCE
2024 / Volume • 12 - Issue • 2

Editorial Board

Journal Info

Please refer to the journal's webpage (www.jemsjournal.org) for " About Us", "Aim and Scope", "Guide for Authors" and "Ethical Policy".

JEMS is currently indexed in Web of Science Emerging Sources Citation Index (ESCI), Tubitak Ulakbim Science Database, Transport Research International Documentation (TRID), Directory of Open Access Journals (DOAJ), EBSCO, J-Gate, Scopus and CNKI.

Owner UCTEA The Chamber of Marine Engineers

Address: Sahrayıcedit Mah. Halk Sk. Golden Plaza No: 29 C Blok K:3 D:6 Kadıköy/İstanbul - Türkiye
Web: gemimo.org **E-mail:** bilgi@gemimo.org **Phone:** +90 216 747 15 51
Fax: +90 216 747 34 35

Publisher Galenos Publishing House
Address: Molla Gürani Mah. Kaçamak Sk. No: 21/1 34093 İstanbul, Türkiye
Phone: +90 (530) 177 30 97 **E-mail:** info@galenos.com.tr **Web:** www.galenos.com.tr

E-ISSN: 2148-9386

Online Publication Date:
June 2024

Journal website:
www.jemsjournal.org

Submit Article:
jag.journalagent.com/jems

Cover Photo:

2024/ Volume 12 / Issue 2
Burak Reis Yavuz (2024).
Maritime Pilot Embarkation in İstanbul Strait

JEMS
JOURNAL OF ETA MARITIME SCIENCE
2024 / Volume • 12 - Issue • 2

Contents

ED **Editorial** 115
Selçuk Nas

AR **Modeling Longshore Sediment Transport for Sustainable Coastal Management in the Damietta Port Area** 116
Ahmed S. A. Ibrahim, Anas M. El Molla, Hany G. I. Ahmed

AR **Energy and Exergy Analysis of Diesel-Hydrogen and Diesel-Ammonia Fuel Blends in Diesel Engine** 128
Kubilay Bayramoğlu

AR **Development of Constructive Measures to Reduce the Consequences of Ship Collisions** 136
Pavel Burakovskiy

AR **Data-Driven Approach for Parameter Estimation and Control of an Autonomous Underwater Vehicle** 144
Tabassum Rasul, Koena Mukherjee

AR **Effect of Exhaust Emissions Produced by Fishing Vessels on Air Pollution: A Case Study of Purse Seine Vessels Operating in the Black Sea** 156
Eralp Özkaya, Ali Yasin Kaya, Fatih Tonoğlu, Özkan Uğurlu, Jin Wang

AR **Decision-Making for Shipping Networks Based on Adaptive Cumulative Prospect Theory: A Case Study in Vietnam** 169
Yen Thi Pham, Ngoc Cuong Truong, Phung Hung Nguyen, Hwanseong Kim

AR **Cruise Passengers' Perceived Service Quality During the Pandemic Period via User-Generated Content** 186
Batuhan Çullu, Nergis Özispa, Gamze Arabelen

AR **Calculation of Time-Independent Maneuvering Coefficients of an Underwater Vehicle Based on Single Grid Structure** 199
Oğuzhan Kırıkbaş, Şakir Bal

AR **Temporal Analysis of Factors Influencing Countries' Maritime Trade Performance with CRITIC-based VIKOR Method** 213
Emrah Akdamar, Ersin Fırat Akgül, Maruf Gögebakan, Evrim Işık

AR **Fire Safety Analysis Onboard Passenger Ships by using Fire Dynamics Simulations: Case Study of a Turkish Domestic Passenger Ship** 224
Tolga Aycı, Barış Barlas, Aykut Ölçer

DOI: 10.4274/jems.2024.40326

Journal of ETA Maritime Science 2024;12(2):115

Selçuk Nas

Dokuz Eylül University Maritime Faculty, Department of Maritime Education and Training, İzmir, Türkiye

The traditional 5th GMC congress, GMC'24, was held on 20-21 May 2024 at Istanbul Technical University Maritime Faculty Tuzla campus. The congress, where a total of 185 papers from 15 different countries were presented in 6 parallel sessions for 2 days, was very successful. The topics of "Autonomous Ships", "Artificial Intelligence" and "carbon emission and energy" were discussed intensively at the congress. It has been decided that the next GMC will be held in Izmir/Turkey in 2026, hosted by Dokuz Eylül University.

It gives me great pleasure to present JEMS 12 (2) to our esteemed readers. Every day, more people are becoming interested in JEMS, and the editorial board and reviewers are becoming pickier. This issue includes some interesting and worthwhile studies. Without a doubt, the maritime area will benefit from these studies. I would like to thank the following people: the publishers, who produced high-quality publications by carefully adhering to our publication policies; our reviewers; the editorial board; the section editors; and the authors, who submitted their insightful studies for publication in this issue.

Best regards,

Prof. Dr. Selçuk NAS
Editor in Chief

Address for Correspondence: Selçuk Nas, Dokuz Eylül University Maritime Faculty, Department of Maritime Education and Training, İzmir, Türkiye
E-mail: snas@deu.edu.tr
ORCID ID: orcid.org/0000-0001-5053-4594

Journal of ETA Maritime Science 2024;12(2):116-127

Modeling Longshore Sediment Transport for Sustainable Coastal Management in the Damietta Port Area

Ahmed S. A. Ibrahim, Anas M. El Molla, Hany G. I. Ahmed

Al-Azhar University, Department of Civil Engineering, Cairo, Egypt

Abstract

Within the framework of constructing mega coastal ports in Egypt, this research aims to achieve coastal management sustainability in its surroundings by modeling the Longshore Sediment Transport "LST". The literature in the fields of modeling and sediment transport was reviewed and scrutinized. The model was calibrated by contrasting the calculated wave data against 2003 measured data at the Damietta Buoy. The model inputs were tuned to produce a result that was similar to the observed data. Moreover, the model results were validated against 2005 measured data at the Damietta Buoy. Likewise, MIKE21 SM was used to estimate 2011 bed levels within Damietta Port, where 2010 bathymetrical survey data were used. Confident with the model results, it was employed to synthesize transport data for 1940-2020 in terms of LST, Gross LST "GLST" and Net LST "NLST" while considering human intervention and implementing ERA5 wave data. Results were obtained and analyzed, and there was a significant correlation between the significant wave height "Hs" and the wave period "Tp" and GLST (i.e. R=0.91-0.79, respectively). The analyzed trend results highlighted that in the pre-construction phase of Damietta Port, increases in GLST and NLST were modest (1139.9 and 243.7 m^3/year, respectively). However, in the post-construction phase of Damietta Port, they escalated between 4679.47 and 3962 m^3/year. The analyzed results indicated that after introducing coastal protection, GLST and NLST decreased to 2978.1 and 2176 m^3/year, respectively.

Keywords: Damietta port, wave, sediment transport, trend analysis, MIKE21

1. Introduction

Coastal regions in the Mediterranean are susceptible to changes in climate. In addition, human intervention amplifies ecosystem vulnerability. However, Egypt is on track to construct mega ports such as Damietta Port. Historically, Damietta Port was constructed in 1982, when two western and eastern jetties were constructed to align its entrance. Additionally, in 2003, breakwaters were constructed within its vicinity. Moreover, from 2016 to 2019, protection was constructed that consists of four T-detached breakwaters.

Accordingly, the literature within the domain of coastal modeling was assembled. Many researchers have investigated this field. Prasad and Kumar [1] documented that the interaction between sea and land is affected by climate change susceptibilities. Likewise, Satterthwaite [2] stated that coastal areas attracted interest because of human development, resulting in population increase and susceptibility to climate threats (i.e. sea-level-rise, wave activity and erosion). Such threats are impaired by human activities [3-6]. The Mediterranean zone is prone to an accelerated temperature increase that amplifies the coastal erosion risks [7-9]. On the other hand, Khalifa [10] documented that Longshore Sediment Transport "LST" plays a significant role in shoreline morphology, where it is induced by waves. Moreover, Aucan [11] stated that climate change affects localized regions in terms of hydrodynamic phenomena.

Numerical models are vital tools for predicting risky wave events [12,13]. However, these tools require development and validation to promote their reliability, and many studies have introduced many approaches for this purpose [14-16]. On the other hand, Başaran et al. [17] indicated that sustainable coastal management is of global significance, as coastal regions account for approximately 75% of the

Address for Correspondence: Ahmed S.A. Ibrahim, Al-Azhar University, Department of Civil Engineering, Cairo, Egypt
E-mail: ahmedsayed.90@azhar.edu.eg
ORCID ID: orcid.org/0009-0005-4402-9889

Received: 09.11.2023
Last Revision Received: 27.02.2024
Accepted: 08.03.2024

To cite this article: A. S. A. Ibrahim, A. M. El Molla, and H. G. I. Ahmed, "Modeling Longshore Sediment Transport for Sustainable Coastal Management in the Damietta Port Area." *Journal of ETA Maritime Science*, vol. 12(2), pp. 116-127, 2024.

Earth's surface. Moreover, they further documented that human activities and climate change transformed the dynamics in coastal zones, which provoked substantial changes in spatial and temporal coastal ecosystems.

Moreover, based on the scrutinized literature, it was obvious that many researchers are delving into LST mechanisms and coastal morphology, whereas Amarouche et al. [18] emphasized that a proper understanding of LST is a prerequisite to effectively manage coastal zones. Likewise, Simav et al. [19] highlighted that the Mediterranean is affected by increasingly human interventions. Focused on the Egyptian coast to offer coastal engineers key factors to effectively manage it [20]. Moreover, Van Rijn et al. [21] suggested that coastal engineers are confronted with a formidable challenge in achieving an accurate prediction of critical factors (i.e. near-shore waves). However, Keshtpoor et al. [22] concentrated on achieving hydrodynamic simulations, LST, and morphological changes, which are imperative for coastal management and planning.

Based on the aforementioned literature, it is important to achieve coastal management sustainability in the vicinity of mega coastal ports in Egypt (i.e., Damietta Port) by modeling the LST, where an 81-year data span was implemented in the present study (i.e. 1940 to 2020 ECMWF-ERA 5 wave data) to consider the long-term impact of climate change and human interventions.

2. Methods and Data

2.1. Study Area Description

The assembled data were analyzed, from which a clear study area description was perceived and presented. Damietta Port is located in the Nile Delta. It was constructed in 1982. It has a 15-m deep navigation channel. It has two jetties (i.e. eastern and western), and the western jetty is 7.9 km long [23]. The study area stretches over 10 km in the vicinity of Damietta Port, which is a significant maritime project that was initiated in 1981 [24]. Its location was selected because of its resilience to waves, where coastal accretion was historically documented [25,26].

The study area is distinguished by its very low tidal range (i.e. 14 cm) with a daily fluctuation of 0.60 m [27]. In addition, the grain size "D_{50}" of the study area is 0.25 mm and the seabed sediments are 0.11 mm, at depths less than 6 m [28]. However, many defensive measures have been constructed to protect Damietta Port [29]. Among them, for example, are four T-detached breakwaters that were constructed to protect Damietta Port's eastern side. They were established between 2016 and 2019. They extend over 1.5 km. These defensive structures altered the wave reflection pattern, erosion, and accretion along the coast, as shown in Figure 1.

2.2. Data Collection

The assembled data encompassed 2003 and 2005 wave data at Damietta Buoy (i.e. located at a depth of 12 m at coordinates of 31.51° N and 31.76° E), as presented in Figure 1. The time series wave data were recorded at 4-h intervals and were obtained from the Egyptian Coastal Research Institute (CoRI). In addition, the ERA5 dataset provides significant data (i.e. wind and waves). Additionally, the available data incorporated 2010 and 2011 bathymetrical data as a set of profiles upstream and downstream of Damietta Port. These bathymetrical data were acquired from CoRI, as shown in Figure 2. Moreover, the data also included wave data from 1940 to 2020 acquired from ERA5. ERA5 data were accessed from https://cds.climate.copernicus.eu/cdsapp#!/dataset/reanalysis-era5-single-levels?tab=form [30]. The ERA5 dataset was developed by the European Centre for Medium-Range Weather Forecasts "ECMWF". It is a reanalysis dataset that provides comprehensive atmospheric and oceanographic information. It encompasses a huge observation array with satellite and buoy readings. ERA5 is renowned for its accuracy. Its resolution is 1 h, while its spatial resolution is 0.25° (i.e. 30 km). The duration of the ERA5 data (81 years) is considered appropriate in considering

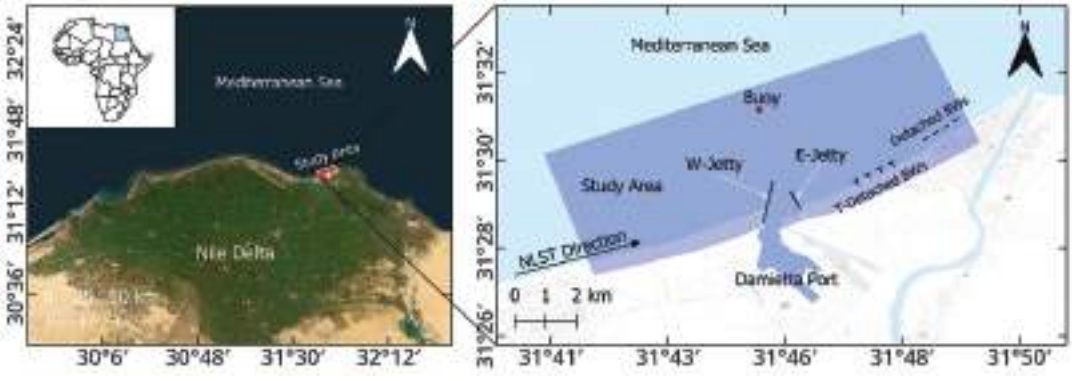

Figure 1. *Study area with defensive structures and Damietta Buoy location*

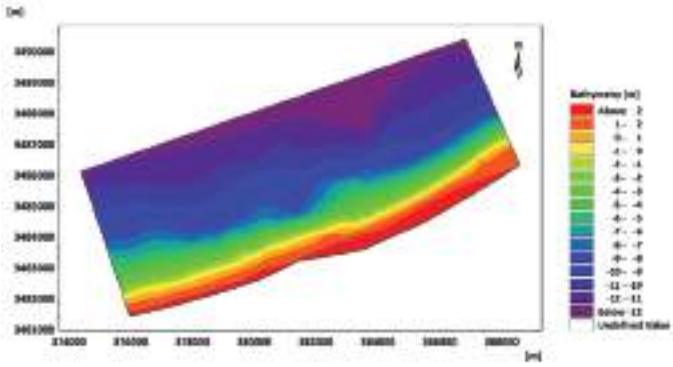

Figure 2. *2010 bathymetric survey of the study area*

the recommendations of both the World Meteorological Organisation "WMO" and the Intergovernmental Panel on Climate Change "IPCC". The World Meteorological Organization recommends investigating climate change using 30-year data [31]. The IPCC recommends using longer datasets to study coastal stability [32]. Unfortunately, the study suffered from a lack of observational data, particularly bathymetric and wave data. The observed wave data were only available for two years (i.e. 2003-2005). Furthermore, bathymetric data for the study area were only available in 2010 and 2011.

2.3. Numerical Simulation

MIKE21 was selected for implementation because it is widely accepted and has proven its reliability in many engineering projects. MIKE21 was developed by the Danish Hydraulic Institute "DHI". It addresses complex morphologies. It performs littoral drift simulations while updating the shoreline morphology [33]. The software encompasses four modules. These are spectral wave "SW" (i.e. MIKE21 SW), hydrodynamic "HD" (i.e. MIKE21 HD), sand transport "ST" (i.e. MIKE21 ST), and shoreline morphology "SM" (i.e. MIKE21 SM) [34].

This section provides a synopsis of the MIKE 21 theoretical background and governing equations.

2.3.1. MIKE21 Governing equations and theoretical background

The governing equations of MIKE21 are the mass equation, momentum equation, salinity, and temperature [35].

Theoretically, MIKE21 SW is a two-dimensional (2-D) wave model [36]. It uses the finite-volume technique on a computational mesh, where differential equations govern the wave dynamics [37,38]. The equations are expressed as follows:

$$\frac{S}{\sigma} = \frac{\partial N}{\partial t} + \nabla(\vec{v}N) \tag{1}$$

Where:

t: time;

v : wave group velocity in the four-dimensional (4-D) phase space formed by x, y, σ and θ $\left(c_\sigma, c_\theta, c_x, c_y\right)$

$\vec{x}$: Cartesian coordinates (x,y)

σ: relative angular frequency

θ: direction of wave propagation

$N(\sigma, \theta, x, t)$: action-density

∇: 4-D differential operator (v, σ and θ)

S: wave energy source

Principally, MIKE21 HD satisfies the Boussinesq assumptions for hydrostatic pressure. It is based on the incompressible Reynolds-averaged Navier-Stokes equations. It encompasses continuous and momentum equations [35]. Moreover, the 3D hydrodynamic equation can be simplified to a 2D shallow water long wave by time variation by integrating the water depth. MIKE21 HD solves the continuity and momentum equations described as follows:

Continuity equation:

$$\frac{\partial h}{\partial t} + \frac{\partial h\bar{u}}{\partial x} + \frac{\partial h\bar{v}}{\partial y} = hS \tag{2}$$

Momentum equation:

$$\begin{aligned}&\frac{\partial h\bar{u}}{\partial t} + \frac{\partial h\bar{u}^2}{\partial x} + \frac{\partial h\bar{v}\,\bar{u}}{\partial y} = f\bar{v}h - gh\frac{\partial \eta}{\partial x} - \frac{h}{\rho_o}\frac{\partial P_a}{\partial x} - \frac{gh^2}{2\rho_o}\frac{\partial \rho}{\partial x}\\ &+ \frac{\tau_{sx}}{\rho_o} - \frac{\tau_{bx}}{\rho_o} - \frac{1}{\rho_o}\left(\frac{\partial S_{xx}}{\partial x} + \frac{\partial S_{xy}}{\partial y}\right) + \frac{\partial}{\partial x}\left(hT_{xx}\right)\\ &+ \frac{\partial}{\partial x}\left(hT_{xy}\right) + hu_sS\end{aligned} \tag{3}$$

$$\begin{aligned}&\frac{\partial h\bar{v}}{\partial t} + \frac{\partial h\bar{v}^2}{\partial y} + \frac{\partial h\bar{v}\,\bar{u}}{\partial x} = f\bar{u}h - gh\frac{\partial \eta}{\partial y} - \frac{h}{\rho_o}\frac{\partial P_a}{\partial y} - \frac{gh^2}{2\rho_o}\frac{\partial \rho}{\partial y}\\ &+ \frac{\tau_{sy}}{\rho_o} - \frac{\tau_{by}}{\rho_o} - \frac{1}{\rho_o}\left(\frac{\partial S_{yx}}{\partial x} + \frac{\partial S_{yy}}{\partial y}\right) + \frac{\partial}{\partial x}\left(hT_{xy}\right)\\ &+ \frac{\partial}{\partial y}\left(hT_{yy}\right) + hv_sS\end{aligned} \tag{4}$$

Where:

t: Time

x, y, and z: Cartesian coordinates

η: Surface elevation

d: Still water depth

h: Total water depth (η + d)

u, v, and w: x, y, and z velocity components

f: Coriolis parameter (f = 2Ω sinØ)

Ω: angular rate of revolution

Ø: geographic latitude

g: Acceleration due to gravity

ρ: Water density

S_{xx}, S_{xy}, S_{yx}, and S_{yy}: radiation stress tensor components

P_a: atmospheric pressure

ρ∘: water reference density

τ_{sx} and τ_{sv}: surface wind stresses

τ_{bx} and τ_{bv}: bottom stresses

T_{xx}, T_{xv}, and T_w: lateral stresses

S: point source discharge

u_S, v_S: water velocity discharged into ambient water.

Theoretically, MIKE21 ST calculates sediment transport while considering wave-current interaction, turbulence, flow velocity, and sediment concentration. It calculates bed load as suspended load by using Shields parameter as flow velocities. It uses a diffusion equation to consider the sediment concentration and vertical fluctuations. Its output provides littoral drift gradients that influence the morphology. Academically, MIKE21 SM utilizes the shoreline continuity equation, where it employs the one-line theory, which divides the shore segment into wedges perpendicular to the shoreline to calculate its position by considering the volumetric sediment changes within each wedge [39].

$$\frac{\Delta N}{\Delta t} = \frac{vol}{dA_z} \quad (5)$$

where:

ΔN: horizontal shoreline changes

dA_z: vertical closure area

vol: is the sediment volume coming in and out of the wedge

Δt denotes the time step.

2.3.2. MIKE21 input data

Damietta Port was discretize to initiate the computation, where the computational mesh was defined. It is defined by the UTM coordinates. Its cross-shore and long-shore dimensions are 4.9 km and 13.1 km, respectively. The mesh encompassed the study area and extended seawards to -13.5 m, where the maximum elemental area was 600 m^2 specified near-shore and 3000 m^2 offshore, as shown in Figure 3. The mesh encompassed 48774 triangular elements and 96726 points. MIKE21 input data encompassed ERA5 wave data and bathymetrical data. MIKE 21 SW was operated, where the JONSWAP formulation was employed. MIKE21 SM input data encompass a baseline, an initial shoreline, an edge map, and predefined coastal profiles. The baseline and edge maps define the spatial domain for MIKE21 SM calculations. Regarding the initial shoreline and predefined coastal profiles, they define the bathymetry inside this domain [34]. However, the baseline orientation specifies the direction of shoreline movement, while the initial shoreline defines the initial position prone to accretion or erosion. The baseline and initial shoreline are polylines with nodes with x coordinates. The baseline node spacing designates the resolution of the initial shoreline, where the nodal spacing is 100 m. The edge map divides the shore face into strips perpendicular to the baseline. The offshore boundary of the edge map is the closure depth (i.e. -7.0 m). Changes in sediment volume move the shoreline edge during the simulation. MIKE21 SM calculates the total sediment volume change in a strip by integrating sediment volume change in all mesh elements.

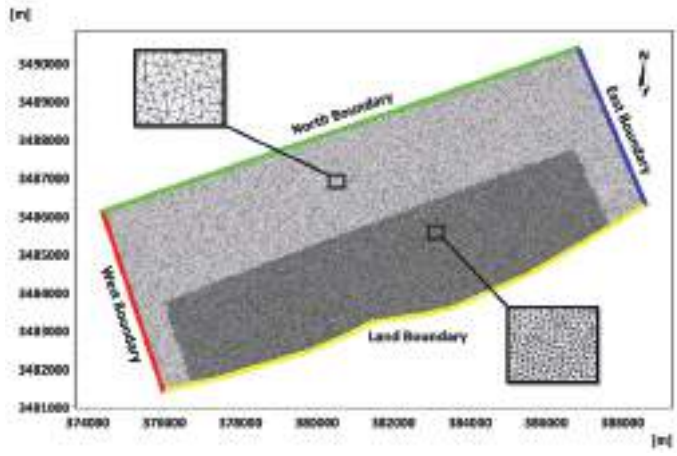

Figure 3. *Discretized study area and computational mesh*

2.3.3. Model calibration and validation

Implemented modules MIKE21 SW and MIKE21 SM were calibrated and validated. The main objective is to find the optimal dissipation coefficients (i.e., wave-breaking factors (γ and α) and bottom friction) that best fit the model results with the observed data. Accurate estimation of wave energy dissipation is crucial for oceanography and wave modeling to predict wave behavior [40].

To calibrate the MIKE21 model, several simulations were run. Each iteration of the trial-and-error procedure-modified specific critical coefficients. where calibration is based on measurements taken in the study area (e.g., 2003 wave data and 2011 bathymetric data). During the calibration process, the model's performance was assessed using statistical metrics (i.e. bias, Root Mean Square Error "RMSE", Scatter Index "SI" and Correlation Coefficient "CC"). Bias designates the difference between the calculated model results and the measured values. The process reduces errors such as RMSE, bias, and SI across all simulation results. This was achieved using the following set of equations:

$$\bar{x} = \frac{1}{n}\sum_{i=1}^{n} x \quad (6)$$

$$CC = \frac{\sum_{i=1}^{n}(x_i-\bar{x})(y_i-\bar{y})}{\sqrt{\sum_{i=1}^{n}(x_i-\bar{x})^2 \sum_{i=1}^{n}(y_i-\bar{y})^2}} \quad (7)$$

$$RMSE = \sqrt{\frac{1}{n}\sum_{i=1}^{n}(y-x)^2} \quad (8)$$

$$BIAS = \frac{1}{n}\sum_{i=1}^{n}(y-\bar{x}) \quad (9)$$

$$SI = \frac{\sqrt{\frac{1}{n}\sum_{i=1}^{n}(y-x-BIAS)^2}}{\frac{1}{n}\sum_{i=1}^{n}|x_i|} \quad (10)$$

Where:

n: number of data

x: measured value

y: estimated or calculated value

MIKE21 SW

MIKE21 The SW was *calibrated*, where 2003 ERA5 wave data were introduced to it and the wave data at Damietta buoy values were obtained. The simulated wave data listed in the calibration and validation process are computed for the point nearest to the buoy. This was achieved by contrasting the calculated wave data against 2003 measured data at the Damietta Buoy. Based on the calibration process, the model results (i.e., H_s and T_p) were tuned to produce analogous data. Moreover, the model results were *validated* against 2005 measured data at the Damietta Buoy.

MIKE21 SM

Similarly, MIKE21 SM was used to provide 2011 bed levels in the vicinity of Damietta Port, where 2010 bathymetrical data was used as an initial condition. MIKE21 SM was calibrated by comparing its calculated bed level data against 2011 measured data at Damietta. Four profiles from 2010 were used (i.e., 2 at port Upstream "US" and 2 at port Downstream "DS"). MIKE 21 was operated, and 2011 profiles were obtained. MIKE21 SM was calibrated by comparing the calculated profiles with the 2011 measured profiles. The model inputs were tuned to produce equivalent levels. Moreover, the model results were validated against another 4 profiles (2 at the US and the other 2 are at the DS).

2.3.4. Long-term simulation

Confident with the calibration and validation process results, MIKE21 was implemented to simulate the study area for a long-time span of 81 years (i.e. 1940-2020), where 1940-2020 ERA5 wave data were implemented and all human interventions were considered according to their construction time (i.e. western and eastern jetties were constructed in 1982, while the 4 breakwaters were established in 2003 and the T-detached breakwaters were constructed during 2016-2019). Consequently, MIKE21 was run and LST, GLST, and NLST were obtained

3. Results and Discussion

Results were obtained and analyzed, from which LST yearly trends were identified. Such trends are fundamental data for further analysis and should be employed in establishing effective development strategies for coastal management. A linear regression equation was used to analyze LST long-term trends, where this relation is described as follows:

$$y = a + b * x \quad (11)$$

Where:

y: meteorological variable

x: time

a and *b*: regression coefficients (i.e. obtained from the least square method).

3.1. Results Analysis and Discussion of the Calibration and Validation

The results of the calibration and validation processes were analyzed. The analyzed results for the calibration process are presented in Table 1, Figure 4, and Figure 5, where Figure 4 and Figure 5 encompass three subfigures: (a), (b), and (c). Table 1 showcases the statistical metrics employed during the model calibration process across different runs. Each run was evaluated using statistical metrics (i.e. CC, RMSE, bias, and SI). The analysis reveals that dissipation coefficients exhibit a limited impact on CC but show significant improvement in reducing bias and RMSE in the simulated results. After analysis, the third model run outperforms the others in all metrics examined. With correlation coefficients of 0.930 for Hs and 0.994 for bed levels, the third run shows a strong relationship between predicted and observed values.

Furthermore, it has low RMSE values of 0.180 m for Hs and 0.212 m for bed levels, indicating little difference between predicted and actual values. In addition, the bias values for Hs (0.030 m) and bed levels (0.054 m) are close to zero, implying unbiased predictions. Furthermore, the scatter index values for Hs (0.041 m) and bed levels (0.150 m) are low, indicating little variation around the observed values. Overall, the third run outperformed the other runs because of its strong correlation, low RMSE, negligible bias, and limited SI. The calibration values for the third run were a friction coefficient of 0.01 and wave-breaking factors (α = 0.95 and γ = 0.8). Additionally, Figure 5 depicts Taylor

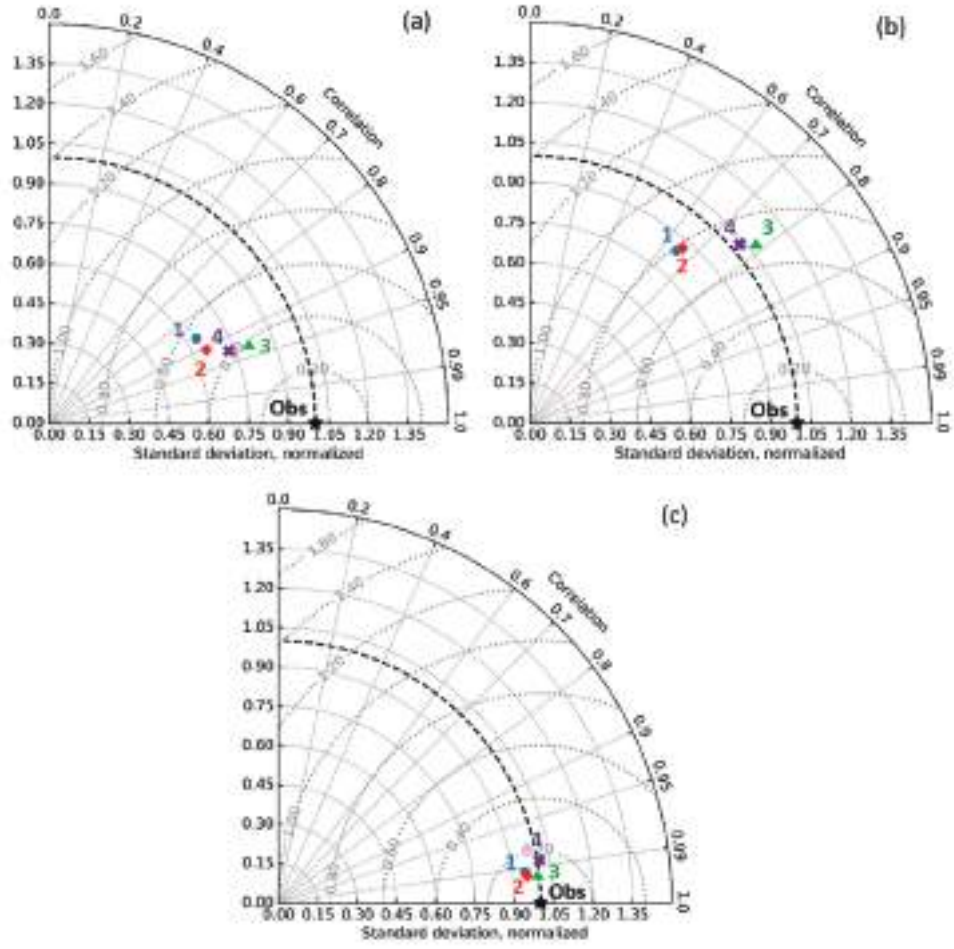

Figure 4. *The Taylor diagram shows the performances of model runs with different bottom frictions during the calibration process. (a) significant wave height, (b) peak wave period, and (c) bed level*

Table 1. *Statistical metrics for the model calibration process across several runs*

Runs	Parameter	CC	RMSE	Bias	SI
1	Significant wave height	0.866	0.250	0.030	0.411
	Peak wave period	0.647	1.213	-0.402	0.172
	Bed level	0.991	0.384	0.287	0.050
2	Significant wave height	0.932	0.184	0.057	0.297
	Peak wave period	0.773	1.090	-0.062	0.163
	Bed level	0.990	0.332	0.248	0.043
3	Significant wave height	0.930	0.180	0.030	0.292
	Peak wave period	0.784	1.040	-0.291	0.150
	Bed level	0.994	0.212	0.054	0.041
4	Significant wave height	0.930	0.191	-0.031	0.312
	Peak wave period	0.771	1.282	-0.814	0.152
	Bed level	0.987	0.324	-0.106	0.061

diagrams of modeled H_s, T_p, and bed levels versus measured values for calibration. Furthermore, Figure 5 contrasts the measured against simulated values (i.e. H_s, T_p and bed levels) for the third run by scatter plots. where the color scale signifies the density of data, and the density of data emphasizes the distribution of observed vs. modeled values. where subfigures (a) and (b) show the calculated and measured values of H_s and T_p, respectively, and subfigure (c) shows the bed levels.

The analyzed results for the validation process are presented in Table 2 and Figure 6, where Figure 6 encompasses 3 subfigures (a), (b), and (c). Table 2 lists the statistical metrics (i.e. CC, RMSE, Bias and SI) for the validation process results. From the table, it was obvious that the value of CC was 0.902 for Hs, while the value of CC for the bed levels was 0.994. Moreover, the table indicates that the RMSE values were low, which signifies a robust agreement between the computed and measured data. However, in certain instances, minor bias was evident, especially for Hs (i.e. negative bias of -0.032). However, the plots presented in Figure 6 provide a visual assessment of the model's performance, emphasizing the agreement between observed and calculated values.

Table 2. *Statistical metrics related to the calculated and measured values for the validation process*

Parameter	CC	RMSE	Bias	SI
Significant wave height	0.902	0.229	-0.032	0.310
Peak wave period	0.723	1.255	-0.186	0.185
Bed level	0.994	0.211	0.095	0.037

3.2. Results Analysis and Discussion of the Wave Climate

Results of the wave climate (i.e., H_s and T_p) were analyzed and presented in Figure 7, which provides monthly wave data. The figure designates that the Hs distribution reaches the minimum during the 1st quartile, while it attains the average in the 3rd quartile. However, the maximum values vary monthly from 1940 to 2020. Moreover, it emphasizes that storms are frequent and intense from February to April. However, the wave statistical distribution varies significantly on a monthly basis. Hs at 12 m depth indicated its variability within the range of 0.01-4.94 m, whereas T_p varied within the range of 2-14.3 s, with a mean wave direction of 326°. Moreover, the figure indicates that during winter, Hs ranged between 0.55 and 1.55 m, with an average of 1.03 m. However, T_p varies between 5.4 and 8.1 s. In contrast, during summer, H_s ranges between 0.61 and 1.28 m, whereas T_p ranges between 4.9 and 7 s. However, in autumn and spring, the mean Hs was 0.85 m, and the monthly variation in H_s indicated that the maximum Hs occurred in November, December, January, February, and March. However, H_s is less than 1 m throughout the year (i.e. 68% of the time), while H_s ranges between 1 m and 2

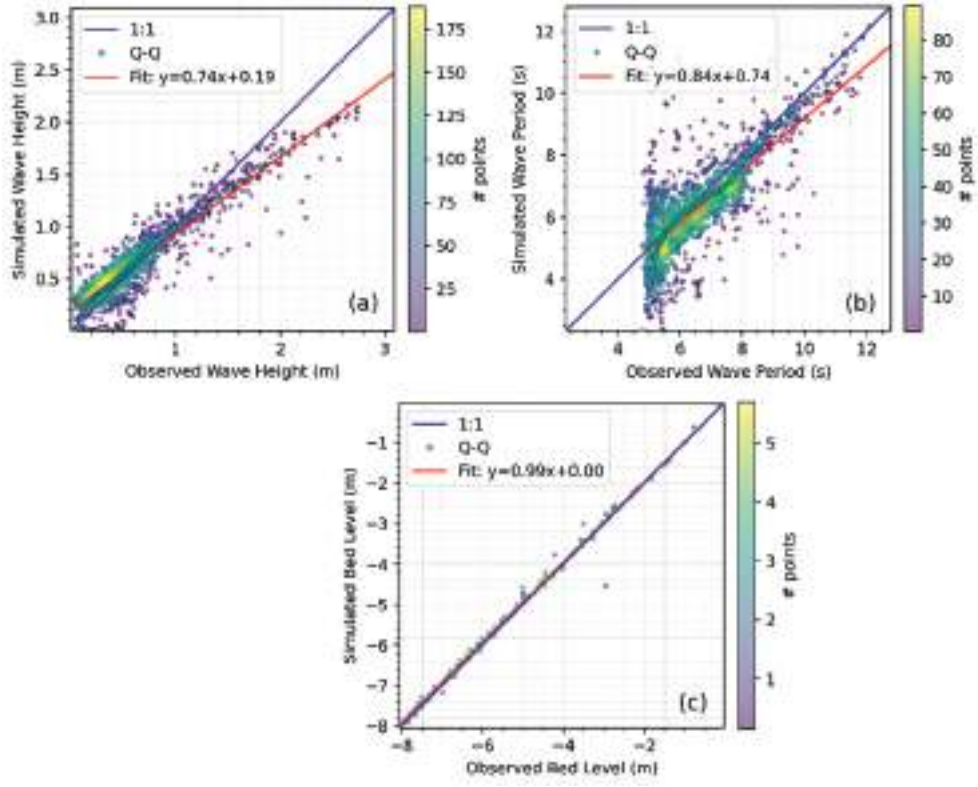

Figure 5. *Scatter plots for the third model run in the calibration process. (a) significant wave height, (b) peak wave period, and (c) bed level*

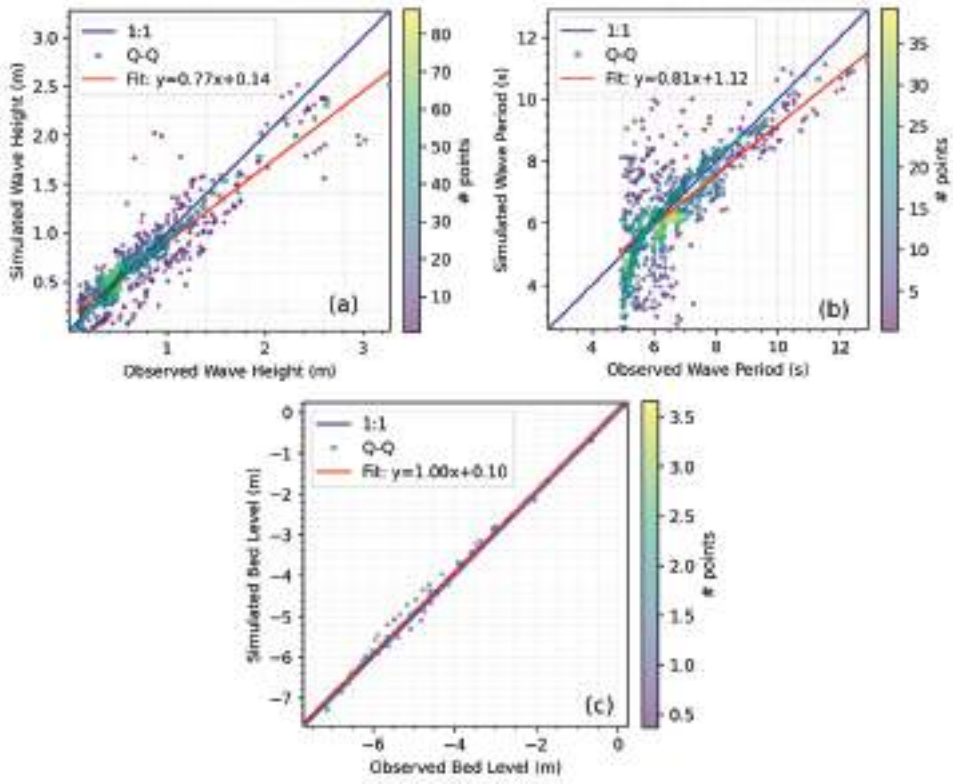

Figure 6. *Scatter plots for the validation process: (a) significant wave height, (b) peak wave period, and (c) bed level*

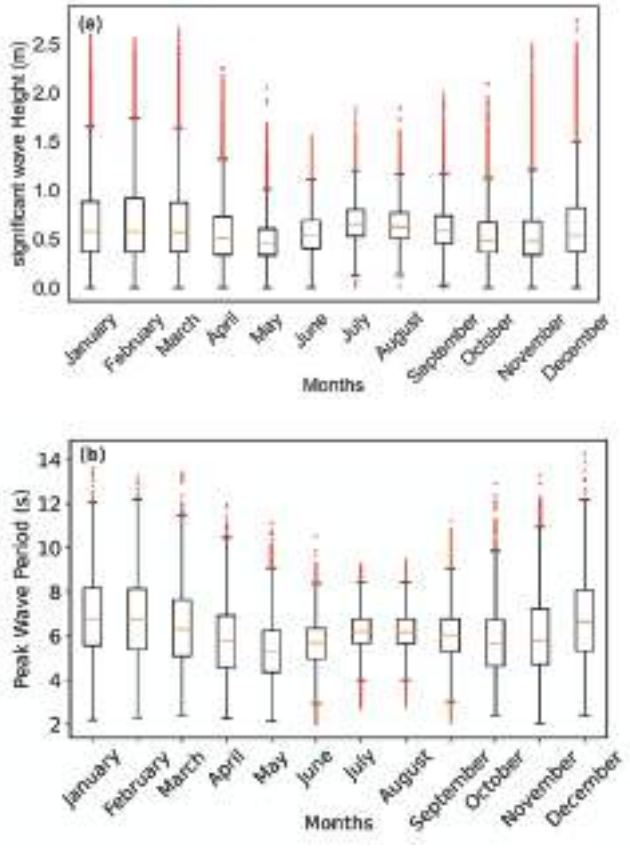

Figure 7. *Monthly variations in wave climate during 1940-2020: (a) significant wave height (m) and (b) peak wave period (s)*

m during 28% of the year, and H_s exceeds 2 m only 0.04% of the year. This agrees with [41,42], who documented that the waves predominantly (i.e. 86%) come from the N-NW sector.

Figure 8 depicts the differences in wave height distribution in the study area during the pre-construction and post-construction phases of Damietta Port. During the pre-construction phase (Figure 8a), the wave height distribution reflected the natural conditions of the area. The distribution of the wave heights changed after construction (Figure 8b). However, the existence of these structures modified the wave climate in the area by changing the wave propagation sequences and heights.

3.3. Results Analysis and Discussion of Sediment Transport

The results of LST analysis are presented in Figure 9, which indicates that LST varies where the sediment is disturbed by human interventions. In addition, the LST long-term trend was achieved using the best-fit line method.

In the pre-construction phase of Damietta Port, GLST ranged between 0.87 and 1.5 x10^6 m^3/year, with an average of 1.1x10^6 m^3/year. Likewise, NLST varied between 0.49 and 1.04x10^6 m^3/year with an average of 0.73x10^6 m^3/year. Sediment transport values agree with previous findings in the study area, where researchers estimated the transport to be 0.66 x10^6 m^3/year to the east and 0.26 x10^6 m^3/year

to the west with anNLST of 0.4x10^6 m^3/year to the east [26]. However, other researchers estimated NLST to be 0.8x10^6 m^3/year [43], while Frihy et al. [44] estimated it to be 0.6-1.8x10^6 m^3/year.

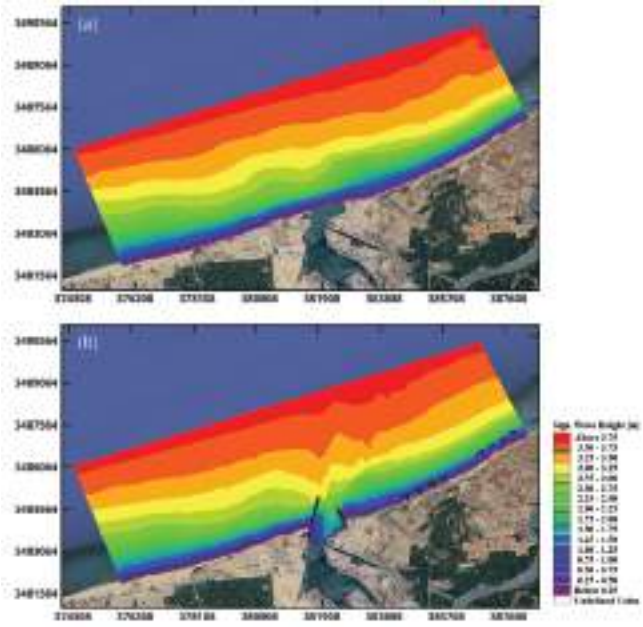

Figure 8. *Significant wave height distributions for two phases: (a) pre-construction phase of Damietta Port and (b) post-construction phase of Damietta Port and associated protection structures*

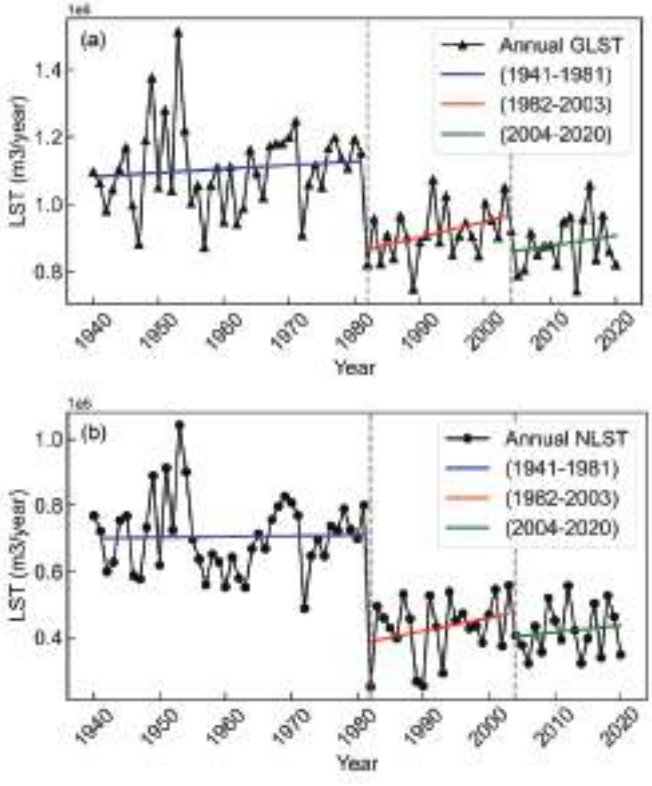

Figure 9. *Annual LST trend during 1940-2020: (a) annual NLST and (b) annual GLST*

In the post-construction phase of Damietta Port, LST experienced a rapid decrease and was trapped within the navigation channel, which eventually obstructed port access.

After implementing the Port structures, GLST fluctuated annually, with the highest GLST recorded in 1992 (i.e. 1.07x10^6 m^3/year), while the lowest GSR occurred in 1989 (i.e. 0.75x10^6 m^3/year); (Figure 9a). However, the annual GLST was 0.9x10^6 m^3/year. Furthermore, the NLST varied, where the highest annual NLST was 0.65x10^6 m^3/year. In contrast, the lowest recorded NLST value was 0.2x10^6, with an average value of 0.42x10^6 m^3/year (Figure 9b). A similar estimate has been previously documented. However, Frihy et al. [42] employed fluorescent tracers to designate the annual LST. The study revealed that GLST was 0.85x10^6 m^3/year, while NLST was 0.49x10^6 m^3/year.

To gain insights into annual LST, we used trend lines to represent the average LST values for each year (Figure 9). The analysis reveals significant positive trends in LST, both before and after the construction of Damietta Port and the implementation of coastal protection structures. These trends underscore the dynamic response of LST to human interventions, potentially impacting coastal geomorphology and sediment management strategies. In the pre-construction phase of Damietta Port, both GLST and NLST exhibited relatively modest trends. The trend in GLST showed a positive average of 1139.9 m^3/year, while the trend in NLST was also positive, averaging 243.7 m^3/year.

In the post-construction phase of Damietta Port, there was a substantial increase in both GLST and NLST trends. The trend in GLST significantly increased to 4679.47 m^3/year, and the trend in NLST also experienced a notable increase, reaching 3962 m^3/year. These findings strongly indicate that the Port's construction had a significant impact on LST processes along the coast. From 2004 to 2020, following the implementation of coastal protection structures, there was a noticeable decrease in both GLST and NLST trends. The trend in GLST decreased to 2978.1 m^3/year, and the trend in NLST decreased to 2176 m^3/year. This decline suggests that the coastal protection structure likely played a crucial role in mitigating LST trends and effectively stabilizing sediment dynamics in the area.

3.4. Results Analysis and Discussion of Sediment Transport and Wave Climate

Results spanning over eight decades (1940-2020) of LST and wave climate (i.e. H_s and T_p) were obtained in the Damietta buoy location, analyzed, and presented in Figure 10. The analysis revealed strong correlations among these parameters. From the figure, clear was the strong correlation between H_s and GLST so as NLST, where R was 0.91; (Figure

10a) and was 0.71; (Figure 10b), respectively. In addition, T_p had a strong correlation between T_p and GLST, similar to NLST, where R was 0.79, as shown in Figure 10c, and o.66, as shown in Figure 10d.

4. Conclusions and Recommendations

This study represents a substantial advancement in our understanding of the complex interactions among wave climate, LST, and human interventions in coastal regions, with a specific focus on the Damietta area in the Eastern Mediterranean. By analyzing an extensive 81-year dataset, which includes four-hour interval data, the study has provided valuable insights into the coastal dynamics of this region. MIKE 21 SW proved its reliability in transforming waves from offshore to the Damietta buoy. MIKE 21 SM proved its trustworthiness in estimating bed levels in the Damietta area. A better understanding of the complex interaction between waves, LST, and human interventions in coastal regions was obtained. Valuable insights were attained into the coastal dynamics of the Damietta region, where it was clear that waves less than 1 m prevailed 68% of the year and waves exceeding 2 m occurred 0.04% of the time. LST has varied significantly over the years, which indicates the dynamic nature of LST in the Damietta area. NLST migrates eastward; however, directional reversals were evident. Implementing protection structures for LST dynamics helped reduce impact of Damietta Port by stabilizing sediment processes and reducing GLST and NLST trends.

Based on the conclusions, the following recommendations were made:

Implement a robust monitoring system for waves and LST to gain better insights into the complexities of coastal dynamics. Coastal planning should be integrated to consider the interaction between wave climate, sediment dynamics, and human activities. Strike a balance between sediment management and coastal processes. The protection work should be sustainable and compatible with the surrounding ecosystem.

Based on the suggested recommendations, future research is advised to:

Investigate temporal wave trends over a shorter time intervals. Conduct a detailed analysis of storm events and their impact on waves and sediment transport. Investigate the socioeconomic impacts of longshore transport on coastal communities. Assess the consequences of changing sediment dynamics on coastal infrastructure. Assess coastal areas' resilience to climate change and human interventions.

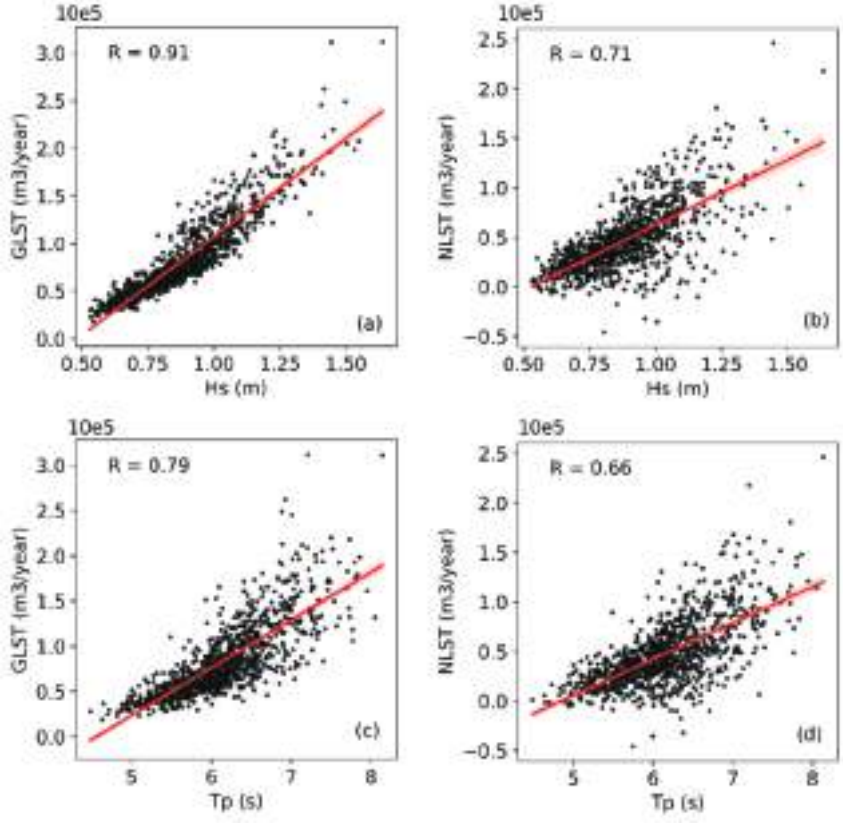

Figure 10. *Longshore sediment transport (i.e. GLST and NLST) versus wave climate (i.e. Hs, Tp)*

Authorship Contributions

Concept design: A. S. A. Ibrahim, A. M. El Molla, and H. G. I. Ahmed, Data Collection or Processing: A. S. A. Ibrahim, Analysis or Interpretation: A. S. A. Ibrahim, A. M. El Molla, and H. G. I. Ahmed, Literature Review: A. S. A. Ibrahim, and H. G. I. Ahmed, Writing, Reviewing and Editing: A. S. A. Ibrahim, A. M. El Molla, and H. G. I. Ahmed.

Funding: The authors declare that no funding was received for this research, authorship, or publication.

References

[1] D. H. Prasad, and N. D. Kumar, "Coastal erosion studies-a review," *International Journal of Geosciences,* vol. 5, pp. 341-345, Mar 2014.

[2] D. Satterthwaite, "The transition to a predominantly urban world and its underpinnings," *Human Settlements Discussion Paper Series- Theme: Urban Change –4,* pp. 1-91, 2007.

[3] A. Arns, S. Dangendorf, J. Jensen, S. Talke, J. Bender, and C. Pattiaratchi, "Sea-level rise induced amplification of coastal protection design heights". *Scientific Reports*, vol. 7, pp. 1-9, 2017.

[4] A. Grases, V. Gracia, M. García-León, J. Lin-Ye, and J. P. Sierra, "Coastal flooding and erosion under a changing climate: Implications at a low-lying coast (Ebro Delta)". *Water (Switzerland)*, vol. 12, 346, Jan 2020.

[5] R. Almar, et al. "Response of the Bight of Benin (Gulf of Guinea, West Africa) coastline to anthropogenic and natural forcing, Part1: Wave climate variability and impacts on the longshore sediment transport". *Continental Shelf Research,* vol. 110, pp. 48-59, Nov 2015.

[6] S. Knobler, D. Liberzon, and F. Fedele, "Large waves and navigation hazards of the Eastern Mediterranean Sea". *Scientific Reports*, vol. 12, pp. 1-17, Oct 2022.

[7] IPCC, "Climate change 2022: impacts, adaptation and vulnerability. Contribution of working group II to the sixth assessment report of the intergovernmental panel on climate change [H.-O. Pörtner, D.C. Roberts, M. Tignor, E.S. Poloczanska, K. Mintenbeck, A. Alegr," Cambridge Univ. Press. Cambridge Univ. Press. Cambridge, UK New York, NY, USA, vol. 3056, 2022.

[8] A. R. Birben, I. H. Özölçer, S. Karasu, and M. I. Kömürcü, "Investigation of the effects of offshore breakwater parameters on sediment accumulation". *Ocean Engineering*, vol. 34, pp. 284-302, Feb 2007.

[9] M. R. Nikmanesh, and N. Talebbeydokhti, "Numerical simulation for predicting concentration profiles of cohesive sediments in surf zone". *Scientia Iranica,* vol. 20, pp. 454-465, Jun 2013.

[10] M. A. Khalifa, "Adoption of recent formulae for sediment transport calculations applied on the Egyptian Nile delta coastal area". *Journal of Coastal Conservation,* vol. 16, pp. 37-49, Oct 2011.

[11] J. Aucan, "Effects of climate change on sea levels and inundation relevant to the pacific islands what is already happening?". *PACIFIC MARINE CLIMATE CHANGE REPORT CARD, Science Review,* pp. 43-49, 2018.

[12] K. E. Saraçoğlu, H. A. Arı Güner, C. Şahin, Y. Yüksel, and E. Özkan Çevik, "Evaluation of the wave climate over the black sea: field observations and modeling". In *Proceedings of 35th Conference on Coastal Engineering, Antalya, Turkey, 2016,* pp. 1-8, Jun 2016.

[13] F. Barbariol, et al. "Wind waves in the mediterranean sea: an ERA5 reanalysis wind-based climatology". *Frontiers in Marine Science*, vol. 8, pp. 1-23, Nov 2021.

[14] P. G. Remya, R. Kumar, S. Basu, and A. Sarkar, "Wave hindcast experiments in the Indian Ocean using MIKE 21 SW model". *Journal of Earth System Science,* vol. 121, pp. 385-392, May 2012.

[15] M. H. Moeini, and A. Shahidi, "Application of two numerical models for wave hindcasting in Lake Erie". *Applied Ocean Research,* vol. 29, pp. 137-145, Jul 2007.

[16] S. Hadadpour, H. Moshfeghi, E. Jabbari, and B. Kamranzad, "Wave hindcasting in Anzali, Caspian Sea: a hybrid approach," *Journal of Coastal Research,* vol. 65, pp. 237-242, Jan 2013.

[17] B. Başaran, A. Güner, and H. Anıl, "Effect of wave climate change on longshore sediment transport in Southwestern Black Sea". *Estuarine, Coastal and Shelf Science,* vol. 258, 107415, Sep 2021.

[18] K. Amarouche, A. Akpınar, N. E. I. Bachari, R. E. Çakmak, and F. Houma, "Evaluation of a high-resolution wave hindcast model SWAN for the West Mediterranean basin". *Applied Ocean Research,* vol. 84, pp. 225-241, Mar 2019.

[19] Ö. Simav, D. Z. Şeker, and C. Gazioğlu, "Coastal inundation due to sea level rise and extreme sea state and its potential impacts: Çukurova Delta case". *Turkish Journal of Earth Sciences,* vol. 22, pp. 671-680, 2013.

[20] J.-L. Chen, T.-J. Hsu, F. Shi, B. Raubenheimer, and S. Elgar, "Hydrodynamic and sediment transport modeling of New River Inlet (NC) under the interaction of tides and waves". *Journal of Geophysical Research: Oceans,* vol. 120, pp. 4028-4047, 2015.

[21] L. C. V. Rijn, J. S. Ribberink, J. V. D. Werf, and D. J. R. Walstra, "Coastal sediment dynamics: recent advances and future research needs". *Journal of Hydraulic Research,* vol. 51, pp. 475-493, 2013.

[22] M. Keshtpoor, J. A. Puleo, F. Shi, and N. R. DiCosmo, "Numerical simulation of nearshore hydrodynamics and sediment transport downdrift of a tidal inlet". *Journal of Waterway, Port, Coastal, and Ocean Engineering,* vol. 141, Jul 2014.

[23] A. M. Khalifa, M. R. Soliman, and A. A. Yassin, "Assessment of a combination between hard structures and sand nourishment eastern of Damietta harbor using numerical modeling". *Alexandria Engineering Journal,* vol. 56, pp. 545-555, Dec 2017.

[24] ASRT, "Sedimentation in Damietta Harbor; Academy of Scientific Research and Technology Final Report; ASRT: Cairo, Egypt," 1988.

[25] H. M. El Asmar, and K. White, "Changes in coastal sediment transport processes due to construction of New Damietta Harbour, Nile Delta, Egypt". *Coastal Engineering,* vol. 46, pp. 127-138, Jul 2002.

[26] M. Sogreah, "Effects on the construction of the Port of Damietta on the evolution of the littoral drift," *Consult. Report, number 35/1202/R9*, p. 35, 1982.

[27] N. El-Fishawi, "Relative changes in sea level from tide gauge records at Burrulus, central part of the Nile Delta coast," *INQUA MBSS Newsl.*, vol. 16, pp. 53 – 61, 1994.

[28] F. M. Eid, S. H. S. El-Din, and K. A. A. El-Din, "Sea level variation along the Suez Canal". *Estuarine, Coastal and Shelf Science,* vol. 44, pp. 613-619, May 1997.

[29] H. M. El-Asmar, M. M. N. Taha, and A. S. El-Sorogy, "Morphodynamic changes as an impact of human intervention at the Ras El-Bar-Damietta Harbor coast, NW Damietta Promontory, Nile Delta, Egypt". *Journal of African Earth Sciences,* vol. 124, pp. 323-339, Dec 2016.

[30] Hersbach, H. *et al.*, "ERA5 hourly data on single levels from 1940 to present," Copernicus Climate Change Service (C3S) Climate Data Store (CDS) doi: 10.24381/cds.adbb2d47 (accessed on 10 March 2023).

[31] P. Vethamony, V. M. Aboobacker, K. Sudheesh, M. T. Babu, and K. Ashok Kumar, "Demarcation of inland vessels' limit off Mormugao port region, India: a pilot study for the safety of inland vessels using wave modelling," *Natural Hazards*, vol. 49, pp. 411-420, 2009.

[32] IPCC, "Climate Change 2013: The Physical Science Basis," *Contrib. Work. Gr. I to Fifth Assess. Rep. Intergov. Panel Clim. Chang. [Stocker, T.F., D. Qin, G.-K. Plattner, M. Tignor, S.K. Allen, J. Boschung, A. Nauels, Y. Xia, V. Bex P.M. Midgley (eds.)]. Cambridge Unive*, p. 1535, 2013.

[33] A. Seenath, "A new approach for handling complex morphologies in hybrid shoreline evolution models," *Applied Ocean Research,* vol. 141, 103754, Dec 2023.

[34] DHI, "Introducting the MIKE 21 Shoreline Morphology Module, Denmark, DHI Headquarters," 2017.

[35] DHI, "MIKE 21 & MIKE 3 Flow Model FM - Hydrodynamic Module, Denmark, DHI Headquarters," 2017.

[36] DHI, "MIKE 21 Wave Modelling - MIKE 21 Spectral Waves FM, Denmark, DHI Headquarters," 2017.

[37] G. J. L. Komen, M. Cavaleri, K. Donelan, S. Hasselmann, and P. A. E. M. Janssen, "Dynamics and modelling of ocean waves," *Cambridge University Press,* vol. UK, pp. 560, 1994.

[38] I. R. Young, "Wind generated ocean waves". *Elsevier*, vol. 2, Apr 1999, [Online]. Available: https://api.semanticscholar.org/

[39] DHI, "MIKE 21 & MIKE 3 Flow Model FM - Sand Transport Module, Denmark, DHI Headquarters," 2017.

[40] A. Akpinar, and S. Ponce de León, "An assessment of the wind re-analyses in the modelling of an extreme sea state in the Black Sea," *Dynamics of Atmospheres and Oceans,* vol. 73, pp. 61-75, Mar 2016.

[41] A. Abo Zed, "Effects of waves and currents on the siltation problem of Damietta harbour, Nile Delta coast, Egypt," *Mediterranean Marine Science,* vol. 8, pp. 33-48, 2007.

[42] O. E. Frihy, A. B. Abd El Moniem, and M. S. Hassan, "Sedimentation processes at the navigation channel of the Damietta Harbour on the Northeastern Nile Delta coast of Egypt". *Journal of Coastal Research,* vol. 18, pp. 459-469, 2002.

[43] T. Tech., "Shoreline master plan for the Nile Delta coast," *Prog. Rep. number 1*, p. 143, 1984.

[44] H. M. El-Asmar and K. White, "Rapid updating of maps of dynamic coastal landforms by segmentation of Thematic Mapper imagery, example from the Nile Delta, Egypt," *In Proceedings of 23rd Annual Conference of the Remote Sensing Society, The University of Reading. Remote Sensing Society, Nottingham*, pp. 515-520, 1997.

ORIGINAL RESEARCH (AR) DOI: 10.4274/jems.2024.46503

Journal of ETA Maritime Science 2024;12(2):128-135

Energy and Exergy Analysis of Diesel-Hydrogen and Diesel-Ammonia Fuel Blends in Diesel Engine

Kubilay Bayramoğlu

Zonguldak Bülent Ecevit University Faculty of Maritime, Department of Marine Engineering, Zonguldak, Türkiye

Abstract

In response to global warming and pollution, the use of alternative fuels in diesel engines is becoming increasingly important. The purpose of this research is to evaluate the effects of hydrogen and ammonia additions to diesel fuel on carbon emissions and energy and the exergy efficiency of diesel engines and to evaluate sustainability. In this study, the effects of adding 5%, 10%, and 15% of both hydrogen and ammonia to conventional diesel fuel on specific fuel consumption, carbon emissions, energy, exergy, and sustainability index (SI) were examined parametrically. Ammonia and hydrogen fuels reduce CO_2 emissions because they are carbon-free. as a result of the research, it was found that compared with ammonia addition, increasing hydrogen addition lowered specific fuel consumption while decreasing engine performance. The findings obtained show that mechanical energy and exergy values increase by 5.5% in the case of hydrogen addition and decrease by approximately 1.1% in the case of ammonia addition. The thermal efficiency and SI increased in the case of hydrogen addition and decreased in the case of ammonia addition. The exergy efficiency was estimated to be 63.37%, an increase of approximately 2.3% over pure diesel. The highest SI and exergetic performance coefficient values were determined 2.73 and 1.63, respectively. In line with the first and second law analyses, the usability of ammonia and hydrogen in diesel engines was evaluated thermodynamically.

Keywords: Alternative fuels, Exergy analysis, Sustainability index, Hydrogen, Ammonia

1. Introduction

Considering that the use of fossil fuels has significant harmful effects on the natural environment and human life, there are numerous regulations. [1]. In particular, reducing CO_2 due to the greenhouse effect has become extremely important. Approximately 3% of the world's carbon resources come from the maritime sector [2]. The Marine Environment Protection Committee (MEPC 80) aims to reduce greenhouse gas emissions by approximately 40% in 2030 and 70% in 2040, and reach net zero CO_2 emissions by 2050 [3]. Therefore, it is essential to employ alternative fuels or renewable energy sources. To reduce carbon emissions, future engines that use zero-carbon fuels, including hydrogen and ammonia, are being actively developed [4].

Hydrogen is considered a potential fuel because it may function as both a medium for storage and a carrier of energy in fuel cells. Hydrogen can be produced using a few fundamental clean energy sources: sunlight, geothermal power, and biomass gasification. In comparison to geothermal and solar hydrogen, hydrogen produced by the gasification of biomass has a high energy and energetic efficiency [5]. Numerous studies on the use of hydrogen in diesel engines have been published in the literature. Şanlı and Uludamar [6] assessed the energy-exergy efficiency and sustainability index (SI) of diesel and hydrogen-added diesel-biodiesel fuels. Li et al. [7] conducted experiments on a four-cylinder common-rail diesel engine using hydrogen-diesel combustion mode. At 20% and 40% loads, the effects of the amount of hydrogen and fuel injection timing on the combustion efficiency and emission parameters of diesel engines were examined. Duan et al. [8] optimized the combustion properties of a turbocharged direct injection hydrogen diesel engine and their engine performance the entire operating map. Wang et al. [9] compared the

Address for Correspondence: Kubilay Bayramoğlu, Zonguldak Bülent Ecevit University Faculty of Maritime, Department of Marine Engineering, Zonguldak, Türkiye
E-mail: k.bayramoglu.b@gmail.com
ORCID ID: orcid.org/0000-0002-5838-6132

Received: 11.12.2023
Last Revision Received: 28.02.2024
Accepted: 18.03.2024

To cite this article: K. Bayramoğlu, "Energy and Exergy Analysis of Diesel-Hydrogen and Diesel-Ammonia Fuel Blends in Diesel Engine." *Journal of ETA Maritime Science*, vol. 12(2), pp. 128-135, 2024.

combustion, injection, and performance of high-energy ignition methods at different ignition energies using computational fluid dynamics. Bayramoğlu and Yılmaz [10] conducted a numerical analysis to investigate how varying injection rates and timings of hydrogen affect the performance of a diesel engine. Bayramoğlu et al. [11] performed a numerical analysis to investigate the impact of varying intake manifold air variable rates and hydrogen addition on the engine performance and emissions parameters of a numerical test diesel engine.

As climate change intensifies, using ammonia as a fuel is considered a reaction to reduce carbon emissions. Because of its auto-ignition, density, and boiling point, ammonia is a fuel that can be used in internal combustion engines [12]. Ammonia has a proven track record as a hydrogen potential carrier and a developed infrastructure for extended distribution and transportation. Ammonia is a suitable green alternative fuel for the decarbonization of diesel engines and power-generating industries because it can be produced using renewable energy sources [13]. Various studies have been conducted on the use of ammonia as fuel. Tian et al. [14] studied the injection strategies of ammonia in internal combustion engines. Qi et al. [15] evaluated the most recent developments in ammonia-hydrogen engines, including ignition methods and combustion techniques, fuel supply, emissions and emission reduction methods. Xu et al. [16] investigated the use of an ammonia diesel mixture in a slow-speed, two-stroke marine diesel engine. Bayramoğlu et al. [17] investigated the effects of methane, hydrogen, and methane, ammonia, and hydrogen combustion combinations on emissions and thermodynamic properties. Pei et al. [18] investigated premixed compression ignition diesel and diesel-piloted engine modes under variable operating parameters to achieve high engine performance and low CO_2 emission in an experimental setup using ammonia-diesel dual fuel. Bani-Hani et al. [19] conducted an energy and exergy analysis of the regenerative Brayton cycle, which uses pentachlorobiphenyl wastes as an alternative fuel. Singh and Paul [20] evaluated the energy, exergy, exhaust emission, exergoeconomic, environmental-economic, and sustainability characteristics of a diesel engine using diesel and pyrolysis oil fuel mixtures. Lin and Wu [21] developed a model to calculate the exergy and energy efficiency of a boiler under various alternative fuel conditions.

The concept of exergy is extremely important in converting the fuel energy used in diesel engines into useful work. In this study, energy, exergy, and sustainability analysis of the use of hydrogen and ammonia fuel in a mixture with diesel fuel was conducted to limit CO_2 emissions against global warming. In contrast to earlier research, this study included analytical balancing equations for the analyses of diesel-hydrogen and diesel ammonia mixtures at 5%, 10%, and 15%. In addition, the change in CO_2 emissions due to the mixture of hydrogen and ammonia was also evaluated in the study.

2. Methodology

The study used a six-cylinder, low-speed marine diesel engine. Table 1 shows the technical specifications of the diesel engine. In general combustion problems, several fuels may be examined together. In a basic combustion problem, the two essential conditions are air and fuel. It is assumed that the combustion products are in balance after combustion. The combustion products and thermodynamic properties depend on the operating parameters, such as temperature and pressure. The diesel-hydrogen and diesel-ammonia combustion processes are given in Equations (1) and (2), respectively [23].

$$xC_\alpha H_\beta + yNH_3 + \frac{a_s}{\phi}(O_2 + 3.76N_2) \rightarrow CO_2 + H_2O + O_2 + N_2 + others \quad (1)$$

$$xC_\alpha H_\beta + yH_2 + \frac{a_s}{\phi}(O_2 + 3.76N_2) \rightarrow CO_2 + H_2O + O_2 + N_2 + others \quad (2)$$

Table 1. *Specifications of the diesel engine [22]*

Specifications	Unit	Value
Engine type	-	6S35ME
Bore	mm	350
Stroke	mm	1550
Power	kW	5220
SFC	g/kWh	190

In the given equations, is the equivalence ratio, represents the air–fuel stoichiometric ratio, and x and y represent the molar ratios of hydrogen and ammonia, respectively. Table 2 shows the parameters of the diesel, hydrogen, and ammonia used in the study.

Table 2. *Specifications of the investigated fuels [4]*

Specifications	Units	NH3	H_2	Diesel
Storage temperature	K	300	300	300
Lower heating value	MJ/kg	18.5	120	42.7
Adiabatic flame temperature	K	2073	2383	2573
Stoichiometric air-fuel ratio in mass	-	6.05	34.6	14.5

In diesel engines, some of the energy generated by the fuel energy is converted to mechanical power transferred to the propeller, combustion products in the exhaust, and heat transfer to the engine body. The energy balance for the diesel engine can be stated as shown in Equations (3) and (4) using the first law of thermodynamics [24].

$$\dot{E}_{in} = \dot{E}_{out} + \dot{E}_{loss} \quad (3)$$

$$\dot{E}_{fuel} = \dot{E}_{work} + \dot{E}_{exhaust} + \dot{E}_{loss} \quad (4)$$

where $\dot{E}_{fuel}$ is the fuel energy. $\dot{E}_{work}$ is the mechanical power. $\dot{E}_{exhaust}$ is the exhaust energy and $\dot{E}_{loss}$ is the energy loss from the combustion chamber. The energy of the fuel is defined by Equation (5).

$$\dot{E}_{fuel} = \dot{m}_{fuel} \cdot LHV \quad (5)$$

Where, $\dot{m}_{fuel}$ is the fuel mass flow and *LHV* is the lower heating value of fuel. Combustion products energy in the exhaust is calculated by Equation (6). In exhaust energy calculations, the mass fraction and energy value of each gas in the exhaust are considered.

$$\dot{E}_{exhaust} = \sum \dot{m}_i \cdot \Delta h_i \quad (6)$$

where Δh_i is the enthalpy difference and $\dot{m}_i$ is the mass fraction of the exhaust gasses. The mechanical work and energy loss from the combustion chamber are calculated by Equations (7) and (8), respectively.

$$\dot{E}_{work} = \dot{W} \quad (7)$$

$$\dot{E}_{loss} = \dot{E}_{fuel} + \dot{E}_{air} - \dot{E}_{work} + \dot{E}_{exhaust} \quad (8)$$

Equation (9) can be used to calculate the balance of exergy for a steady-state system [25,26].

$$\sum \dot{E}x_{in} = \sum \dot{E}x_{out} + \sum \dot{E}x_{dest} \quad (9)$$

The exergy balance can be determined using Equation (10) [27].

$$\dot{E}x_{fuel} = \dot{E}x_{work} + \dot{E}x_{exhaust} + \dot{E}x_{loss} + \dot{E}x_{dest} \quad (10)$$

Where, $\dot{E}x_{fuel}$ is the fuel exergy. $\dot{E}x_{work}$ is the mechanical work exergy, $\dot{E}x_{exhaust}$ is the exhaust exergy, $\dot{E}x_{lost}$ is the exergy of the heat loss from combustion chamber and $\dot{E}x_{dest}$ is the exergy destruction. Exergy of fuel can be calculated using Equation (11).

$$\dot{E}x_{fuel} = \dot{m}_{fuel} \cdot LHV \cdot \varepsilon_{fuel} \quad (11)$$

The chemical energy factor ε_{fuel} can be written as Equation (12) [28].

$$\varepsilon_{fuel} = 1.0401 + 0.1728\frac{H}{C} + 0.0432\frac{O}{C} + 0.2169\frac{S}{C}\left[1 - 2.0628\frac{H}{C}\right] \quad (12)$$

where *H*, *O*, *C*, and *S* are the mass ratios of hydrogen, oxygen, carbon, and sulfur in the fuel, respectively. Equation (13) can be used to calculate the loss of exergy [29].

$$\dot{E}x_{loss} = \dot{E}_{loss}\left[1 - \frac{T_0}{T_s}\right] \quad (13)$$

Where $\dot{Q}_{loss}$ is the heat transfer from the diesel engine, T_o =300 K is the environmental temperature and T_S is the engine temperature. The exhaust, thermomechanical, and chemical exergy are given by Equations (14), (15), and (16) [30].

$$\dot{E}x_{exhaust} = \sum \dot{m}_i (\varepsilon_{ch} + \varepsilon_{thm})_i \quad (14)$$

$$\varepsilon_{ch} = \sum y_i E^o{}_{ch} + \bar{R}T_0 \sum y_i \ln(y_i) \quad (15)$$

$$\varepsilon_{thm} = \sum (h - h_0) - T_0(s - s_0) \quad (16)$$

Where *R* is the gas constant, y_r is the exhaust gas mole fraction of each product. *h* is the enthalpy, *s* is the entropy and *T* is the temperature. $E^o{}_{ch}$ is the standard chemical exergy [31]. The mechanical exergy can be expressed as Equation (17).

$$\dot{E}x_{work} = \dot{W} \quad (17)$$

The thermodynamic efficiency of the first and second laws are given in Equations (18) and (19) [32].

$$\eta_I = \frac{E_{work}}{E_{fuel}} \quad (18)$$

$$\eta_{II} = 1 - \frac{\dot{E}x_{dest}}{\dot{E}x_{fuel}} \quad (19)$$

Obtaining information on exergy losses in the combustion process depends on the use of another performance criterion known as the exergetic performance coefficient (EPC). Equation (20) is used to calculate the EPC function, which is defined as the ratio of total exergy output to availability loss [33-35].

$$EPC = \frac{\dot{E}x_{fuel} - Ex_{des.}}{Ex_{des.}} \quad (20)$$

The SI is a significant criterion for comparing alternative engine fuels [27]. The SI evaluates the environmental impact of energy systems [36]. The SI can be determined using Equation (21).

$$SI = \frac{1}{1 - \eta_{II}} \quad (21)$$

3. Results and Discussion

In addition to conventional diesel fuels, alternative fuels that reduce carbon emissions, such as hydrogen and ammonia, are used in marine diesel engine systems. The first and second laws of thermodynamics and sustainability of 5%, 10%, and 15% hydrogen and ammonia fuel blends are evaluated. In the study, the adiabatic flame temperatures for hydrogen, diesel, and ammonia fuel were taken as 2400 K, 2000 K, and 1600 K, respectively. The exhaust temperatures were calculated by proportioning the adiabatic flame temperature. In addition, for pure combustion values, it has been assumed that hydrogen fuel increases by 25% compared with diesel fuel, while ammonia reduces it by 10% [37]. The combustion process of hydrogen and ammonia added to diesel fuel was performed under the same fuel energy conditions. Figure 1 shows the specific fuel consumption because of 5%, 10%, and 15% hydrogen and ammonia addition to diesel fuel.

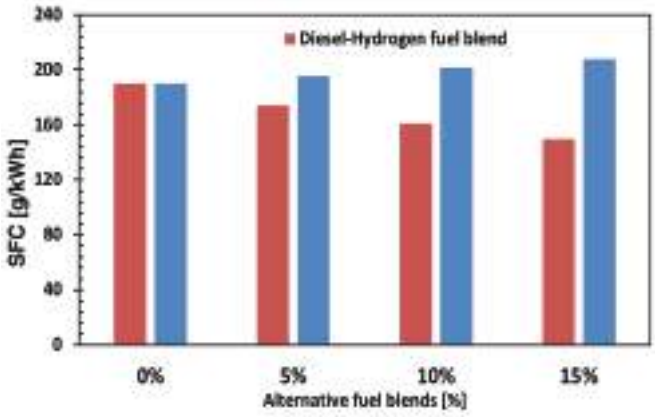

Figure 1. *Specific fuel consumption of diesel-hydrogen and diesel-ammonia fuel blends*

Considering the calorific values of hydrogen and ammonia, specific fuel consumption decreases as hydrogen addition increases. This is because hydrogen provides more energy per unit mass than diesel. With ammonia addition, specific fuel consumption increases because the lower calorific value of ammonia is less than that of diesel fuel. To provide the same amount of energy, the amount of ammonia per unit energy increase. Carbon emissions have decreased for both hydrogen and ammonia fuels because they are carbon-free fuels. Carbon dioxide emissions for hydrogen and ammonia fuels are shown in Figure 2.

Fuel is injected into the diesel engine to provide approximately 11.7 MW of energy. This energy was assumed to be equal for 5%, 10%, and 15% hydrogen additions and balanced against the amount of fuel. It was determined that there was an increase in the mechanical energy with increasing hydrogen addition. In addition, when the amount of hydrogen added to diesel fuel increased, the exhaust energy decreased. This is due to a decrease in the exhaust flow rate as hydrogen addition increases. In addition, it is observed that mechanical energy increases by 5% for 15% hydrogen addition. Figure 3 shows the diesel engine energy balance for hydrogen addition.

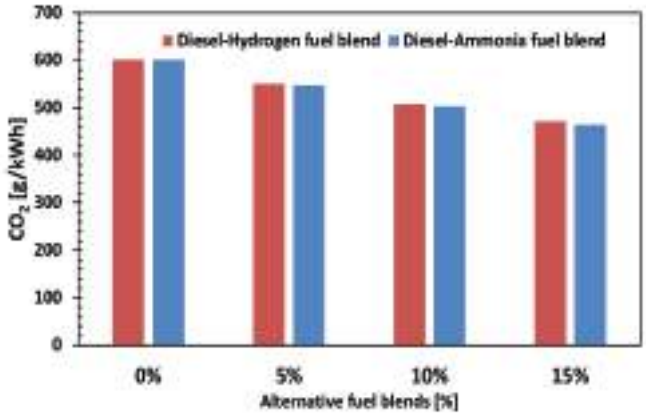

Figure 2. *CO_2 emissions of diesel-hydrogen and diesel-ammonia fuel blends*

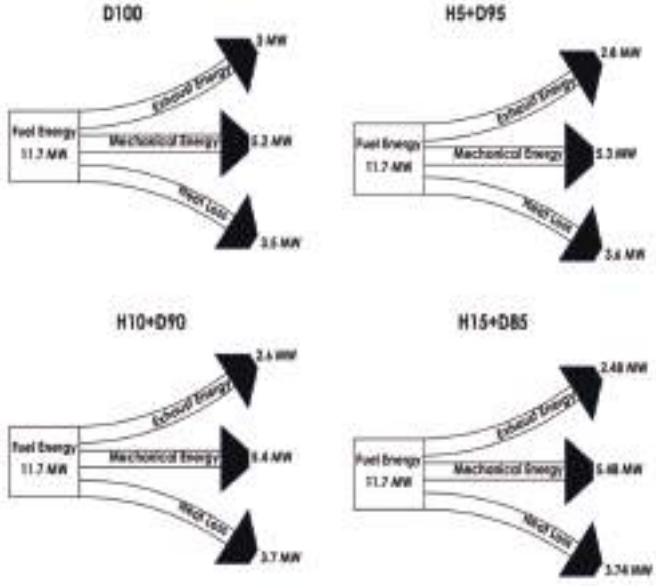

Figure 3. *Energy balance for diesel-hydrogen blends*

Figure 4 demonstrates the energy balance with the addition of ammonia. Mechanical energy decreased with increasing ammonia addition. The addition of ammonia reduces the combustion chamber temperature of the fuel. The main reason for the decrease in mechanical energy is that ammonia reduces the combustion chamber temperature and pressure. Similar to the addition of hydrogen, the heat

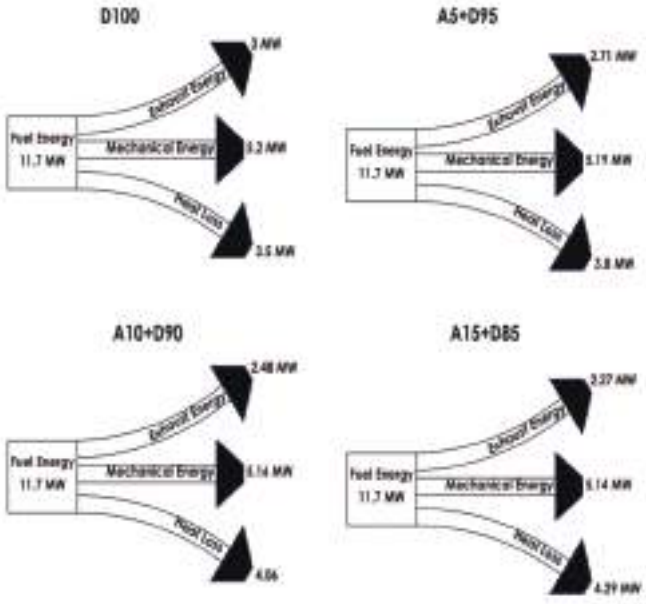

Figure 4. *Energy balance for diesel-ammonia blends*

loss from the combustion chamber also increases with the addition of ammonia.

In diesel engines, fuel exergy is calculated depending on the atomic balance and the lower heating values in the fuel. The fuel exergy determined for the addition of both hydrogen and ammonia to diesel fuel is approximately 12.56 MW. Unlike the concept of energy, exergy destruction is also calculated. Irreversibility, based on the second rule of thermodynamics, causes exergy destruction. It was determined that with increasing hydrogen energy, mechanical exergy and heat exergy increased, whereas exhaust exergy decreased. In addition, exergy destruction accounts for approximately 40% of the total exergy. It can be seen that exergy destruction decreases with increasing hydrogen addition. The exergy balance of diesel-hydrogen addition is shown in Figure 5.

Figure 6 shows the exergy balance for the diesel-ammonia fuel mixture. With increasing ammonia addition, exergy destruction and heat exergy increase, whereas mechanical exergy and exhaust exergy decrease. It can be evaluated that mechanical exergy decreases because of the decrease in engine performance of ammonia addition. This can also be explained by the fact that ammonia increases irreversibility and exergy destruction.

Thermal efficiency values calculated using the first law of thermodynamics and the second law of exergy efficiency for diesel-hydrogen and diesel-ammonia fuel blends are shown in Figure 7. It was determined that the thermal efficiency increased with increasing hydrogen addition and decreased with increasing ammonia. Thermal efficiency increases by approximately 5% for 15% hydrogen addition. It was determined that in the case of 15% ammonia addition, the thermal efficiency decreased by 1.5%. The findings show that the highest thermal efficiency is in the 15% diesel-hydrogen blends and the lowest thermal efficiency is in the 15% diesel-ammonia blends. When the second law efficiencies are compared, in the case of 15% hydrogen addition, the exergy efficiency was determined to be

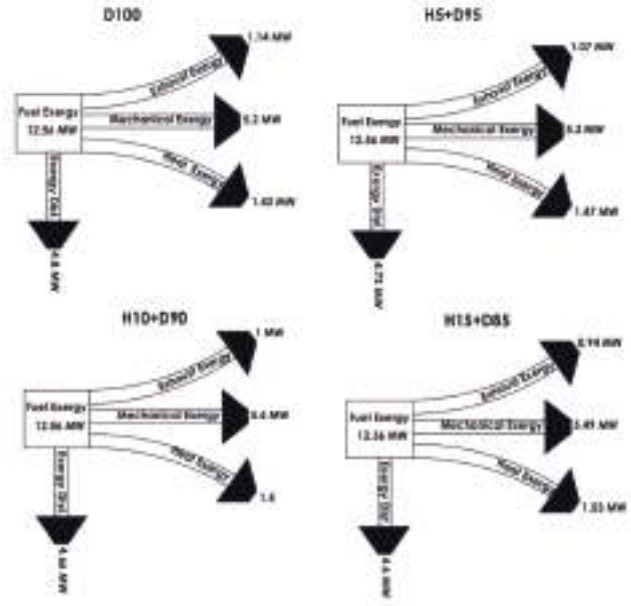

Figure 5. *Exergy balance for diesel-hydrogen blends*

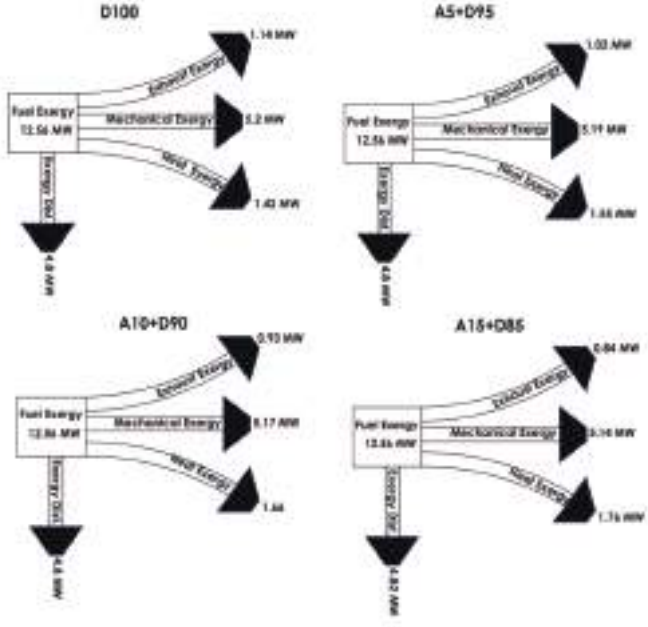

Figure 6. *Energy balance for diesel-ammonia blends*

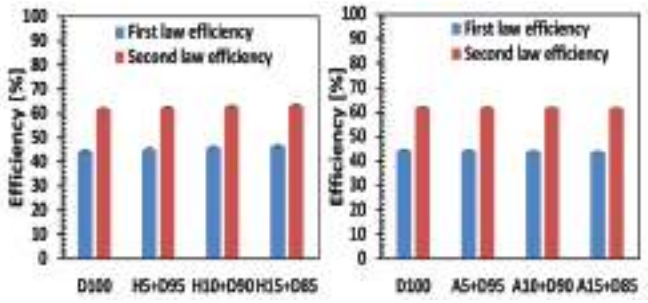

Figure 7. *First and second law efficiency*

63.37%, an increase of approximately 2.3% compared with the use of pure diesel. With 15% ammonia addition, the exergy efficiency was 61.62%.

Figure 8 shows the model findings according to the EPC criteria. Determining the ecological performance of combustion processes and comparing the findings with second-law characteristics are essential technical parameters. The findings show that the EPC value in diesel combustion is approximately 1.63. It was observed that in the case of 15% hydrogen addition, the EPC value was approximately 1.73, and in the case of 15% ammonia addition, the EPC value was 1.63.

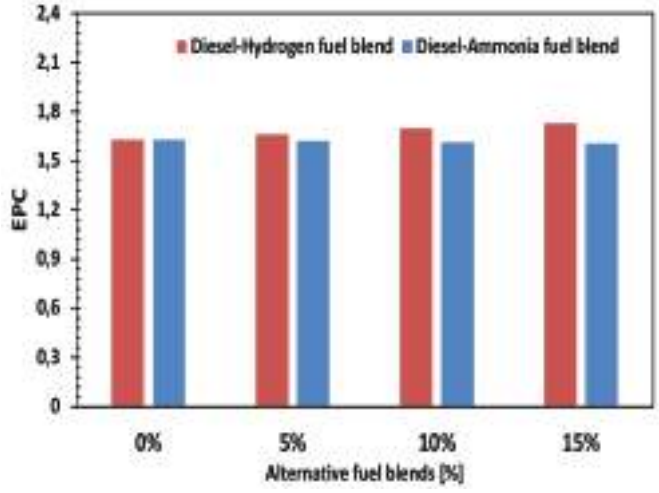

Figure 8. *Variations in EPC*

EPC: Exergetic performance coefficient

Figure 9 demonstrates the SI, which is a derivative of the second law for hydrogen and ammonia addition. Based on exergy data, it was determined that diesel-hydrogen addition increased the SI, whereas ammonia-diesel addition decreased the SI. The SI was determined to be approximately 2.73 for 15% hydrogen addition and approximately 2.6 for 15% ammonia addition.

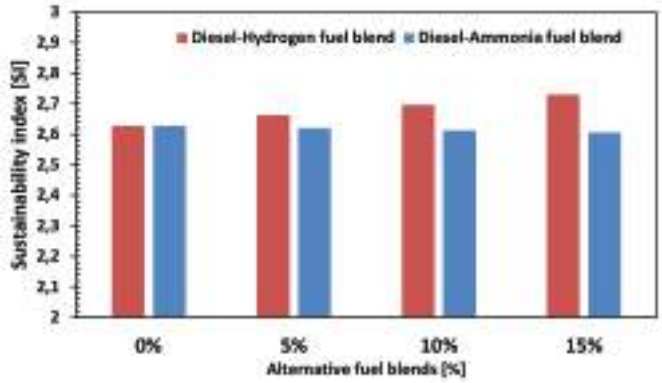

Figure 9. *Sustainability index*

4. Conclusion

This study investigated the effects of 5%, 10%, and 15% hydrogen and 5%, 10%, and 15% ammonia to conventional diesel fuel on energy, exergy, and carbon emissions. The model includes analytical evaluation of the energy and exergy impact of hydrogen and ammonia additions based on fuel consumption under the same fuel energy conditions. With the investigation, the following main findings were obtained:

• Specific fuel consumption was determined under the same fuel energy conditions according to the lower calorific values of the fuels used. It has been determined that 15% hydrogen addition reduces specific fuel consumption by approximately 21%, whereas 15% ammonia addition increases it by 9.5%.

• The main reason why hydrogen and ammonia fuels will be preferred in the future is that they are carbon-free. Therefore, it was determined that carbon emissions decreased for both fuels. It has been observed that carbon emissions per hour are lower because hydrogen fuel reduces engine fuel consumption.

• Energy efficiency is higher with hydrogen fuel addition. Therefore, the mechanical energy increase was determined to be higher in the case of hydrogen addition. In a 15% diesel-hydrogen blend, mechanical energy increased by 5%. For the 15% diesel-ammonia blend, mechanical energy decreased by 1.1%.

• In exergy balance, while exergy destruction increased in the diesel-ammonia mixture, it decreased in the diesel-hydrogen mixture. Mechanical exergy increases with the addition of hydrogen and decreases with the addition of ammonia, depending on the mechanical energy.

• The thermal efficiency, which is the first law energy, was determined to be approximately 46.59% with 15% hydrogen addition. It was determined to be 43.71% in 15%

ammonia addition. The second law efficiency is 63.37% with 15% hydrogen addition and 61.62% with 15% ammonia addition. The SI increases with the addition of hydrogen and decreases with the addition of ammonia.

• In this study, SI and EPC calculations were carried out. The SI was calculated to be approximately 2.73 for 15% hydrogen addition and 2.6 for 15% ammonia addition. The results indicate that the EPC value for diesel combustion is approximately 1.63. The EPC value for 15% hydrogen addition was around 1.73, whereas that for 15% ammonia addition was around 1.63.

In future studies, LCA guidelines, and wake-up well calculations, including well-to-tank and tank-to-wake emission factors, could be analyzed for the impact on carbon emissions of ammonia and hydrogen fuels used as alternative fuels. Additionally, energy, exergy, and sustainability analyses of alcohol and biodiesel fuels can be performed as alternative fuels.

Funding: The author declare that no funding was received for this research, authorship, or publication.

References

[1] Z. Lin, et al. "Numerical investigation of ammonia-rich combustion produces hydrogen to accelerate ammonia combustion in a direct injection SI engine". *International Journal of Hydrogen Energy,* vol. 49, pp. 338-351, Jan 2024.

[2] A. Sánchez, M. A. Martín Rengel, and M. Martín, "A zero CO2 emissions large ship fuelled by an ammonia-hydrogen blend: Reaching the decarbonisation goals". *Energy Conversion and Management,* vol. 293, 117497, Oct 2023.

[3] IMO. *2023 IMO strategy on reduction of GHG emissions from ships,* 2023.

[4] J. Shin, and S. Park, "Numerical analysis for optimizing combustion strategy in an ammonia-diesel dual-fuel engine". *Energy Conversion and Management,* vol. 284, 116980, May 2023.

[5] A. Roy, and S. Pramanik, "A review of the hydrogen fuel path to emission reduction in the surface transport industry". *International Journal of Hydrogen Energy,* vol. 49, pp. 792-821, Jan 2024.

[6] B. Şanlı, and E. Uludamar, "Effect of hydrogen addition in a diesel engine fuelled with diesel and canola biodiesel fuel: Energetic-exergetic, sustainability analyses". *International Journal of Hydrogen Energy,* vol. 49, pp. 1148-1159, Jan 2024.

[7] Z. Li, J. Liu, Q. Ji, P. Sun, X. Wang, and P. Xiang, "Influence of hydrogen fraction and injection timing on in-cylinder combustion and emission characteristics of hydrogen-diesel dual-fuel engine". *Fuel Processing Technology,* vol. 252, 107990, Dec 2023.

[8] Y.-h. Duan, B.-g. Sun, Q. Li, X.-s. Wu, T.-g. Hu, and X.-h. Luo, "Combustion characteristics of a turbocharged direct-injection hydrogen engine". *Energy Conversion and Management,* vol. 291, 117267, Sep 2023.

[9] Y. Wang, Z. Xu, C. Zhang, and L. Liu, "Combustion optimization of a hydrogen free-piston engine with high-energy ignition". *International Journal of Hydrogen Energy,* vol. 49, pp. 483-494, Jan 2024.

[10] K. Bayramoğlu, and S. Yılmaz, "Emission and performance estimation in hydrogen injection strategies on diesel engines". *International Journal of Hydrogen Energy,* vol. 46, pp. 29732-29744, Aug 2021.

[11] K. Bayramoğlu, S. Yilmaz, and M. Nuran, "Energy and exergy analyses of hydrogen addition in a diesel engine". *International Journal of Exergy,* vol. 37, pp. 377-392, 2022.

[12] W.-H. Chen, P. Sarles, A. K. Sharma, S. S. Lam, E. E. Kwon, and A. B. Culaba, "Analysis of ammonia combustion for decarbonization followed by selective non-catalytic reduction of nitrogen oxides". *International Journal of Hydrogen Energy,* vol. 48, pp. 39553-39569, Dec 2023.

[13] C. Kurien, and M. Mittal, "Utilization of green ammonia as a hydrogen energy carrier for decarbonization in spark ignition engines". *International Journal of Hydrogen Energy,* vol. 48, pp. 28803-28823, Aug 2023.

[14] J. Tian, et al. "Visualization study on ammonia/diesel dual direct injection combustion characteristics and interaction between sprays". *Energy Conversion and Management,* vol. 299, 117857, Jan 2024.

[15] Y. Qi, W. Liu, S. Liu, W. Wang, Y. Peng, and Z. Wang. "A review on ammonia-hydrogen fueled internal combustion engines". *eTransportation,* vol. 18, 100288, Oct 2023.

[16] X. Xu, Z. Wang, W. Qu, M. Song, Y. Fang, and L. Feng, "Optimizations of energy fraction and injection strategy in the ammonia-diesel dual-fuel engine". *Journal of the Energy Institute,* vol. 112, 101455, Feb 2024.

[17] K. Bayramoğlu, A. Bahlekeh, and K. Masera, "Numerical investigation of the hydrogen, ammonia and methane fuel blends on the combustion emissions and performance". *International Journal of Hydrogen Energy,* vol. 48, pp. 39586-39598, Feb 2023.

[18] Y. Pei, D. Wang, S. Jin, Y. Gu, C. Wu, and B. Wu, "A quantitative study on the combustion and emission characteristics of an Ammonia-Diesel Dual-fuel (ADDF) engine". *Fuel Processing Technology,* vol. 250, 107906, Nov 2023.

[19] E. Bani-Hani, et al. "Energy and exergy analyses of a regenerative Brayton cycle utilizing monochlorobiphenyl wastes as an alternative fuel". *Energy,* vol. 278, 127861, Sep 2023.

[20] D. Singh, and A. Paul, "Energy, exergy, emission, exergoeconomic, enviroeconomic, and sustainability analysis of diesel engine, fueled by waste cooking oil and waste polyethylene co-pyrolysis oil-diesel blends". *Journal of Cleaner Production,* vol. 426, 139186, Nov 2023.

[21] K.-W. Lin, and H.-W. Wu, "Emissions and energy/exergy efficiency in an industrial boiler with biodiesel and other fuels". *Case Studies in Thermal Engineering,* vol. 50, 103474, Oct 2023.

[22] MAN. *MAN B&W ME-C two-stroke engines*. 2024.

[23] C. R. Ferguson. International combustion engines; Applied thermosciences. United States: John Wiley and Sons, New York, NY; 1985.

[24] G. Kökkülünk, "Energy and exergy analyses of a bulk carrier diesel generator for different loads". *Journal of Eta Maritime Science,* vol. 7, pp. 43-50, Mar 2019.

[25] Y. Zhang, B. Li, H. Li, and B. Zhang, "Exergy analysis of biomass utilization via steam gasification and partial oxidation". *Thermochimica Acta,* vol. 538, pp. 21-28, Jun 2012.

[26] K. Bayramoğlu, and M. Nuran, "Energy, exergy, sustainability evaluation of the usage of pyrolytic oil and conventional fuels in diesel engines". *Process Safety and Environmental Protection,* vol. 181, pp. 324-333, Jan 2024.

[27] B. Doğan, M. Çelik, C. Bayındırlı, and D. Erol, "Exergy, exergoeconomic, and sustainability analyses of a diesel engine using biodiesel fuel blends containing nanoparticles". Energy, vol. 274, 127278, Jul 2023.

[28] Kotas T. The Exergy Method of Thermal Plant Analysis. Florida: Krieger Publishing Company; 1985.

[29] E. J. C. Cavalcanti, "Energy, exergy and exergoenvironmental analyses on gas-diesel fuel marine engine used for trigeneration system". *Applied Thermal Engineering,* vol. 184, 116211, Feb 2021.

[30] M. K. Yesilyurt, "The examination of a compression-ignition engine powered by peanut oil biodiesel and diesel fuel in terms of energetic and exergetic performance parameters". *Fuel,* vol. 278, 118319, 2020.

[31] M. A. Rosen, and I. Dincer, "Exergy as the confluence of energy, environment and sustainable development". *Exergy, An International Journal*, vol. 1, pp. 3-13, 2001.

[32] N. Panigrahi, M. K. Mohanty, S. R. Mishra, and R. C. Mohanty, "Energy and exergy analysis of a diesel engine fuelled with diesel and simarouba biodiesel blends". *Journal of The Institution of Engineers (India): Series C,* vol. 99, pp. 9-17, 2018.

[33] Y. Ust, A. S. Karakurt, and U. Gunes, "Performance analysis of multipurpose refrigeration system (MRS) on fishing vessel". *Polish Maritime Research,* vol. 23, pp. 48-56, Apr 2016.

[34] Y. Ust, B. Sahin, A. Kodal, and I. H. Akcay, "Ecological coefficient of performance analysis and optimization of an irreversible regenerative-Brayton heat engine". *Applied Energy,* vol. 83, pp. 558-572, Jun 2006.

[35] Y. Ust, F. Arslan, I. Ozsari, and M. Cakir, "Thermodynamic performance analysis and optimization of DMC (Dual Miller Cycle) cogeneration system by considering exergetic performance coefficient and total exergy output criteria". *Energy,* vol. 90, 552-559, Oct 2015.

[36] S. Sarıkoç, İ. Örs, and S. Ünalan, "An experimental study on energy-exergy analysis and sustainability index in a diesel engine with direct injection diesel-biodiesel-butanol fuel blends". *Fuel,* vol. 268, 117321, May 2020.

[37] M. Faizal, and R. Saidur, "Comparative thermodynamics analysis of gasoline and hydrogen fuelled internal combustion engines". *International Journal of Advanced Scientific Research and Management,* vol. 2, pp. 12-18, Mar 2017.

ORIGINAL RESEARCH (AR) DOI: 10.4274/jems.2024.24582

Journal of ETA Maritime Science 2024;12(2):136-143

Development of Constructive Measures to Reduce the Consequences of Ship Collisions

Pavel Burakovskiy

Kaliningrad State Technical University, Department of Navigation and Maritime Safety, Kaliningrad, Russia

Abstract

An analysis of the damage caused to vessels by collisions shows that the wreck of most struck ships is mainly due to underwater damage developed because of the accident. Such damage is caused, as a rule, by the presence of bulbs on striking ships that have high longitudinal rigidity and strength exceeding the load-bearing capacity of the framing system several times. Scientists in many countries are looking for ways to reduce the consequences of collisions with ships that have bulbs. Based on the results of the research, schemes for modernizing the forward end of ship hulls by installing bulbs with increased longitudinal compliance to reduce the consequences of ship collisions were proposed, and recommendations were developed for the selection of their characteristics, which make it possible to avoid underwater holes on a struck ship. Bulbs with increased longitudinal compliance were designed using methods of plastic limit analysis. The effectiveness of a modernized deformable bow structure was studied using ANSYS LS-DYNA non-linear finite element method computations. The developed technical solutions ensure that in case of collision in the underwater part of a struck vessel, the deformations of the framing systems will remain insignificant, thereby avoiding the appearance of damage below the waterline.

Keywords: Ship collisions, Corrugated bulb, Bearing capacity, FEM, Plastic limit analysis

1. Introduction

An analysis of the damage caused to vessels by collisions shows that the wreck of most struck ships is mainly due to underwater damage developed because of the accident [1,2]. Such damage is caused, as a rule, by the presence of bulbs on striking ships that have high longitudinal rigidity and strength exceeding the load-bearing capacity of the framing system several times.

According to some data [1], in 80% of cases, damage to struck ships is located below the operational waterline, and the probability of ship destruction is determined by the size of the damage and the design features of the ship (position of watertight bulkheads, distance between double sides, etc.) affecting the number of compartments flooded [1,3].

In [4], it is shown that for more than 30% of the collision scenarios, the damage vertical position lower limit is above the waterline, but typically due to scenarios with collision angles close to 0° or 180° with limited penetration. During the risk assessment, the scenarios leading to these damages were discarded, and damage stability analysis was carried out [4]. In the study [5], it is shown that the bulb structure is most threatening to struck ships. In paper [6], a bulbous bow is a threat to a struck ship because most large ships have a bulbous bow and it usually contacts the struck ship first, then it might penetrate the side shell.

A typical example of the influence of bulb design on the consequences of an accident is the collision of the SS "Admiral Nakhimov" with the MS "Pyotr Vasev" that occurred on August 31, 1986 in Tsemes Bay near Novorossiysk. It resulted in the loss of 423 lives [2,7]. The MS "Petr Vasev" crashed into the hull of the SS "Admiral Nakhimov" in the area of 90-110 frames on the starboard side with the upper part of the stem and the bulb below the waterline. The bulb ripped up an underwater hole in the ship's hull with an area of 84 m^2 stretching from the seventh to tenth watertight compartments that housed the second boiler room, engine room, tanks with fuel oil and diesel fuel, food warehouses, and hold No. 4. At the same time, the bulb of the striking ship remained practically undeformed [2,7].

Address for Correspondence: Pavel Burakovskiy, Kaliningrad State Technical University, Department of Navigation and Maritime Safety, Kaliningrad, Russia
E-mail: paul_b@mail.ru
ORCID ID: orcid.org/0000-0002-2813-1788

Received: 18.09.2023
Last Revision Received: 31.01.2024
Accepted: 20.03.2024

To cite this article: P. Burakovskiy, "Development of Constructive Measures to Reduce the Consequences of Ship Collisions." *Journal of ETA Maritime Science*, vol. 12(2), pp. 136-143, 2024.

It is known that the use of bulbs can reduce wave resistance by approximately 15% or more, depending on the hull design. However, there is a contradiction between a small gain in speed, and a few percent in fuel economy, and colossal losses in the case of collision. If there is a bulb on the striking ship, the struck ship in case of collision, even at low speed, receives damage below the waterline that often leads to a ship wreck. The economic side of this issue is also a subject of ship insurance because insurers consider the issue of "taking into account bulbs in insurance conditions" [8,9].

2. Analysis of the Existing Design Solutions

Scientists in many countries are looking for ways to reduce the consequences of collisions with ships with bulbs [10-13]. The concept of soft bow design was proposed in [14]. Thus, in 1990, Woisin [8] developed recommendations for reducing the consequences of collisions with ships with bulbous bows. It was proposed to reduce the size of the bulb shapes or to make the bulb flexible in the longitudinal direction so that it would collapse under low longitudinal force, while the force destroying the bulb should be less than that which violates the integrity of the shell plate of the framing system.

As an alternative to a bulbous bow to reduce the consequences of collisions, according to Woisin [8], the Mayer's bow shape should be considered. It is also recommended to reduce the thickness of the shell plate and stem to create a "lightweight" structure, but the practical implementation of these provisions has not yet been carried out.

In paper [15], the probability of rupture of cargo oil tank in the struck VLCC in cases where all the spiking ships use buffer bulbous bows was compared with the case where all the striking ships use conventional bulbous bows. It is estimated from the calculation that the probability of rupture of cargo oil tank in the struck VLCC decrease about 10-12% by the effect of using buffer bulbous bow.

In [16], various softening methods for the fore part of an LNG carrier are proposed and their influence on reducing the damage of a struck ship and the impact transmitted to the striking ship are studied. The effectiveness of a buffer bow is highlighted in [5] by focusing on the performance and how much the risk of oil outflow is decreased. In [17], the introduction of buffer bulbous bows has been proposed. Relatively soft buffer bows absorb part of the kinetic energy of the striking ship before penetrating the inner hull of the struck vessel.

Papers [6] and [18] show that buffer bow design (bulbous bow stiffened with vertical ring frames) may effectively reduce the risk of oil spill and/or seawater ingress in various cases of collision between large ships. It is noted that a lower crushing pressure of the bulbous bow is preferable to avoid the early and easy rupture of the side structure.

A comparative collision study of the new SEA-Arrow buffer bow and the conventional bulbous bow was conducted in [19] using elasto-plastic finite element analysis. It is shown that the buffer bow characteristic of the SEA-Arrow is superior to that of the conventional bulbous bow because much more energy is dissipated by the plastic deformation of striking and struck ships until the inner shell of the struck ship ruptures.

To reduce the consequences of collisions with ships equipped with bulbs, new designs of bow bulbs have been proposed [13,20,21]. It is possible to eliminate underwater damage by making the longitudinal bearing capacity of the bulb lower than the bearing capacity of the side framing system of the vessels, which is achieved by making the shell plate of the bulb in the form of annular corrugations.

This design of the bulb has a cone-shaped or cylindrical shape, contains a fairing and an insert made in the form of corrugations and reinforced with brackets, and the cross-sectional corrugations of the insert have the shape of a drop or a circle. These designs have some disadvantages; therefore, this paper proposes new technical solutions.

Thus, in the bulb design [21], the ultimate load for corrugations with a large perimeter is significantly higher than that for corrugations with a small perimeter located in the bow part of the bulb, which leads to an increase in the longitudinal rigidity of the bulb. Reducing the longitudinal rigidity of the bulb is possible by increasing the height of the corrugations with an increase in their perimeter; however, this leads to a loss of useful volume inside the bulb and also increases the labor intensity of manufacturing the bulb because of the need to manufacture corrugations of various heights.

An increase in the compliance of the bulb due to a decrease in the thickness of the corrugations is limited by the fact that during operation, the bow end of the ship is subjected to intense hydrodynamic loads.

This paper presents new design solutions that make it possible to regulate the compliance of bulb fitting within a wide range through the implementation of some measures. In particular, to regulate the compliance of the corrugated insert, it is proposed to use grooves of a certain depth in the corrugations. To fill the space in the corrugations to give the bulb fitting a streamlined shape, it is proposed to use elastic containers with a working medium. In addition, the bulb fitting can be made of separate sections that slide inside the bulb during the interaction of the bulb fitting with the side grillage of the struck vessel. In addition, the bulb fitting can

be attached to the hull of the vessel with the possibility of its separation if there is a threat of collision between vessels. The following sections provide a detailed description of the proposed technical solutions and an analysis of their effectiveness. The proposed technical solutions have no analogs in world practice, which is confirmed by invention patents.

3. New Design Measures

In particular, this work proposes a design for a corrugated bulb, in the upper and lower parts of the corrugated walls there is a groove (Figure 1).

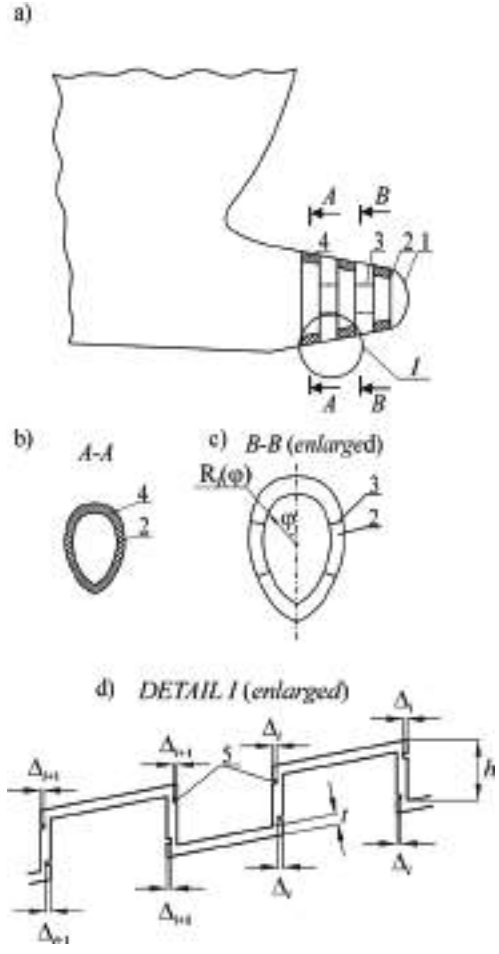

Figure 1. *Diagram of a corrugated bulb with grooves in the walls of the corrugations: a) general view; b) section A-A; c) section B-B; d) detail I; 1- fairing; 2- corrugated insert; 3- brackets; 4- elastic filler; 5- grooves*

To determine the relationship between the depth of the groove and the thickness and height of the corrugation at which the required compliance of the bulb fitting is ensured, plastic limit analysis can be used [22,23]. Let us consider the deformation of a corrugation with unit width b (Figure 2).

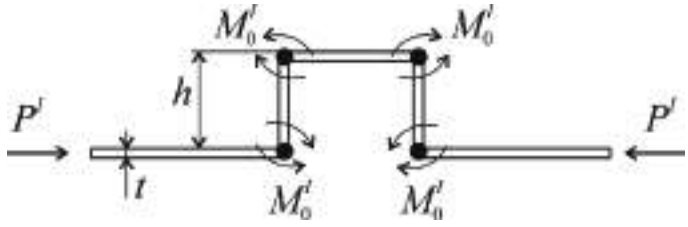

Figure 2. *Corrugation deformation diagram*

Limiting moment M_0^l of the section of a corr nit width b according to [22]

$$M_0^l = \sigma_T \cdot \frac{b \cdot t^2}{4} \quad (1)$$

where t – corrugation thickness, m;

b – corrugation width, m;

σ_T – yield strength of the corrugation material, Pa.

In this case, the ultimate load P^l leading to the folding of the corrugation can be determined within the framework of plastic limit analysis [22] as follows:

$$P^l \cdot h = 2 \cdot M_0^l \quad (2)$$

where h – corrugation height, m.

The limiting moment M_0^K for an annular corrugation can be determined by integrating (1) along the entire perimeter of the corrugation, considering the symmetry of the corrugation relative to the vertical plane

$$M_0^K = 2\int_0^{\pi} \frac{M_0^l}{b} \sqrt{[R'(\varphi)]^2 + [R(\varphi)]^2}\, d\varphi = \sigma_T \cdot \frac{t^2}{2} \int_0^{\pi} \sqrt{[R'(\varphi)]^2 + [R(\varphi)]^2}\, d\varphi \quad (3)$$

where $R(\varphi)$ – function describing the cross-sectional shape of the corrugation, m.

Equating the moment created by the force acting on the bulb fitting from the side of the side grillage at the moment of collision with the limiting moments acting at the vertices of the annular corrugation, in the absence of grooves, as in

$$P \cdot h = \sigma_T \cdot t^2 \int_0^{\pi} \sqrt{[R'(\varphi)]^2 + [R(\varphi)]^2}\, d\varphi \quad (4)$$

For a corrugation with grooves, condition (4) is transformed to

$$P \cdot h = \sigma_T \cdot (t - \Delta_i)^2 \int_0^{\pi} \sqrt{[R'(\varphi)]^2 + [R(\varphi)]^2}\, d\varphi \quad (5)$$

From this expression, we can determine the depth of the recess to determine the required compliance of the bulb

$$\Delta_i = t - \frac{h \cdot P_{0i}}{\sigma_T \cdot \int_0^{\pi} \sqrt{[R_i'(\varphi)]^2 + [R_i(\varphi)]^2}\, d\varphi} \quad (6)$$

where Δ_i is the depth of the recess of the *ith* corrugation, m;

h – corrugation height, m;

t – corrugation thickness, m;

P_{0i} – ultimate load of the ith corrugation, ensuring the required compliance of the bulb, *N*;

σ_T – yield strength of the corrugation material, Pa;

$R_i(\varphi)$ – function describing the cross-sectional shape of the ith corrugation, m.

Expression (6) was obtained within the framework of plastic limit analysis [22,23], according to which the deformation of the corrugations occurs with the formation of plastic hinges in their corners in the area where the grooves are located. The proposed design of the bulb fitting of the ship's hull (Figure 1) consists of a fairing 1, a corrugated insert 2, and brackets 3. The voids between the brackets installed on the outside are molded with elastic filler 4. In the upper and lower parts of the corrugation walls, grooves 5 of a certain depth are located [24].

In this technical solution, in the event of a ship collision, the deformation of the bulb begins with corrugations that have a minimum ultimate load that is regulated by changing the depth of the groove, thereby ensuring the required compliance of the bulb in the longitudinal direction.

In previously developed structures [20,21], the presence of an elastic filler increases the longitudinal rigidity of the bulb fitting because during its deformation during a ship collision, the outer edges of the corrugations begin to approach each other and clamp the elastic filler together, preventing it from being pushed out of the corrugation space.

This increases the force required to deform the bulb and prevents the reduction in the length of the bulb when the corrugations are deformed, which reduces the efficiency of using these structures.

This problem can be solved by installing elastic containers with a working medium in the voids between the surfaces of the corrugations and brackets instead of elastic filler [25], pressure relief devices in the walls of the corrugations, and shells on the outside (Figure 3).

The proposed design of the bulb of the ship's hull consists of a fairing 1, a corrugated insert 2, and brackets 3. In the voids between the brackets, which are installed on

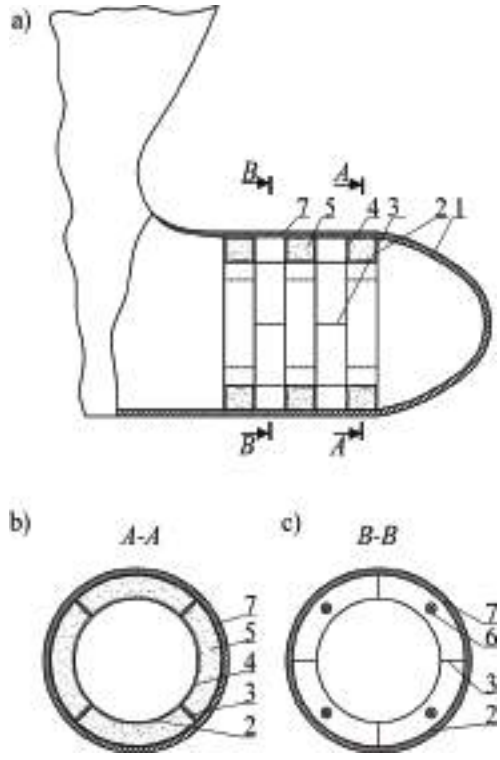

Figure 3. *Scheme of a corrugated bulb with elastic containers: a) general view; b) section A-A; c) section B-B; 1- fairing; 2- corrugated insert; 3- brackets; 4- elastic containers; 5- working medium; 6- pressure relief devices; 7- shell*

the outside, there are elastic containers 4 with a working medium 5, and in the walls of the corrugations there are pressure relief devices 6. From the outside of the bulb insert, there is a shell 7.

When ships collide, the bulb comes into contact with the underwater part of the side framing system. In the above-water part, as the bulb is deformed, the upper part of the ship's stem comes into contact. Because the compliance in the longitudinal direction of the bulb is high, when ships collide, it is deformed with the formation of plastic hinges in the corners of the corrugated insert.

This is accompanied by an increase in pressure in the elastic containers and removal of the working medium using pressure relief devices that can be either safety valves or special structural elements that collapse when the pressure in the elastic containers exceeds a certain value.

The use of pressure relief devices would enable us removal of the working medium at a speed sufficient to allow unhindered deformation of the corrugated insert. Based on this condition, the number of pressure relief devices per elastic container must be selected considering its volume. Both liquid and gas under a certain pressure can be used as the working medium.

The shell located on the outer side of the structure improves the hydrodynamic characteristics of the bulb and does not prevent its deformation in case of collision, as it can be made of elastic materials such as rubber.

To achieve the necessary bulb compliance, it can also be designed in the form of separate sections. Their diameter increases toward the stern. The sections of the bulb must be fastened together, and the circular transverse frames must be attached to the shell plate with connecting elements. Their strength is determined by the given axial load on the bulb frame (Figure 4, where 1- shell plate; 2- circular transverse frame; 3- section of the bulb; 4- connecting element; 5- elastic shell).

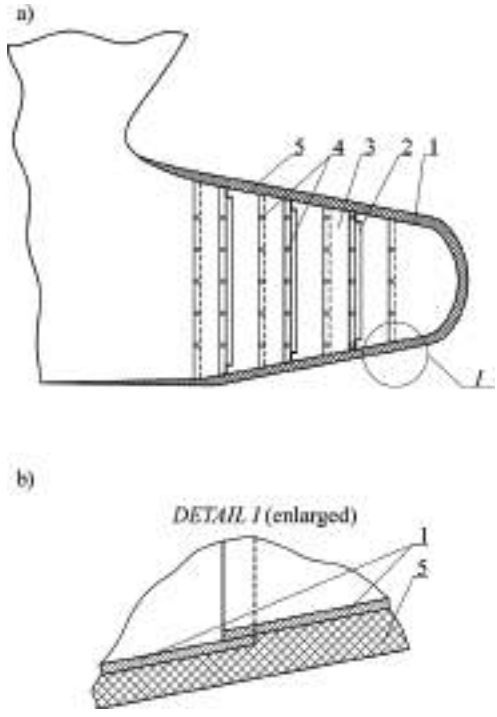

Figure 4. *Bulb with increased longitudinal compliance from individual sections: a) general view; b) detail I; 1-shell plate; 2- circular transverse frame; 3- section of the bulb; 4- connecting element; 5- elastic shell*

To ensure the required compliance, the number of connecting elements for each of the joints of the sections and the corresponding connections of the circular transverse frames should be determined using the following formula:

$$N_i = \frac{P_{0i}}{S \cdot \tau_B} \qquad (7)$$

where P_{0i} is the maximum load of the ith connection of the sections of the bulb, ensuring the required compliance of the bulb, N;

N_i– number of connecting elements in the ith connection;

S– is the area of the connecting element, m^2;

τ_B– tensile strength of the material of the connecting element for shear, Pa.

In this technical solution [26], in case of a ship collision, the deformation of the bulb is carried out due to the cutting of the connecting elements and the movement of a section of the bulb with a minimum load limit of the connection inside the adjacent section of the bulb. The appropriate compliance of the bulb in the longitudinal direction can be ensured by the proper choice of the number of connecting elements, their cross-section, and material.

It is also possible to prevent the occurrence of underwater damage in the event of a collision by disconnecting the bulb of the striking vessel immediately before the collision. To achieve this, the bulb-shaped fairing should be secured to the ship's hull with adecision number: connection using explosive bolts (Figure 5). The proposed design consists of a casing 1, reinforced with stiffening ribs 4, and contains a bulb flange 2. Using explosive bolts 6 and nuts 7, the bulb flange 2 is attached to thedecision number: vessel hull flange 3, and gasket 5 is installed to seal the connection.

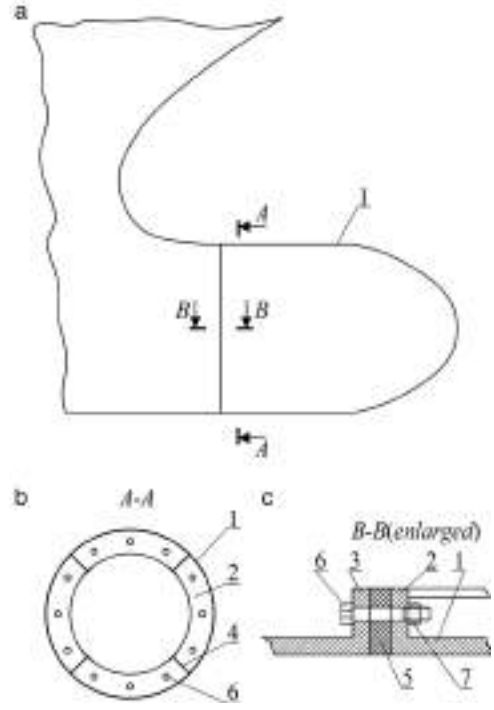

Figure 5. *Scheme of a detachable bulb: a) general view; b) section A-A; c) section B-B; 1- casing; 2- bulb flange; 3- vessel hull flange; 4- stiffening ribs; 5- gasket; 6- explosive bolts; 7- nuts*

If a danger of collision arises and it is impossible to avoid it by maneuvering, the explosive bolts connecting the

bulbdecision number: to the ship's hull are undermined, which leads to the separation of the bulb and its flooding. In this case, during a collision, the upper part of the ship's stem comes into contact with the struck ship, resulting in deformation of the hull structures above the waterline. The command to detonate explosive bolts can be given either by the person steering the vessel or by the onboard intelligent system in automatic mode [27,28].

4. Analysis of the Effectiveness of the Developed Design Solutions

To evaluate the effectiveness of the developed design solutions, numerical modeling of the deformation of the bulbs of the proposed structures was performed using the ANSYS software package. Figure 6 shows a three-dimensional model of a bulb.

Figure 6. *Three-dimensional model of a corrugated bulb with grooves*

Figure 7 shows a bulb during the deformation process and the distribution of plastic deformations under bulb loading.

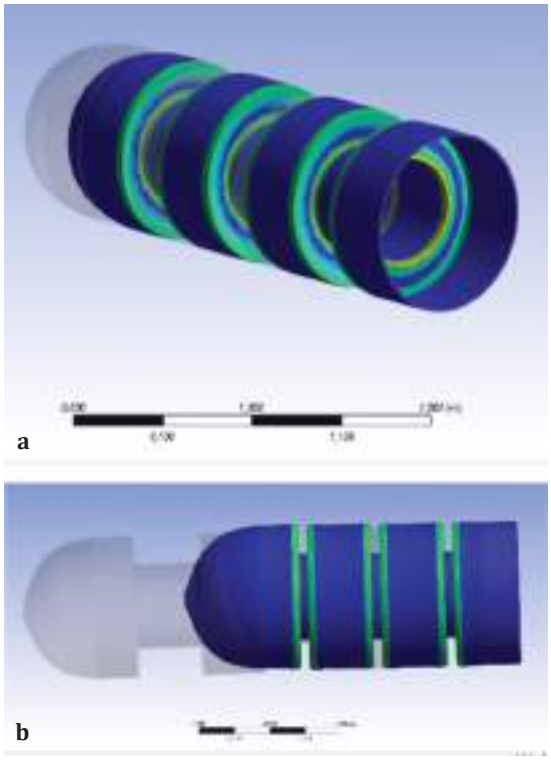

Figure 7. *Distribution of plastic deformations upon loading the bulb*

It can be seen that plastic deformations are concentrated in the area of corrugation corners, which confirms the advisability of using the plastic limit analysis when determining the load-bearing capacity of corrugated bulbs.

As the study has shown, formulas of the form (6), obtained using methods of plastic limit analysis [22,23], can be used to assess the load-bearing capacity of corrugated bulb structures of the proposed design.

To confirm the effectiveness of the proposed design solutions, a simulation of the process of interaction between the bulb structure and the side grillage of the struck vessel was performed using ANSYS LS-DYNA software. The thickness of the plating of the bulb fittings of the proposed and traditional designs was assumed to be the same and equal to 16 mm. Models of the bulb fitting and the side grillage before the start of testing are presented in Figure 8, and the results are presented in Figure 9. It can be seen that until the bulb is almost completely folded, the deformations of the side grillage of the struck vessel do not exceed 0.5 m, whereas destruction of the side floor does not occur. The highest stresses in the beam of the side floor of the struck vessel are approximately 512 MPa.

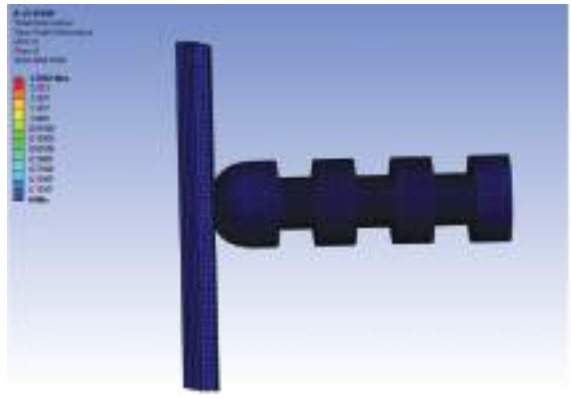

Figure 8. *Models of the side grillage and bulb of the proposed design before testing*

Figure 10 shows the results of the interaction between a traditional bulb structure and a side grillage. It can be seen that the bow bulb remains practically free of distortion, the deformation of the side grillage is 0.75 m, and the stress is 560 MPa, while a collapse of the side grillage set is observed. With further impact of the bulb fitting on the side grillage, its destruction is observed.

The nature of the interaction between a traditional bulb structure and a side grillage obtained as a result of a computational experiment is in good compliance with the data of [1,3,5,6].

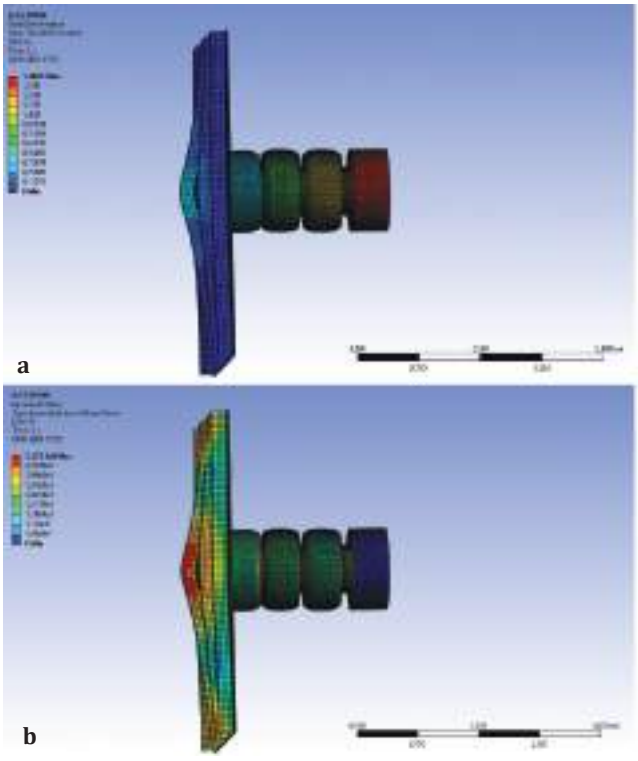

Figure 9. *Results of modeling the collision process when using the bulb of the proposed design: a) deformation; b) stress*

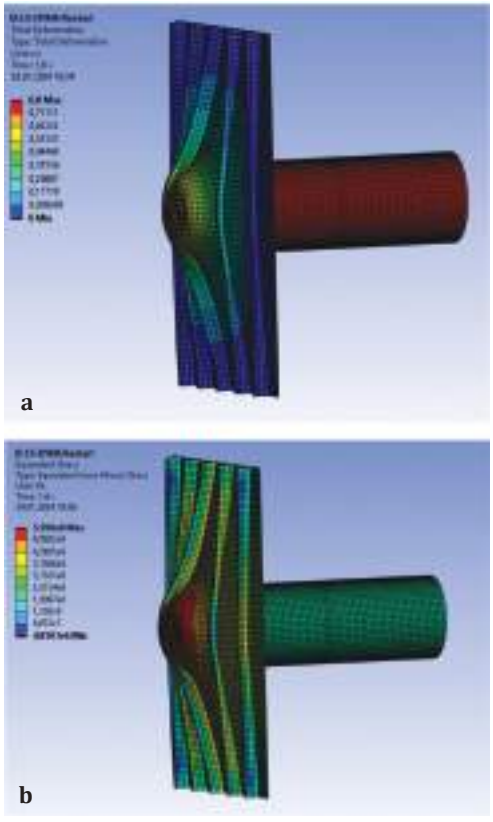

Figure 10. *Results of modeling the collision process when using a traditional bulb design: a) deformation; b) stress*

5. Discussion

As the study showed, the use of bow bulbs with increased longitudinal compliance can significantly reduce the deformation of the side grillage of a struck vessel, preventing its destruction and leakage of transported cargo, which is especially important for tankers. The obtained result complies with the results of the studies presented in [5,6,18].

The use of the design solutions proposed in this work makes it possible to implement the concept of a flexible bow extremity [14]. In this case, energy dissipation during the implementation of the proposed design must be carried out mainly because of the deformation of the hull in the above-water part. A similar approach was proposed earlier in [29], and the bulb design presented there was constructed with non-tight shells and stiffened with vertical ring frames to reduce the axial crushing rigidity to a minimal level.

Note that in the case of implementing structures [24,25], it is possible to increase the amount of energy dissipated during bulb deformation by changing the height and number of corrugations. In this case, the required compliance of the bulb will be maintained because of the appropriate choice of the thickness of the corrugations and the depth of the recesses. The design presented in [26], compared to [24,25], has a lower energy intensity, and to increase it, additional deformable elements made of material with relatively low strength characteristics can be placed in the inner part of the bulb fitting. In this case, after cutting the connecting elements, the load during bulb deformation will not increase, and the energy intensity will increase.

If the design presented in Figure 4 is implemented, energy dissipation will occur only due to the deformation of the above-water part of the hull. In this case, it is necessary to make the above-water part of the vessel with increased longitudinal compliance, as proposed in [16].

6. Conclusion

Based on the results of the research, schemes for modernizing the forward end of ship hulls by installing bulbs with increased longitudinal compliance to reduce the consequences of ship collisions were proposed, and recommendations were developed for the selection of their characteristics, which make it possible to avoid underwater holes on a struck ship. The developed technical solutions ensure that in case of collision in the underwater part of a struck vessel, the deformations of the framing systems will remain insignificant, thereby avoiding the appearance of damage below the waterline. Thus, it seems possible to avoid a ship wreck and crew losses, environmental pollution, and significantly decrease the amount of repairs

due to reduced damage to the hull in case of collision. The relevance of the proposed design solutions is proved by invention patents; their implementation into repair and ship hull modernization will significantly reduce the damage from navigation accidents. Conducting further research in this direction must include a design study of the proposed technical solutions in relation to specific ship designs for subsequent trial operations.

Funding: The author received no financial support for the research, authorship, and/or publication of this article.

References

[1] M. N. Aleksandrov, *Safety of life at sea*. Leningrad: Shipbuilding, 1983 (in Russian).

[2] D. T. Chapkis, *The loss of SS "Admiral Nakhimov"*. Rostov-on-Don: Prof-Press, 1995 (in Russian).

[3] K. Wendel, "Die Wahrscheinlichkeit des Überstehens von Verletzungen", *Schiffstechnik*, Heft 34, pp. 47-61, 1960.

[4] M. Zhang, et al. "A method for the direct assessment of ship collision damage and flooding risk in real conditions", *Ocean Engineering*, vol. 237, 109605, Oct 2021.

[5] H. Endo, and Y. Yamada, "Performance of buffer bow structure against collision-on the effect in preventing oil outflow", *Marine Technology and SNAME News*, vol. 45, pp. 54-62, Jan 2008.

[6] H. Endo, Y. Yamada, O. Kitamura, and K. Suzuki, "Model test on the collapse strength of the buffer bow structures," *Marine Structures*, vol. 15, pp. 365-381, Jul-Oct 2002.

[7] V. Gennadiev, "Lessons from Tsemes Bay: on the 20th anniversary of the loss of SS "Admiral Nakhimov", *Marine Fleet*, pp. 27-32, 2006 (in Russian).

[8] G. Woisin, "Möglichkeiten des baulichen Schutzes gegen das Austreten von für die Umwelt gefährlichen Stoffen, insbesondere Öl, bei Schiffskollisionen", *Seewirtschaft*, № 10, pp. 66-72, 1990.

[9] G. Woisin, "Schiffbauliche Forschungsarbeiten für die Sicherheit kernenergiegetriebener Handelsschiffe", in *Jahrbuch der Schiffbautechnischen Gesellschaft*, Vol. 65. Hamburg: Schiffbautechnische Gesellschaft, 1971, pp. 225-263.

[10] J. Peschmann, "*Berechnung der Enerieabsorption der Stahlstruktur von Schiffen bei Kollision und Grundberührung*", Institut für Schiffbau, Hamburg, Germany, Tech. Rep. 613, 2001.

[11] J. Amdahl, "*Energy Absorption in Ship-platform Impacts*", Department of Marine Technology, The University of Trondheim, Norway, Tech. Rep. UR-83-34, 1983.

[12] Y. Yamada, "*Bulbous buffer bows: a measure to reduce oil spill in tanker collisions*", Ph.D. dissertation, Danish University of Technology (DTU), Denmark, 2006.

[13] I. Tautz, M. Schöttelndreyer, W. Fricke, and E. Lehmann, "Experimental investigations on collision behavior of bow structures", in *Proc. of the 5th International Conference on Collision and Grounding of Ships, ICCGS 2010, Espoo, Finland, June 14-16, 2010*. Espoo: Aalto University, pp. 179-183, 2010.

[14] L. Cheung, "A soft bow for ships", *European Shipbuilding*, pp. 52-53, 1969.

[15] Y. Yamada, P. T. Pedersen, and P. F. Hansen, "The effect of buffer bow structures on probabilistic collision damages of oil tankers", in *Proc. of the 4th International Conference on Collision and Grounding of Ships, ICCGS 2007, Hamburg, Germany, September 9-12, 2007*. Hamburg: Schiffbautechnische Gesellschaft, pp. 235-242, 2007.

[16] S. R. Cho, K. W. Kang, J. H. Kim, J. S. Park, and J. W. Lee, "Optimal soft bow design of an LNG carrier", in *Proc. of the 4th International Conference on Collision and Grounding of Ships, ICCGS 2007, Hamburg, Germany, September 9-12, 2007*. Hamburg: Schiffbautechnische Gesellschaft, pp. 227-234, 2007.

[17] Y. Yamada, H. Endo, and P. T. Pedersen, "Effect of buffer bow structure in ship-ship collision," *International Journal of Offshore and Polar Engineering*, vol. 18, pp. 133-141, 2008.

[18] O. Kitamura, *Buffer Bow Design for the Improved Safety of Ships*. IMO, 2000; MEPC45/INF.5, Annex.

[19] S. Yagi, H. Kumamoto, O. Muragishi, and Y. Takaoka, "A study on collision buffer characteristic of sharp entrance angle bow structure", *Marine Structures*, vol. 22, pp. 12-23, Jan 2009.

[20] E. P. Burakovskiy, "Bulb of the ship's hull", SU1197918, 1985.

[21] E. P. Burakovskiy, and I. V. Zhukova, "Bulb of the ship's hull", RU2108940, 1998.

[22] L. M. Belenkiy, *Handbook on Plastic Analysis in Engineering*. Paramus, NJ USA: Backbone Publishing Company, 2006.

[23] S. Kaliszky, I. Sajtos, B. A. Lógó, J. M. Lógó, and Z. Szabó, "Gábor Kazinczy and His Legacy in Structural Engineering", *Periodica Polytechnica Civil Engineering*, vol. 59, pp. 3-7, 2015.

[24] P. E. Burakovskiy, and E. P. Burakovskiy, "Bulb of the ship's hull", RU2518695, 2014.

[25] P. E. Burakovskiy, "Bulb of the ship's hull", RU2527619, 2014.

[26] P. E. Burakovskiy, "Bulb of the ship's hull", RU2652502, 2018.

[27] Yu. I. Nechaev, Ed., *Artificial intelligence systems in intelligent technologies of the 21st century*. Saint Petersburg: Art-Express, 2011 (in Russian).

[28] E. P. Burakovskiy, P. E. Burakovskiy, and V. A. Dmitrovskiy, *Constructive assurance of navigation safety*. Saint Petersburg: Lan', 2020 (in Russian).

[29] O. Kitamura, T. Kuroiwa, Y. Kawamoto, and E. Kaneko, "A study on the improved tanker structure against collision and grounding damage", in *Proc. of the 7th International Symposium on Practical Design of Ships and Mobile Units*, *Hague, Netherlands, September 20-25, 1998*. Amsterdam: Elsevier, pp. 173-179, 1998.

DOI: 10.4274/jems.2024.10438

Journal of ETA Maritime Science 2024;12(2):144-155

Data-Driven Approach for Parameter Estimation and Control of an Autonomous Underwater Vehicle

Tabassum Rasul, Koena Mukherjee

National Institute of Technology Silchar, Department of Electronics and Instrumentation Engineering, Silchar, India

Abstract

This paper showcases a data-driven non-linear adaptive controller design employing an unfalsification approach to attain optimal estimates for unknown parameters in an autonomous underwater vehicle (AUV). These estimates are applied to the controller to enable precise trajectory tracking. The controller design presented is capable of adapting to parametric changes and uncertainties while fulfilling the desired performance criteria using an effective parameter update method of unfalsification. The results were validated through simulations conducted using MATLAB/SIMULINK.

Keywords: Adaptive control, Autonomous underwater vehicle, Data-driven control, Unfalsified control

1. Introduction

A complex non-linear dynamical system like autonomous underwater vehicle (AUV) undergoes changes in environmental conditions throughout its operation. In addition, the effects of added mass, which is the additional inertia encountered when a body accelerates through a fluid, must be accounted for while describing the dynamic equations. This causes uncertainty in the system parameters. As a result, modeling an AUV system accurately becomes an error-prone task. In addition, the presence of environmental disturbances like waves and ocean currents makes the process of AUV modeling even more difficult. Therefore, AUV control remains an ongoing research topic, and all the latest advancements in control methodologies are being tested on AUVs. These methodologies include robust control techniques, as seen in [1-3], adaptive control methods, as explored by [4], and optimal control, as demonstrated in [5], among others, which were applied to AUVs to obtain better performance in navigation and communication. Disturbance observer-based control methods have also been employed to address environmental disturbances, as evident in [6,7].

In the current scenario, researchers are increasingly drawn toward data-driven methods looking for alternatives to model-based techniques, as relying on model-based techniques for controlling non-linear dynamic systems like AUV systems comes with plenty of assumptions. This paper introduces a data-driven method rooted in the unfalsification theory, which was initially devised by Safonov and Tsao [8] in 1995. It is an iterative procedure that relies on the system's input and output values. Unfalsified control theory is a supervisory technique in which the system is adapted to different scenarios by switching between controllers from among a finite set of candidate controllers. Controllers that meet the specified performance criteria are integrated into the closed-loop control system, whereas those that fail are excluded.

This method differs from gain scheduling, which relies on predefined controller gains without feedback to compensate for inaccuracies in scheduling and is a model-dependent technique [9,10]. Unfalsified control, on the contrary, evaluates the candidate controller a priori using the concept of fictitious reference and past measurement data and performs the selection procedure online. At any point in time, if the present controller fails to satisfy the desired criteria, it is removed from the loop and the next best candidate is brought into the loop. This method was applied to a 2-degree-of-freedom (DOF) robotic arm

Address for Correspondence: Tabassum Rasul, National Institute of Technology Silchar, Department of Electronics and Instrumentation Engineering, Silchar, India
E-mail: tabassum_rs@ei.nits.ac.in
ORCID ID: orcid.org/0000-0002-4456-7442

Received: 19.10.2023
Last Revision Received: 09.02.2024
Accepted: 22.03.2024

To cite this article: T. Rasul, and K. Mukherjee, "Data-Driven Approach for Parameter Estimation and Control of an Autonomous Underwater Vehicle." *Journal of ETA Maritime Science*, vol. 12(2), pp. 144-155, 2024.

system for parameter estimation in [11]. The mathematical framework of this method and its several properties have been explored in [12]. The method was also tested for robustness in [13], and its stability properties were analyzed in [14]. In [15,16], the concept of unfalsification is combined with model reference adaptive control for set point tracking. It has been stated that the selection of an unfalsified controller may be performed either from a fixed set of candidates or via online optimization techniques. The online optimization technique was inspected in [17]. Furthermore, the control design was tried on a knee joint for the process of neuroprostheses in [18]. In [19], it was applied to a reactor system for temperature control. In a previous study, the application of this method to dynamic positioning in an AUV system was discussed [20]. In addition, data-driven methods have found utility in sample collection for oceanographic studies [21,22]. The design of a data-driven H_∞ loop shaping controller is detailed in [23], and more recently, its examination in non-linear time-varying plants is presented in [24-26].

1.1. Symbols and Abbreviations

$[\ ]^T$ denotes the transpose of a matrix, $\|\|$ represents the Euclidean norm of the signal, and $\int$ indicates the integration of a function. J is a rotation matrix determined by a choice of Euler angles, and $\mathfrak{J}$ is the cost function, which depends on the system output, control input, and a fictitious reference. L_{2e} represents the extended Euclidean norm space and $\|\ \|_\tau$ denotes the truncated norm. Further details on these concepts are explored in the forthcoming sections.

The SNAME notation, as presented in [27], is adopted for describing the motion of AUVs in six DOF. Specifically, as illustrated in Figure 1, linear motion along the X-axis is denoted by x, while rotational motion along the X-axis is denoted by φ. Along the Y-axis, linear motion is denoted by y and rotational motion is denoted by θ. Along the Z-axis, linear motion is denoted by z, and rotational motion is denoted by ψ.

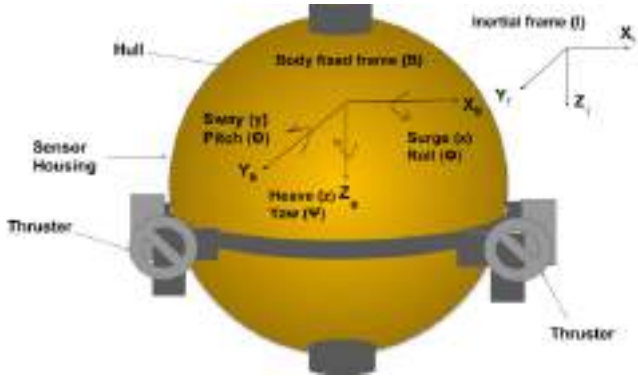

Figure 1. *Position and angle representation in the reference frames*

1.2. Structuring the Paper

The paper is structured as follows: Section 2 provides a summary of the AUV system and its mathematical model. Section 3 outlines the problem statement, and the adaptive unfalsified controller design is expounded in section 4. The stability analysis of the controller design is shown in Section 5. Section 6 discusses the simulation results, and the conclusion is presented in Section 7.

2. System Description and Model of the AUV

2.1. Construction of an AUV

An AUV is a propeller-driven platform commonly powered by lithium-ion batteries for propulsion. The key elements in the structure of an AUV encompass a hull, a propulsion system, a submersion mechanism, an electric power supply, navigation sensors, and a communication system. The AUV incorporates navigation sensors such as the inertial measurement unit (IMU) and sonar. In addition, it is equipped with pressure sensors, temperature sensors, battery monitoring sensors, leakage sensors, etc.

For AUVs, a pressure hull is essential to house its components in a dry, watertight environment. This hull accommodates electronic components and facilitates access for maintenance or modifications.

The volume of the AUV remains constant underwater, necessitating an increase in the downward force to dive deeper and counteract buoyancy. This can be achieved by adding mass through ballast tanks or external thrusters. Ballasting, which involves pumps and compressed air, is a common method, whereas thrusters pointing downwards offer a simpler but less power-efficient alternative.

All AUVs require propulsion, with motors being the prevalent choice due to their availability and cost-effectiveness. The placement of the motors affects the controllability across various DOF. Power consumption increases significantly with vehicle speed, posing an optimization challenge for achieving an ideal speed within the limited energy supply. Sealed batteries are used to supply electric power in AUVs.

Common methods for AUV navigation include dead reckoning, inertial navigation using IMUs, and acoustic navigation. However, to enhance the accuracy of inertial navigation sensors like IMU, additional aids such as differential global positioning systems for position estimation, Doppler velocity logs for velocity estimation, and pressure sensors for depth estimation are necessary. Acoustic navigation relies on the acoustic signals from the AUV transponder to determine its position. The primary methods used are long baseline and ultra-short baseline.

Underwater wireless communication in AUVs is usually achieved using acoustic communication. Acoustic modems are used for transmitting and receiving signals underwater.

AUVs are developed in different shapes and sizes, each equipped with a different number of thrusters. The most common configurations include cylindrical or torpedo-shaped models, such as the REMUS and HUGIN, and spherical-shaped models like the ODIN.

The AUV under consideration in this study has a spherical model configuration, as shown in Figure 1. It comprises a closed spherical body featuring eight thruster assemblies to propel the vehicle and provide six DOF motion capabilities. In the autonomous mode, the vehicle is controlled by an on-board computer, whereas in the manual mode, control can be achieved by connecting to a ground station computer via TCP/IP through a tether. The tether, in autonomous mode, serves for monitoring and safety purposes. The sensor housing encloses the usual sensors for navigation and position estimation. In addition, other sensors such as oxygen or pH sensors are included based on the application of the designed AUV.

2.2. Mathematical Model and its Properties

Analyzing an AUV requires consideration of two reference frames, the body-fixed frame {B} and the inertial frame {I}, as illustrated in Figure 1. The mathematical model of the AUV characterizes its motion along various axes in 6 DOF through Euler angles.

The vehicular velocities with respect to the inertial frame (η) are described in relation to the velocities relative to the body-fixed reference frame (ν) by [27]

$$\dot{\eta} = J(\eta)\nu \tag{1}$$

Here $\eta = \left[\eta_1^T, \eta_2^T\right]^T = \left[x, y, z, \varphi, \theta, \psi\right]^T$

and $\nu = \left[\nu_1^T, \nu_2^T\right]^T = \left[u, v, w, p, q, r\right]^T$

x, y, z represent linear displacements and φ, θ, ψ represent angular displacements in the inertial frame. Similarly u, v, w represent linear velocities and p, q, r represent angular velocities in the body fixed frame. $J(\eta)$ is the transformation matrix.

The dynamic model of an AUV considers hydrostatics, hydrodynamic forces, viscous damping, and propulsion forces and torques that act on the vehicle's body. The additional force due to the added mass is also accounted for. These components are encompassed in the non-linear hydrodynamic equation of motion of the AUV and are represented as;

$$M(\eta)\ddot{\eta} + C(\eta, \dot{\eta})\dot{\eta} + D(\eta, \dot{\eta})\dot{\eta} + g(\eta) = T + T_E \tag{2}$$

In the above equation, $M(\eta)$ represents the matrix containing mass and inertia coefficients, $M \in R^{6\times6}$, $C(\eta, \dot{\eta}) \in R^{6\times6}$, $D(\eta, \dot{\eta}) \in R^{6\times6}$ denotes the damping matrix, $g(\eta) \in R^6$ represents the gravitational matrix, T_E accounts for disturbances induced by environmental factors and $T \in R^6$ is the control input in the inertial reference frame encompassing both propulsion forces and torques. When the vehicle is fully actuated, the control input vector T can be expressed as

$$T = [T_x, T_y, T_z, T_\varphi, T_\theta, T_\psi]^T \tag{3}$$

The work presented in this paper focuses on an AUV with 4 DOF motion. The dynamic equation is given by

$$M\ddot{\eta} + D(\eta, \dot{\eta})\dot{\eta} = T + T_E \tag{4}$$

Here $\eta = [x, y, z, \psi]^T$ and $\eta, \dot{\eta}, \ddot{\eta} \in R^4$, $M \in R^{4\times4}$, $D(\eta, \dot{\eta}) \in R^{4\times4}$, T and $T_E \in R^4$.

Note:

N1. Here, the gravitational term is presumed to be zero given the constant desired motion along the Z-axis. The Coriolis and centripetal force terms are considered negligible due to the low speed of the vehicle and hence are omitted from the equation.

N2. The reference trajectory is expressed in the inertial frame; therefore, for mathematical gravity, the dynamical equation of the AUV is expressed in the same frame.

2.2.1. Properties

P1. The mass and inertia matrix is a positive definite symmetric matrix.

$$\delta_m I_n \le M(\eta) \le \delta_M I_n, \quad n = 1, 2, \ldots, 6 \tag{5}$$

δ_m, δ_M are positive constants and I_n is the identity matrix of the nth order.

P2. The Damping matrix is non-symmetric and strictly positive definite.

$$D(\eta, \dot{\eta}) > 0 \tag{6}$$

The AUV model in Equation (4) is assumed to have unknown parameters; therefore, the mass and damping matrices are expressed in regressor form as;

$$Y(\eta, \dot{\eta}, \ddot{\eta})\Phi = T + T_E \tag{7}$$

where $Y(\eta, \dot{\eta}, \ddot{\eta}) \in R^{4\times p}$ is a known regressor matrix and $\Phi = \left[\phi_1, \ldots, \phi_p\right]^T$ is the unknown parameter vector.

3. Problem Description

3.1. Problem Statement

Given an input-output set $D_\tau = \{T_\tau, \Upsilon_\tau\}$ such that $D_\tau \in \mathfrak{L}_{2e}$ of the AUV system in (7) has uncertain parameters, the proposed adaptive unfalsified controller drives the AUV to follow a desired trajectory.

To realize this problem statement, the following assumption is required.

Assumption: The input-output data of the system, T and $\Upsilon = [\eta, \dot{\eta}, \ddot{\eta}]$ are measurable and available.

With the above assumption, the input-output data of the system are used to design the controller according to the proposed design. Because an infinite signal cannot be measured in real time, the input-output data of the system is truncated over a finite time.

Lemma 1: A truncated signal x_τ is defined as the signal $x(t)$ for a time period $\tau \in R$, if

$$x_\tau = \begin{cases} x(t), & t \in [0, \tau] \\ 0, & otherwise \end{cases}$$

A truncated L_2 norm of a truncated signal x_τ is given as

$$\| x \|_\tau = \int_0^\tau |x(t)|^2 \, dt$$

Here $\| x \|$ stands for the Euclidean norm of $x(t)$ for time τ. Also $x \in L_{2e}$, if $\| x \|_\tau$ exists $\forall \tau < \infty$ where L_{2e} is the extended L_2 norm space.

The AUV system (4) is simulated and run such that the input $T_T = T(t)_{t=0}^{\infty}$ when fed to the system generates the corresponding output $\Upsilon_T = \Upsilon(t)_{t=0}^{\infty}$ which is measured. This dataset $D_T = \{T_T, \Upsilon_T\}$ is truncated up to a period $t \in [0, \tau]$ to obtain the resultant set $D_\tau = \{T_\tau, \Upsilon_\tau\}$ and $D_\tau \in L_{2e}$. For mathematical simplicity the subscript τ is removed from the resultant data set $D_\tau = \{T_\tau, \Upsilon_\tau\}$, which is referred to as $\{T, \Upsilon\}$ from here on in the paper.

4. Controller Design

Unfalsified control is a data-based supervisory control technique that offers the advantages of both a robust and an adaptive control method. Non-linear systems like AUVs are affected mainly by parametric uncertainties and environmental disturbances. Thus, it is favorable to resort to a model-independent control method that is adaptive and can also tackle disturbances and non-linearities. Figure 2 illustrates the block diagram of the controller design.

4.1. Unfalsified Control Design

The closed loop structure in Figure 2 consists of the AUV system, whose parameters are not certain, a controller bank $C_B = [C_1, C_2, ..., C_n]$ of n non-linear controllers designed using randomly chosen parameter values from a finite set within a given bound. The input from the controller and the output from the system are available for measurement. The unfalsified control method uses the measured data in iterations to find the most suitable controller from the aforementioned controller bank. To achieve this, a switching algorithm is devised. Controllers meeting the specified performance criteria are incorporated into the closed-loop system, whereas those falling short of the criteria are excluded. This is achieved by generating a fictitious

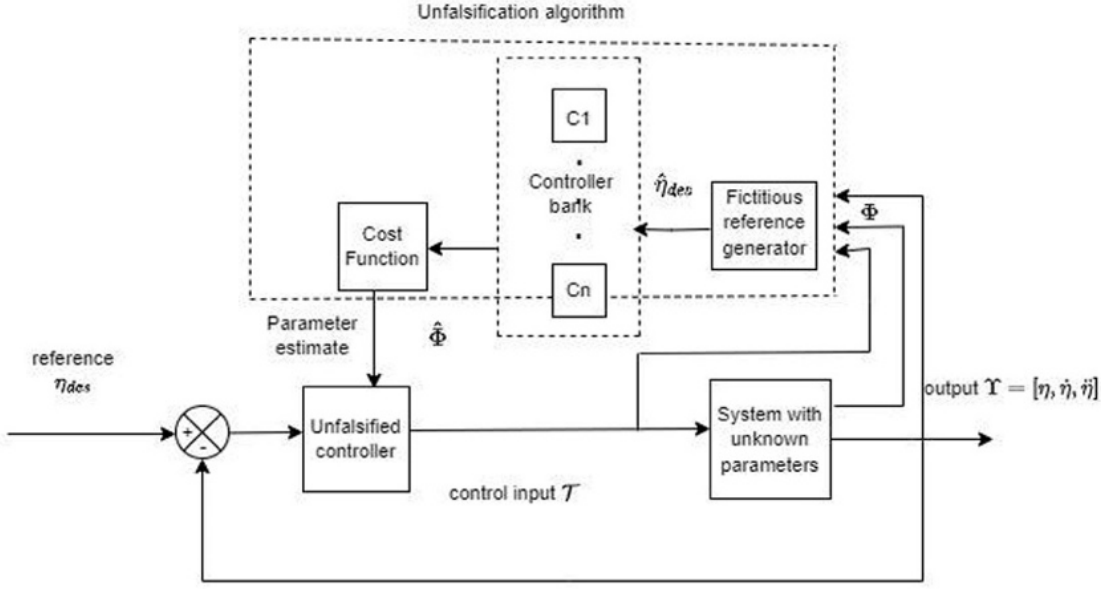

Figure 2. *Adaptive unfalsified control system design*

reference signal by which the controllers are evaluated by mathematical computation and are not required to be placed in the closed loop. Only the selected controller is placed in the closed-loop system.

The following terms are defined for comprehension.

D1: Fictitious Reference: A virtual signal that, if it were part of the closed loop system, would have generated the given set of input-output values for a specific controller is called the fictitious reference signal. For input T and output Y the fictitious reference can be computed as [28].

$$\dot{\eta}_{des} = C^{-1}T + Y \tag{8}$$

D2: Cost Function: To govern the system's performance and stability criteria, a function incorporating the system's input, output, and fictitious reference is defined as the cost function. All candidate controllers aim to minimize this cost function. The cost detectability property (Lemma 4 in section 4.4 of the paper) associated with the cost function ensures the closed-loop stability of the unfalsified controller [28].

4.2. Adaptive Unfalsified Control Design

The control problem is to design an adaptive unfalsified controller that allows the AUV to track a desired trajectory in the presence of parameter uncertainties and external disturbances without using explicit model information. The controller design is segmented into three stages.

Stage 1: A non-linear controller like a computed torque controller (CTC) is constructed, assuming all the parameters of the AUV system are known. Consider the difference between the desired and actual positions as the error given by

$$e_\eta = \eta_{des} - \eta \tag{9}$$

The control input obtained from the CTC is given by

$$T = M[\ddot{e}_\eta + \Lambda_1\dot{e}_\eta + \Lambda_2 e_\eta] + M\ddot{\eta} + D(\eta,\dot{\eta})\dot{\eta} \tag{10}$$

Λ_1 and Λ_2 are positive gains that determine the speed of convergence of the tracking error to zero. Putting the value of T in equation (4), we obtain,

$$M\ddot{\eta} + D(\eta,\dot{\eta})\dot{\eta} = M[\ddot{e}_\eta + \Lambda_1\dot{e}_\eta + \Lambda_2 e_\eta] + M\ddot{\eta} + D(\eta,\dot{\eta})\dot{\eta} + T_E \tag{11}$$

Stage 2: A set of n random values for unknown parameters forms the candidate set of controllers.

$$\begin{aligned} Y(\eta,\dot{\eta},\ddot{\eta})\Phi &= M[\ddot{e}_\eta + \Lambda_1\dot{e}_\eta + \Lambda_2 e_\eta] + M\ddot{\eta} + D(\eta,\dot{\eta})\dot{\eta} + T_E \\ &= M[\ddot{e}_\eta + \Lambda_1\dot{e}_\eta + \Lambda_2 e_\eta] + Y(\eta,\dot{\eta},\ddot{\eta})\Phi_i + T_E, \quad i = 1,2,\ldots,n \end{aligned}$$

Stage 3: Using the method of unfalsification, near-optimal values are estimated for the unknown parameters, and the CTC with the estimated parameters is inserted into the feedback loop. The CTC takes care of the trajectory tracking by the AUV.

Let the unknown mass matrix M be approximated as $\hat{M}$, an assumption for the bound of $\hat{M}^{-1}$ is made. By property P1, M is positive definite and symmetric. Therefore, $\hat{M}^{-1}$ exists and

$$0 < \hat{M}^{-1} \le \Delta_{im} \tag{12}$$

where Δ_{im} is a positive. Hence, using the method of unfalsification, the unknown parameter Φ is estimated as $\hat{\Phi}$. The control law is modified to

$$T = \hat{M}[\ddot{e}_\eta + \Lambda_1\dot{e}_\eta + \Lambda_2 e_\eta] + Y(\eta,\dot{\eta},\ddot{\eta})\hat{\Phi} + T_E \tag{13}$$

Using Equations (7) and (13) the system dynamics thus becomes

$$Y(\eta,\dot{\eta},\ddot{\eta})\Phi = \hat{M}[\ddot{e}_\eta + \Lambda_1\dot{e}_\eta + \Lambda_2 e_\eta] + Y(\eta,\dot{\eta},\ddot{\eta})\hat{\Phi} + T_E \tag{14}$$

which implies

$$\hat{M}[\ddot{e}_\eta + \Lambda_1\dot{e}_\eta + \Lambda_2 e_\eta] + Y(\eta,\dot{\eta},\ddot{\eta})\hat{\Phi} - Y(\eta,\dot{\eta},\ddot{\eta})\Phi + T_E = 0 \tag{15}$$

$$\hat{M}[\ddot{e}_\eta + \Lambda_1\dot{e}_\eta + \Lambda_2 e_\eta] + Y(\eta,\dot{\eta},\ddot{\eta})e_\Phi + T_E = 0 \tag{16}$$

where $e_\Phi = \hat{\Phi} - \Phi$ is the estimation error.

$$\ddot{e}_\eta + \Lambda_1\dot{e}_\eta + \Lambda_2 e_\eta + \hat{M}^{-1}Y(\eta,\dot{\eta},\ddot{\eta})e_\Phi + \hat{M}^{-1}T_E = 0 \tag{17}$$

$$\ddot{e}_\eta = -\Lambda_1\dot{e}_\eta - \Lambda_2 e_\eta - \hat{M}^{-1}Y(\eta,\dot{\eta},\ddot{\eta})e_\Phi - \hat{M}^{-1}T_E \tag{18}$$

In matrix form

$$\begin{bmatrix}\dot{e}_\eta \\ \ddot{e}_\eta\end{bmatrix} = \begin{bmatrix}0 & 1 \\ -\Lambda_2 & -\Lambda_1\end{bmatrix}\begin{bmatrix}e_\eta \\ \dot{e}_\eta\end{bmatrix} + \begin{bmatrix}0 \\ -\hat{M}^{-1}Y(\eta,\dot{\eta},\ddot{\eta})e_\Phi - \hat{M}^{-1}T_E\end{bmatrix} \tag{19}$$

Equation (19) constitutes the error dynamics of the system. The closed-loop stability analysis is discussed in the next section. Once the control law is designed according to Equation (13), a fictitious reference (8) is computed for each controller of the bank as

$$\dot{\eta}_{des} + \Lambda_1\dot{\eta}_{des} + \Lambda_2\eta_{des} = \hat{M}^{-1}[T + T_E + \hat{M}(\Lambda_1\eta + \Lambda_2\eta) - \hat{D}(\Phi,\eta,\dot{\eta})\dot{\eta}] \tag{20}$$

$\hat{M}, \hat{D}$ represents mass matrix and damping matrix estimates. This fictitious reference is used to evaluate the cost function that determines the selection of controllers.

Note: N3. The controller inverse, in this case, requires the inverse of the mass matrix, which is invertible and bounded as given in Equation (12).

4.3. Algorithm of Unfalsification

The hysteresis algorithm applied for the falsification procedure involves the following steps:

1. Given input and output data $D_\tau = \{T, Y\}$ of the system with initial states.

2. *for* $i = 1,2,...,n$, Formulate control law using (13) to constitute the candidates of the controller bank $C_B = [C_1, C_2, ..., C_n]$.

3. Compute the fictitious reference $\hat{\eta}_{des_i}$ (20) for C_i.

4. Calculate the fictitious error $\hat{e}_{\eta i} = \hat{\eta}_{des_i} - \eta$ for C_i.

5. Evaluate the performance of C_i by minimizing the cost function $\mathfrak{J}$ given in Equation (30). Let at $\tau = 0, C = C_{initial}$ and $\mathfrak{J} = \mathfrak{J}_{initial}$

6. *if* for i^{th} iteration $\mathfrak{J}_i < \mathfrak{J}_{initial}$, then $\mathfrak{J} = \mathfrak{J}_i$ and $C = C_i$
else $C = C_{initial}$

End if

7. Increment *i*.

8. End for

9. Repeat steps 4 to 6 to find the arg min $\mathfrak{J}$.

10. Terminate when the minimum J is achieved.

C is the controller that remains unfalsified and runs in the closed loop system.

4.4. Stability Analysis and Proof

To establish the stability of an adaptive unfalsified controller, knowledge of a few relevant terms is required. These are defined as follows:

Lemma 2: The control problem is deemed feasible for a system S_ζ if there exists at least one stabilizing controller in the bank of candidate controllers C_B at any point in time [29].

Lemma 3: Unfalsified Stability: The stability of the system S_ζ is considered falsified by the data (T, Y) if

$$sup_{T\in L_{2e}\|T\|\neq 0}\frac{\|Y\|_\tau}{\|T\|_\tau} < \infty \tag{22}$$

Otherwise, the stability of the system S_ζ is asserted to be falsified by the input-output pair (T, Y) [29].

T1: Stability Theorem: Given a plant in (7) and a bank of controllers $C_B = [C_1, C_2, ..., C_n]$ with at least one stabilizing controller as in (13), the closed loop system is said to be stable if the unfalsified controller minimizes the cost function $\mathfrak{J}(t)$ which satisfies the cost detectability property.

Proof: To prove closed-loop stability in an unfalsified control approach, we must meet the following three conditions. First, there must be at least one stabilizing controller in the controller bank. Second, an iterative algorithm leading to a finite number of switches is necessary. Finally, the cost function considered must satisfy the cost detectability property. According to the stability theorem stated above, it is imperative to demonstrate the stability of at least one candidate controller to fulfill the feasibility (Lemma 2) of the control problem.

Let system (7) lies in the space

$S_\zeta = \left\{\zeta \in R: \| \zeta \| \leq \frac{2\Gamma \| P \|}{\kappa_{min}(Q)}\right\}$ where $\zeta = \begin{bmatrix} e_\eta \\ \dot{e}_\eta \end{bmatrix}$ represents the error matrix. Error dynamics (19) can be written as

$$\dot{\zeta} = A_C\zeta + \chi \tag{23}$$

where $\zeta = \begin{bmatrix} e_\eta \\ \dot{e}_\eta \end{bmatrix}$, $\dot{\zeta} = \begin{bmatrix} \dot{e}_\eta \\ \ddot{e}_\eta \end{bmatrix}$, $A_C = \begin{bmatrix} 0 & 1 \\ -\Lambda_2 & -\Lambda_1 \end{bmatrix}\zeta$,

$$\chi = \begin{bmatrix} 0 \\ -\bar{M}^{-1}Ye_\Phi - \bar{M}^{-1}d \end{bmatrix}.$$

A Lyapunov function candidate is considered as follows:

$$V(\zeta) = \frac{1}{2}\zeta^T P\zeta \tag{24}$$

where P is symmetric and positive definite. From Equation (24)

$$\kappa_{min}(P) \| \zeta \|^2 \leq V(\zeta) \leq \kappa_{max}(P) \| \zeta \|^2 \tag{25}$$

The time derivative of the Lyapunov function is obtained as

$$\begin{aligned} \dot{V}(\zeta) &= \zeta^T P\dot{\zeta} + \dot{\zeta}^T P\zeta \\ &= \zeta^T P(A_C\zeta + \chi) + (A_C\zeta + \chi)^T P\zeta \\ &= \zeta^T PA_C\zeta + \zeta^T P\chi + \zeta^T A_C^T P\zeta + \chi^T P\zeta \\ &= \zeta^T(PA_C + A_C^T P)\zeta + 2\chi P\zeta \end{aligned} \tag{26}$$

By design, we can ensure that

$$PA_C + A_C^T P = -Q \tag{27}$$

Then, Equation (25) becomes

$$\dot{V} = -\zeta^T Q\zeta + 2\chi P\zeta \leq -\kappa_{min}(Q) + 2 \| \chi \| \| P \| \| \zeta \| \tag{28}$$

Now,

$$\begin{aligned} \| \chi \| &= \left\| \begin{bmatrix} 0 \\ -\bar{M}^{-1}Ye_\Phi - \bar{M}^{-1}T_E \end{bmatrix} \right\| \\ &\leq \| \bar{M}^{-1} \| \left(\| Ye_\Phi \| + T_{E_{max}} \right) \\ &\leq \Gamma\left(\| Ye_\Phi \| + T_{E_{max}} \right) \\ &\leq -\kappa_{min}(Q) \| \zeta \|^2 + 2\Gamma \| P \| \| \zeta \| \\ &\leq -\kappa_{min}(Q) \| \zeta \| \left(\| \zeta \| - \frac{2\Gamma\|P\|}{\kappa_{min}(Q)} \right) \end{aligned} \tag{29}$$

Hence

$$\| \zeta \| \leq \frac{2\Gamma\|P\|}{\kappa_{min}(Q)} \tag{30}$$

In Equation (30), $\frac{2\Gamma}{\kappa_{min}(Q)}$ is a positive constant, and $\| P \|$ is positively bounded. Thus, it can be concluded that the system is ultimately bounded by the Lyapunov stability theory within the range given by Equation (30). This confirms the feasibility condition (Lemma 2) of theorem (T1).

Next, as stated in the stability theorem (T1), the proof of stability requires knowledge of cost detectability, defined as follows:

Lemma 4: Cost Detectability: A cost function $\mathfrak{J}(t)$ is considered cost detectable if it fulfills the conditions given as follows [29]:

1. The function $\mathfrak{J}_i(t)$ monotonically increases in time t for all $\left(C_i, T, Y, \hat{\eta}_{des_i}\right), i = 1,2,3\ldots$
2. $lim_{t\to\infty}\mathfrak{J}_i(t)$ remains uniformly bounded for all $\left(C_i, T, Y, \hat{\eta}_{des}\right), i = 1,2,3\ldots$ when C_i is stabilizing.

The cost function considered is

$$\mathfrak{J}(t) = \frac{\|\hat{e}_\eta\|^2 + \alpha\|T\|^2}{\|\hat{\eta}_{des}\|^2 + \rho} \tag{31}$$

$\alpha, \rho > 0$ are positive constants. $\hat{\eta}_{des}$ represents the fictitious reference and the fictitious error $\hat{e}_\eta = \hat{\eta}_{des} - \eta$ is the deviation of output from the fictitious reference.

To prove that $\mathfrak{J}(t)$ is monotonically increasing in time, equation (31) is differentiated w.r.t time t as follows:

$$\begin{aligned}
\dot{\mathfrak{J}}(t) &= \frac{d}{dt}\left\{\frac{\|\hat{e}_\eta\|^2 + \alpha\|T\|^2}{\|\hat{\eta}_{des}\|^2 + \rho}\right\} \\
&= \frac{d}{dt}\left\{\frac{\left((\int_0^\infty |\hat{e}_\eta|^2\,dt)^{\frac{1}{2}}\right)^2 + \alpha\left((\int_0^\infty |T|^2\,dt)^{\frac{1}{2}}\right)^2}{\left((\int_0^\infty |\hat{\eta}_{des}|^2\,dt)^{\frac{1}{2}}\right)^2 + \rho}\right\} \\
&= \frac{d}{dt}\left\{\frac{\int_0^\infty |\hat{e}_\eta|^2\,dt + \alpha(\int_0^\infty |T|^2\,dt)}{\int_0^\infty |\hat{\eta}_{des}|^2\,dt + \rho}\right\} \\
&= \frac{(\int_0^\infty |\hat{\eta}_{des}|^2\,dt + \rho)\frac{d}{dt}\left[(\int_0^\infty |\hat{e}_\eta|^2\,dt) + \alpha(\int_0^\infty |T|^2\,dt)\right]}{-\left[(\int_0^\infty |\hat{e}_\eta|^2\,dt) + \alpha(\int_0^\infty |T|^2\,dt)\right]\frac{d}{dt}(\int_0^\infty |\hat{\eta}_{des}|^2 + \rho)} \\
&= \frac{(\int_0^\infty |\hat{\eta}_{des}|^2\,dt + \rho)(|\hat{e}_\eta|^2 + \alpha|T|^2) - (\int_0^\infty |\hat{e}_\eta|^2\,dt + \alpha\int_0^\infty |T|^2\,dt)|\hat{\eta}_{des}|^2}{(\int_0^\infty |\hat{\eta}_{des}|^2\,dt + \rho)^2} \\
&= \frac{(\|\hat{\eta}_{des}\|^2 + \rho)(|\hat{e}_\eta|^2 + \alpha|T|^2) - (\|\hat{e}_\eta\|^2 + \alpha\|T\|^2)|\hat{\eta}_{des}|^2}{(\|\hat{\eta}_{des}\|^2 + \rho)^2} \\
&= \frac{(\|\hat{\eta}_{des}\|^2 + \rho)(|\hat{e}_\eta|^2 + \alpha|T|^2)}{(\|\hat{\eta}_{des}\|^2 + \rho)^2} - \frac{\|\hat{e}_\eta\|^2|\hat{\eta}_{des}|^2}{(\|\hat{\eta}_{des}\|^2 + \rho)^2} - \frac{\alpha\|T\|^2|\hat{\eta}_{des}|^2}{(\|\hat{\eta}_{des}\|^2 + \rho)^2} \\
&= \frac{|\hat{e}_\eta|^2 + \alpha|T|^2}{\|\hat{\eta}_{des}\|^2 + \rho} - \frac{\|\hat{e}_\eta\|^2|\hat{\eta}_{des}|^2}{(\|\hat{\eta}_{des}\|^2 + \rho)^2} - \frac{\alpha\|T\|^2|\hat{\eta}_{des}|^2}{(\|\hat{\eta}_{des}\|^2 + \rho)^2}
\end{aligned} \tag{32}$$

Since, $\frac{\|\hat{e}_\eta\|^2|\hat{\eta}_{des}|^2}{(\|\hat{\eta}_{des}\|^2 + \rho)^2} \geq 0$ and $\frac{\alpha\|T\|^2|\hat{\eta}_{des}|^2}{(\|\hat{\eta}_{des}\|^2 + \rho)^2} \geq 0$

Therefore,

$$\dot{\mathfrak{J}}(t) \leq \frac{|\hat{e}_\eta|^2 + \alpha|T|^2}{\|\hat{\eta}_{des}\|^2 + \rho} \tag{33}$$

Hence, $0 \leq \dot{\mathfrak{J}}\left(t\right) \leq \frac{|e_\eta|^2 + \alpha|T|^2}{\|\hat{\eta}_{des}\|^2 + \rho}$ for all $\left(C_i, T, Y, \hat{\eta}_{des}\right)$, $i = 1,2,3\ldots$

This confirms the cost detectability of $\mathfrak{J}(t)$ which by theorem (T1) fulfills a condition of stability. As the selection of the unfalsified controller depends on minimizing the cost function that depends on the actual and fictitious errors, the convergence of the errors can be assured. Moreover, the candidate set of controllers is generated using the lower and upper bounds of the unknown parameters, which in any case confirms the boundedness of the estimates. The controller $C = C_f$ satisfies $\mathfrak{J}(t)$ and remains unfalsified at $t = \tau_f$ thus results in

$$\lim_{t\to\tau_f} \|\hat{\eta}_{des_f} - \eta_{des}\| = 0 \tag{34}$$

where $\hat{\eta}_{des_f}$ is the fictitious reference for controller $C = C_f$.

Hence, by Equation (34), and by the arguments stated above, it is concluded that the control system is stable.

4.5. Finiteness of Parameter Switching

Switching of controllers depending on the attainment of the minimum cost function is performed by the following algorithm:

Hysteresis Switching Algorithm-$\Gamma_k \in R$ is a continuous logic input signal and δ is the output switching signal. δ and k belong to the normed vector space K. If at $t = t_0$, $\delta(0) = \arg\min_{k\in K}\left\{\Gamma_k(0)\right\}$ and at some subsequent time $t = t_m$, δ is switched to $l \in K$. In this scenario case δ remains constant for time $t_{m+1} > t_m$ such that $(1+n)\min\left\{\Gamma_k(t_{m+1})\right\} \leq \Gamma_l(t_m)$, n being the hysteresis constant. This generates a piecewise constant signal δ [30]. If Γ_k is uniformly bounded and $\Gamma_k \geq \omega$, such that $\omega > 0, \forall k \in K$ and all $t \geq 0$, the switching remains finite.

The monotonically decreasing set of unfalsified controllers bounded below by an empty set ensures a finite amount of switching among controllers. If there are n number of candidate controllers and at the minimum one stable controller satisfies the specified performance criteria, then by the algorithm stated above, after a maximum of n-1 switches the convergence of the switching of unfalsified controllers can be assured.

5. Results

The proposed controller design is applied to the system in Equation (7), and its performance is assessed via simulation in MATLAB/SIMULINK. The system parameters are described as follows:

$$M = \begin{bmatrix} m_{11} & 0 & 0 & 0 \\ 0 & m_{22} & 0 & 0 \\ 0 & 0 & m_{33} & 0 \\ 0 & 0 & 0 & m_{44} \end{bmatrix}, D = \begin{bmatrix} d_{11} & 0 & 0 & 0 \\ 0 & d_{22} & 0 & 0 \\ 0 & 0 & d_{33} & 0 \\ 0 & 0 & 0 & d_{44} \end{bmatrix}, \eta = \begin{bmatrix} x \\ y \\ z \\ \psi \end{bmatrix}, \text{and } T = \begin{bmatrix} T_x \\ T_y \\ T_z \\ T_\psi \end{bmatrix} \tag{35}$$

The regressor matrix is defined as

$$Y(\eta, \dot{\eta}, \ddot{\eta})\Phi^T = \begin{bmatrix} \ddot{x} & |\dot{x}|\dot{x} & 0 & 0 & 0 & 0 & 0 & 0 \\ 0 & 0 & \ddot{y} & |\dot{y}|\dot{y} & 0 & 0 & 0 & 0 \\ 0 & 0 & 0 & 0 & \ddot{z} & |\dot{z}|\dot{z} & 0 & 0 \\ 0 & 0 & 0 & 0 & 0 & 0 & \ddot{\psi} & |\dot{\psi}|\dot{\psi} \end{bmatrix} \begin{bmatrix} m_{11} \\ d_{11} \\ m_{22} \\ d_{22} \\ m_{33} \\ d_{33} \\ m_{44} \\ d_{44} \end{bmatrix} \tag{36}$$

Let the desired trajectory be

$$\eta_{des} = \begin{bmatrix} x_{des} \\ y_{des} \\ z_{des} \\ \psi_{des} \end{bmatrix} = \begin{bmatrix} 10\sin(t) \\ 10\cos(t) \\ 10 \\ \frac{\pi}{3} \end{bmatrix} \quad (37)$$

The initial values of the states of the AUV are taken as $\eta(0) = [1,1,0.5,0.1]^T$ and $\eta(0) = [0,0,0,0]^T$. For the CTC, the control gain values are $\Lambda_1 = 25$ and $\Lambda_2 = 625$. The nominal values of these parameters are taken from [31], and a minimum and maximum bound on the variation of these parameter values is considered based on the nominal values. The nominal, minimum, and maximum values for each parameter are given in Tables 1 and 2. Next, a set of 20 random values is generated between the upper and lower bounds for each $[\phi_1,...,\phi_8]^T$ using the MATLAB function. These 20 random values, applied to the control law in Equation (13), constitute the 20 candidates of the controller bank. Using these values of C_i, $i = 1,2,...,20$ a fictitious reference $\hat{\eta}_{des_i}$ is derived for each candidate controller using the relation in Equation (20). The cost function $\mathfrak{J}(t)$ considered is the minimum of the performance specification $T_{spec}(\hat{\eta}_{des}, T, Y)$, i.e. $\mathfrak{J}(t) = min\, T_{spec}(\hat{\eta}_{des}, T, Y)$. The performance specifications considered are given below.

$$T_{spec} = \frac{W_1\|(\hat{\eta}_{des}(t) - \eta(t))\|^2 + W_2\|\dot{\eta}(t)\|^2}{W_3\|\hat{\eta}_{des}(t)\|^2 + \rho} \quad (38)$$

wwhere W_1, W_2, and W_3 are weighting factors and ρ is a constant. The results satisfying the performance criterion (38) are presented in this paper.

The unknown parameters are estimated using the unfalification algorithm, which gives the near-optimal values of the aforementioned parameters. The parameters ϕ_1, ϕ_3, ϕ_5, and ϕ_7 are mass parameters of the system and are plotted against their nominal values, as given in Table 1. The parameters ϕ_2, ϕ_4, ϕ_6, and ϕ_8 are damping parameters, as shown in Table 2. The estimated values obtained by minimizing the performance specification in (38) are also presented in Tables 1 and 2 along with the estimation error. The switching in the parameter values of ϕ_1,ϕ_3, ϕ_5, and ϕ_7 can be observed in Figure 3.

The switching in the values of ϕ_2, ϕ_4, ϕ_6, and ϕ_8 is shown in Figure 4.

As the algorithm runs for a complete iteration, the change in plant dynamics changes parameter values. Hence, causing the switching in parameter values. It is observed that the parameter estimates obtained are quite close to the nominal values of the parameters. Due to the inclusion of the norm of the control input term, switching shows a high variation during the transient period. The AUV is effectively guided by the controller that remains unfalsified to follow the specified trajectory, thereby achieving the control objective. Figure 5 shows the tracking at each DOF, while Figure 6 depicts the circular trajectory plot.

In Figure 7, the error convergence plot is shown.

The results obtained are compared with those of the classical adaptive control design proposed in [31]. The tracking results presented in [31] show absolute convergence in 10 s, whereas in the proposed design, as evident from the results presented, absolute convergence is attained in 7 s. Thus, confirming faster and better convergence. Furthermore, the absence of parameter update dynamics in the closed-loop system, which is a characteristic of other adaptive methods, results in reduced computational complexity, providing an additional advantage in the proposed design.

Table 1. *Unknown mass parameters*

Sl. No.	Unknown parameter	Mass parameter	Nominal value (kg)	Min. value	Max. value	Estimated value	Absolute error
1	Φ_1	$м_{11}$	100	90	110	98.04	1.96
2	Φ_3	$м_{22}$	109	100	120	116.8	7.8
3	Φ_5	$м_{33}$	125	115	135	127.2	2.2
4	Φ_7	$м_{44}$	28.8	20	40	21.93	6.87

Table 2. *Unknown damping parameters*

Sl. No.	Unknown parameter	Damping parameter	Nominal value (kg/s)	Min. value	Max. value	Estimated value	Absolute error
1	Φ_2	$д_{11}$	10	1	20	3.5	6.5
2	Φ_4	$д_{22}$	400.18	390	410	393.5	6.48
3	Φ_6	$д_{33}$	10	1	20	18.84	8.84
4	Φ_8	$д_{44}$	1.8	1	3	2.95	1.15

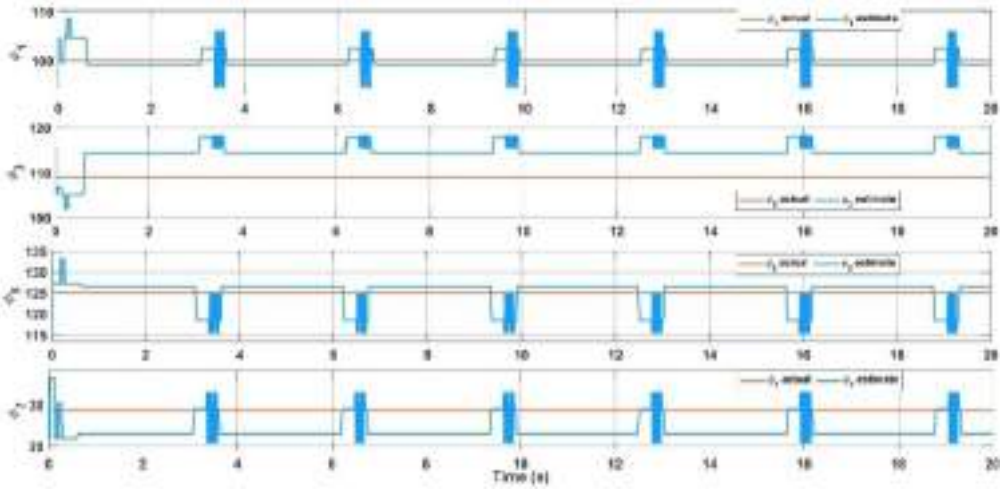

Figure 3. *Parameter switching* $(\Phi_1 - \hat{\Phi}_1, \Phi_3 - \hat{\Phi}_3, \Phi_5 - \hat{\Phi}_5, \Phi_7 - \hat{\Phi}_7)$

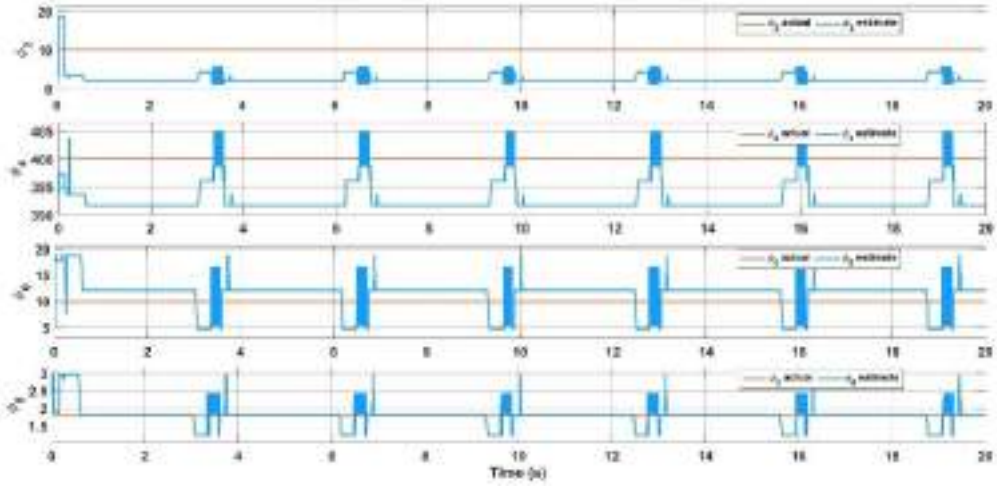

Figure 4. *Parameter switching* $(\Phi_2 - \hat{\Phi}_2, \Phi_4 - \hat{\Phi}_4, \Phi_6 - \hat{\Phi}_6, \Phi_8 - \hat{\Phi}_8)$

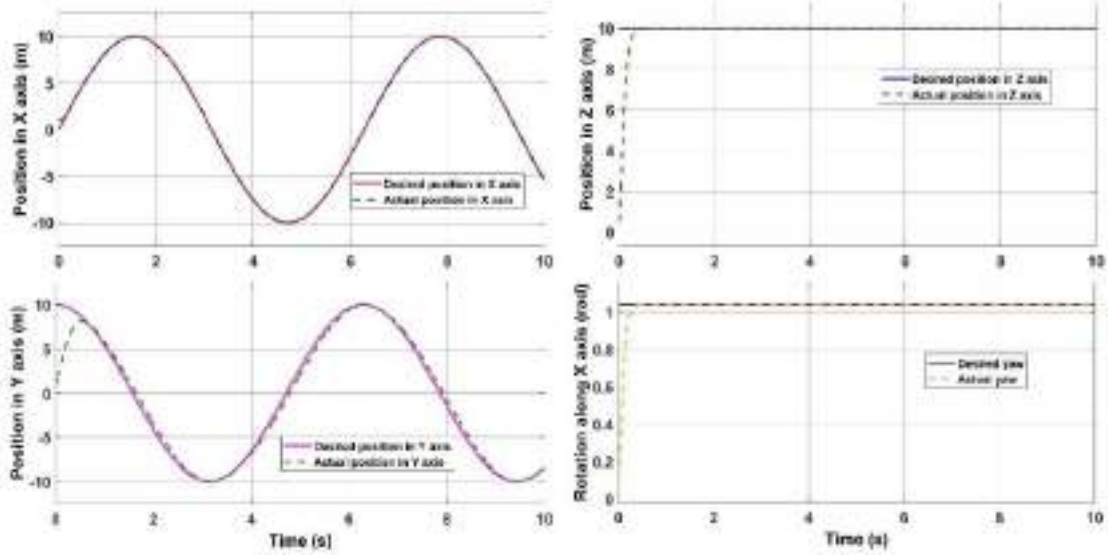

Figure 5. *Trajectory tracking along the X, Y, and Z axes*

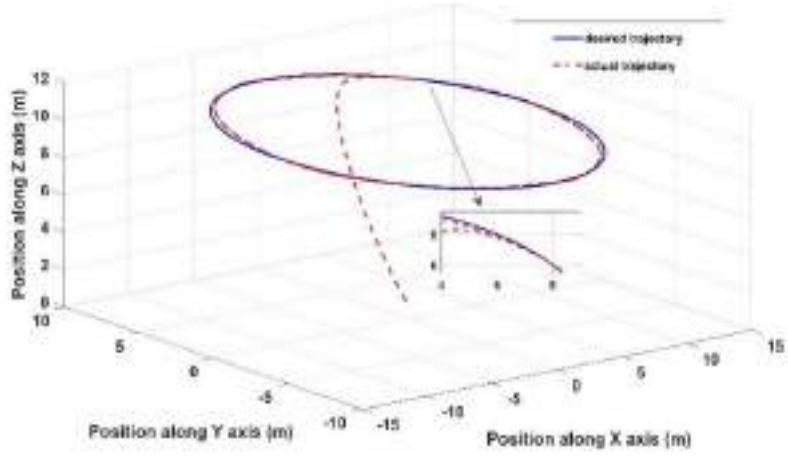

Figure 6. *Circular trajectory tracking*

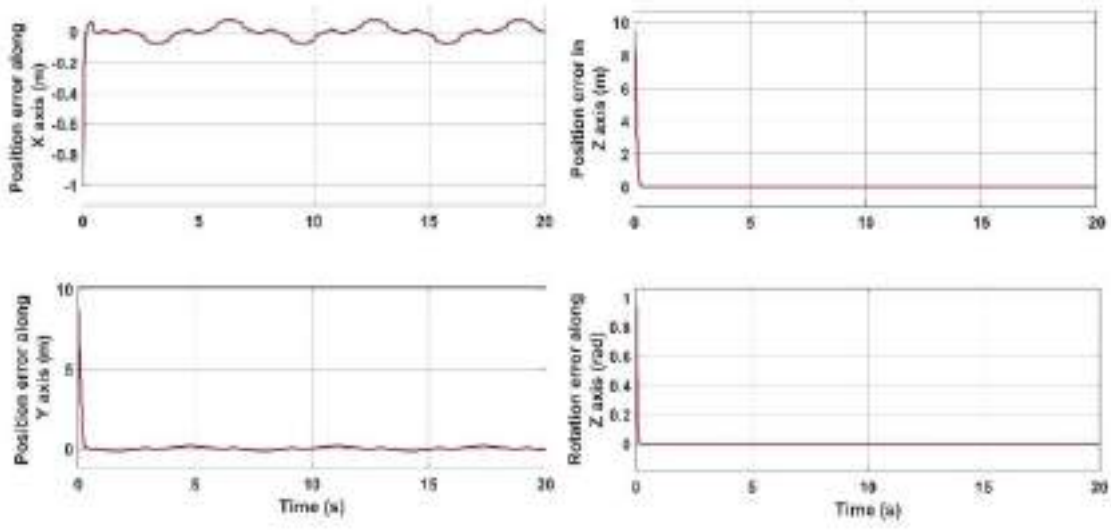

Figure 7. *Error convergence in adaptive unfalsified control*

6. Conclusion

The functioning of an AUV is likely to be affected by its physical non-linearities and environmental disturbances. Thus, it is favorable to use an adaptive plus data-driven method to control an AUV. This paper proposes adaptive control using the method of falsification with real-time input-output data. The approach utilizes measured information of input and output to select a controller from the candidate set. The plant used here is unknown, and the method uses the concept of a fictitious reference to obtain the parameter estimates. Near-optimal values of the parameter estimates are obtained by minimizing a designated cost function that considers the performance criteria. The controller utilizes these estimated values of parameters to guide the AUV toward the reference trajectory.

Simulation results verify the adaptiveness of the controller in estimating unknown parameters and prove its efficacy in attaining tracking objectives. The proposed design of the controller has also been corroborated with stability analysis and proof. The results have been substantiated with comparative results from another established method. In future work, it is planned to broaden the controller's scope by incorporating robust controllers into the controller bank and applying it to higher DOF robotic systems, thereby establishing the robustness of the controller design. In addition, in this work, a fixed convex set of candidates has been used for parameter estimation. This can be upgraded for non-convex sets using the latest optimization techniques.

Authorship Contributions

Concept design: T. Rasul, and K. Mukherjee, Data Collection or Processing: T. Rasul, Analysis or Interpretation: T. Rasul, Literature Review: T. Rasul, Writing, Reviewing and Editing: T. Rasul, and K. Mukherjee.

Funding: The authors did not receive any financial support for the research, authorship and /or publication of this article.

References

[1] M. Jun, and M. G. Safonov, "Automatic PID tuning: an application of unfalsified control". in *Proceedings of the International Symposium on Computer Aided Control System Design*, Hawai, USA, 1999.

[2] S. Liu, D. Wang, and E. Poh, "Nonlinear adaptive observer design for tracking control of AUVs in wave disturbance condition," *OCEANS 2006, Asia Pacific,* pp. 1-8.

[3] K. M. Tan, A. Anvar, and T.F. Lu, "Autonomous underwater vehicle (AUV) dynamics modelling and performance evaluation". *World Academy of Science, Engineering and Technology International Journal of Mechanical and Mechatronics Engineering,* vol. 6, Dec 2012.

[4] O. Hassanein, S. G. Anavatti, S. Hyungbo, and T. Ray, "Model-based adaptive control system for autonomous underwater vehicles". *Ocean Engineering*, vol. 127, pp. 58-69, Nov 2016.

[5] C. Silvestre, and A. Pascoal, "Nonlinear $H\infty$ optimal control scheme for an underwater vehicle with regional function formulation". *Journal of Applied Mathematics*, 2013.

[6] S. Liu et al., "Nonlinear adaptive observer design for tracking control of AUVs in wave disturbance condition," in *Proceedings of 2004 IEEE International Conference on Intelligent Robots and Systems*, Japan, 2004.

[7] K. Mukherjee, I. N. Kar, and R. K. P. Bhatt, "Ocean Waves: A disturbance observer approach for an autonomous underwater vehicle". *OCEANS 2019 Marseille.*

[8] M. G. Safonov, and T. C. Tsao, "The unfalsified control concept: A direct path from experiment to controller," *Feedback Control, Nonlinear Systems, and Complexity*, vol. 202, pp. 196-214, 1995.

[9] D. J. Leith, and W. E. Leithead, "Appropriate realization of gain-scheduled controllers with application to wind turbine regulation," *International Journal of Control*, vol. 65, pp. 223-248, 1996.

[10] D. J. Leith, and W. E. Leithead, "Survey of gain-scheduling analysis and design". *International Journal of Control*, vol. 73, pp. 1001-1025, 2000.

[11] T. C. Tsao, and M. G. Safonov, "Unfalsified direct adaptive control of a two-link robot arm". *International Journal of Adaptive Control and Signal Processing*, Apr 2001.

[12] M. G. Safonov, and S. Y. Cheong, "Unfalsified Control: Theory and Applications". In *IEEE Conference on Decision and Control, San Diego, CA* Dec 2006.

[13] M. G. Safonov, "Data-driven robust control design: Unfalsified Control". In *Proceedings of NATO Lecture Series 236, Robust Integrated Control Systems Design Methods for 21st Century Military Applications*, NATO Research and Technology Office, 2003.

[14] C. Manuelli, S. G. Cheong, E. Mosca, and M. G. Safonov, "Stability of unfalsified adaptive control with non-SCLI controllers and related performance under different prior knowledge". In *2007 European Control Conference (ECC), Kos, Greece, 2007,* pp. 702-708.

[15] A. Paul, M. Stefanovic, M. G. Safonov, and M. Akar, "Multi-controller adaptive control (MCAC) for a tracking problem using an unfalsification approach". In *Proceedings of the 44th IEEE Conference on Decision and Control*, pp. 4815-4820, 2005.

[16] F. B. Cabral, and M. G. Safonov, "Unfalsified model reference adaptive control using the ellipsoid algorithm". In *Proceedings of IEEE Conference on Decision and Control*, 2013.

[17] R. S. Sanchez-Pena, P. Colmegna, and F. Bianchi, "Unfalsified control based on the $H\infty$ controller parametrization". *International Journal of Systems Science*, vol. 46, pp. 1-12, Dec 2014.

[18] F. Previdi, T. Schauer, S. M. Savaresi, and K. J. Hunt, "Data-driven control design for neuroprostheses: a virtual reference feedback tuning (VRFT) approach*". IEEE Transactions on Control Systems Technology*, vol. 12, pp. 176-182, Jan 2004.

[19] Jing Wang and Yue Wang and Liulin Cao and Qibing Jin, "Adaptive iterative learning control based on unfalsified strategy for Chylla-Haase reactor". *IEEE/CAA Journal of Automatica Sinica*, vol. 1, 2014.

[20] V. Hassani, T. F Onstein, and A. M. Pascoal, "Application of data-driven control to dynamic positioning". *IFAC-PapersOnLine*, vol. 50, pp. 12392-12397, 2017.

[21] J. Das, et al. "Data-driven robotic sampling for marine ecosystem monitoring". *The International Journal of Robotics Research*, vol. 34, pp. 1435-1452, Aug 2015.

[22] T. O. Fossum, "*Intelligent autonomous underwater vehicles: a review of AUV autonomy and data-driven sample strategies*". PhD Dissertation from Applied Underwater Robotic Laboratory, Norwegian University of Science and Technology, Trondheim, Norway, 2016.

[23] Y.-C Sung, S. V. Patil, and M. G. Safonov, "Data-driven $H\infty$ loop-shaping controller design". *International Journal of Robust and Nonlinear Control*, vol. 28, pp. 3678-3693, Jul 2016.

[24] S. V. Patil, Y.-C Sung, and M. G. Safonov, "Nonlinear unfalsified adaptive control with bumpless transfer and reset". *IFAC-PapersOnLine*, vol. 49, pp. 1066-1072, 2016.

[25] Y.-C Sung, S. V. Patil, and M. G. Safonov, "Robustness of uncertain switching nonlinear feedback systems against large time-variation". *IEEE Transactions on Automatic Control*, vol. 67, pp. 993-1000, Feb 2022.

[26] S. V. Patil, Y.-C Sung, and M. G. Safonov, "Unfalsified adaptive control for nonlinear time-varying plants". *IEEE Transactions on Automatic Control*, vol. 67, pp. 3892-3904, Aug 2022.

[27] T. I. Fossen, *Guidance and control of ocean vehicles*, John Wiley and Sons, 1994.

[28] R. Wang, and M. G. Safonov, "Stability of unfalsified adaptive control using multiple controllers". *American Control Conference*, 2005.

[29] M. Stefanovic, A. Paul, and M. G. Safonov, "Safe adaptive switching through infinite controller set: Stability and convergence". *IFAC Proceedings Volumes*, vol. 38, pp. 73-78, 2005.

[30] J. P. Hespanha, *Logic-based switching algorithms in control*, Yale University, 1998.

[31] B. K. Sahu, and B. Subudhi, "Adaptive tracking control of an autonomous underwater vehicle". *International Journal of Automation and Computing*, vol. 11, pp. 299-307, Mar 2015.

ORIGINAL RESEARCH (AR) DOI: 10.4274/jems.2024.61214

Journal of ETA Maritime Science 2024;12(2):156-168

Effect of Exhaust Emissions Produced by Fishing Vessels on Air Pollution: A Case Study of Purse Seine Vessels Operating in the Black Sea

Eralp Özkaya[1], Ali Yasin Kaya[2], Fatih Tonoğlu[2], Özkan Uğurlu[2], Jin Wang[3]

[1]Directorate General of Coastal Safety, Ministry of Transport and Infrastructure, İstanbul, Türkiye
[2]Ordu University Faculty of Marine Sciences Fatsa, Department of Maritime Transportation and Management Engineering, Ordu, Türkiye
[3]Liverpool John Moores University Faculty of Engineering and Technology, Liverpool Logistics, Offshore and Marine (LOOM) Research Institute, Liverpool, UK

Abstract

In this study, exhaust emissions originating from purse seine fishing vessels were calculated. A bottom-up method based on ship activities was used for emission calculations. Necessary information for the calculations was obtained from the BAGIS (Fishing Vessels Monitoring System) system. Eighteen purse seiners in the Black Sea region with a length of 20 m or more engaged in fishing activities in the 2017-2018 fishing season were used as samples. These vessels were categorized into three different groups according to their length. The emissions produced by each length group were calculated separately under different conditions for vessels identified as "port", "operation", and "navigation". The total emissions in the Black Sea region and Türkiye were estimated. This study provides emission estimates using operational conditions and real data from Turkish-flagged purse seiners engaged in fishing in the Black Sea. In this respect, this research presents novelty and addresses an important gap in the existing literature. The annual emission amount of purse seine fishing vessels in the Black Sea is 260,000 tons, while the annual emission amount from purse seine vessels throughout Türkiye has been calculated as 440,000 tons. As a result, the effectiveness of the Emission Control Area (ECA)/Sulphur ECA region implementation in reducing emissions from maritime activities has been demonstrated. In addition, this study constitutes a source for the exhaust emission inventory of purse seiners in the Black Sea region.

Keywords: Ship emissions, Fishing vessels, Black Sea, Air pollution, Automatic identification system

1. Introduction

It is now well known that emissions due to fossil fuels have adverse environmental effects on a global scale, such as global warming, acidification, and eutrophication. Since the fishing industry is highly dependent on fossil fuel use, it produces significant amounts of greenhouse gasses (GHG) and other atmospheric pollutants [1]. Although emissions produced by ships are considered effective only in the sea, these emissions can affect hundreds of kilometres inland from the sea due to wind and other factors. Therefore, emissions produced by ships significantly contribute to air pollution and pose health risks to coastal residents. It is known that 70% of ship-borne emissions occur within the 200 nautical miles area [2], and fishing vessels contribute to air pollution because of their intense operations in the coastal area [3]. While GHG emissions from all maritime activities were 977 million tonnes in 2012, they increased by 9.6% and reached 1.076 billion tonnes in 2018 [4]. According to estimations based on data in 2015 [5], CO_2 emissions from global shipping were calculated as 932 million tons. This amount was 2.6% of the total CO_2 emissions estimated to be 36.062 billion tonnes worldwide.

Address for Correspondence: Fatih Tonoğlu, Ordu University Faculty of Marine Sciences Fatsa, Department of Maritime Transportation and Management Engineering, Ordu, Türkiye
E-mail: fatihtonoglu@odu.edu.tr
ORCID ID: orcid.org/0000-0003-3372-2977

Received: 09.10.2023
Last Revision Received: 19.01.2024
Accepted: 22.03.2024

To cite this article: E. Özkaya, A. Y. Kaya, F. Tonoğlu, Ö. Uğurlu, and J. Wang. "Effect of Exhaust Emissions Produced by Fishing Vessels on Air Pollution: A Case Study of Purse Seine Vessels Operating in the Black Sea." *Journal of ETA Maritime Science*, vol. 12(2), pp. 156-168, 2024.

Of the total emissions from all maritime activities, 87% (812 million tonnes) is from international shipping, 9% from cabotage (78 million tonnes) and 4% from fishing (42 million tonnes). A study based on data from the Sea Around Us initiative revealed that CO_2 emissions from fishing significantly exceed previously documented levels [6]. In addition to CO_2 emissions, policies and academic studies have intensified in recent years to reduce other types of emissions such as CO, NO_x, SO_x, particulate matter (PM), volatile organic compounds, and NH_3 [7]. In this respect, a more inclusive approach would be to consider all exhaust emission types from fishing vessels. To comply with increasingly stringent environmental regulations, exhaust emissions from fishing vessels need to be reduced. Responding to climate change by reducing waste and toxic substances released into the environment would be wise for the fishing industry. Otherwise, ensuring sustainable fishing and a clean environment will not be possible for new generations. As stated in The Food and Agriculture Organization State of World Fisheries and Aquaculture Report 2008, "Fishing and aquaculture activities make a small but significant contribution to GHG emissions during production processes and the transport, processing, and storage of fish" [8].

There are three approaches used to calculate the fuel consumption of ships and therefore the emissions they cause: The bottom-up method based on the ship, the bottom-up method based on ship activities, and the top-down method based on fuel statistics [9]. In the literature, they are also referred to as the "full bottom-up" method, the "bottom-up" method, and the "top-down" methods, respectively. The difference between the two bottom-up methods is the ship position and the time spent in different ship operations. There are differences in the data obtained using different calculation methods in determining the GHG emissions from ships. Carbon dioxide equivalent (CO_2e) is a standard unit that expresses the total GHG emissions from various sources in terms of the equivalent amount of CO_2 that would have the same global warming potential [10]. Annual GHG emissions (all GHG emissions in CO_2e, excluding black carbon-BC) from ships in 2017 were calculated as 704 million tonnes CO_2e according to the top-down method. Additionally, they were determined to be 760 million tons CO_2e according to the voyage-based bottom-up method and 946 million tons CO_2e according to the vessel-based bottom-up method [4]. There may be incomplete information, errors, or inconsistencies in the fuel statistics. Therefore, fuel-based methods can cause problems in achieving clear results in emission calculations. On the other hand, activity-based methods can estimate fuel consumption more consistently because they use many common inputs and assumptions [11]. The emissions produced by global fisheries are estimated to be much higher than previously reported due to differences in fuel use intensity, unreported catches, and insufficient data [6]. An activity-based calculation method is a practical approach that significantly eliminates the aforementioned negativities so that emissions from fishing vessels can be revealed more clearly.

The anchovy catch constitutes approximately 65% of the pelagic species living near the sea surface in Turkish territorial waters, with approximately 85% of the catch occurring in the Black Sea region [12]. Most of the fishing vessels engaged in anchovy fishing within the Black Sea region are purse seiners [13]. Additionally, these purse seiners operating in the Black Sea catch approximately 55.25% of the pelagic species residing near the sea surface within Turkish territorial waters. To evaluate the emission levels caused by pelagic fishing activities in Turkish territorial waters, it is essential to scrutinize the emission characteristics of purse seiners in the Black Sea. In this context, it is crucial to determine the volume of exhaust emissions originating from purse seine fishing in the Black Sea region.

This study determines the exhaust emissions produced by ships engaged in purse seine fishing in the Black Sea region. The bottom-up method based on ship activities introduced by Trozzi [14] was adopted for emission calculations. This method considers the ship's technical characteristics, duration of different ship operations, fuel types, and emission types for the emission calculation. This approach is preferred because it allows for detailed data entry. The fact that all ship parameters are used with this method increases the sensitivity compared with other methods and provides a high level of accuracy in terms of emission estimations. The study will reveal exhaust emissions from ships engaged in purse seine fishing in the Black Sea region. The study's estimates of exhaust emissions will be an important part of the puzzle necessary to determine the emissions from fishing activities worldwide. It will also be an important reference for estimating emissions from ships that are similar in size, main engine power, auxiliary engine power, and mode of operation.

2. Literature Review

In the literature, there are studies that reveal ships' emissions by creating data sets with a remote monitoring system. Although many studies are widely conducted, it has been observed that studies focused on ships with high engine power and in port/strait areas where ship traffic is intense. When the literature is examined, a wide range of studies have been conducted on the calculation of emissions originating from ships, both regionally and internationally.

In particular, studies on the sensitivity of modelling focus on access to information and evaluation of ship data.

The Automatic Identification System (AIS) is a mandatory collision avoidance system on ships that allows ships to electronically share much information, including identity, position, speed, and course, with other ships and vessel traffic services stations [15,16]. Goldsworthy and Goldsworthy [17] calculated exhaust emissions separately for each ship according to the main engine, auxiliary engine, and boiler load factors based on AIS data for modelling exhaust emissions at ports and intense coastal navigation areas in Australia. They used Class-A AIS data because they believed that this approach would yield more accurate results in their studies. Class-A AIS contains much more detailed information and is installed on commercial vessels navigating international seas within the scope of SOLAS. Coello et al. [1] used the AIS-based method to calculate emissions from the British fishing fleet by limiting the operation between certain latitudes and longitudes. It is stated in the study that the methods in which ship movements are actively used will give more precise results. Nunes et al. [18] studied ship movements over two years to evaluate exhaust emissions from ships in four Portuguese ports and developed an AIS movement-based approach. Perez et al. [16] examined ship activities in Texas state waters based on the AIS system and estimated the ships' emissions by considering the ship traffic and the speed, condition of the ships (navigation, port and anchorage), and port arrival and departure times. Buber et al. [19] calculated the GHG emissions caused by domestic ship traffic in the Gulf of İzmir using the bottom-up method and examined these results by combining them with the geographic information system method. They found that the highest emission types in the region were CO_2, NO_x and SO_2, respectively. In addition, they reported that the highest emissions were during manoeuvres and that the emissions at the two piers where ships with more powerful machinery operated corresponded to more than half of the total emissions in the region. In terms of emission amounts per day, they stated that the highest emission was in the cruise condition.

In addition to estimating emissions, the importance of remote monitoring systems for fishing vessels in terms of sustainable fishing has been demonstrated by some studies. The ship remote monitoring system, established in Taiwan in 1990, has become a system in which 2,200 ships are under control after 20 years. The system has become an important data source for the control of illegal fishing, its contribution to the control of fish stocks on board and land, and scientific monitoring of fishing efforts [20]. Parker et al. [21] revealed that the global fishing vessel fleet grew by 28% between 1990 and 2011, resulting in approximately 179 million tons of CO_2 emissions in 2011. Dağtekin et al. [22] conducted an economic analysis of anchovy fishery in the Black Sea and stated that 0.17-0.59 tons of CO_2 emissions were emitted for each ton of fish caught. To prevent the increase in emissions produced by the fishing fleet, they made suggestions in their study, such as preventing excessive and unnecessary fishing, determining the fishing times, and arranging the distances of fishing activities from the coast. Winther et al. [23] created an emission inventory based on AIS data from ships in the Arctic. The study revealed that fishing vessels caused the highest emissions among other types of vessels in the Arctic, accounting for 45% BC, 38% NO_x, and 23% SO_2. Koričan et al. [3] conducted a comparison by analyzing the emission values of 163 purse seiners and 82 trawlers active in the Adriatic Sea. Emission calculations were performed using the bottom-up method. The study findings indicated that trawlers exhibit higher emission indices than purse seiners. This is primarily attributed to the relatively high energy demands and lower fish landing quantities associated with trawlers. However, the researchers noted that the disparity in emission indices between trawlers and purse seiners was relatively minor, especially when considering the income derived from fishing activities.

Different data sets can be used to calculate emissions from ships and to conduct impact analysis; Endresen et al. [24] used Automated Mutual-Assistance Vessel Rescue System data for the data set and Compherensive Ocean-Atmosphere Data Set data for calculating the effect. The use of an emission measuring device is one of the approaches that give the clearest results, but there are serious difficulties in their implementation. Liu et al. [25] used an emission measuring device system in their study and made instant gas measurements under different conditions, such as navigation, manoeuvring, and operation on offshore fishing vessels. As a result of the study, it has been determined that there are differences in terms of quantity in different types of exhaust emissions depending on the ship's activities. This method is very effective because it minimizes the assumptions. Winnes et al. [26] made an assessment by using the port of Gothenburg as an example of reducing GHG emissions from ships in ports. In the study, emission reduction measures were listed as "alternative fuel use", "changes in ship design" and "operation". It was stated that among the scenarios, the highest amount of emission reduction would occur in the "operation condition". In their extensive investigation, Xing et al. [27] investigated the strategies available for minimizing CO_2 emissions from ships. They categorized these strategies into technological measures, operational measures, eco-friendly fuels, and alternative power sources. The challenges in implementation were also highlighted, considering the impediments associated with adopting these measures. Based on their analysis, the researchers concluded that the

diversification of ship power systems and marine fuels is an unavoidable necessity.

As a result of the literature review, although there are studies on the emission estimation of fishing vessels, no study has revealed the exhaust emissions produced by purse seiners in the Black Sea region. In this respect, the estimation of exhaust emissions produced by purse seine fishing vessels in the Black Sea region will fill an important knowledge gap. In addition, this study will contribute to the literature by comparing the emissions according to the size of the ships, as it reveals the exhaust emissions by considering the dimensions of the fishing ships. In this study, the activity-based bottom-up method, which considers the times in different ship activities (navigation, operation, port) and the technical characteristics of the ships, was applied by using BAGIS (Fishing Vessels Monitoring System) data. The BAGIS system is an AIS-like system developed for tracking the Turkish fishing fleet, which must be installed on vessels of 12 m and above in length. In this respect, detailed datasets obtained from the BAGIS devices of fishing vessels are a practical approach for estimating exhaust emissions to obtain clearer and more accurate results. This study differs from other studies in the literature with its mentioned aspects.

3. Methodology

3.1. Data Collection

This study aims to determine the exhaust emissions of Turkish fishing vessels with a length of 20 m or more engaged in purse seine fishing in the Black Sea region. In the study, as a sample, the data of 18 fishing boats engaged in purse seine fishing in the 2017-2018 fishing season (from 1 September 2017 to 15 April 2018) were examined. As a part of the research, the study analyzed data from 18 fishing vessels involved in purse seine fishing during the 2017-2018 fishing season (from September 1, 2017, to April 15, 2018). The data of 18 ships were evaluated in three categories. In this respect, they provide useful outputs for purse seiner exhaust emissions with similar characteristics. The number of purse seiners was limited due to the study's limitations and the detailed data that needed to be analyzed. Considering the data obtained, inferences were made about purse seiners in the Black Sea and Türkiye. Data showing the time spent by 18 purse seine fishing vessels under different operational conditions in the Black Sea region were obtained from the BAGIS system. BAGIS is a system that can only be accessed by engineers authorized by the Ministry of Agriculture and Forestry of the Republic of Türkiye and officials of the Coast Guard Command. The authorization to access certain data was obtained with the permission of the ministry officials. Information that can be accessed when querying ships in this system includes the ship's name, license number, mooring number, width, overall length, equipment ownership, fleet registration number, log length, vessel group, current ship speed, and position.

A typical representation of fishing vessels on the BAGIS system screen is presented in Figure 1. The meanings of icon colours are as follows (Figure 1): light green colour indicates fishing vessels with location information via GSM; dark green colour indicates fishing vessels with location information via satellite; blue colour indicates AIS track information received from the Ministry of Transport; red colour indicates fishing vessel violating a rule defined by the ministry, orange colour indicates the ship that needs to be introduced to the system because any information is missing [28]. Using Microsoft Excel, a raw data set was structured. The data taken from the BAGIS system were used to form the raw data. While using the speed data in the raw dataset, the study of Campbell et al. [29] is taken as a reference. In addition, the opinions of the captains of the fishing vessels examined in this study were considered. Thus, a ship is assumed to be stopped at a speed range of 0-1 knots (confirmed to be in port condition by mapping), manoeuvring or operating at a speed range of 1-6 knots, and navigating at speeds of 6 knots and above. The purse seine fishing vessels considered in the study were classified into three different size groups: length group A represents 20-30 m range; length group B represents 30-40 m range; and length group C, 40 m and above. The numbers of main and auxiliary engines of purse seine fishing vessels examined in this study differ. Hence, in the computation of both main engine and auxiliary engine powers, the cumulative main engine power in vessels equipped with multiple main engines and the cumulative auxiliary engine power in vessels featuring more than one auxiliary engine were considered.

Figure 1. *The display of fishing vessels on the BAGIS system [28]*

3.2. Stages of the Study

First, a literature review was conducted to reveal the exhaust emissions produced by purse seine fishing vessels in the Black Sea region. As a result of the literature review,

the most appropriate method is to use the activity-based bottom-up method for the most precise calculation of emissions. Ship navigation information and technical data of 18 purse seine fishing vessels of groups A, B, and C in the study were obtained from the BAGIS system. A dataset was created in Excel for easier analysis of the data. This dataset contains the following information: ship length, main engine power, auxiliary engine power, total operating time (days), total stay in port (hours), total operation/ manoeuvre time (hours), total navigation time (hours), average navigation speed (knots), total distance navigated (Nm), and type of ship activity (port, operation, navigation). In the next step, numerical values of NO_x, SO_x, CO_2, hydrocarbons (HC), and PM emissions from the vessels were calculated using the bottom-up method. Then, emission estimates of purse seiners in the Black Sea and Türkiye were made according to the emissions calculated for the sample ships. In the last stage of the study, the emissions from purse seine fishing vessels were compared with those reported in the literature, and recommendations were made to reduce

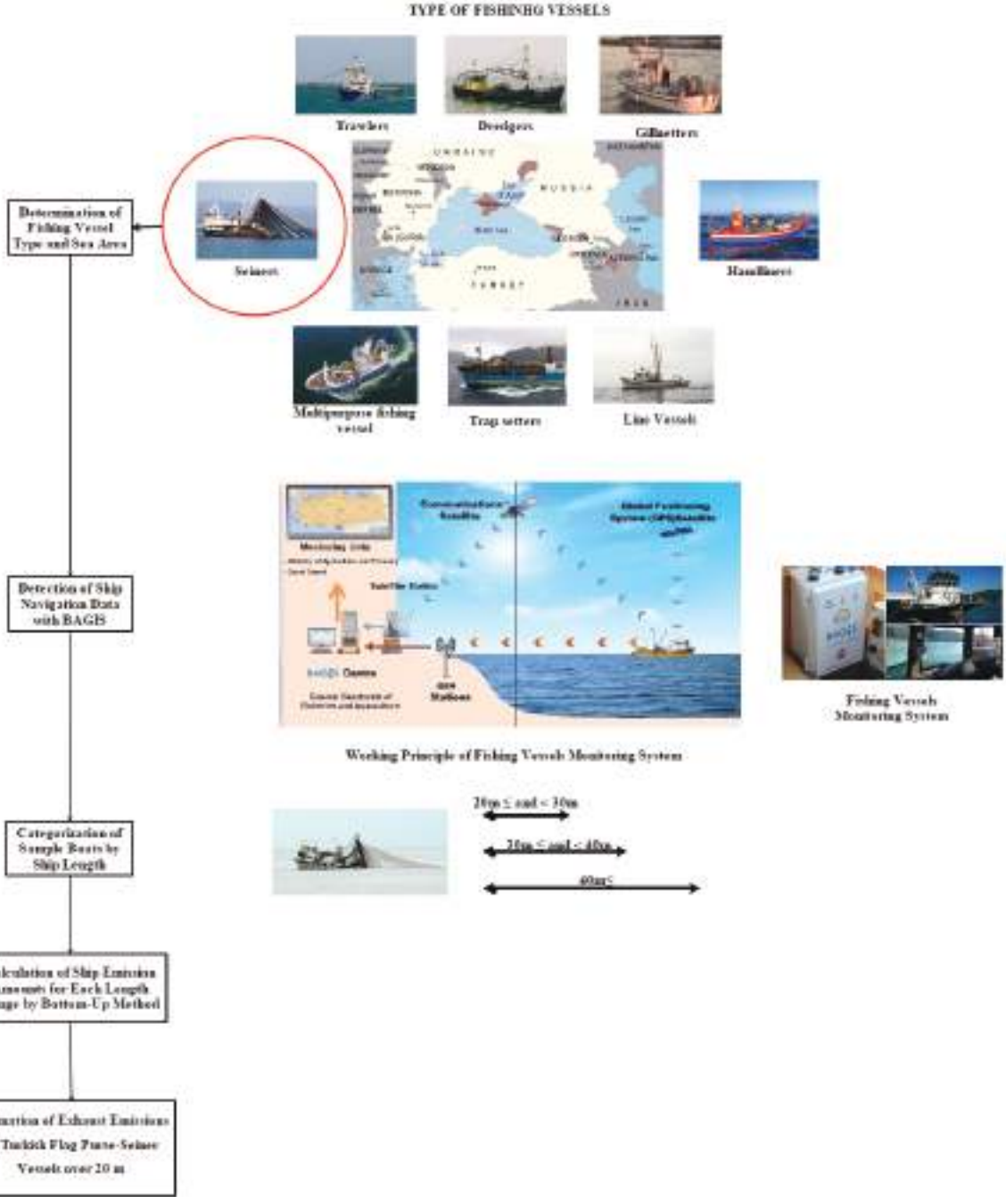

Figure 2. *Flow chart of the research*

emissions and create awareness. The research flowchart is shown in Figure 2.

3.3. Research Method

In this study, the approach introduced by Trozzi [14] within the framework of the EMEP/EEA air pollution emission inventory guidebook was used within the scope of the bottom-up method. In the literature, there have been many studies using the approach presented in Trozzi's [14] study [30,31]. The bottom-up method derives emission estimates using data sources that describe maritime activities; these data are AIS data, including a ship's identity, position, speed, draft, and other information [32]. AIS data serves as an essential input to enhance bottom-up inventory, offering the potential for positive outcomes in research through this approach. Instead of AIS data, this study utilized BAGIS data, which, similar to AIS, encompasses navigational details such as ship identity, location, time, speed, and route. To apply the "full bottom-up" method based on ship activities, data such as main engine power, auxiliary engine power, speed, position, and type of ship activity should be considered. Using a ship's full parameters in this method increases its sensitivity compared with other methods. The formulation is expressed as:

$$E_{trip,i,j,m} = \sum_p [T_p \times \sum (P_e \times LF_e \times EF_{e,i,j,m,p})] \quad (1)$$

EF: Emission factor (g/kWh)

LF: Load Factor

P: Power according to engine type (kW)

T: Time (hours)

p: Different phases of the trip (navigation, port, operation)

j: Engine type (low speed, medium speed, high speed)

i: Emission type (NO_x, SO_x, etc.)

m: Fuel type (MDO-Marine Diesel Oil, HFO-Heavy Fuel Oil)

trip: The navigation, manoeuvre, or port condition the ship is in

$E_{trip,i,j,m}$: Sum of emissions under all conditions

e: Engine type (main, auxiliary)

In this study, while calculating the main engine and auxiliary engine emission factors, the EMEP/EEA 2016 air pollution inventory was used as a reference, and similar studies were used [14,32]. Emission factors in this study are those used for vessels with high-speed diesel engines. All the emission factors used are shown in Table 1. The uncertainty ratios in the emission factors used can be calculated as ±20% for NO_x, ±20% for SO_x, and ±10% for PM ±25% [33].

Diesel engines can be classified as slow, medium, or fast, depending on their rated speed. Low-speed diesel engines have engines with a maximum operating speed of 0-300 rpm. Medium-speed diesel engines have a maximum operating speed in the 300-900 rpm range. High-speed diesel engines have an operating speed of 900 rpm and above. Approximately 18% of existing engines are slow, 55% are medium, and 27% are fast diesel engines [33]. All ships in this study have high-speed diesel engines. Load factors are 0.8% for "navigation condition" for main engines, 0.2% for "port conditions", and 0.2% for "operation conditions". For auxiliary engines, it is 0.3%, 0.4%, and 0.5% for navigation, port, and operational conditions, respectively [33]. The emission factors in Table 1 and daily ship movement data from BAGIS were transferred to a Microsoft Excel table, and daily NO_x, SO_x, CO_2, HC, and PM emissions were calculated according to the ship's operation, port, and navigation conditions.

Table 1. *Main engine and auxiliary engine emission factors [33]*

Main engine (g/kWh)					
Emission factor	**NO_x**	**SO_x**	**CO_2**	**HC**	**PM**
Navigation	11.20	1.00	697	0.45	0.30
Port	9.30	1.00	725	0.50	0.90
Operation	9.30	1.00	747	0.97	0.90
Auxiliary engine (g/kWh)					
Emission factor	**NO_x**	**SO_x**	**CO_2**	**HC**	**PM**
Navigation	13.20	1.00	697	0.46	0.30
Port	13.20	1.00	725	0.50	0.30
Operation	11.80	1.00	747	0.97	0.30

4. Results

Trozzi [14] stated that to calculate the emissions produced by ships in detail, the voyage of a ship should be evaluated separately as navigation, port, and manoeuvre. In the study, it was emphasized that the most sensitive method for calculating emissions would be the sum of the emissions under these three conditions. In this study, the emission factor values in the manoeuvre condition stated by [14] were assumed to be equivalent to the values in the "operation conditions" of the vessels. The information on each purse seine fishing vessel's technical characteristics and activities used in the emission calculation is given in Table 2.

The average "port", "operation", and "navigation" times of the ships within the scope of the study were 2,839, 566.8, and 854 h in group A, respectively; 2,097.5, 531.3, and 890.5 h in group B; and 1,429.8, 539, and 706.5 h in group C. The ships with the longest average operating time were group ships with a rate of 40.76% (Table 2).

The average "main engine" powers of the ships in groups A, B, and C were calculated as 825.2, 1,077.6, and 1,675 kW, respectively. The average "auxiliary engine" powers were 109.4, 142.0, and 201.7 kW, respectively. In terms of total

Table 2. *Information on technical specifications and activities of each purse seine fishing vessel*

Vessel	Length (m)	Main engine (kW)	Auxiliary engine (kW)	Duration of all conditions (Day)	Duration of port (Hour)	Duration of operation (Hour)	Duration of navigation (Hour)	Average ship speed (Knot)	Total distance (Nm)
A1	27.9	797.8	126.8	220	3,370	754	1,162	7.38	8,571.9
A2	24.5	850	102.1	130	2,056	488	571	7.27	4,149.3
A3	26.5	708.3	104.4	170	2,951	459	668	10.52	7,027.1
A4	22	895	90	197	3,110	612	1,006	7.50	7,549.2
A5	27	1,137	136	163	2,544	578	790	8.15	6,440.1
A6	29.8	563	97	185	3,003	510	927	7.99	7,406.8
B1	39	1,744.7	79.8	102	1,274	436	743	8.07	5,996.8
B2	33	1171	120	202	2,839	844	1,180	7.25	8,555.5
B3	31.44	1,159.4	119.3	108	1,988	260	344	7.55	2,596.3
B4	33.8	768	134	175	2,744	665	791	7.50	5,935.8
B5	36.3	862	101	138	1,976	411	925	7.40	6,841.5
B6	38	760	298	154	1,764	572	1,360	7.77	10,572.8
C1	44	1,823	160.3	186	2,800	621	1,048	7.91	8,288.7
C2	40	1,749.2	203.5	99	1,035	511	828	7.70	6,374.4
C3	42	1,647.8	223.7	102	1,164	526	751	8.59	6,454.6
C4	42.2	1,897	224	97	1,210	534	584	7.88	4,603.1
C5	42.7	1,315	149	92	1,175	496	537	8.15	4,377.6
C6	42	1,618	249.8	93	1,195	546	491	7.77	3,817.1

engine power (main engine + auxiliary engine), group C ships constituted 46.56% of the total engine power in the study. This rate is approximately twice that of group A ships (23.19%) (Table 2).

Using Equation 1, the total emissions for each ship were calculated (Table 3). The total emissions from the 18 vessels in the study were 22,447.55 tonnes. Ship groups making an enormous contribution to the total emissions were listed as group C (38.86%) > group B (32.08%) > group A (29.06%) (Table 3).

The purse seine fishing vessels in group C made the largest contribution to total emissions in all emission categories. The purse seine fishing vessels in group C accounted for 40.26% of total NO_x emissions, 38.84% of SO_x emissions, 38.84% of CO_2 emissions, 39.84% of HC emissions, and 37.76% of PM emissions. While the purse seine fishing vessels in group B were in second place in terms of contribution to total emissions, their contribution rates were between 31.54% and 32.09%. These rates were between 28.14% and 30.70% for the purse seine fishing vessels in group A that made the least contribution to the total emissions (Table 3). The vessels included in the study were in the "port condition" for 60.90% of the entire operating time (Table 2).

Table 3. *Total emissions of each purse seine fishing vessel (Tonnes)*

Vessel	NO_x	SO_x	CO_2	HC	PM
A1	16.53	1.94	1,376.53	1.08	0.58
A2	10.22	1.33	945.38	0.74	0.40
A3	11.26	1.51	1,068.71	0.82	0.45
A4	16.71	1.57	1,123.22	0.81	0.85
A5	17.73	1.67	1,189.48	0.87	0.93
A6	10.86	1.01	718.06	0.52	0.54
B1	18.23	1.89	1,349.25	1.08	0.57
B2	23.53	2.73	1,925.81	1.55	0.82
B3	10.30	1.54	1,095.57	0.83	0.46
B4	13.58	1.26	956.94	0.67	0.69
B5	12.85	1.19	796.53	0.61	0.61
B6	15.10	1.35	965.34	0.65	0.70
C1	32.82	3.89	2,771.73	2.16	1.17
C2	20.56	1.89	1,344.03	1.12	0.57
C3	19.21	1.91	1,353.66	1.12	0.57
C4	18.95	1.77	1,263.34	0.96	0.93
C5	12.24	1.15	817.73	0.62	0.60
C6	15.46	1.44	1,029.89	0.80	0.77
Sum	296.13	31.03	22,091.19	16.99	12.20

Table 4. *Emissions of each purse seine fishing vessel according to different conditions (Tonnes)*

Vessel	Condition	NO_x	SO_x	CO_2	HC	PM
A1	Port	6.98	1.39	984.33	0.70	0.42
	Operation	1.43	0.25	189.51	0.25	0.08
	Navigation	8.12	0.29	202.70	0.14	0.09
A2	Port	4.64	0.98	696.25	0.49	0.29
	Operation	1.01	0.19	138.83	0.18	0.06
	Navigation	4.58	0.16	110.30	0.08	0.05
A3	Port	5.92	1.20	849.76	0.60	0.36
	Operation	0.83	0.15	111.46	0.15	0.05
	Navigation	4.51	0.16	107.49	0.08	0.05
A4	Port	7.01	0.70	504.34	0.35	0.54
	Operation	1.28	0.13	98.17	0.13	0.11
	Navigation	8.42	0.75	520.71	0.34	0.20
A5	Port	7.66	0.75	544.57	0.38	0.57
	Operation	1.59	0.16	121.62	0.16	0.13
	Navigation	8.47	0.75	523.29	0.34	0.23
A6	Port	5.07	0.48	350.63	0.24	0.35
	Operation	0.77	0.08	57.66	0.08	0.06
	Navigation	5.03	0.44	309.76	0.20	0.13
B1	Port	4.81	1.16	836.12	0.58	0.35
	Operation	1.58	0.32	237.69	0.31	0.10
	Navigation	11.85	0.41	275.44	0.19	0.12
B2	Port	8.43	1.83	1,297.80	0.92	0.55
	Operation	2.29	0.44	319.79	0.42	0.13
	Navigation	12.81	0.46	308.23	0.21	0.14
B3	Port	5.85	1.27	906.39	0.64	0.38
	Operation	0.71	0.13	99.34	0.13	0.04
	Navigation	3.74	0.13	89.84	0.06	0.04
B4	Port	6.35	0.61	493.06	0.30	0.44
	Operation	1.37	0.14	102.97	0.13	0.10
	Navigation	5.86	0.52	360.92	0.23	0.16
B5	Port	4.49	0.44	319.33	0.22	0.34
	Operation	0.86	0.09	13.06	0.09	0.07
	Navigation	7.51	0.67	464.14	0.30	0.20
B6	Port	5.97	0.53	385.23	0.27	0.32
	Operation	1.61	0.16	115.96	0.09	0.10
	Navigation	7.51	0.67	464.14	0.30	0.29
C1	Port	12.46	2.78	1,984.45	1.39	0.83
	Operation	2.58	0.49	368.01	0.48	0.15
	Navigation	17.78	0.62	419.27	0.29	0.19
C2	Port	4.76	1.01	719.22	0.51	0.30
	Operation	2.15	0.40	298.16	0.39	0.12
	Navigation	13.64	0.49	326.65	0.22	0.15
C3	Port	5.29	1.09	773.08	0.55	0.33
	Operation	2.17	0.39	294.13	0.38	0.12
	Navigation	11.75	0.42	286.45	0.19	0.13
C4	Port	6.06	0.60	431.04	0.30	0.45
	Operation	2.45	0.25	187.08	0.24	0.20
	Navigation	10.45	0.93	645.23	0.42	0.28
C5	Port	4.03	0.40	287.60	0.20	0.30
	Operation	1.56	0.16	119.56	0.16	0.13
	Navigation	6.65	0.59	410.57	0.27	0.18
C6	Port	5.57	0.54	388.55	0.27	0.39
	Operation	2.29	0.23	172.73	0.22	0.18
	Navigation	7.60	0.67	468.61	0.30	0.20
Sum		296.13	31.03	22,091.19	16.99	12.20

Accordingly, among the total emissions, the emission rate in the "port condition" was 57.45%, while the emission rate in the "navigation condition" was 28.81%, and the emission rate in the "operation condition" was 13.74% (Table 4).

In the "port condition", the purse seine fishing vessels in group C made the greatest contribution to the total emissions with 35.93%, while the vessels in group B contributed 33.22% and the vessels in group A 30.84%. In the "operation condition", the contribution of the vessels in group C to total emissions was 47.26%, whereas the contribution of the vessels in group B was 29.19% and in group A was 23.56%. In the "navigation condition", the contribution rate of the vessels in group C to the total emissions was 40.69%, while the vessels in group B contributed 31.19% and the vessels in group A 28.11%. While the difference between the emission contribution rates of the groups is 5.09% (the difference between group C and group A) in the case of the port, this difference increases to 23.70% in the "operation condition" (Table 4). Because the total time spent by purse seine fishing vessels in each condition differed, the emissions per unit time were calculated to make a more consistent comparison. The emissions per unit time of each purse seine fishing vessel under different conditions are given in Table 5.

In the "port condition", the emissions of the purse seine fishing vessels in group C per unit time varied between 2.01 times and 2.12 times more than the emissions produced by the purse seine fishing vessels in group A. While these ratios were similar in the "operation condition" (between 2.00 and 2.09), they decreased between 1.96 and 2.05 in the "navigation condition". In all emission categories except HC, the highest emissions per hour were observed in the "navigation condition". In the HC category, the highest emissions per hour occurred in the "operation condition". This result was expected because HC has a higher emission factor (approximately two times) in the "operation condition" than in the other conditions (Table 1).

In Table 3, the total emissions produced by each vessel according to emission types were presented. The total emissions produced by the 18 vessels that constituted the sample are as follows: 296.13 tons of NO_x, 31.03 tons of SO_x, 22,091.19 tons of CO_2, 16.99 tons of HC, and 12.20 tonnes of PM. In the study, 18 purse seine fishing vessels were examined as a sample that were allowed to catch in the 2017/2018 fishing season. The 18 purse seine fishing vessels examined as a sample in the study constituted approximately 13% of the 139 active purse seine fishing vessels with a length of 20 m and above in the Black Sea in the 2017/2018 fishing season. In the 2020/2021 fishing season (from 1 September 2020 to 15 April 2021), this rate was approximately 9% of 209 purse seine fishing vessels with a

Table 5. *Emissions of each purse seine fishing vessel under different conditions per hour (10^{-3} tons)*

	Port					Operation					Navigation				
Vessel	NO_x	SO_x	CO_2	HC	PM	NO_x	SO_x	CO_2	HC	PM	NO_x	SO_x	CO_2	HC	PM
A1	2.07	0.41	292.08	0.21	0.12	1.89	0.34	251.34	0.33	0.10	6.99	0.25	174.44	0.12	0.08
A2	2.26	0.48	338.64	0.24	0.14	2.06	0.38	284.50	0.37	0.11	8.02	0.29	193.16	0.13	0.09
A3	2.01	0.41	287.96	0.20	0.12	1.81	0.32	242.84	0.32	0.10	6.75	0.24	160.91	0.11	0.07
A4	2.25	0.22	162.17	0.11	0.17	2.09	0.21	160.41	0.21	0.17	8.37	0.74	517.60	0.33	0.20
A5	3.01	0.30	214.06	0.15	0.22	2.76	0.28	210.42	0.27	0.22	10.73	0.95	662.39	0.43	0.28
A6	1.69	0.16	116.76	0.08	0.12	1.50	0.15	113.06	0.15	0.11	5.43	0.48	334.16	0.22	0.14
B1	3.77	0.91	656.29	0.46	0.27	3.62	0.73	545.16	0.71	0.22	15.95	0.55	370.72	0.25	0.16
B2	2.97	0.65	457.13	0.32	0.19	2.71	0.52	378.89	0.50	0.16	10.86	0.39	261.21	0.18	0.12
B3	2.94	0.64	455.93	0.32	0.19	2.72	0.51	382.08	0.50	0.15	10.86	0.38	261.16	0.18	0.12
B4	2.31	0.22	179.69	0.11	0.16	2.06	0.21	154.84	0.20	0.15	7.41	0.65	456.28	0.29	0.20
B5	2.27	0.22	161.60	0.11	0.17	2.08	0.21	31.78	0.21	0.17	8.12	0.72	501.77	0.32	0.22
B6	3.38	0.30	218.39	0.15	0.18	2.82	0.27	202.73	0.15	0.17	5.53	0.49	341.28	0.22	0.21
C1	4.45	0.99	708.73	0.50	0.30	4.15	0.79	592.61	0.77	0.24	16.97	0.60	400.07	0.27	0.18
C2	4.60	0.98	694.90	0.49	0.29	4.21	0.78	583.48	0.76	0.23	16.48	0.59	394.51	0.27	0.18
C3	4.54	0.94	664.15	0.47	0.28	4.12	0.75	559.19	0.73	0.22	15.65	0.56	381.42	0.26	0.17
C4	5.01	0.49	356.23	0.25	0.38	4.59	0.47	350.33	0.46	0.37	17.89	1.59	1104.85	0.71	0.48
C5	3.43	0.34	244.77	0.17	0.26	3.15	0.32	241.05	0.31	0.25	12.37	1.10	764.56	0.49	0.33
C6	4.66	0.45	325.15	0.22	0.33	4.19	0.42	316.36	0.41	0.32	15.49	1.37	954.40	0.62	0.41

length of 20 m and above in the Black Sea [34]. Considering these data, a proportional estimation of the total emissions produced by purse seine fishing vessels in the Black Sea region and Türkiye in the 2020/2021 fishing season has been made. The purse seine fishing vessels of the 2020/2021 fishing season were classified into size groups in a similar way as in the study (groups A, B and C), and the emissions were calculated for each size group. In Table 6, the average emissions of 18 purse seine fishing vessels are given for each size group. In studies where access to the main dataset is not possible or data processing is extremely challenging due to the dataset's size, emission predictions can be made by relying on a sample group with similar ship characteristics and operational features. There are studies in the literature that have been conducted using this method. In their study, Koričan et al. [3] established a validation group consisting of 12 vessels, including 10 purse seiners and 2 trawlers, to assess the emissions caused by the Croatian fishing fleet, which comprises 163 purse seiners and 82 trawlers.

5. Discussion

This study investigated exhaust emissions produced by purse seine fishing vessels operating in the Black Sea. The "bottom-up" method, which is frequently used in the literature and has a higher consistency than other methods, was used for emission calculations. Contrary to the study of Demirci and Karagüzel [35], which concluded that the highest emissions occurred in the "operation condition", in this study, it was determined that the largest share of the contribution to the total emission occurred in the "port condition". The most important factor leading to this result is the long stay of the ships in the port. Ay et al. [36] also included the "auxiliary engine/main engine power" ratios per ship for different ship types in their study. This rate was found to be higher in fishing vessels than in other ship types. The ships in the study were "in port condition" for an average of 60% of the examination duration (Table 2). The primary source of emissions in the port is the boilers and auxiliary engines operating to meet the electricity needs. The inadequacy of infrastructure to meet the electricity needs of ships at fishing ports in Türkiye is one of the main causes of emissions in the port. Such vessels in group A were in port for 66.65% of the entire working time, the vessels in group B for an average of 59.60%, and the vessels in group C for 53.45% (Table 2). The largest emissions were observed "in port condition", similar to the results of Song and Shon [37]. Nunes et al. [18] estimated that CO_2, NO_x, and SO_x emissions represent more than 95% of navigation and in-port emissions.

It was observed that the total emissions of the vessels in group C were higher than those in groups A and B in all emission categories in port, operation, and navigation conditions. Therefore, the high emissions produced by the vessels in group C, which have the lowest total working

Table 6. *Average emissions for each size group and estimated emissions in the Black Sea and Türkiye (Tonnes)*

Sample purse seiners							
	Size definition	**Num.**	**NO_x**	**SO_x**	**CO_2**	**HC**	**PM**
Group A	20 m≤ and <30 m	6	13.89	1.50	1,070.23	0.81	0.62
Group B	30 m≤ and <40 m	6	15.60	1.66	1,181.57	0.90	0.64
Group C	40 m≤	6	19.87	2.01	1,430.06	1.13	0.77
Sum		18	296.13	31.03	22,091.19	16.99	12.20
Purse seiners in the Black Sea							
	Size definition	**Num.**	**NO_x**	**SO_x**	**CO_2**	**HC**	**PM**
Group A in the Black Sea	20 m≤ and <30 m	51	839.05	87.92	62,591.71	48.14	34.57
Group B in the Black Sea	30 m≤ and <40 m	91	1,497.12	156.87	111,683.25	85.89	61.68
Group C in the Black Sea	40 m≤	67	1,102.28	115.50	82,228.33	63.24	45.41
Sum in the Black Sea		209	3,438.44	360.29	256,503.30	197.27	141.67
Purse seiners in Türkiye							
	Size Definition	**Num.**	**NO_x**	**SO_x**	**CO_2**	**HC**	**PM**
Group A in Türkiye	20 m≤ and <30 m	107	1,760.35	184.46	131,319.87	101.00	72.53
Group B in Türkiye	30 m≤ and <40 m	153	2,517.14	263.76	187,775.14	144.42	103.71
Group C in Türkiye	40 m≤	92	1,513.57	158.60	112,910.54	86.84	62.36
Sum in Türkiye		352	5,791.06	606.81	432,005.55	332.25	238.60

time (25.60%), can be attributed to their high engine power. This result confirms the conclusion of previous studies that "increasing engine power also increases the emissions" [18,38,39]. In this respect, the main engine power and ship size are among the most important parameters in terms of the amount of emissions from fishing vessels. Some studies in the literature reveal the relationship between the size and tonnage of a ship and its fuel consumption [38].

In this study, the total emissions in the "navigation condition" were higher than those in the "operation condition" for all emission types. This result is in contrast to the study of Liu et al. [25], which made instant emission measurements on fishing vessels with the help of an emission measuring device. The difference between the operation and navigation times of the purse seine vessels in this study may be the main reason for the difference between the studies. Indeed, the total operating time of the ships in this study was 9,823 h, while the total navigation time was 14,706 h. In other words, the navigation time was approximately 50% more than the operation time. As a requirement of purse seine fishing, navigation time is higher than operation time to reach the fishing area and detect shoals. In this respect, reductions in exhaust gas emission values will be possible with technological developments in detecting shoals and some methods that purse seiners will spend less time for navigation. Another study on emissions contributed to marine fishing in China revealed that GHG emissions, which were 16,479 million tons in 2001, increased to 18,601 million tons in 2020, and a significant portion of these GHG emissions is attributed to trawl and purse seine fishing operations [40].

To prevent air pollution produced by ships and take the necessary precautions, the sources causing the pollution should be determined correctly. In the long term, the effect of seemingly small increases in emissions per unit time on general air pollution is quite large. Therefore, the emissions per unit time are important data that can be used for this purpose. In the study, it was concluded that although more than half of the total emissions occurred in the "port condition", the emissions per unit time occurred most in the "navigation condition". Thus, it has been revealed that not only the total emissions but also the emissions per unit time increase with increasing engine power. This result is valuable because it highlights the importance of calculating emissions per unit time.

CO_2 emissions from fishing vessels in 2016 were approximately 207 million tons [6]. In addition, the International Maritime Organization (IMO) 2014 GHG Study stated that 22 million tons of CO_2 were produced globally in 2012 by 22,130 fishing vessels of 100 GT or more. As a result of the estimation made in this study, CO_2 emissions from purse seine fishing vessels in Türkiye were calculated as approximately 432 thousand tons. This accounts for 0.21% of total global CO_2 emissions and 1.96% of IMO's CO_2 emissions from fishing vessels. According to the IMO data, CO_2 emissions per fishing vessel were 994.13 tonnes,

while in this study, CO_2 emission per vessel was calculated as 1227.29 tons. This value is 23.45% higher than the IMO average. While this value is observed to be above the IMO average, when compared to the study conducted by Chassot et al. [41] on purse seine, it appears to be significantly lower than their calculated CO_2 emissions per ship (2077 tonnes).

The estimated emissions for Türkiye were compared with the results of studies in different countries [1,16]. Accordingly, the estimated annual NO_x, SO_x, and CO_2 emissions in Türkiye are 24.05, 57.79, and 25.77 times higher than the annual NO_x, SO_x, and CO_2 emissions of purse seiners in the UK, respectively. Additionally, they are 61.22 and 39.15 times higher than the annual NO_x and SO_x emissions of fishing vessels in the Texas area. One of the main reasons for the large emission difference between Türkiye and the other two countries is that the UK and US waters are largely in the Emission Control Area (ECA) / Sulphur Emission Control Area (SECA) region. This result shows the effectiveness of the ECA/SECA region implementation in reducing air pollution. The expansion of ECA and SECA regions around the world, especially in closed basins with heavy maritime traffic such as the Mediterranean and the Black Sea, can be one of the most effective steps toward reducing global air pollution.

6. Conclusion

Combating air pollution is a serious issue that countries cannot cope with alone and that all countries must deal with in a joint effort. This cooperation becomes even more important when considering emissions from a global industry such as shipping. Therefore, in this study, emissions originating from purse seine fishing vessels in the Black Sea region, which constitute 1.96% of the world's fishing vessel fleet of 100 GT and above, were calculated [32]. As a result of this study, it has been determined that purse seiners in the Black Sea region produce more than 260,000 tons of exhaust emissions per year. This represents approximately 60% of the annual emissions produced by purse seiners only in Türkiye. Considering the fishing activities in the other Black Sea countries, such emissions will be much higher.

To keep exhaust emissions originating from fishing vessels in the Black Sea under regular control, it is essential for riparian countries to work together. For this purpose, the scope of the BAGIS system used in this study can be expanded, and a joint instant monitoring and coordination center can be established with other Black Sea countries.

Because unregistered fishing activities cannot be included in the studies, there is no doubt that the actual emissions are higher than the calculated. Technological developments that will enable instant monitoring of all seas and ships to prevent uncontrolled emissions will be an important step in global emission control.

Approximately 60% of the motorized fishing fleet of 20 m and above in Türkiye are purse seine fishing vessels examined in this study [42]. Similar to this study, studies to be conducted for specific types of fishing vessels and determination of the main emission sources in each type of vessel can serve as a reference for taking precautions specific to vessel types. In addition, studies on new fishing techniques or ship designs that will lead to minimum emissions while providing maximum catch in global fishing activities can also help reduce air pollution from fishing.

The "bottom-up" method used in this study is very useful in emission estimation because it can process data from the AIS system. The use of AIS data in emission calculations allows local determination of emissions. Thus, it can be determined where to focus for emission control. However, the lack of data from AIS devices revealed that AIS devices used on fishing vessels should also be developed and standardized. In addition, the correct processing of the ship's operational status depends on whether the crew on the ship has set the "ship status" setting. For this reason, training the personnel working on the fishing vessels on this subject is also extremely important.

In this study, the estimated emissions produced by purse seiners across Türkiye were calculated as approximately 440,000 tons. The fact that such emissions are quite high compared to the countries in the ECA/SECA region is one of the most important results of the study. As in this study, a comparison of the exhaust emissions produced in the special areas declared as ECA/SECA regions and the other areas can provide a basis for evaluating the effectiveness of the special area implementation.

In terms of future studies; conducting research that encompasses the entire Black Sea region to reveal the emissions caused by purse seiners would be beneficial. Studies can be conducted to estimate emissions based on the working conditions and real data of other types of fishing vessels besides purse seiners, such as trawlers. Comparisons can be made between emissions caused by different types of fishing activities; emissions from surface fishing and deep-sea fishing can be compared. Thus, emission values caused by fishing activities based on different fish species can be evaluated.

Differences in emission levels among fishing vessels are believed to stem primarily from variations in engine power. Therefore, developing a global monitoring system integrated into fishing vessels could enable real-time and simultaneous tracking of GHG emissions from fishing vessels worldwide. This system could serve as an effective resource when determining measures to achieve the IMO's zero-emission goals. By providing real-time monitoring and assessment of emissions from vessels,

it can assist in understanding variations among fishing vessels of different sizes. Such a monitoring system can contribute to supporting sustainability efforts in the maritime industry by facilitating the development of more specific strategies, considering various types of vessels and their engine powers, in pursuit of the IMO's zero-emission goals.

In this study, ship size is equated with ship length. On the other hand, ships intended for deep-sea fishing may prioritize stability and seaworthiness, while fishing ships operating in shallow waters may prioritize manoeuvrability. In this context, future studies may consider characteristics that affect the design and manoeuvrability of ships, such as the ship's beam, ship's length/beam ratio, and total sea surface area, in addition to the ship's length. Thus, optimum ship design ideas that will contribute to reducing GHG emissions can be proposed.

Authorship Contributions

Concept design: E. Özkaya, and Ö. Uğurlu, Data Collection or Processing: E. Özkaya, and Ö. Uğurlu, Analysis or Interpretation: E. Özkaya, Literature Review: E. Özkaya, and A. Y. Kaya, Writing, Reviewing and Editing: E. Özkaya, A. Y. Kaya, F. Tonoğlu, Ö. Uğurlu, and J. Wang.

Funding: The authors declare that no funds, grants, or other support was received during the preparation of this manuscript.

References

[1] J. Coello, I. Williams, D. A. Hudson, and S. Kemp, "An AIS-based approach to calculate atmospheric emissions from the UK fishing fleet." *Atmospheric Environment*, vol. 114, pp. 1-7, Aug 2015.

[2] V. Eyring, et al. "Transport impacts on atmosphere and climate: Shipping." *Atmospheric Environment*, vol. 44, pp. 4735-4771, 2010.

[3] M. Koričan, N. Vladimir, and A. Fan, "Investigation of the energy efficiency of fishing vessels: Case study of the fishing fleet in the Adriatic Sea." *Ocean Engineering*, vol. 286, pp. 115734, Oct 2023.

[4] International Maritime Organization (IMO), "Fourth IMO GHG Study 2020 Executive Summary and Final Report", London, UK, 2020.

[5] N. Olmer, B. Comer, B. Roy, X. Mao, and D. Rutherford, "Greenhouse Gas Emissions From Global Shipping, 2013-2015," in *International Council on Clean Transportation, Washington, DC, USA, 2017*. pp. 1-38.

[6] K. Greer, et al. "Global trends in carbon dioxide (CO_2) emissions from fuel combustion in marine fisheries from 1950 to 2016", *Marine Policy*, vol. 107, pp. 103382, Sep 2019.

[7] H. Lee, H. T. Pham, M. Chen, and S. Choo, "Bottom-up approach ship emission inventory in port of incheon based on VTS data", *Journal of Advanced Transportation*, vol. 2021, pp. 1-16, Apr 2021.

[8] Food and Agriculture Organization of the United Nations (FAO), "The state of world fisheries and aquaculture", 2008.

[9] GEF-UNDP-IMO GloMEEP Project and IMarEST, 2018: Ship Emissions Toolkit, Guide No. 1, Rapid assessment of ship emissions in the national context.

[10] M. Brander, and G. Davis, "Greenhouse gases, CO_2, CO_2e, and carbon: What do all these terms mean", *Econometrica*, White Papers, 2012.

[11] International Maritime Organization (IMO), "Second IMO GHG Study 2009 Executive Summary and Final Report", London, UK, 2009.

[12] Balıkçılık ve Su Ürünleri Genel Müdürlüğü (BSGM), "7. Hamsi Çalıştayı; Anchovy Workshop", Trabzon, Türkiye, 2019.

[13] S. F. Koyun, T. Yıldız, and A. Ulman, "The rich get stronger: the purse seine fishery of the Turkish straits system", *Fishes*, vol. 7(6), pp. 301, 2022.

[14] Trozzi, C., "Emission Estimate Methodology for Maritime Navigation, EMEP/EEA Air Pollutant Emission Inventory Guide Book Technical Report No 9", 2010.

[15] A. Harati-Mokhtari, A. Wall, P. Brooks, and J. Wang, "Automatic identification system (AIS): Data reliability and human error implications." *Journal of Navigation*, vol. 60, pp. 373-389, Aug 2007.

[16] H. M. Perez, R. Chang, R. Billings, and T. L. Kosub, "Automatic Identification Systems (AIS) data use in marine vessel emission estimation", in *18th Annual International Emission Inventory Conference*, vol. 14, pp. 1-17. 2009.

[17] L. Goldsworthy, and B. Goldsworthy, "Modelling of ship engine exhaust emissions in ports and extensive coastal waters based on terrestrial AIS data-an Australian case study." *Environmental Modelling & Software*, vol. 63, pp. 45-60, Jan 2015.

[18] R. A. O. Nunes, M. C. M. Alvim-Ferraz, F. G. Martins, and S. I. V. Sousa, "Assessment of shipping emissions on four ports of Portugal." *Environmental Pollution*, vol. 231, pp. 1370-1379, Dec 2017.

[19] M. Buber, A. C. Toz, C. Sakar, and B. Koseoglu, "Mapping the spatial distribution of emissions from domestic shipping in Izmir Bay." *Ocean Engineering*, vol. 210, 107576, Aug 2020.

[20] S. K. Chang, "Application of a vessel monitoring system to ADVANCE sustainable fisheries management-benefits received in Taiwan." *Marine Policy*, vol. 35, pp. 116-121, 2010.

[21] R. W. Parker, et al. "Fuel use and greenhouse gas emissions of world fisheries." *Nature Climate Change*, vol. 8, pp. 333-337, Apr 2018.

[22] M. Dağtekin, A. C. Gücü, and Y. Genç, "Concerns about illegal, unreported and unregulated fishing, carbon footprint, and the impact of fuel subsidy-An economic analysis of the Black Sea anchovy fishery." *Marine Policy*, vol. 140, pp. 105067, Jun 2022.

[23] M. Winther, J. H. Christensen, M. S. Plejdrup, E. S. Ravn, Ó. F. Eriksson, and H. O. Kristensen, "Emission inventories for ships in the arctic based on satellite sampled AIS data." *Atmospheric Environment*, vol. 91, pp. 1-14, Jul 2014.

[24] Ø. Endresen, et al. "Emission from international sea transportation and environmental impact." *Journal of Geophysical Research: Atmospheres*, vol. 108, pp. 1-17, Sep 2003.

[25] Y. Liu, et al. "emission characteristics of offshore fishing ships in the Yellow Bo Sea, China." *Journal of Environmental Sciences*, vol. 65, pp. 83-91, Mar 2018.

[26] H. Winnes, L. Styhre, and E. Fridell, "Reducing GHG emissions from ships in port areas." *Research in Transportation Business and Management*, vol. 17, pp. 73-82, Dec 2015.

[27] H. Xing, S. Spence, and H. Chen, "A comprehensive review on countermeasures for CO_2 emissions from ships." *Renewable and Sustainable Energy Reviews*, vol. 134, pp. 110222, Dec 2020.

[28] H. B. Şen, "Balıkçı Gemileri İzleme Sistemi (BAGIS)," *tarimorman.gov.tr*, 2017. Available: https://www.tarimorman.gov.tr/BSGM/Lists/Haber/Attachments/79/IBS_BAGIS_HBSEN.pdf [Accessed: 30.06.2022].

[29] M. S. Campbell, K. M. Stehfest, S. C. Votier, and J. M. Hall-Spencer, "Mapping fisheries for marine spatial planning: Gear-specific vessel monitoring system (VMS), marine conservation and offshore renewable energy." *Marine Policy*, vol. 45, pp. 293-300, Mar 2014.

[30] D. Chen, et al. "High-spatiotemporal-resolution ship emission inventory of China based on AIS data in 2014", *Science of The Total Environment*, vol. 609, pp. 776-787, Dec 2017.

[31] Y. H. Kumar, and R. Vijayakumar, "Development of an energy efficient stern flap for improved EEDI of a typical high-speed displacement vessel." *Defence Science Journal*, vol. 70, pp. 95-102, Feb 2020.

[32] International Maritime Organization (IMO), "Third IMO Greenhouse Gas Study 2014", London, UK, 2015.

[33] European Environment Agency (EEA), "EMEP/EEA Air Pollutant Emission Inventory Guidebook 2016: technical guidance to prepare national emission inventories". EEA-Report, 21, Copenhagen, Denmark, 2016.

[34] Balıkçılık ve Su Ürünleri Genel Müdürlüğü (BSGM), Balıkçılık ve Su Ürünleri Genel Müdürlüğü, General Directorate of Fisheries and Aquaculture, Ankara, Türkiye, 2021.

[35] A. Demirci, and M. Karagüzel, "The evaluation of fishing vessels fuel consumption and pollutions emissions in the İskenderun Bay." *Fresenius Environmental Bulletin*, vol. 27, pp. 508-514, 2018.

[36] C. Ay, A. Seyhan, and E. B. Beşikçi, "Quantifying ship-borne emissions in Istanbul Strait with bottom-up and machine-learning approaches." *Ocean Engineering*, vol. 258, pp. 111864, Aug 2022.

[37] S. K. Song, and Z. H. Shon, "Current and future emission estimates of exhaust gases and particles from shipping at the largest port in Korea." *Environmental Science and Pollution Research*, vol. 21, pp. 6612-6622, Feb 2014.

[38] J. W. Kwon, S. Yeo, and W. J. Lee, "Assessment of shipping emissions on Busan Port of South Korea", *Journal of Marine Science and Engineering*, vol. 11, pp. 1-18, Mar 2023.

[39] P. De Meyer, F. Maes, and A. Volckaert, "Emissions from international shipping in the Belgian part of the North Sea and the Belgian Seaports." *Atmospheric Environment*, vol. 42, pp. 196-206, Jan 2008.

[40] Y. Xu, J. Lin, B. Yin, P. Martens, and T. Krafft, "Marine fishing and climate change: A China's perspective on fisheries economic development and greenhouse gas emissions." *Ocean & Coastal Management*, vol. 245, pp. 1-11, Nov 2023.

[41] E. Chassot, et al. "Fuel consumption and air emissions in one of the world's largest commercial fisheries." *Environmental Pollution*, vol. 273, 116454, Jan 2021.

[42] Balıkçılık ve Su Ürünleri Genel Müdürlüğü (BSGM), "Su Ürünleri İstatistikleri", Balıkçılık ve Su Ürünleri Genel Müdürlüğü, Fisheries Statistics, General Directorate of Fisheries and Aquaculture, Ankara, Türkiye, 2018.

Journal of ETA Maritime Science 2024;12(2):169-185

Decision-Making for Shipping Networks Based on Adaptive Cumulative Prospect Theory: A Case Study in Vietnam

Yen Thi Pham[1], Ngoc Cuong Truong[1], Phung Hung Nguyen[2], Hwanseong Kim[1]

[1]National Korea Maritime & Ocean University, Department of Logistics, Busan, South Korea
[2]Ho Chi Minh City University of Transport, Maritime Academy, HCM, Ho Chi Minh City, Vietnam

Abstract

This paper proposes an optimal method designed for use in a real-life situation to deal with port route choice decisions for evaluating and aggregating the daily net profit for liner shipping services to assist shipping lines in making optimal decisions under risk in the choice of the optimal route with the highest average daily profit for container liner shipping under the following un-certain combination factors: Freight rate, shipment demand, and fuel oil price. A cumulative prospect theory approach considers the decision-maker's attitude to describe decision-making under uncertainty applicable for any number of consequences to calculate the daily net profit model for container vessels. The results are compared with benchmark methods such as expected utility theory. This paper includes an application of the proposed approach to Hai An container shipping lines in Vietnam in 2022. Furthermore, adaptive parameters are presented to improve a model's performance when data distribution varies over time or across different contexts. The results show that the larger the adaptive parameter, the higher the daily profit, but the growth rate diminishes. The findings suggest that the Hai Phong-Ho Chi Minh route emerges as the safest with the least effect and the lowest variation in cumulative prospect value of daily profit. The Hai Phong (HP)-Tan Cang Cai Mep (TCIT)-Ho Chi Minh (HCM)-Hai Phong route is recommended as the most effective and economically favorable strategy for managers seeking the highest cumulative daily profit. This paper not only explains that the actual calculated results align with decision makers' behavior, such as risk aversion, decision makers who prioritize stability are inclined to choose options or strategies that offer a higher level of certainty, even if it means foregoing higher profits, but also provides a practical and easy-to-apply method for choosing a shipping network.

Keywords: Adaptive cumulative prospect theory, Cumulative prospect theory, Daily profit model, Decision-making, Shipping network

1. Introduction

For many years, containerized trade has been recognized as the fastest growing and critically important segment of maritime trade. To adapt to the growth of maritime trade, shipping companies are increasingly prioritizing routes to optimize their network, promote higher quality service, profit, and competitive advantage, and meet customer demands. However, decision making in the shipping network is challenging due to a complex operating landscape fraught with risk and uncertainty combined with disruptions and unprecedented problems [1]. These complexities make decision-making in the shipping network necessary to help manage efficiently and choose the optimal network. In addition, container carriers, faced with challenges of increased costs, make a strategic decision to reroute to alternative ports of call to seek greater profitability. Route choice models are essential tools for decision makers to identify the best strategies to improve efficiency and enhance the network's overall sustainability as well as adapt to the rapidly changing maritime industry.

There are a few methods that can be used to support decision making, including cost-benefit analysis (CBA) [2], SWOT analysis [3], multiple criteria decision making [4,5], Pareto analysis [6], Analytical Hierarchy Processes [7,8], TOPSIS [3], and game theory [9]. Programs and algorithms are too complex and difficult for many decision makers [10]. In addition, they often lack a reflection of the complexity of human psychology in decision making when faced with

Address for Correspondence: Hwanseong Kim, National Korea Maritime & Ocean University, Department of Logistics, Busan, South Korea
E-mail: kimhs@kmou.ac.kr
ORCID ID: orcid.org/0000-0002-5074-6623

Received: 04.08.2023
Last Revision Received: 04.03.2024
Accepted: 25.03.2024

To cite this article: Y. T. Pham, N. C. Truong, P. H. Nguyen, and H. Kim. "Decision-Making for Shipping Networks Based on Adaptive Cumulative Prospect Theory: A Case Study in Vietnam." *Journal of ETA Maritime Science*, vol. 12(2), pp. 169-185, 2024.

choices under risk and uncertainty. Traditional methods, such as expected utility theory (EUT), have numerous applications across a range of fields, including economics, agriculture, finance, psychology, and management [11]. Nevertheless, the EUT has some limitations when assuming that decision makers are rational [12-14]. In contrast, decision-making is a complex process, and decision-makers are influenced by risk and uncertainty factors; involving their past experiences, emotions, and the way choices are framed [13]. Cumulative prospect theory (CPT) overcomes EUT's deficiencies and considers perception bias of diminishing sensitivity, probability weighting, risk-seeking, loss aversion, source dependence, and preference reversals [13,15]. Therefore, this paper proposes an average daily profit model with uncertain combination factors influencing shipping route choice behavior by applying CPT [13].

Many studies have looked into liner shipping network problems from network design and fleet deployment, with the objective being to determine the ports that the ship should call and the sequence in which they should be visited to maximize profits or minimize costs [16]. A set-partitioning approach involves generating all conceivable shipping service routes and consolidating individual shipping routes into multiple routes if possible [17]. A previous paper investigated the influence of the environment on speed and fuel oil consumption; the findings expressed that strategically utilizing ocean currents in routing could decrease the yearly fuel expenses of both the US and global commercial fleets by $10 million and $70 million, respectively [18]. Various sources of uncertainty, such as political factors, international trade volume, bunker price, freight rate, shipbuilding and chartering costs, interest rates, and currency exchange rates, pose significant challenges and should be considered in the decision-making on shipping networks [16].

The main contributions of this paper include the following: first, the development of a daily profit model for container shipping lines based on the fluctuation of the season in shipping market demand from an easier method approach is the decision tree; second, the presentation of a method that is relatively easy to implement in real life for decision-makers in liner shipping when facing selection under uncertainties from the CPT approach in choosing the optimal route to achieve the highest profit; third, bringing an entire horizon about liner shipping company's psychology bias, their preference in decision-making.

The rest of this paper is organized as follows. Section 2 provides a review of the existing literature on shipping network choice. The system modeling and methodology are proposed in section 3 to evaluate the daily business effectiveness in container operation. Section 4 presents an empirical study of Vietnam. Adaptive CPT is then deployed to an empirical study, and the results are analyzed. Finally, section 5 provides the conclusions.

2. Literature Review

2.1. Decision Making for the Shipping Network

Shipping networks have a long research history in the maritime industry and cover a wide range of topics, including network design, route optimization, fleet management, and strategic planning from economic, strategic tactical, and operational perspectives. Decision making in liner shipping can be divided into three different levels: strategic, tactical, and operational planning levels [19]. Liner shipping networks are designed to match the requirements of customers and consider their own operational costs. Several ship routing and scheduling studies have been conducted, and a significant number of comprehensive reviews about ship routing can be found in [16,20,21] that are referred for a review of shipping network problems.

Most of the existing research on shipping networks has considered the network design problem to minimize costs or maximize profits that highlight uncertainty factors such as container shipment demand, uncertain port time, uncertain wait time, and uncertain container handling time [22-25]. Almost all studies concentrated on optimization techniques that are often applied to determine the optimal shipping network for shipping lines. A dynamic cost-based model can assist in choosing the optimal system for serving particular trade routes with known trade requirements for providing liner services, with the goal of minimizing overall expenses [26]. Another study demonstrated the theme of container liner shipping networks, and a mixed-integer linear programing model was proposed to develop the design problem for the intermodal liner shipping service network [27]. A linear programing model to minimize the total operating and lay-up costs for the fleet [28]. A method for scheduling containerships in a liner shipping network was introduced using a mixed-integer linear programing model that can be efficiently solved by CPLEX for real-world shipping activities connecting Asia, Europe, and Oceania [29]. Another study on the liner ship route was designed under the assumption that the container shipment demand was not a precise value but rather a fuzzy number was performed by [30]. However, optimization techniques not only make decision makers encumbered but also psychological factors such as decision makers' behavior can be ignored.

There are not many studies on decision-making for choosing a route, networks, and maritime networks to perform from various approaches including AHP, TOPSIS, CBA, SWOT, Fuzzy Delphi, Fuzzy ELECTRE I method, and game theory [3,5,7,8]. An analytic hierarchy process multi-criteria decision-making methodology that could optimize the supply chain

delivery network by considering not only qualitative but also quantitative factors was performed [3,9]. CBA is used to assess the profitability of maritime networks for shipping companies to achieve greater efficiency and sustainability in short shipping networks [31]. Another study developed a game theory model for resolving route choices in intermodal transport networks with the aim of decreasing transport costs for carriers who are adopted as rational players [9]. In these studies, the definition of rational decision making has not been clearly defined [9]. In actuality, as mentioned above, decision making has some limitations. Decision making is a rational view with many limitations and criticisms. Therefore, this study focuses on irrational decision-making to reflect reality in the psychology of decision-making behavior.

2.2. Cumulative Prospect Theory Application to Shipping Networks

Numerous studies have been dedicated to several fields like designing and selecting product concepts [32], location selection of emergency rescue centers [33], charging mode for electric vehicles [34], Grey Multi-attribute Emergency Decision-Making Method for Public Health Emergencies [35], decision-making of investment in navigation safety improving schemes [36], and the path selection model of emergency logistics [37]. Published studies related to the CPT application are presented in Table 1.

There has been limited investigation into the adaptation of optimization techniques in ship routing under uncertainty. Chen (1978) created an adaptive optimization approach called "open-loop feedback", in which a ship's route is changed based on deterministic factors when updated information indicates that environmental conditions are significantly different from the initial estimates. In this study, the method used is primarily deterministic in nature and does not incorporate an explicit representation of uncertainty and does not consider decision-makers' psychological factors [38].

This paper proposes an adaptive approach to CPT in which a decision maker's behavior is irrational for liner shipping that distinguishes itself from previous research. This paper aims to fill the research gaps on decision-making in shipping networks by providing a model to calculate daily voyage profit from the viewpoints of CPT that consider the complexity of psychology when people face an uncertain situation.

3. Methodology

This study proposes a daily profit model based on the cumulative prospect approach of daily profit equal to the resulting daily revenue minus daily cost.

3.1. Model Formulation

3.1.1. Notation

c^t: total cost of the round voyage;

r^t: total revenue of the round voyage;

pr^d: daily profit of the round voyage;

j: index of port: $j = \overline{1,n}$;

gr: vessel gross tonnage in GT;

c^{bun}: total bunker expenses for the round voyage;

d_z: distance between port o and e in leg $z(z \in Z)$ of round route;

v_z^{as}: average sailing speed on a round voyage (knots);

c_z^{hc}: cargo handling cost on the leg $z(z \in Z)$ of round route;

c_z^{ts}: the transshipment service cost on the leg $z(z \in Z)$ of round route;

q_z^{ts}: transshipment volume in TEU via two ports on the leg z $(z \in Z)$;

u_z^{ts}: transshipment unit price in USD via two ports on the leg $z(z \in Z)$;

c_z^{pc}: port charges on the leg $z(z \in Z)$ of round route;

c_z^{inv}: inventory cost on the leg $z(z \in Z)$ of round route;

c_z^{cmm}: commission fees on leg $z(z \in Z)$ of round route;

c_z^{br}: broker fees on the leg $z(z \in Z)$ of round route;

c^{oth}: other cost of the round route (USD)

c^{dv}: daily running cost of a vessel (USD/day)

Table 1. *Summary of the literature review of the cumulative prospect theory approach*

Article	Key finding	Method
[32]	Designing and selecting product concepts	QFD and the cumulative prospect theory
[33]	Location selection of the emergency rescue centers	Pythagorean fuzzy multi-attribute decision-making evaluation method and CPT
[34]	Charging mode for the electric vehicle	CPT
[35]	Grey multi-attribute emergency decision-making method for public health emergencies	Interval gray grey number method, CPT, and AHP
[36]	Decision-making in navigation safety improvement schemes	CPT, linear programing model, and projection method data
[37]	Path selection model of emergency logistics	CPT
CPT: Cumulative prospect theory		

3.1.2. Objective function

This section presents the cumulative prospect value function of the average daily profit as the objective function to support decision making. The average daily profit is calculated by the profit earned from the voyage divided by the total time (days) spent on the round voyage. In this paper, it means that the daily profit is earned before interest and tax. The daily profit function is proposed in Equation (1), and the more detailed components are rewritten in Equation (2).

$$pr^d = \frac{r^t - c^t}{t^{tcv}} \quad (1)$$

$$pr^d = \frac{\sum_{kxy}\sum_{xyz}(fr_z^k q_z^k) - (c^{crc} + c^{bun} + \sum_{xyz} c_z^{pc} + \sum_{xyz} c_z^{ts} + \sum_{xyz} c_z^{cnm} + c^{ocl})}{t^{tcv}} \quad (2)$$

Where the first term on the numerator of (2) is the total revenue of the round voyage; the second term is the total cost of the round voyage.

Tversky and Kahneman [13] improved the prospect theory in 1992; the cumulative prospect value (*CPV*) is calculated by accumulating losses and gains. *CPV* values indicate preferences for choices and should be positive. If the value between two choices is negative, the preference for choice is the one that brings the least loss. It is possible to obtain the cumulative prospect values of the average daily profit using Equation (3).

$$CPV(pr^d) = \sum_{i=1}^{m} v^-(pr_i^d)\pi^-(p_i) + \sum_{i=1}^{m} v^+(pr_i^d)\pi^+(p_i) \quad (3)$$

Where $v^-(pr_i^d)$, $v^+(pr_i^d)$ denote prospect value for gains and losses, respectively, which are illustrated by the value function as Equation (4):

$$v(pr_i^d) = \begin{cases} (pr^d)^\alpha \text{ if } pr^d \geq 0 \\ -\lambda(-pr^d)^\beta \text{ if } pr^d < 0 \end{cases} \quad (4)$$

In the above formula, the median exponent of the value function was $\alpha = \beta = 0.88 < 1$ in accordance with diminishing sensitivity; it is convexity in losses and concave in gains. The loss aversion coefficient $\lambda = 2.25 > 1$ could explain individual risk aversion level, which means that an individual perceives loss 2.5 times more than gain, and the graph of losses is steeper than gains. $\pi^+(p_i)$, $\pi^-(p_i)$ are considered crucial elements of prospect theory are the probability weighting function for gains and losses, respectively, by Equations (5), and Equation (6).

$$\pi^+(p_i) = \frac{p_i^\delta}{[p_i^\delta + (1-p_i)^\delta]^{1/\delta}} \quad (5)$$

$$\pi^-(p_i) = \frac{p_i^\theta}{[p_i^\theta + (1-p_i)^\theta]^{1/\theta}} \quad (6)$$

Where δ=0.61, θ = 0.69 are the prospect parameters that indicate the risk-taking attitudes of decision makers [13]. p is the stated probability for the result to i. To improve the performance of a model in situations where the distribution of the data changes over time or across different contexts, a parametric parameter was proposed. In other words, it involves modifying the values of the model's parameters to better fit the new data. This term refers to the process of adjusting the parameters of a mathematical or statistical model based on new data. Therefore, we propose adaptive weighting functions for gains and losses, respectively, as Equations (7), and (8) below:

$$\hat{\pi}^+(p_i) = \frac{p_i^{0.61+\sigma_1}}{[p_i^{0.61+\sigma_1} + (1-p_i)^{0.61+\sigma_1}]^{1/(0.61+\sigma_1)}} \quad (7)$$

$$\hat{\pi}^-(p_i) = \frac{p_i^{0.69+\sigma_2}}{[p_i^{0.69+\sigma_2} + (1-p_i)^{0.69+\sigma_2}]^{1/(0.69+\sigma_2)}} \quad (8)$$

Where $\hat{\pi}^+(p_i)$ and $\hat{\pi}^-(p_i)$ are adaptive parameters that are automatically updated using the gains and loss function. $\sigma_1 = \mu_1 p(fr_i^{sd}) p_i^{FO}$, $\sigma_2 = \mu_2 p(fr_i^{sd}) p_i^{FO}$; μ_1, μ_2 and are the positive parametric adaptation coefficients in gains and losses, respectively, that are used to update parameters for δ and θ.

3.1.3. Revenue function

Now determine the voyage revenue function as resulting from the component sea freight. Revenue is mainly obtained from container transportation. In reality, shipping companies can earn revenue from document, seal, container cleaning, and container repair fees. However, these revenues are considered to be able to cover various costs, including inventory and container repair costs. Assume that the shipment demand in each of the high, medium, and off-seasons accounts for d_1, d_2, and d_3, respectively (noted that $d_1 + d_2 + d_3 = 100\%$). Liner shipping companies often re-decide the freight rate depending on the market supply and demand estimated as well as the change in fuel oil price and the change in services tariffs. Assume that the freight rate is adjusted to increase or decrease together for all. When the season comes, if the shipment demand increases, the freight rate also rises, and on the other hand, if the shipment demand decreases, the freight rate will also go down.

Assume that the customer type x has shipment demand probability container type k in season y on the leg z is d_z^{kxy} satisfied with condition $\sum_{x\in X} d_z^{kxy} = 1$. r^t is total revenue obtained from the round voyage and is expressed as Equation (9) below:

$$r^t = \sum_{x\in X}\sum_{y\in Y}\sum_{z\in Z}\sum_{k\in K}(fr_z^{kxy} q_z^{kxy} d_z^{kxy}) \quad (9)$$

Where fr_z^{kxy} the freight rate of k -type container ($k \in K$) is applied for x - type customer ($x \in X$) in the season y ($y \in Y$) on the leg z ($z \in Z$); q_z^{kxy} indicates volume of container type k ($k \in K$) is transported for customer type x ($x \in X$) in the season y ($y \in Y$) on the z ($z \in Z$).

Routing depends on the strategies of shipping lines and the shipment demand of shippers for specific seasons. To respond to these fluctuations in demand, tactical decision making is necessary, and it typically involves planning every 3-4 months. This ensures that companies can adapt to changes in demand and make informed decisions accordingly [39]. Therefore, accept the argument that the shipment demand is determined in a year and is divided into three ranges with different probabilities: off-season, high season, and medium season. Off-season refers to the period of lowest demand, during which the freight rate is lower than in other seasons. Relating to the high season, the shipment demand surges to higher levels, and the container freight rates also increase and events escalate and reach highs. Various factors can cause high demand, including container shortages, port congestion, and delays. The length of this high-demand period can vary and is dependent on a range of factors [40]. Assume that the shipment demand in each of the high, medium, and off-seasons accounts for d_1, d_2, and d_3, respectively (noted that $d_1 + d_2 + d_3 = 100\%$). Liner shipping companies often re-decide the freight rate depending on the market supply and demand estimated as well as the change in fuel oil price and the change in services tariffs. Assume that the freight rate is adjusted to increase or decrease together for all. When the season comes, if the shipment demand increases, the freight rate also rises, and on the other hand, if the shipment demand decreases, the freight rate will also go down.

Normally, in liner shipping companies, sea freight rates are classified into several customer groups depending on the shipment volume and frequency of service use. It can be called customer policy, price policy, or price strategy and can be adjusted flexibly by surcharges. Adopt the assumption that there are three groups of customers, meaning that the liner shipping company has three ranges of the freight rate. The probability of shipment volume is estimated including occasional customers is r_1 (%), the regular customer is r_2 (%), and the contractual customers is r_3 (%), in where $r_1 + r_2 + r_3 = 100\%$. Note that in each season, the probability of shipment for each customer group is stable. In addition, it should be noted that this work mainly concentrates on the method to support decision making; hence, it assumes that the weight of shipment demand d_1 ($i = \overline{1,3}$) and r_i ($i = \overline{1,3}$) is fixed for each voyage and season. Therefore, in the case where shipment demand is d_1, obtained revenue equals the sum of revenue from group customer 1 in which freight rate is fr_{11}, group customer 2 with freight rate is fr_{12}, and customer 3 with freight fr_{13}. A decision tree is proposed to select the optimal route from the planned set of alternatives.

The decision tree is deployed as shown in Figure 1. As mentioned above, the sea freight rate is also arranged by clusters of seasons and customers. From n scenarios of total cost and three probabilities of shipment demand. This study presents 3n probabilities of average daily profit called consequences.

3.1.4. Cost function

Total cost components are proposed, including [41]: Vessel running costs, bunker costs; port dues; liners costs such as administration, agency fees, brokerage, and other costs. In this study, terminal handling charges (THC) are considered to be the responsibility of payment by the shipper; therefore, in this study, terminal handling costs will not be considered and were eliminated from the shipping line's cost model in Equation (10).

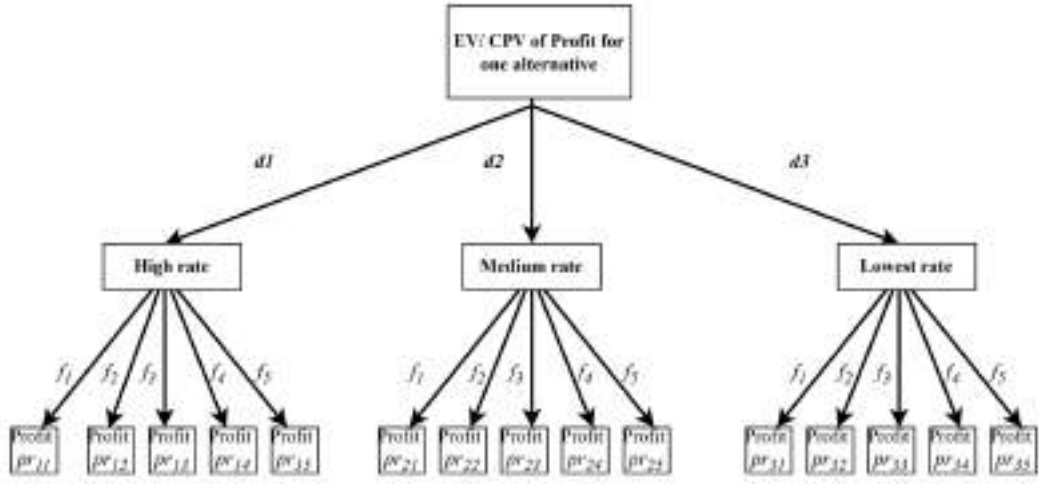

Figure 1. *Decision tree for one alternative in a case study*

$$c^t = c^{trc} + c^{bun} + \sum_{z\in Z} c_z^{pc} + \sum_{z\in Z} c_z^{ts} + \sum_{z\in Z} c_z^{cmn} + c^{otk} \quad (10)$$

Port dues include tonnage, navigation, pilotage, berth, tugboat, mooring/unmooring, quarantine, anchorage, customs declaration, clearance, and canal tolls, if any. Port dues in port j is described as Equations (11) and (12).

$$c_j^{pc} = c_j^{ton} + c_j^{nav} + c_j^{plt} + c_j^{ber} + c_j^{tug} + c_j^{m/u} + c_j^{qrt} + c_j^{anc} + c_j^{d} + c_j^{c} \quad (11)$$

$$= r_j^{ton} gr + r_j^{nav} d_j^{nav} gr + d_j^{plt} r_j^{plt} gr + r_j^{ber} d_j^{ber} gr + n^{tug} hp_j^{tug} r_j^{tug} + c_j^{m/u} + c_j^{qrt} + c_j^{anc} + c_j^{d} + c_j^{oc} + c_j^{cl} + c_j^{c} \quad (12)$$

The above addition notations are explained as follows:

r_j^{ton}: tonnage due rate in USD/GT in port j is built for each tonnage group of vessels and at the berth or at the lifebuoy;

r_j^{nav}: navigation rate in USD/GT is calculated on the basis of gross tonnage for each nautical mile;

d_j^{nav}: the distance in nautical miles when the vessel travels through the navigable port j;

r_j^{plt}: pilot rate in USD per ton per nautical mile in port j;

d_j^{plt}: the distance in nautical when the vessel is assisted in navigating through a complex waterway by port authority service when a vessel enters or leaves the port j;

r_j^{ber}: daily berth rate in USD per day is charged per day for the use of the berth;

d_j^{ber}: number of days in the berth;

n^{tug}: number of tugboats used to support the ship in entering and leaving the port j safety;

hp^{tug}: tugboat measurement of power in horse power;

r^{tug}: tugboat rate in USD per hour charged on the basis of the vessel's gross tonnage per hour;

$c_j^{m/u}$: mooring/unmooring price in USD in port j;

c_j^{qrt}: quarantine, disinfection fees in USD port j;

c_j^{anc}: anchorage dues in USD charged by port authorities for the use of anchorage facilities in port j;

c_j^{d}: customs declaration fees in USD that are charged by custom authorities for processing the declaration of goods being imported or exported in port j;

c_j^{cl}: clearance fees in USD in port j;

The total running cost (USD) is determined by multiplying the total number of days spent on the round voyage by the average daily running cost (c^{dv}). It includes wage and insurance expenses incurred by crews and administration; maintenance costs (inspections, repairs…); cost of insurance like hull and machinery insurance; protection and indemnity insurance (P&I insurance); and war risk insurance. Equation (13) is used to calculate the total running cost per voyage:

$$c^{trc} = c^{dv} t^{tcv} \quad (13)$$

Now consider the bunker cost in USD for the round voyage. Bunker cost is the expense of consumption that is spent on vessels at sea and in port. Bunker cost is influenced by various factors, including the vessel's speed, the duration of time the vessel is in port or at sea, the distance of the voyage leg, the price of the bunker, and the exchange rate if purchasing bunker fuel using foreign currency. For simplification, this paper only considers two major bunkers: diesel and fuel oil cost, and other factors are neglected and given by Equation (14):

$$c^{bun} = s^{tcv} \sum_{i=1}^{n} f_i^{fo} c_i^{fo} + t^{tcv} f^{do} c^{do} \quad (14)$$

Where: s^{tcv}indicates sailing time at sea, f^{fo}presents average daily fuel oil consumption in tons per day; f^{do}shows average diesel oil consumption per day in tons per day; $c^{fo}$is fuel oil price in USD/ton; and c^{do}: diesel oil price in USD/ton. As mentioned above, the range of fuel oil prices is divided into n clusters with the probabilities are $f_i^{fo}$and the fuel oil cost is, $\sum f_i = 1, (i = \overline{1,n}$, nis the number of range fuel oil price).

If there is no direct route from the origin to the destination, containers can be transshipped. The total transshipment cost is illustrated in Equation (15).

$$\sum_{z\in Z} c_z^{ts} = \sum_{z\in Z} (q_z^{ts} u_z^{ts}) \quad (15)$$

In this paper, "other cost" refers to other cost components such as equipment charges, liner management charges, and carrier insurance and claims that are estimated as a percentage of revenue or sea freight.

3.1.5. Total time function

Total time (days) spent on a round voyage includes total sailing time and total port time spent on the round voyage and can be expressed as the following equation:

$$t^{tcv} = \frac{\sum_{z\in Z} d_z}{24 v^{as}} + 2\sum_{j=1}^{n} m_j^{f} + \sum_{j=1}^{n} \left(\frac{q_j^{l}}{r_j^{l}} + \frac{q_j^{d}}{r_j^{d}}\right) \quad (16)$$

The initial value on the right side of Equation (16) is the total sailing time at sea on the round voyage; the second term shows the total maneuver time in all ports of call of the round voyage, including the time spent on embarking and disembarking port; the third term indicates the total time for cargo handling works on the round voyage consisting of loading and unloading in all ports of call of the round voyage. Where: 24 is the number of hours per day; $r_j^{l}$is rate of loading in port j (TEU/day); and r_j^{d}represents the rate of discharging in port j (TEU/day); q_j^{l}shows the volume of

cargo in TEU loaded in port *j*; and q_j^dindicates volume of cargo discharged in port *j* (TEU).

3.2. Methodology

This paper focuses on the route decision-making problem for container liner shipping facing uncertain shipment demand, fuel oil price, and freight rate. In the framework of this paper, we assumed that the variable factors affecting the results of daily average profit are divided into ranges of probabilities. The round route between port *m* and *n* consists of predetermined and unchanging sailing distances and sailing times for each leg. The daily vessel cost of containerships is established and remains constant. Other periodic and unexpected costs are disregarded. Moreover, the vessel is assumed to be parallel, to follow the same route, and to have a capacity that is adapted to transport demand. This work aims to consider a container transportation network that involves not only direct routes but also combines with transshipment, which may help shipping lines save time and increase their ability to turn around. For simplicity, the carrier's empty containers are not considered in this study. To simplify the process by assuming that does not consider other variation factors. Argue that the Break Even Point is the reference point in the model. This means that at the reference point, total revenues equal total costs, and on the other hand, in the case of the model, the outcome is the average daily profit, and the reference point at a daily profit equals zero (0). If the average daily profit is better than 0, then gains and vice versa are losses.

This paper refers to the calculation steps introduced by Gungor and Barlas [10]. Table 2 shows a visual representation of the calculation sequence. First, fill in the column "pr_i^d" vessel's daily profit (consequences) and arrange from the top to the bottom in ascending order. The consequences are arranged in ascending order from top to bottom to adhere to the CPT. The lowest value of the outcome is listed at the top of the column, and the highest value is listed at the bottom. An average daily profit less than 0 is distinguished by the column number "no" marking the sequence number with a negative sign. In this table, assume that there are five values of daily profit that are negative. Group the freight rate and estimate the probability $p(fr_i^{sd})$, next, classify and estimate the probability of fuel oil price p_i^{FO}can be referenced in Table 3 for a case study. On the table of order of operation, assume that there are three probability clusters of freight rate and five probability clusters of fuel oil price. The probability of each scenario is calculated by $p_i = p(fr_i^{sd})p_i^{FO}$. The expected values of the consequences of each alternative are calculated using: $EV = \sum_{i=1}^{n}[p_i(\frac{r_i{}^t - c_i{}^t}{t^{tcv}})]$ and recorded in the column labeled "$EV(pr_i^d)$". The sum of all values of consequences is shown in the row labeled "Total". The prospect value of outcomes is recorded in the column labeled $v(pr_i^d)$ by using Equation (4). The probabilities of gains and losses are shown in the column labeled "cp_i" which is calculated cumulatively p_i from top to bottom for losses and from bottom to top for gains. Then, we demonstrate the probability transformation of cumulated probabilities by Equation (7) for gains and Equation (8) for losses. The column labeled "dcp_i^{trf}" is described by multiplying the accumulated probabilities. The obtained results from $v(pr_i^d)dcp_i^{trf}$is referred to as the cumulative prospect value, which is recorded in the "*CPV*" column. The sum of all CPT values for the consequences of each alternative is given in the row labelled "Total".

4. A Case Study in Vietnam

4.1. Current Status of the Shipping Network in Vietnam

In Vietnam, the form of container transport began to develop in the early 1990s. There are some shipowners who have many years of experience, such as Gemadept, Vinafco, Vinalines. Others have just been established in recent years, including Viet Sun, Viconship, Hai An, and GLS. In where, Hai Phong to Ho Chi Minh and vice versa is well-known as the bustle and dynamic container shipping route that attracted almost all container shipping lines. Other operating routes include Hai Phong - Da Nang - Ho Chi Minh - Hai Phong and Hai Phong - Ho Chi Minh - Tan Cang Cai Mep - Hai Phong. Several companies, such as East Sea, Gemadept, and Vinalines, operate feeder routes to transshipment ports located in the region, such as Singapore, Hong Kong, and Port Klang. At present, Vietnam has approximately 10 domestic container shipping companies, which primarily operate on the North Central South route, as well as some short routes within Southeast Asia and Northeast Asia.

The most popular Vietnam sea freight destinations are Hai Phong, Da Nang, Sai Gon, and Vung Tau ports. TCIT and VICT are two of the five largest terminals in the Ho Chi Minh - Ba Ria Vung Tau port. VICT is authorized to operate as a 40-year joint venture, which involves Southern Waterborne Transport Corporation (SOWATCO) of Vietnam and MITORIENT, a Singaporean company. MITORIENT holds a majority stake of 63% as part of a partnership with Japan's Mitsui & Co and the CMA CGM Group, while SOWATCO holds the remaining 37% of the company's shares [42]. Tan Cang-Cai Mep International Terminal Co., Ltd (TCIT) is a company formed through a partnership between Saigon Newport Corporation and Mitsui O.S.K. Lines (Japan), Wan Hai Lines (Taiwan), and Hanjin Transportation (Korea) [43]. The percentage of cargo throughput in Vietnam's major ports in 2022 is presented in Figure 2.

Table 2. *Order of operations*

No	pr_i^d	$v(pr_i^d)$	$p(fr_i^{sd})$ (%)	p_i^{FO} (%)	p_i (%)	cp_i (%)	cp_i^{trf} (%)	dcp_i^{trf} (%)	CPV	EUV(pr_i^d)
-1	pr_1^d	$-2.25(-pr_1^d)^{0.88}$	$p(fr_1^{sd})$	p_1^{FO}	$p(fr_1^{sd})*p_1^{FO}$	p_1	$\frac{cp_1^{0.69}}{[cp_1^{0.69}+(1-cp_1)^{0.69}]^{0.69^{-1}}}+\hat{\sigma}_1$	cp_1^{trf}	$v(pr_1^d)*dcp_1^{trf}$	$pr_1^d*p_1$
-2	pr_2^d	$-2.25(-pr_2^d)^{0.88}$	$p(fr_1^{sd})$	p_2^{FO}	$p(fr_1^{sd})*p_2^{FO}$	p_1+p_2	$\frac{cp_2^{0.69}}{[cp_2^{0.69}+(1-cp_{12})^{0.69}]^{0.69^{-1}}}+\hat{\sigma}_2$	$cp_2^{trf}-cp_1^{trf}$	$v(pr_2^d)*dcp_2^{trf}$	$pr_2^d*p_2$
-3	pr_3^d	$-2.25(-pr_3^d)^{0.88}$	$p(fr_1^{sd})$	p_3^{FO}	$p(fr_1^{sd})*p_3^{FO}$	$p_1+p_2+p_3$	$\frac{cp_3^{0.69}}{[cp_2^{0.69}+(1-cp_{23})^{0.69}]^{0.69^{-1}}}+\hat{\sigma}_3$	$cp_3^{trf}-cp_2^{trf}$	$v(pr_3^d)*dcp_3^{trf}$	$pr_3^d*p_3$
-4	pr_4^d	$-2.25(-pr_4^d)^{0.88}$	$p(fr_1^{sd})$	p_4^{FO}	$p(fr_1^{sd})*p_4^{FO}$	$p_1+p_2+...+p_4$	$\frac{cp_4^{0.69}}{[cp_3^{0.69}+(1-cp_4)^{0.69}]^{0.69^{-1}}}+\hat{\sigma}_4$	$cp_4^{trf}-cp_3^{trf}$	$v(pr_4^d)*dcp_4^{trf}$	$pr_4^d*p_4$
-5	pr_5^d	$-2.25(-pr_5^d)^{0.88}$	$p(fr_1^{sd})$	p_5^{FO}	$p(fr_1^{sd})*p_5^{FO}$	$p_1+p_2+...+p_5$	$\frac{cp_5^{0.69}}{[cp_5^{0.69}+(1-cp_5)^{0.69}]^{0.69^{-1}}}+\hat{\sigma}_5$	$cp_5^{trf}-cp_4^{trf}$	$v(pr_5^d)*dcp_5^{trf}$	$pr_5^d*p_5$
6	pr_6^d	$(pr_6^d)^{0.88}$	$p(fr_2^{sd})$	p_1^{FO}	$p(fr_2^{sd})*p_1^{FO}$	$p_{15}+p_{14}+...+p_6$	$\frac{cp_6^{0.61}}{[cp_6^{0.61}+(1-cp_6)^{0.61}]^{0.61^{-1}}}+\hat{\sigma}_6$	$cp_6^{trf}-cp_7^{trf}$	$v(pr_6^d)*dcp_6^{trf}$	$pr_6^d*p_6$
7	pr_7^d	$(pr_7^d)^{0.88}$	$p(fr_2^{sd})$	p_2^{FO}	$p(fr_2^{sd})*p_2^{FO}$	$p_{15}+p_{14}+...+p_7$	$\frac{cp_7^{0.61}}{[cp_7^{0.61}+(1-cp_7)^{0.61}]^{0.61^{-1}}}+\hat{\sigma}_7$	$cp_7^{trf}-cp_8^{trf}$	$v(pr_7^d)*dcp_7^{trf}$	$pr_7^d*p_7$
8	pr_8^d	$(pr_8^d)^{0.88}$	$p(fr_2^{sd})$	p_3^{FO}	$p(fr_2^{sd})*p_3^{FO}$	$p_{15}+p_{14}+...+p_8$	$\frac{cp_8^{0.61}}{[cp_8^{0.61}+(1-cp_8)^{0.61}]^{0.61^{-1}}}+\hat{\sigma}_8$	$cp_8^{trf}-cp_9^{trf}$	$v(pr_8^d)*dcp_8^{trf}$	$pr_8^d*p_8$
9	pr_9^d	$(pr_9^d)^{0.88}$	$p(fr_2^{sd})$	p_4^{FO}	$p(fr_2^{sd})*p_4^{FO}$	$p_{15}+p_{14}+...+p_9$	$\frac{cp_9^{0.61}}{[cp_9^{0.61}+(1-cp_9)^{0.61}]^{0.61^{-1}}}+\hat{\sigma}_9$	$cp_9^{trf}-cp_{10}^{trf}$	$v(pr_9^d)*dcp_9^{trf}$	$pr_9^d*p_9$
10	pr_{10}^d	$(pr_{10}^d)^{0.88}$	$p(fr_2^{sd})$	p_5^{FO}	$p(fr_2^{sd})*p_5^{FO}$	$p_{15}+p_{14}+...+p_{10}$	$\frac{cp_{10}^{0.61}}{[cp_{10}^{0.61}+(1-cp_{10})^{0.61}]^{0.61^{-1}}}+\hat{\sigma}_{10}$	$cp_{10}^{trf}-cp_{11}^{trf}$	$v(pr_{10}^d)*dcp_{10}^{trf}$	$pr_{10}^d*p_{10}$
11	pr_{11}^d	$(pr_{11}^d)^{0.88}$	$p(fr_3^{sd})$	p_1^{FO}	$p(fr_3^{sd})*p_1^{FO}$	$p_{15}+p_{14}+...+p_{11}$	$\frac{cp_{11}^{0.61}}{[cp_{11}^{0.61}+(1-cp_{11})^{0.61}]^{0.61^{-1}}}+\hat{\sigma}_{11}$	$cp_{11}^{trf}-cp_{12}^{trf}$	$v(pr_{11}^d)*dcp_{11}^{trf}$	$pr_{11}^d*p_{11}$
12	pr_{12}^d	$(pr_{12}^d)^{0.88}$	$p(fr_3^{sd})$	p_2^{FO}	$p(fr_3^{sd})*p_2^{FO}$	$p_{15}+p_{14}+...+p_{12}$	$\frac{cp_{12}^{0.61}}{[cp_{12}^{0.61}+(1-cp_{12})^{0.61}]^{0.61^{-1}}}+\hat{\sigma}_{12}$	$cp_{12}^{trf}-cp_{13}^{trf}$	$v(pr_{12}^d)*dcp_{12}^{trf}$	$pr_{12}^d*p_{12}$
13	pr_{13}^d	$(pr_{13}^d)^{0.88}$	$p(fr_3^{sd})$	p_3^{FO}	$p(fr_3^{sd})*p_3^{FO}$	$p_{15}+p_{14}+p_{13}$	$\frac{cp_{13}^{0.61}}{[cp_{13}^{0.61}+(1-cp_{13})^{0.61}]^{0.61^{-1}}}+\hat{\sigma}_{13}$	$cp_{13}^{trf}-cp_{14}^{trf}$	$v(pr_{13}^d)*dcp_{13}^{trf}$	$pr_{13}^d*p_{13}$
14	pr_{14}^d	$(pr_{14}^d)^{0.88}$	$p(fr_3^{sd})$	p_4^{FO}	$p(fr_3^{sd})*p_4^{FO}$	$p_{15}+p_{14}$	$\frac{cp_{14}^{0.61}}{[cp_{14}^{0.61}+(1-cp_{14})^{0.61}]^{0.61^{-1}}}+\hat{\sigma}_{14}$	$cp_{14}^{trf}-cp_{15}^{trf}$	$v(pr_{14}^d)*dcp_{14}^{trf}$	$pr_{14}^d*p_{14}$
15	pr_{15}^d	$(pr_{15}^d)^{0.88}$	$p(fr_3^{sd})$	p_5^{FO}	$p(fr_3^{sd})*p_5^{FO}$	p_{15}	$\frac{cp_{15}^{0.61}}{[cp_{15}^{0.61}+(1-cp_{15})^{0.61}]^{0.61^{-1}}}+\hat{\sigma}_{15}$	cp_{15}^{trf}	$v(pr_{15}^d)*dcp_{15}^{trf}$	$pr_{15}^d*p_{15}$
Total					100			100	$\sum_{i=1}^{15}v(pr_i^d)*dcp_i^{trf}$	$\sum_{i=1}^{15}pr_i^d*p_i$

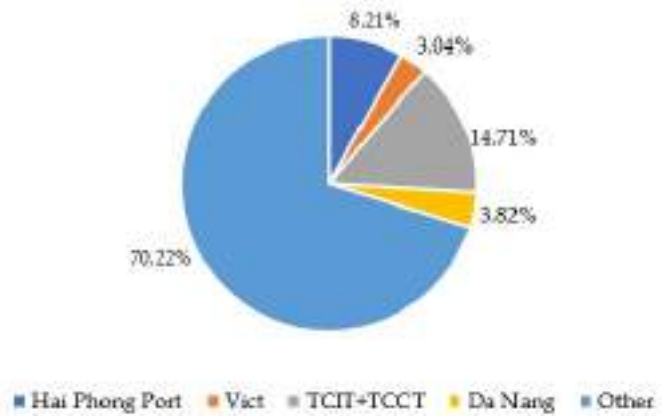

Figure 2. *Percentage of cargo throughput in Vietnam's major ports by 2022*

4.2. Alternative Shipping Network

This study evaluates three alternatives to networking for shipping lines. Shipment demand is estimated using data obtained from the final freight reports for 144 voyages in 2022 of Hai An shipping line on Bravo software, and interview results of marketing department manager and commercial team leader. Furthermore, port dues and transshipment costs by barge are collected from "vessel cost reports" of the Hai An shipping line, which are managed by vessel management, the commercial department, and the ports' official website. In addition, other relevant costs also use data obtained from vessel cost reports of the Hai An container transport company.

Data for the three main routes are gathered to benefit from the decision-making issue. Three main routes including Hai Phong to Ho Chi Minh and vice versa are called alternative 1; alternative 2 is the journey Hai Phong - TCIT - Ho Chi Minh - Hai Phong (directly) and the sailing Hai Phong - Ho Chi Minh - TCIT - Ho Chi Minh - Hai Phong (transshipment between Ho Chi Minh and TCIT) is considered alternative 3. The three alternatives are described further in Figure 3. Note that there is no revenue for the leg from Tan Cang - Cai Mep International Terminal (TCIT) to Ho Chi Minh port. Containers from TCIT are transported to Vietnam International Container Terminals (HCM) and continue to be transported to the Hai Phong port (HP). The goods operated in this leg belong to main lines such as MOL lines, Hapag-Lloyd, and OOCL, meaning that in this situation, the vessel acts as a feeder for the main lines.

In this work, IFO 380 (used for the main engine) is the only fuel type considered, and its price is calculated in 1 year according to the live fuel oil price. Three hundred sixty-five days in 2022 of statistics for Singapore oil prices are determined fuel oil probabilities (Table 3) [44].

"Probability" is calculated by the number of days that the price levels in each interval appear divided by 365, which is the number of days in a year. Fuel consumption during operation is assumed to stabilize. Thus, the fuel costs of

Table 3. *Fuel oil price probabilities*

Price range (USD)	Average value of IFO 380 price (USD)	Probability $p(FO)$ (%)
300-400	385	15
400-500	440	29
500-600	529	25
600-700	651	22
700-800	745	9

Figure 3. *Networks for a case study*

the containerships depend on the price of fuel oil for each voyage leg.

The average loading factor of 20-foot dry container (20'DC) and 40-foot dry container (40'DC) for each way of the round voyages of main and feeder containerships is different and according to the booking confirmation and not over vessel capacity and suitable with the vessel's stable, considering the light and heavy legs of the container transportation line. For this study, marketing manager and commercial manager interviews were also conducted. The ship's specifications are listed in Table 4.

Data output from the software for peak, low, and medium seasons account for 18%, 23%, and 59% of the total annual transport volume, respectively. All voyages in each season are counted, and the average number of containers per voyage for each season is calculated and filled in the corresponding "volume" column for 20, and 40 feet containers. Hai An shipping line reserves 15% of slot booking for contractual customers who sign dead-slot contracts and enjoy the best rates; 55% of slot booking for regular customers; and 30% for occasional customers. Data are arranged by season, each customer group, and the average value of the freight in the "freight rate" column. The average container volume and freight rate in each dimension of alternative 1 are illustrated in Table 5. Table 6 summarizes the average container volume in each dimension of alternatives 2, 3.

For simplicity of calculation, assume that the average daily running cost is 137,920,300 VND/day; an average FO consumption is 16 MTs/day; an average DO consumption is 0.25 MT/day. DO is usually used when the machine is in the maintenance mode. DO consumption when maneuvering the machine forward and backward. Using DO mainly to run the channel and mannequin in and out of the port; DO unit price is unchanged, taken as 20,825,000 VND/MT; marine and port expense in each port of call is similar; other costs include vessel husbanding agency fees, general operations agency fees, booking commissions, management and operation consultant fees, the vessel on/off hire survey (if any), and others. The average of additional agency fees gathered on various voyages is used to calculate other agency costs. The characteristics of all networks are shown in Table 7.

Table 4. *Ship's specifications*

Vessel's criteria	Specifications
Gross tonnage due	1728
IMO number Call sign	9245158 XVLV9
Flag	Vietnam
Average speed	13.5 NM
Sources: Author's computation	

Table 8 expresses the CPV and EUV of Alternative 1 when the parametric adaptation coefficient $\mu_1 = 0$.

4.3. Comparison with the Traditional Method

TTo examine how behavioral biases impact decisions made on shipping networks, this paper calculates voyage daily profit from the CPT approach and compares the obtained results to EUT, according to which decision makers are irrational. Many previous studies have compared CPT and EUT [45-50]. Results reveal that many barriers identified in the literature have potential explanations offered through CPT. According to the EUT, decision makers choose the

Table 5. *Average container volume and freight rate in each dimension of alternative 1*

	HP-HCM				HCM-HP			
Season	**Volume 20'**	**Freight rate/ probability (USD/%)**	**Volume 40'**	**Freight rate/ probability (USD/%)**	**Volume 20'**	**Freight rate/ probability (USD/%)**	**Volume 40'**	**Freight rate/ probability (USD/%)**
High season (18%)	371	242/30	343	279/30	317	166/30	352	229/30
		271/55		313/55		179/55		242/55
		296/15		346/15		187/15		254/15
Off-season (23%)	283	226/30	258	263/30	230	150/30	255	221/30
		255/55		297/55		163/55		234/55
		280/15		330/15		171/15		246/15
Medium season (59%)	320	234/30	291	271/30	260	158/30	288	221/30
		263/55		305/55		171/55		234/55
		288/15		338/15		179/15		246/15
Types of goods	Bricks, lime, stone powder, food, plastic pellets, plywood, automobiles, motor vehicles, electronics				Plastic granules, aluminum, building materials, rice, coffee, bran, and paper			
Sources: Author's computation								

Table 6. *Average container volume in each dimension of alternatives 2, 3*

HP-HCM					HCM-HP			
Season (Probability)	**Volume 20'**	**Freight rate/ probability (USD/%)**	**Volume 40'**	**Freight rate/ probability (USD/%)**	**Volume 20'**	**Freight rate/ probability (USD/%)**	**Volume 40'**	**Freight rate/ probability (USD/%)**
High season (18%)	264	242/30	240	279/30	241	166/30	268	229/30
		271/55		313/55		179/55		242/55
		296/15		346/15		187/15		254/15
Off-season (23%)	176	226/30	160	263/30	170	150/30	155	221/30
		255/55		297/55		163/55		234/55
		280/15		330/15		171/15		246/15
Medium season (59%)	220	234/30	200	271/30	220	158/30	200	221/30
		263/55		305/55		171/55		234/55
		288/15		223/15		176/15		246/15
	HP-TCIT				**TCIT-HP**			
High season (18%)	91	251	182	290	72	230	144	280
		292		332		272		320
		324		355		305		345
Off-season (23%)	60	235	120	273	47	214	94	264
		276		316		256		310
		308		339		289		331
Medium season (59%)	76	243	152	281	60	222	120	272
		284		324		264		318
		312		347		297		337
Types of goods	Main line goods (Empty container and other)				Main line goods (Empty container and other)			
Sources: Author's computation								

Table 7. *Characteristics of all networks*

Parameters	Alternative 1	Alternative 2	Alternative 3
Tonnage dues (GT)	17280	17280	17280
Sailing time (day)	4.94	5.02	4.94
Time in port (day)	2.44	2.89	2.89
Total time	7.38	7.91	7.38
Navigation aid dues (VND)	16,588,800	16,588,800	16,588,800
Clearance fees	320,000	480,000	320,000
Pilot dues (VND)	61,344,000	86,227,200	61,344,000
Berth dues (VND)	9,720,000	12,485,664	9,720,000
Mooring/unmooring (VND)	4,441,500	5,541,500	4,441,500
Tugboat charges	69,200,000	100,109,090	69,200,000
Quarantine fees	0	0	0
Customs others (VND)	54,200,000	39,151,200	54,200,000
DO expenses (VND)	20,825,000	38,432,248	41,160,709
Daily fixed cost (VND/day)	137,920,300	137,920,300	137,920,300
Agency others	312,138,000	367,090,000	367,090,000
Average value of revenue in one voyage	Rev1	Rev2	Rev3
Equipment charge (est.)	0.058 Rev1	0.058 Rev2	0.058 Rev3
Liner management fees	0.035 Rev1	0.035 Rev2	0.035 Rev3
Obtained revenue from sea freight	TR^1_{SF}	TR^2_{SF}	TR^3_{SF}
Carrier insurance and claim	$0.01TR^1_{SF}$	$0.01\ TR^2_{SF}$	$0.01TR^3_{SF}$
Source: Author's computation			

option that will result in the highest expected utility value. The expected utility value of each alternative is expressed as follows:

$$EV(pr^d) = \sum_{i=1}^{n} p_i pr_i^d \quad (17)$$

Where: $\sum_{i=1}^{n} p_i = 1$, i is indicates alternative, n is the number of alternative payoffs, p_i presents the probability of alternative and $p\,r_i^d$indicates the payoff of an alternative.

In this section, perform the same steps of the operation for alternatives 1, 2, and 3; then, the CPV and EUV values of all alternatives are summarized in the decision tree of Figures 4, 5, and 6, respectively.

The results obtained from the two methods are depicted in Figure 7. The results from the two methods indicate that the preference in decision-making for Hai An shipping lines is the same and greater than 0. Based on the given information, it can be argued that the Hai An company is operating efficiently. In this case, daily profit cumulative prospect values of alternatives 42,694,100 < 44,371,043 < 44,470,292 show that the prescriptive approach prefers alternative 2 as the first best economical route, with the order of preference being alternative 3 ≺ alternative 1 ≺ alternative 2. The daily profit expected values of alternatives also have the same prescriptive preference as cumulative prospect values.

Focusing on ratios rather than absolute values is one of the important fundamentals of CPT. Hence, this study investigates the relative comparison between alternatives

Table 8. *CPV and EUV calculation of alternative 1*

No	$p\,r_i^d$	$v(p\,r_i^d)$	$p(fr_i^{sd})$ (%)	p_i^{FO} (%)	p_i (%)	cp_i (%)	cp_i^{trf} (%)	dcp_i^{trf} (%)	*CPV*	$EUV(p\,r_i^d)$
1	351,436,719	33,139,464	59	9	5.31	100.00	100.00	21.30	7,060,303	18,661,290
2	376,124,102	35,179,643	59	22	12.98	94.69	78.70	16.47	5,792,339	48,820,908
3	408,165,174	37,803,815	59	25	14.75	81.71	62.23	10.77	4,073,271	60,204,363
4	426,791,963	39,317,897	18	9	1.62	66.96	51.46	0.99	387,390	6,914,030
5	431,539,399	39,702,513	59	29	17.11	65.34	50.47	9.31	3,696,629	73,836,391
6	445,984,144	40,869,666	59	15	8.85	48.23	41.16	4.47	1,826,978	39,469,597
7	451,479,347	41,312,487	18	22	3.96	39.38	36.69	2.02	832,711	17,878,582
8	483,520,419	43,881,861	18	25	4.50	35.42	34.67	2.35	1,029,470	21,758,419
9	506,894,643	45,743,309	18	29	5.22	30.92	32.33	2.85	1,305,856	26,459,900
10	521,339,389	46,888,471	18	15	2.70	25.70	29.47	1.56	732,669	14,076,164
11	660,030,553	57,705,387	23	9	2.07	23.00	27.91	1.25	722,770	13,662,632
12	684,717,936	59,600,554	23	22	5.06	20.93	26.66	3.34	1,990,442	34,646,728
13	716,759,008	62,048,085	23	25	5.75	15.87	23.32	4.58	2,840,776	41,213,643
14	740,133,233	63,825,278	23	29	6.67	10.12	18.74	7.88	5,031,949	49,366,887
15	754,577,978	64,920,167	23	15	3.45	3.45	10.86	10.86	7,047,490	26,032,940
Total						**100**		**100**	**44,371,043**	**493,002,474**

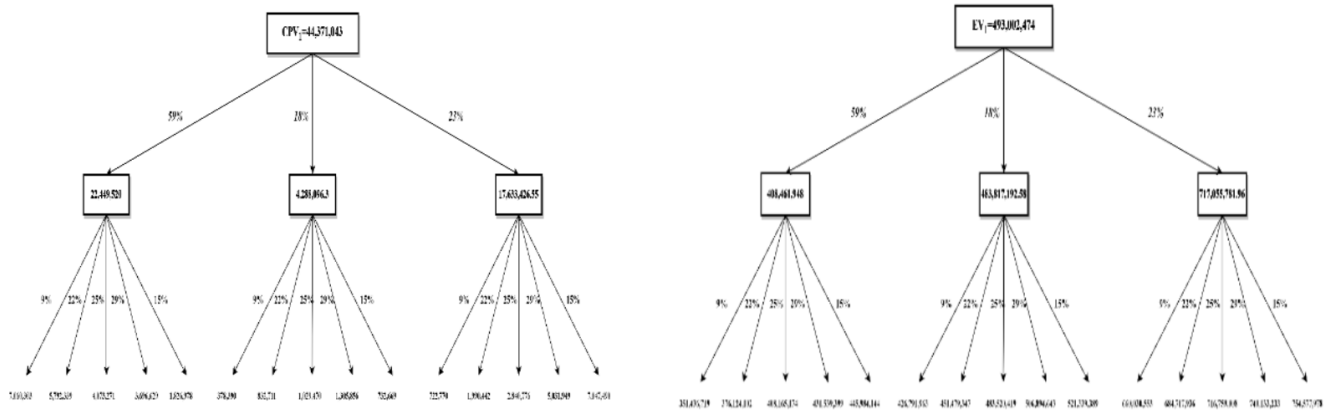

(a) **(b)**

Figure 4. *Decision tree analysis for alternative 1. (a) CPV; (b) EV*

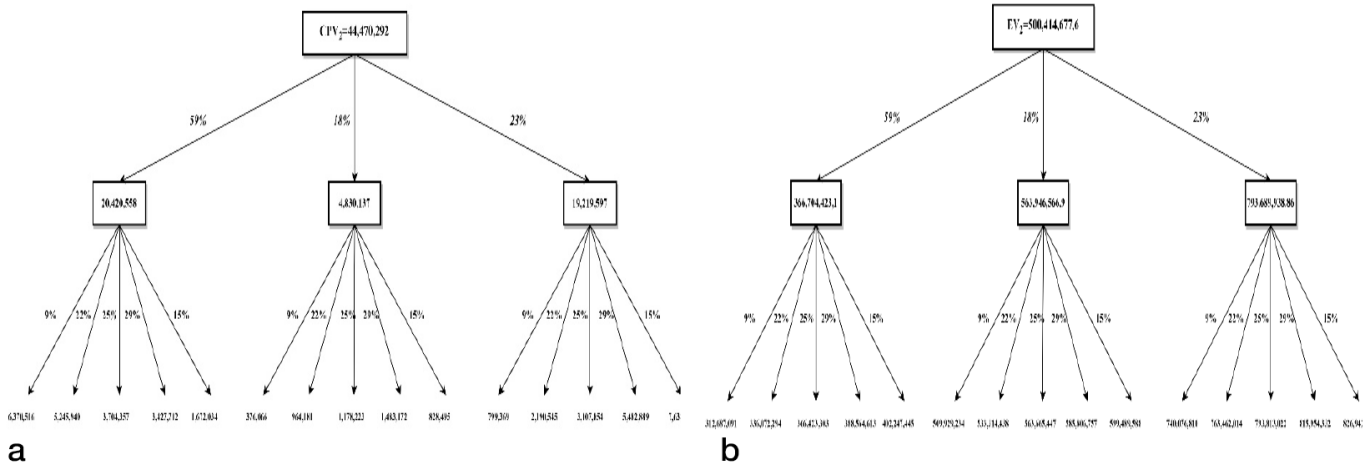

Figure 5. *Decision tree analysis for alternative 2. (a) CPV; (b) EV*

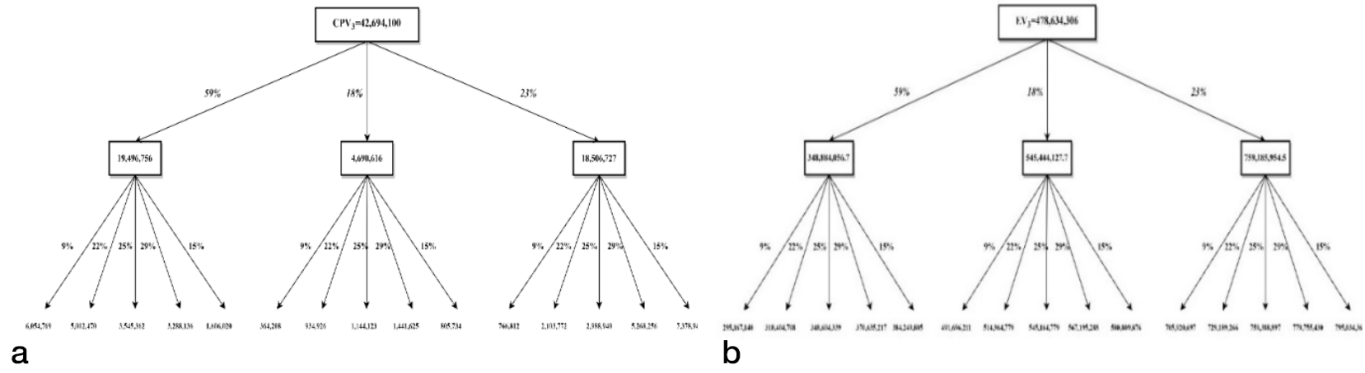

Figure 6. *Decision tree analysis for alternative 3. (a) CPV; (b) EV*

and grasp the decision-making behavior, as listed in Table 9. In this case study, assume that the obtained results from alternative 3 are indicated as the reference point. The following table illustrates the relative comparison.

From the above comparison results, if access is obtained from the EUT approach, the shipping company would choose alternative 2 as the optimal option and would ignore alternatives 1 and 3. Nevertheless, from the CPT method, options 1 and 2 are both worthy options because they are both profitable compared to the reference point. In addition, the profit gap between the two options equal to 0.22% is negligible. In contrast, the profit gap between the two options is higher and equals 1.55% from the EUT approach. Therefore, decision makers will consider additional factors such as the stability of goods to deploy the shipping route. Alternative 1 is the busiest and most dynamic route in Vietnam's domestic shipping market and is of interest to many major Vietnam shipping lines. Even though the shipping line's selection does not follow EUT, their decisions are consistent with the concept of CPT.

The next step will investigate the relationship between the change of parametric adaptation coefficient μ_1 and the variation of CPV and EUV of each alternative by assigning a value to the coefficient ensuring that μ_1 is greater than 0, starting from 0.1 to 2.0 under the rule of arithmetic progression with a common difference of 0.1. The results are shown in Table 10.

It is interesting to observe that the EUV remains unaffected by modifying the model's parameters. As a result, EUV does

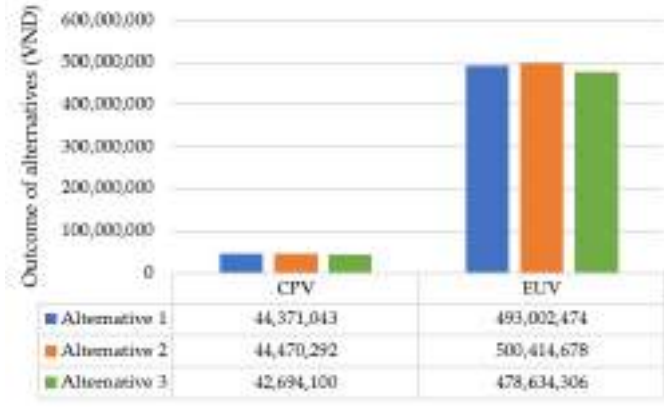

Figure 7. *CPV and EUV of the alternatives*

not consider complexity factors that can influence decision making, such as prejudices and cognitive biases, which may not adequately reflect the complexities inherent in decision making under uncertainty. Figure 8 depicts the relationship between the parametric adaptation coefficient and the variation of CPV of the three alternatives.

It is possible to realize the peculiarity of the effect of the parameter on the variation of the cumulative prospect value. The higher the parametric adaptation coefficient value, the higher the cumulative prospect of daily profit, but the growth rate diminishes. This means a greater emphasis on risk aversion, demonstrating that prioritizing risk aversion leads to diminishing growth rates despite higher daily profits. Furthermore, alternative 1 is least affected by the adaptive parameters. Under the influence of the adaptive parameter, the CPV of alternative 3 has the highest and fastest variation growth rate compared to the other two options, although it has the lowest CPV. It can be concluded that alternative 1, which is considered a safer choice due to its stability and minimal susceptibility to changes in the uncertainty factor. While alternative 3 may offer a higher potential for CPV, it also carries a greater risk. Similarly, alternative 2 also has a higher possibility of achieving a higher CPV than alternative 1. These findings underscore the importance of risk aversion, safety, and stability in the decision-making process. Combined with the aforementioned arguments, domestic carriers in Vietnam, who prefer certainty, are willing to sacrifice higher profits for stable profits, which aligns with the concept of CPT.

5. Conclusion

This paper proposes a quantitative method that uses econometric cognitive parameters to calculate the round voyage efficiency of shipping network decisions. This paper has demonstrated and compared values from two backbone methods for decision analysis: EUT, in which decision-makers following the EUT are rational, and CPT, in which decision-makers are irrational. This work will be useful and easier for strategy makers of liner shipping companies to consider when making decisions in an uncertain environment. This paper adds to the literature by improving comprehension of the demand for transport, cost, and revenue components by analyzing both shipment demand and clusters of customer and freight rates in the comparison between route scenarios. Networks are constructed, and daily profit formulation is introduced to choose the best optimal shipping network.

For the case study, the results are obtained as follows. Alternative 2 was investigated as the best route. Furthermore, the decision-maker's behavior is not consistent with the fundamentals of EUT, but it was explained from the CPT approach. The preference results from the CPT and the EUT approach are the same. Based on the comparison results mentioned earlier, according to the EUT approach, the relative comparison of average daily profit between alternatives 2 and 1 equal to 1.55% is greater than this gap from the CPT approach in that the difference is only 0.22%, which is very small. The shipping company would choose alternative 2 as the first best option if approached from the EUT perspective and would disregard both alternatives 1 and 3. From the CPT perspective, alternatives 1 and 2 can be considered efficient options. Shipping lines will consider other factors besides the average cumulative profit when choosing option 1 or option 2.

After assessing the impact of adaptation parameters on the model, alternative 1 emerged as the safest with the least effect and the lowest variation in CPV. Alternative 2 is suggested as the most effective option for managers seeking the highest potential CPV and opportunities to achieve greater CPV on daily profit. Alternative 3, on the other hand, offers the lowest profitability and is heavily influenced by uncertainty. As a result, it is recommended to eliminate Alternative 3 as a feasible choice. In fact, the Hai

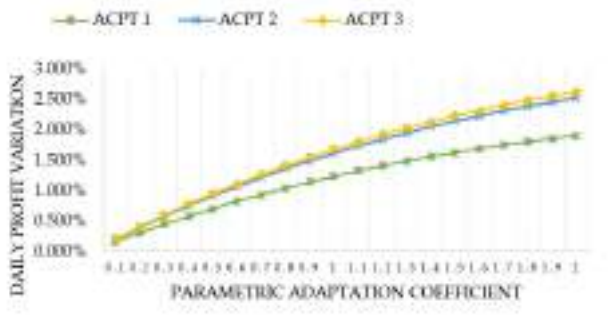

Figure 8. *Effect of adaptive parameter on average daily profit*

Table 9. *Relative comparison between alternatives from the CPV and EUV approaches*

Alternative/Comparison	CPV	EUV
Alternative 1	44,371,043	493,002,474
Alternative 2	44,470,292	500,414,678
Alternative 3	42,694,100	478,634,306
RC23 (Relative comparison between alternative 2 and alternative 3)	4.16%	4.55%
RC13 (Relative comparison between alternative 1 and alternative 3)	3.93%	3.0%
RC21 (Relative comparison between alternative 2 and alternative 1)	0.22%	1.5%

Table 10. *Relationship between the parametric adaptation coefficient and the variation in CPV and EV*

μ_1	Variation in CPV (%)			Variation in EUV (%)		
	Alternative 1	Alternative 2	Alternative 3	Alternative 1	Alternative 2	Alternative 3
0.1	0.156	0.202	0.209	0	0	0
0.2	0.305	0.393	0.409	0	0	0
0.3	0.449	0.576	0.599	0	0	0
0.4	0.578	0.750	0.779	0	0	0
0.5	0.705	0.915	0.951	0	0	0
0.6	0.824	1.071	1.113	0	0	0
0.7	0.937	1.219	1.267	0	0	0
0.8	1.044	1.360	1.414	0	0	0
0.9	1.144	1.493	1.552	0	0	0
1.0	1.239	1.619	1.682	0	0	0
1.1	1.328	1.738	1.806	0	0	0
1.2	1.411	1.849	1.922	0	0	0
1.3	1.489	1.954	2.032	0	0	0
1.4	1.562	2.054	2.135	0	0	0
1.5	1.631	2.147	2.231	0	0	0
1.6	1.694	2.234	2.322	0	0	0
1.7	1.753	2.315	2.407	0	0	0
1.8	1.808	2.392	2.490	0	0	0
1.9	1.858	2.463	2.560	0	0	0
2.0	1.905	2.529	2.629	0	0	0

An shipping line has also mainly operated with a frequency of three voyages per week on the Hai Phong to Ho Chi Minh round voyage, while the number of voyages to TICT is only one voyage per week. Furthermore, in Vietnam's domestic shipping market, routing as alternative 1 is not only the most popular route because the demand for shipment is stable and regular but also has the longest history route and is deployed by many liner shipping companies with the same operating routes and ship size, including Vosco, Vinafco, Vietsun, Tan Cang shipping, Vsico, and GLS shipping companies. This fact with the above proof and argument can be explained by the fact that decision makers who prefer certainty tend to be averse to risks in gains and are willing to sacrifice potentially high profit for a greater level of assurance. This paper presents a case study that explains why alternative 1 is preferred over alternative 2, despite not having the highest daily profitability. The findings indicate that decision makers in the Vietnam domestic container shipping market value stability and predictability over potential revenue, which is consistent with the principles of CPT.

Notwithstanding efforts to perform a comprehensive analysis with real data, several assumptions were made because of missing data and accompanying uncertainty. One shipping line contributed the data for this study, which is considered a major drawback and resulted in a limited amount of data. Another limitation of this study is its exclusive focus on economic aspects, neglecting technical considerations. Future research could broaden the scope of research by incorporating diverse criteria beyond quantitative measures like voyage time. Qualitative factors, such as reliability of transportation modes, route characteristics (such as navigational safety and security), weather conditions, and the influence of government policies, could be explored using linguistic variables in fuzzy and uncertain environments and should be investigated through expert surveys. Moreover, future studies could enhance the algorithm by using random forest instead of decision tree to deal with larger, more intricate datasets, thereby enhancing accuracy.

Acknowledgement

This research was supported by the 4th Educational Training Program for the Shipping, Port, and Logistics from the Ministry of Oceans and Fisheries.

Authorship Contributions

Concept design: Y. P. Thi, and H. Kim, Data Collection or Processing: Y. P. Thi, and P. H. Nguyen, Analysis or Interpretation: Y. P. Thi, N. C. Truong, and P. H. Nguyen, Literature Review: Y. P. Thi, and N. C. Truong, Writing, Reviewing and Editing: Y. P. Thi, N. C. Truong, P. H. Nguyen, and H. Kim.

Funding: The authors declare that no funds, grants, or other support was received during the preparation of this manuscript.

References

[1] The United Nations Conference on Trade and Development, UNCTAD, *Review of Maritime Transport*, 2022.

[2] S. T. Koçak, and F. Yercan, "Comparative cost-effectiveness analysis of arctic and international shipping routes: a fuzzy analytic hierarchy process". *Transport Policy*, vol. 114, pp. 147-164, Dec 2021.

[3] M. Celik, S. Cebi, C. Kahraman, and I. D. Er, "Application of axiomatic design and TOPSIS methodologies under fuzzy environment for proposing competitive strategies on Turkish container ports in maritime transportation network". *Expert Systems with Applications*, vol. 36, pp. 4541-4557, Apr 2009.

[4] N. Koohathongsumrit, and W. Meethom, "An integrated approach of fuzzy risk assessment model and data envelopment analysis for route selection in multimodal transportation networks". *Expert Systems with Applications*, vol. 171, 114342, Jun 2021.

[5] N. Koohathongsumrit, and W. Meethom, "Route selection in multimodal transportation networks: a hybrid multiple criteria decision-making approach," *Journal of Industrial and Production Engineering*, vol. 38, pp. 171-185, Feb 2021.

[6] G. Xiong, and Y. Wang, "Best routes selection in multimodal networks using multi-objective genetic algorithm". *Journal of Combinatorial Optimization*, vol. 28, pp. 655-673, Oct 2014.

[7] M. J. Sharma, I. Moon, and H. Bae, "Analytic hierarchy process to assess and optimize distribution network". *Applied Mathematics and Computation*, vol. 202, pp. 256-265, Aug 2008.

[8] A. Kengpol, S. Tuammee, and M. Tuominen, "The development of a framework for route selection in multimodal transportation". *The International Journal of Logistics Management,* vol. 25, pp. 581-610, Nov 2014.

[9] L. Bukvić, J. Pašagić Škrinjar, B. Abramović, and V. Zitrický, "Route selection decision-making in an intermodal transport network using game theory". *Sustainability*, vol. 13, pp. 4443, Apr 2021. [Online]. Available: MDPI.

[10] A. Gungor, and B. Barlas, "Decision-making under risk: a ship sale and purchase problem by utilizing cumulative prospect theory". *Journal of ETA Maritime Science*, vol. 10, pp. 16-28, Mar 2022.

[11] J. Meyer. "Expected utility as a paradigm for decision making in agriculture". In: Just, R.E., Pope, R.D. (eds) A Comprehensive Assessment of the Role of Risk in U.S. Agriculture. Natural Resource Management and Policy, vol 23. Springer, Boston, MA, 2002.

[12] M. O. Rieger, M. Wang, and T. Hens, "Estimating cumulative prospect theory parameters from an international survey". *Theory and Decision*, vol. 82, pp. 567-596, Nov 2017.

[13] A. Tversky, and D. Kahneman, "Advances in prospect theory: Cumulative representation of uncertainty". *Journal of Risk and Uncertainty*, vol. 5, pp. 297-323, Oct 1992.

[14] D. Kahneman, and A. Tversky, "Prospect theory: An analysis of decision under risk". in *Handbook of the Fundamentals of Financial Decision Making: Part I,* pp. 99-127, Jul 2013. https://doi.org/10.1142/9789814417358_0006

[15] S. Ebrahimigharehbaghi, Q. K. Qian, G. de Vries, and H. J. Visscher, "Application of cumulative prospect theory in understanding energy retrofit decision: A study of homeowners in the Netherlands". *Energy and Buildings*, vol. 261, pp. 111958, Apr 2022.

[16] Meng, Q., Wang, S., Andersson, H., & Thun, K, "Containership routing and scheduling in liner shipping: overview and future research directions". *Transportation Science*, vol. 48, pp. 265-280, May 2014.

[17] K. Fagerholt, "Optimal fleet design in a ship routing problem," *International Transactions in Operational Research*, vol. 6, pp. 453-464, Aug 2006.

[18] H. K. Lo, M. R. McCord, and C. K. Wall, "Value of ocean current information for strategic routing". *European Journal of Operational Research*, vol. 55, pp. 124-135, Nov 1991.

[19] J. Mulder, and R. Dekker, "Methods for strategic liner shipping network design". *European Journal of Operational Research*, vol. 235, pp. 367-377, Jun 2014.

[20] D. Ronen, "Ship scheduling: The last decade". *European Journal of Operational Research*, vol. 71, pp. 325-333, Dec 1993.

[21] M. Christiansen, K. Fagerholt, and D. Ronen, "Ship routing and scheduling: Status and perspectives". *Transportation Science*, vol. 38, pp. 1-18, Feb 2004.

[22] X. Qi, and D. P. Song, "Minimizing fuel emissions by optimizing vessel schedules in liner shipping with uncertain port times". *Transportation Research Part E: Logistics and Transportation Review*, vol. 48, pp. 863-880, Jul 2012.

[23] Q. Meng, T. Wang, and S. Wang, "Short-term liner ship fleet planning with container transshipment and uncertain container shipment demand". *European Journal of Operational Research*, vol. 223, pp. 96-105, Nov 2012.

[24] S. Wang, and Q. Meng, "Robust schedule design for liner shipping services". *Transportation Research Part E: Logistics and Transportation Review*, vol. 48, pp. 1093-1106, Nov 2012.

[25] S. Wang, and Q. Meng, "Liner ship route schedule design with sea contingency time and port time uncertainty". *Transportation Research Part B: Methodological*, vol. 46, pp. 615-633, Jun 2012.

[26] D. E. Lane, T. D. Heaver, and D. Uyeno, "Planning and scheduling for efficiency in liner shipping". *Maritime Policy & Management*, vol. 14, pp. 109-125, 1987.

[27] Q. Meng, S. Wang, and Z. Liu, "Network design for shipping service of large-scale intermodal liners". *Transportation Research Record*, vol. 2269, pp. 42-50, Dec 2012.

[28] D. I. Jaramillo, and A. N. Perakis, "Fleet deployment optimization for liner shipping Part 2. Implementation and results". *Maritime Policy and Management*, vol. 18, pp. 235-262, May 2006.

[29] Q. Meng, and S. Wang, "Liner shipping service network design with empty container repositioning". *Transportation Research Part E: Logistics and Transportation Review*, vol. 47, pp. 695-708, Sep 2011.

[30] T. N. Chuang, C. T. Lin, J. Y. Kung, and M. D. Lin, "Planning the route of container ships: A fuzzy genetic approach". *Expert Systems with Applications*, vol. 37, pp. 2948-2956, Apr 2010.

[31] G. Fancello, P. Serra, M. Carta, V. Aramu, and P. Fadda, "Decision-making for maritime networks: evaluating corporate and social profitability of an integrated short sea shipping network in the Upper Tyrrhenian Sea". In *Computational Science and Its Applications-ICCSA 2020: 20th International Conference, Cagliari, Italy, July 1-4, 2020, Proceedings, Part VII 20*, pp. 83-95, Springer International Publishing, 2020.

[32] Z. Wang, R. Y. K. Fung, Y. Li, and Y. Pu, "An integrated decision-making approach for designing and selecting product concepts based on QFD and cumulative prospect theory". *International Journal of Production Research*, vol. 56, pp. 1-16, Jul 2017.

[33] J. Jiang, "A multi-attribute decision-making method for the location selection of emergency rescue centers based on improved cumulative prospect theory under the background of ecological sustainable development". *Journal of Intelligent & Fuzzy Systems*, vol. 43, pp. 8151-8175, Nov 2022.

[34] Y. Ren, Y. Zhou, and L. Shi, "Decision-making approach in charging mode for electric vehicle based on cumulative prospect theory". In *2012 China International Conference on Electricity Distribution, CICED 2013, 10-14 September 2012, Shanghai, China* [Online]. Available: IEEE Xplore, http://www.ieee.org. [Accessed: 10 Feb 2023].

[35] H. Wang, "Grey multiattribute emergency decision-making method for public health emergencies based on cumulative prospect theory". *Mathematical Problems in Engineering*, vol. 2022, 3240483, May 2022. [Online]. Available: https://www.hindawi.com [Accessed: 10 Feb 2023].

[36] L. Wang, Q. Liu, and T. Yin, "Decision-making of investment in navigation safety improving schemes with application of cumulative prospect theory". In *Proceedings of the Institution of Mechanical Engineers, Part O: Journal of Risk and Reliability*, vol. 232, pp. 710-724, Feb 2018.

[37] Y. Yuan, and D. Wang, "Path selection model and algorithm for emergency logistics management," *Computers & Industrial Engineering*, vol. 56, pp. 1081-1094, Apr 2009.

[38] H. Fennema, and P. Wakker, "Original and cumulative prospect theory: A discussion of empirical differences". *Journal of Behavioral Decision Making*, vol. 10, pp. 53-64, Dec 1998.

[39] X. Liu, H. Q. Ye, and X. M. Yuan, "Tactical planning models for managing container flow and ship deployment". *Maritime Policy & Management*, vol. 38, pp. 487-508, Aug 2011.

[40] The United Nations Conference on Trade and Development, UNCTAD, *Review of Maritime Transport*, 2021. https://unctad.org/

[41] I. Kurt, M. Aymelek, E. Boulougouris, and O. Turan, "Operational cost analysis for a container shipping network integrated with offshore container port system: A case study on the West Coast of North America". *Marine Policy*, vol. 126, 104400, Apr 2021.

[42] V. I. C. Terminal, Vietnam International Container Terminal, *Our Story So Far*. [Online]. Available: https://www.vict-vn.com/our-story?l=en [Accessed: 02 March 2023].

[43] SNP Corporation, Saigon Newport Corporation, *Welcome to Tan Cang - Cai Mep International Terminal.* [Online]. Available: https://www.tcit.com.vn/information/about-us.html [Accessed on 02 March 2023].

[44] Ship & Bunker, *Singapore Bunker Prices*. [Online]. Available: https://shipandbunker.com/prices/apac/sea/sg-sin-singapore#IFO380 [Accessed: 09 January 2023].

[45] A. Khan, "Expected utility versus cumulative prospect theory in an evolutionary model of bargaining". *Journal of Economic Dynamics and Control*, vol. 137, 104332, Apr 2022.

[46] B. Häckel, S. Pfosser, and T. Tränkler, "Explaining the energy efficiency gap-expected utility theory versus cumulative prospect theory". *Energy Policy*, vol. 111, pp. 414-426, Dec 2017.

[47] Ş. Gazioğlu, and N. Çalışkan, "Cumulative prospect theory challenges traditional expected utility theory". *Applied Financial Economics*, vol. 21, pp. 1581-1586, Jul 2011.

[48] G. W. Harrison, and E. E. Rutström, "Expected utility theory and prospect theory: One wedding and a decent funeral". *Experimental Economics*, vol. 12, pp. 133-158, Jun 2009.

[49] H. K. Chung, P. Glimcher, and A. Tymula, "An experimental comparison of risky and riskless choice—limitations of prospect theory and expected utility theory". *American Economic Journal: Microeconomics*, vol. 11, pp. 34-67, Aug 2019.

[50] G. W. Harrison, and D. Ross, "The empirical adequacy of cumulative prospect theory and its implications for normative assessment". *Journal of Economic Methodology*, vol. 24, pp. 150-165, Apr 2017.

ORIGINAL RESEARCH (AR) DOI: 10.4274/jems.2024.35403

Journal of ETA Maritime Science 2024;12(2):186-198

Cruise Passengers' Perceived Service Quality During the Pandemic Period via User-Generated Content

Batuhan Çullu[1], Nergis Özispa[2], Gamze Arabelen[3]

[1]Aydın Adnan Menderes University, Söke Business Administration Faculty, Aydın, Türkiye
[2]Mersin University Faculty of Maritime, Department of Maritime Business Administration, Mersin, Türkiye
[3]Dokuz Eylül University Faculty of Maritime, Department of Maritime Business Administration, İzmir, Türkiye

Abstract

The coronavirus epidemic, which emerged in Wuhan at the end of 2019, spread worldwide and caused more than 4 million deaths as of 2021. The cruise industry, whose goal is to maintain customer satisfaction at the highest possible level, like all service industries, has passed a difficult test with serious coronavirus disease-2019 (COVID-19) cases that emerged on various ships. The new rules of the COVID-19 pandemic are reflected in the service processes of the ships that started to sail again after a long-term pause in the sector. The main motivation of this study is to determine whether the factors affecting customers' perceived service quality have changed during the pandemic period in the cruise industry, which is one of the sectors where service quality should be maintained high. Therefore, this study aims to determine the factors affecting the perceived service quality of cruise passengers and determine the new factors that occurred during the pandemic. To achieve this goal, the online narratives of 418 passengers cruising in the European Region between September 2020 and September 2021 were analyzed using Leximancer software, and key elements of passengers' perceptions of service quality were determined. As a result of the study, it was found that cabin location, restaurant quality, and COVID-related variables became significant factors affecting the perceived service quality of cruise passengers during the pandemic period. Additionally, disembarkation and embarkation, which were important variables in the pre-COVID period, were reclassified under the COVID category. The study also determined that adherence to COVID-19 measures by cruise companies positively impacted customer satisfaction during this period.

Keywords: Leximancer, Service quality perception, User generated content

1. Introduction

Historically, the early 20th century was a preferred time for cruise travel due to maritime transportation being a strong alternative for passenger transport. Cruise ships, which were widely used by people with high incomes in the 1920s, lost their popularity due to developments in air transportation after the second world war. By the end of the 20th century, cruise lines, which focused on marketing activities by expanding into different market segments and with the help of technological opportunities, have regained their former popularity today and have increased their market shares significantly with features that can appeal to almost every demographic group [1,2].

Because of these efforts, the global cruise industry revenue has exceeded US$ 27 million in recent years; however, the travel restrictions imposed by the coronavirus disease-2019 (COVID-19) pandemic have adversely affected the industry in 2020, and the value of the cruise industry has decreased to US$ 3.37 million in 2021. According to 2021 data, while the cruise industry experienced a decrease of 87.8% in its total revenue and a loss of approximately 2,500 jobs worldwide, only 5.8 million passengers preferred cruise travel [3]. To mitigate these negative impacts, ensuring the health and safety of passengers, crew, and communities became the top priority for all stakeholders in the cruise industry, including cruise companies, travel agencies, ports, destinations,

Address for Correspondence: Nergis Özispa, Mersin University Faculty of Maritime, Department of Maritime Business Administration, Mersin, Türkiye
E-mail: nergis.ozispa@deu.edu.tr
ORCID ID: orcid.org/0000-0002-2467-5286

Received: 05.11.2022
Last Revision Received: 20.01.2024
Accepted: 27.03.2024

*The initial version of this study was presented orally at V. National / I. International Port Congress and published as an abstract in the proceeding book of the congress. Which can be found at https://ulk2021.deu.edu.tr/tr/7-2/.

To cite this article: B. Çullu, N. Özispa, and G. Arabelen. "Cruise Passengers' Perceived Service Quality During the Pandemic Period via User-Generated Content." *Journal of ETA Maritime Science*, vol. 12(2), pp. 186-198, 2024.

and suppliers. In this context, Cruise Lines International Association and its member organizations have invested in R&D studies, worked with global experts, and collaborated closely with authorities in the health, transportation, and safety fields to develop health and safety protocols. The safe resurgence of the industry in Europe, the United Kingdom, some parts of Asia, and North America, on the other hand, gives strong signals that cruising is imminent when the right precautions are taken [4].

According to [5], customer perception is their opinion of the service they received, and service quality is a generic evaluation tool like attitude. Literature described the perception of service quality as a judgment or attitude about how much better the service is [6]. In the cruise industry, in addition to concerns such as health and safety arising from the COVID-19 pandemic, many elements affect the cruise experience and service quality perceptions of tourists, such as food and beverage services, events, customer service, tours, itineraries, shopping [2,7,8], entertainment, embarkation, disembarkation, excursions [9], Wi-Fi, and mobile phone connections. It is argued that these factors affect perceived service quality, cruise experience, and overall customer satisfaction.

Therefore, the purpose of this study is to give an answer to questions as; "how COVID-19 pandemic restrictions changed passengers' perceived services?", "which cruise service quality attributes have altered in pandemic conditions?" and "how passengers responded to changes?"

2. Literature Review

COVID-19 virus emerged in China in 2019, affected the entire world in a very short time period, and was declared a pandemic by the World Health Organization in 2020 [10]. In this study, which aims to examine the effects of COVID-19 on the perceived service quality variables in the cruise sector, it has been determined that the literature examining the COVID-19 process in the cruise industry is quite limited.

Because of the query made on the Web of Science database on 08.02.2022, using the key words and phrases Cruise Industry + COVID and Cruising + COVID, it was determined that there were 43 studies in total. Of these studies, 37 were published as articles, 2 as proceeding paper and editorial material, and one as review and one as letter. All published studies, because of the timeline of the existence of the COVID-19 virus, were published between 2020 and 2021. Web of science categories of the studies are examined, and it is seen that the studies mainly focus on hospitality leisure sport tourism (11 study) and environmental studies (9 study). These categories are followed by management (7 study), public environmental occupational health (6 study), environmental sciences (6 study) and green sustainable science technology (5 study) respectively. While only four studies were found in the business category, no study was found in the marketing category. Likewise, when the research areas of these studies are examined, environmental sciences ecology (11 study), social sciences (11 study), and business economics (10 study) stand out as the main research areas. When WOS categories were examined in the existing literature, no study was found in the marketing category. Given that the cruise service sector can be classified as a luxury segment, where the emphasis on service quality is particularly intense and generally appeals to an upper-class customer base, it should be examined from a marketing science perspective. Therefore, this study aims to fill this gap in the literature.

2.1. Service Quality Dimensions in the Cruise Industry

The concept of product and service quality entered the marketing literature the 1980s and was divided into two categories: physical product and service marketing. In physical product marketing, quality has been defined and measured with increasing levels of precision, but when it comes to services marketing, difficulties have arisen in defining, measuring, and controlling quality. Since services are performances rather than objects, it is nearly impossible for uniform quality to be established and enforced [11]. However, the obvious benefits that service quality will provide to organizations include customer satisfaction and increased profitability [12], have caused researchers and managers to attach great importance to this issue in the last four decades. In 2003, [13] defined the concept as "service quality is a focused evaluation that reflects the customer's perception of specific dimensions of service namely reliability, responsiveness, assurance, empathy, tangibles". In 1984, [14] argued that businesses should understand how consumers' perceptions of quality and service quality are affected in order to gain competitiveness, and with the "technical and functional quality model" they developed, they decided that the three components of service quality are "image, technical quality and functional quality". In [5], a service quality model was created based on the gap analysis between customer expectations and business performance. The GAP model argues that service quality is a function of the gaps between expectation and performance across quality dimensions. Since the 1980s, with the emergence of the service quality concept, many scholars, academics, and researchers have examined the concept of service quality and developed many models that aim to measure or increase service quality. Some of these models are given below;

- IT-based model [15],
- Synthesized model of service quality [16],
- Model of e-service quality [17].

- Model of perceived service quality and satisfaction [18],
- Evaluated performance and a normed quality model [19],
- Attribute and overall affect model [20],
- IT alignment model [21],
- Internet banking model [22],
- Internal service quality model [23],
- Retail service quality and the perceived value model [24],
- The ideal value model of service quality [25],
- Antecedents and mediator model [26],
- PCP attribute model [27],
- Internal service quality DEA model [28],
- Service quality, customer value, and customer satisfaction model [29],
- Attribute service quality model [30],
- Performance only model [31].

When all these models related to service quality are examined, it is concluded that the service quality literature is generally shaped in line with customer expectation, satisfaction, and perception. In addition to the aforementioned inference, when the nature of the service sector is considered, which changes according to the characteristics of the service provided, the necessity of examining the concept of service quality in the triangle of the specific characteristics of the sector in which the service is provided, the competencies of the service provider, and the service perception of the potential customers expected to buy the service comes to the fore. The SERVQUAL model proposed by [6] to measure perceived service quality has been adapted by many researchers to measure service quality in different sectors such as accommodation and tourism, restaurants, destinations, and outbound guide package tours. Among the adaptations of the SERVQUAL model, the model created for historical houses was named HISTOQUAL, the model created for ecotourism service quality was named ECOSERV, the model created for the measurement of vacation experience satisfaction was named HOLSAT, and the model created for cruise experience satisfaction was named SERV-PERVAL [32].

The SERV-PERVAL scale was used in 2014 to examine the relationship between the "cognitive perceived value, affective perceived value, satisfaction with the cruise experience and the basic structures of behavioral intentions" because of the cruise travel experience of Asian cruise passengers [33]. In the study, five main components designed to measure cognitive perceived value which are, "emotional response as emotional perceived value, level of satisfaction, behavioral intention and demographic variables". The cognitive value perceived by cruise passengers was obtained through explanatory factor analysis in four dimensions: "cruise ship facilities, food and beverage service, entertainment, and service provided by the crew" [33]. The SERV-PERVAL model was also used by [34] in a study that aimed to test the relationships between cruise passengers' "emotional response, reputation, behavioral price, perceived value, monetary price, quality and repurchase intentions". That study used a measurement tool consisting of 25 items under five main factors: "quality, monetary price, behavioral price, emotional response, and reputation". The study revealed that "reputation, emotional response and monetary price" were the antecedents of quality perceptions of both first-time visitors and repeaters.

Reference [8] aimed to determine the satisfaction levels of Hong Kong cruise passengers and the factors affecting their satisfaction. They used 31 attributes in five main categories as variables, named "accommodation, food and beverage, entertainment, other facilities, and the staff". The study's findings led to the following conclusion: The key factors influencing the rejoining of the cruise were "accommodation, food and beverage and entertainment", respectively. A conceptual framework has been created that measures the experiential performance of cruise voyages in a study, which aims to examine the information on tourist behavior in navigational environments by analyzing the effects of the physical environment on a cruise experience. In the proposed model, there are eight sub-variables under the main variables: perceived servicescape, cruise experience, intention to recommend, and intention to return [35]. Authors suggested;

Ambient factors (sounds, cleanliness, lighting, music, temperature);

1. Design and functionality factors (decor, colors, layout, size, entertainment, architecture, seating comfort)

2. Social factors (crowding, queues, cruiser cues, crew friendship)

3. As subvariables of the main variable perceived servicescape [35].

In 2006 [36] examined the "moment of truth" of cruise passengers using the critical incident technique in their study, in which they examined the "overall satisfaction, perceived value, word-of-mouth communication and repurchase intentions" of cruise passengers via a survey method. Emphasizing that the truth of moments is an effective management tool for the cruise industry, the study grouped negative "service, staff/crew, food/beverage, entertainment, ship facilities, port of calls, children/teen issues, policies, and price" and positive "service, staff/crew, food/beverage, entertainment, ship facilities, port of calls and cabin" incidents and concluded that negative incidents

were much more effective than positive incidents on cruise passengers' post hoc cruise evaluations.

On the other hand, [37] analyzed the perceived importance and performance of service attributes offered to cruise passengers and attributes related to the US cruise industry using the importance-performance analysis method. In the study in which the data were collected by the survey method, the results were classified into three main groups; attributes of high importance "overall cleanliness, employee appearance, courteous and polite employees, make passengers feel safe, always willing to help passengers, responsive to passengers' needs, perform passengers' requests without error, dependable service, understanding passengers' specific needs, pay individualized attention to passengers", attributes of average importance "lighting, music, cruise motion, entertainment, recreation and sports facilities, fitness and health facilities, supplementary facilities, facilities for children" and attributes of low importance "interior and exterior décor, ship layout, and size of ship".

In 2020, a study approached this subject from a different perspective, analyzing cruise passengers' comments on online platforms in a study that aimed to determine cruise passengers' experiential perceptions of service quality regarding higher or lower money scores. In the study, they concluded that the perceived quality of cruise travel was determined by 10 basic elements: "ship, staff, food, entertainment, room, area, embarkation, excursion, disembarkation, and port" [9].

2.2. User-generated Content

In the past, when technology and social platforms were not as developed as today, interview and focus group methods were the main methods preferred by companies to determine customer needs in matters such as determining marketing strategies and product development. However. nowadays, when the industrial revolution is taking place, user-generated content (UGC) produced by users themselves, in line with their own wishes, instantly or whenever they feel appropriate/ready, is accepted as an alternative and reliable source to determine customer needs [38]. As of the early 2000s, smart web services based on new technology have enabled users to produce digital media and communicate with other users [39]. Conducted a systematic review of the research on UGCs and found that this phenomenon was included in the literature with references such as UGC, social media, participatory web, and Web 2.0. According to [39], UGC in the literature should have three basic features; must contain a personal contribution, be published, and be produced outside the professional field/professional routine.

UGC is characterized by personal contributions. This contribution can be summarized as commenting, researching, and preparing information within the framework of existing services or uploading individual texts, images, sounds, and visuals. For these contents and contributions produced by users to be classified as UGC, they must be open to the public or at least a group. Therefore, content contained in applications that only allow bilateral communication, such as e-mail or instant messaging applications, is not characterized as UGC. Finally, these UGC must be produced outside professional routines. In content produced within the scope of the UGC, design authority is generally in the hands of amateurs, as in citizen journalism [39].

The use of these contents (restaurant ratings, videos, tweets, road traffic situations), produced voluntarily by ordinary users, has become widespread in recent years. The reasons for this are that the content is cheap to obtain, the process is rewarding for content providers (appreciation, recognition, etc.), and the content produced is considered to be more reliable data because it consists of the experiences of real people, not modified by ordinary media organizations [40].

3. Methodological Approach

In keeping with the current trend, customers are increasingly posting reviews of the goods and services they have used online [41-43]. From the viewpoint of tourism, these internet forums where previous visitors' opinions are expressed are developing into an effective tool to direct other travelers' decisions [44]. The analysis of UGC, as recent studies have shown, also provides a chance to present passengers' current service perceptions.

Content analysis is a method for establishing reliable and valid assumptions about the content in which texts are used [45]. In the past decade, the content analysis method has become a useful tool with the rapid development of the internet [9]. However, manually coding the large amount of text data that the Internet provides has become time consuming [46]. To avoid time allocation, Leximancer online software was used in this study. Leximancer analyzes the meanings of chunks of text by extracting the major concepts and ideas using sophisticated algorithms that perform mathematical and scientific calculations using the Bayesian method of prediction [47,48].

Leximancer is a software tool designed for quantitative content analysis that utilizes a machine learning approach to discern key concepts within a text and their interrelations. This tool performs both thematic and semantic analyses of the textual data. The software generates data on the frequency and co-occurrence of concepts within textual data [49], operating a process that autonomously transforms

co-occurrence data from natural language into semantic patterns. This process is executed in two distinct phases: semantic and relational, each using a unique algorithm. These algorithms are fundamentally statistical and incorporate elements of nonlinear dynamics and machine learning techniques [50]. Upon identifying a concept via the machine learning mechanism, Leximancer develops a corresponding thesaurus, compiling words linked to the identified concept, thereby providing its semantic or definitional essence [51]. The resulting concept map provides a conceptual synopsis of the initial textual source.

In other words, the software first identifies concepts, which are groups of words that appear together in the text, and then ranks them according to their frequency of occurrence and relative incidence compared to identified concepts. Then, the software resolves concept co-occurrences in the text as well as direct relationships between concepts, which means that the concepts located in the central area of the concept map most frequently cooccur with other defined concepts in the text. Lastly, the software creates themes by clustering the concepts by their similarities and creates a concept map [52-55].

Leximancer software, which integrates content analysis methodologies with sophisticated analytical techniques for textual data, has gained widespread adoption across various research domains. Researchers use this tool in particular to extract important features of customer perceptions and experiences, which yields invaluable insights for various studies. Mahr et al. [52] systematically reviewed the concepts and theories underlying customer service experience (CSE) and its five dimensions using a text mining approach with Leximancer software. They emphasized the contribution of the sensorial dimension to CSE research. [9] used Leximancer software to analyze 2000 guest reviews from Cruisecritic.com, identifying ten major themes related to cruise service quality. Brochado et al. [53] used Leximancer software to analyze in-depth interviews and explore locals' perceptions in two highly tourism-dependent southern European cities. This study examined the impacts of the COVID-19 pandemic on local communities affected by city tourism and highlighted the variables that residents perceived as having the most influence on city tourism. Huang and Wang [54] used Leximancer to conduct a thematic content analysis of COVID-19-related empirical research in tourism and hospitality journals. This study identified research themes/ subthemes, research methods, and countries/regions of research.

This research aims to explore whether the COVID-19 pandemic induced changes in the service dimensions perceived by cruise passengers. To this end, it draws upon reviews from passengers on the first European routes to reopen after the pandemic. Given the voluminous and unstructured nature of these textual data, the use of text mining techniques was deemed appropriate by the authors. The choice of Leximancer as the analytical tool is attributed to its proven effectiveness in extracting themes and identifying common topics from text, its previous applications in similar academic fields, its robust user interface, and ease of use.

Following a description of the data source and data gathering technique, descriptive statistics are presented. The dataset was then examined using Leximancer software, and the results were presented. The study was summarized in the conclusion after the findings were examined along with the literature in the discussion part.

4. Data Collection and Preprocessing

Cruisecritic.com is a prominent website where users can share their past cruise experiences. From this perspective, it stands out as one of the most vital platforms for user-generated content in the cruise industry. Potential cruisers can utilize the user-generated content on the website to make informed decisions about their upcoming trips.

Reviews on cruisecritic.com may include the name of the ship, the route, the travel date, the username, the age of the person, the number of times that the person has taken part in the cruises, the assessment title, and the cabin selection. "Cabins, Dining, Entertainment, Public Rooms, Fitness Recreation, Family, Shore Excursion, Enrichment, Service, and Value for Money" are also included in the evaluation areas. Passengers may also add photos to their reviews.

The study scraped the reviews of passengers who went on a cruise on European Routes between September 2020 and September 2021 from Cruisecritic.com. The data was collected from the website via the website scraping script created by the authors in the Python programing language. A total of 418 reviews written in English, which contain 208,849 words, were collected from the website and stored in as Comma Delimited data file (CSV). The data file included the ship name and review content. Other star-based-evaluations were not taken into consideration. Convenience sampling was used in this study. To ensure that the number of reviews needed to employ Leximancer software was met, as well as to match the sample size of prior relevant studies. For example, one study explored travelers' multisensory place experiences on Mediterranean port of call destinations (n=248) [56-58], another examined cruise travelers' service perceptions (n=2000) [9], and another investigated visitors' experiences in a natural world heritage site (n=351) [59].

Text mining models are significantly reliant on the preprocessing of unstructured textual data. According to [57], typical preprocessing steps include tokenizing,

stemming, bi-gram or tri-gram searches, and removal of stop words, punctuation, and irrelevant words or characters. This process can be complex and varies widely, often depending on the researcher's expertise. Leximancer, however, simplifies this process by offering a more streamlined and user-friendly approach to text preprocessing and model application, with limited scope for user customization of settings. Figure 1 illustrates the process of building a model using Leximancer Software. UGC from passengers, collated as text files, is uploaded into the software. The text processing settings are maintained by default.

However, the Leximancer application automates the content analysis, eliminates the effect of the researcher's subjective judgments on the output, and shortens the analysis time. It can also include erroneous concepts that are frequently mentioned in the text [56]. Therefore, the authors limited the total number of concepts to 60 via concept seed settings and eliminated erroneous concepts after careful reading. Erroneous concepts such as time expressions such as day, days, night, time, and times and frequently used words that reduce the depth of analysis such as cruise, cruises, and company names were eliminated via concept coding settings. Following the identification of initial concept seeds by the software, we refine the output by removing concepts (tokens) lacking significant meaning, erasing negotiation terms, and incorporating a sentiment lens.

The final output is a concept map that visually represents the service dimensions as experienced by cruise passengers. Additionally, the data exports from Leximancer provided us with valuable metrics on token co-occurrence and sentiment analysis. This enabled a more nuanced understanding of the underlying patterns and sentiments present in the cruise passengers' feedback.

5. Findings

Before the dataset was analyzed, descriptive statistics were obtained. Table 1 shows the age of the passengers, how many times they have cruised before, which route they commented on, the number of comments according to the cruise lines, and their percentage values in the dataset.

The dataset includes passenger comments from a total of 80 ships sailing on European routes with different itineraries. More than 74% of the passengers who write reviews are over the age of fifty. In normal times, it is expected that the average age of cruise passengers is high. However, the COVID-19 is more lethal in the elderly. Despite this, it is seen that middle-aged and older passenger boarded cruise ships during the pandemic period. Additionally, first-time cruisers account for less than 16% of the entire dataset, with approximately 48% of reviews coming from the Europe-British Isles & Western route.

After gaining key insights about the dataset, passenger reviews were analyzed using Leximancer Software. Once 418 comments were analyzed, Leximancer revealed 53 concepts that are clustered into 10 themes, which are presented in Figure 1. While smaller gray dots indicate the concepts, larger colorful circles indicate themes. In addition, the prominence of the themes is shown by heat mapping. According to the color wheel, the "hottest" or most significant theme appears in red, followed by orange for the next-hottest theme. For the sake of readability, the heat map indicators are given in Figure 1. The size of a concept's dot on the concept map also indicates a concept's connectivity. In other words, the larger the concept dot, the more often the concept is coded in the text with the other concepts on the map. In this context, connectivity refers to the total number of times a concept appears in print alongside every other concept on the map [55].

Figure 1. *Process of building the model*

As previously mentioned, 10 attributes were identified in the content analysis of passengers' online reviews of their perceived cruise quality. These attributes, ranked by their connectivity rates, are: Ship (100%), Staff (41%), COVID (37%), Cabin Location (31%), Public Area (27%), Restaurant (24%), Cabin (12%), Excursions (11%), and Ports (5%). In addition, Figure 2 represents the concept clusters within attributes.

The attributes and the words that make them up in Figure 3 are presented together with the relevancy percentages.

The 10 attributes that emerged at the end of the analysis support the literature. However, COVID emerged as a new attribute in the perceived service quality of passengers. The concepts that make up the COVID attribute are "experience, test, port, embarkation, tests, restrictions, mask, pandemic and itinerary". At the same time, it is seen that the port and excursions attributes are connected to other themes through the COVID attribute.

Accordingly, the use of the defining concepts of the COVID attribute with favorable and unfavorable structures has

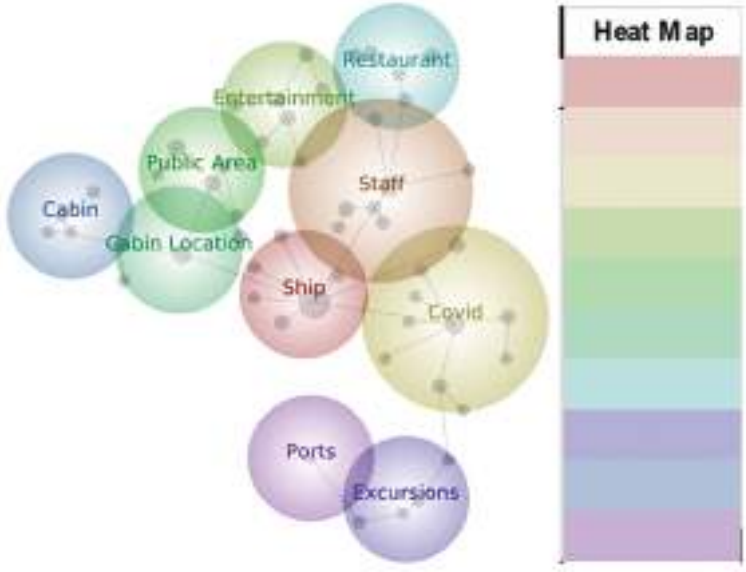

Figure 2. *Theme map*

Table 1. *Descriptives of dataset*

Age of the reviewers	Count	Percentage	Times sailed	Count	Percentage
10's	2	0.48%	First Timer	66	15.79%
20's	11	2.63%	2-5	75	17.94%
30's	35	8.37%	6-10	67	16.03%
40's	54	12.92%	10+	210	50.24%
50's	110	26.32%			
60's	122	29.19%			
70's	77	18.42%			
80's	7	1.67%			
Route	**Count**	**Percentage**	**Lines**	**Count**	**Percentage**
Europe, British Isles, and Western	199	47.61%	Virgin	158	37.80%
Europe-All	79	18.90%	Other	121	28.95%
Baltic Sea	65	15.55%	MSC	56	13.40%
Europe: River Cruise	40	9.57%	Celebrity	33	7.89%
Europe and Eastern Mediterranean	20	4.78%	VIKING	26	6.22%
Mediterranean	10	2.39%	AMA	13	3.11%
Europe-Western Mediterranean	5	1.20%	Royal Caribbean	11	2.63%

been examined, and the results are presented in Table 2. Considering all the comments of the passengers, 1887 positive structures were found, while 550 negative structures were used. However, all words describing the COVID attribute are associated with more positive structures than negative structures.

6. Discussions

In this study, the narratives of 418 people who went on a cruise on the European route during the COVID process were collected via a script written by the authors in Python. The collected texts were analyzed using Leximancer software. Leximancer software revealed the main attributes that affect passengers' perceived service quality. As a result, ten attributes that mostly affect passengers' perceived service quality has been revealed as; ship, staff, COVID, cabin location, public area, entertainment, restaurant, cabin, excursions, and ports. Since this study aims to determine the factors affecting the perceived service quality of cruise passengers and determine the new factors that occurred during the pandemic, the results obtained from this analysis were compared with the results obtained by [9], who examined the main attributes affecting the service quality perceived by cruise passengers in the pre-COVID period using the same method. Comparisons related to the pre-COVID and COVID periods of the main perceived service quality attributes are given in Table 3.

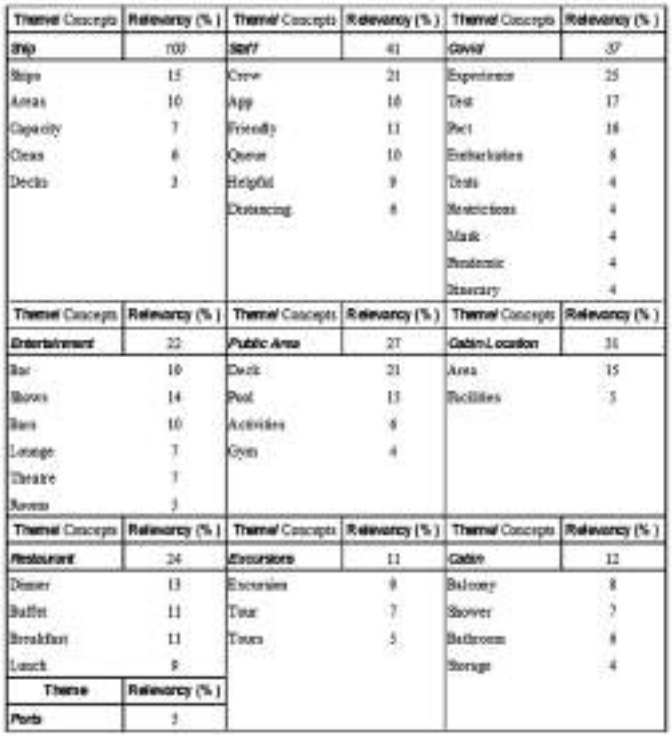

Figure 3. *Concepts under attributes*

As can be seen in Table 3, COVID, cabin location, and restaurant themes have been added to the factors affecting the perceived service quality of customers during the pandemic period. Although food, embarkation, and disembarkation themes were important themes in the pre-COVID period, they were not positioned as the main themes during the COVID period. While food became a restaurant theme, embarkation was coded as a concept under the COVID theme, and disembarkation completely disappeared. While [9] indicated that embarkation and disembarkation are factors that affect passengers' perceptions of service quality, [60] stressed the importance of embarkation for passenger satisfaction. However, embarkation was identified in our analysis as a concept falling under the COVID attribute. This is due to changes made to the boarding procedures during the pandemic. It has been noted that before boarding the ship, guests view all pre-testing and the supply of required documents (vaccination card, passport, special permissions) as a component of the service quality. The reviews of the passengers specifically indicated the time, queue, and compliance pandemic constraints. Some customer reviews on this subject are shown below:

"We were expecting the embarkation to take some time due to several documents that had to be handed in during check-in, lateral flow COVID tests to be carried out on every passenger

Table 2. *Related concepts*

Concept	Related concept	Count	Related concept	Count
All reviews	Favourable	1887	Unfavourable	550
Experience	Favourable	117	Unfavourable	33
Port	Favourable	44	Unfavourable	15
Test	Favourable	39	Unfavourable	14
Embarkation	Favourable	18	Unfavourable	5
Restrictions	Favourable	15	Unfavourable	6
Itinerary	Favourable	13	Unfavourable	4
Mask	Favourable	8	Unfavourable	5

Table 3. *Comparison of pre-COVID and COVID periods' main perceived services quality attributes*

Pre-COVID Period		COVID Period	
Theme	**Concept**	**Theme**	**Concept**
Ship	Ship, family, reservation, expensive	Ship	Ship, area, capacity, clean, decks
Staff	Staff, friendly, helpful, nice	Staff	Crew, app, friendly, queue, helpful, distancing
	Food, breakfast, restaurants, delicious, elevators	**COVID**	Experience, test, port, embarkation, restriction, mask, pandemic, itinerary
Area (public spaces)	Area, pool, deck, and bar	**Cabin Location**	Area, facilities
Room/Cabin	Room, bathroom, bed	Public Area	Deck, pool, activities, and gym
Entertainment	Entertainment, crowded, spa	Entertainment	Bar, shows, lounge, theater, and rooms
	Embarkation, line, comfortable	**Restaurant**	Dinner, buffet, breakfast, and lunch
Excursions	Excursions, cancellation, itinerary	Room/Cabin	Balcony, shower, bathroom, and storage
	Disembarkation, smooth	Excursions	Excursions, tours
Port	Port	Ports	Port
Comparison with Araslı et al. [9]			
COVID: Coronavirus disease			

boarding the cruise, and waiting for the results to come back as negative before being allowed to board. However, the entire process was handled very well by [Line] and cruise terminal staff."

"The embarkation process involved a 4 1/2 hr queue, which was not COVID safe as we were all in close contact for the 4 1/2 hrs, with other passengers before we were tested."

As it can be seen in Table 3, COVID became the third most important attribute, which includes the concepts of test, COVID, pandemic, restrictions, mask, embarkation, experience, and itinerary. According to customer reviews, passengers from pre-cruise to post-cruise must undergo rapid antigen tests. Although it differs from tour to tour, the test may be applied 3 days before embarkation, just before embarkation, before and/or after disembarkation, before or after excursions/tours, or even as a daily routine. For this reason, it has been observed that the test applications and informing the passenger in all stages of processes affect the service quality perception of the passengers. Some customer reviews of these situations are shown below:

"But the policy differed when we boarded. While the website stated that IF we did not have a test within 48 h of boarding, we would be required to have a test at boarding. "We went out of our way to get a test within the proscribed time."

"Even the paperwork they showed at boarding said the same thing. Perhaps [Line] should be clearer and simply state that a test will be required at the boarding time."

"Pre-boarding required a COVID test, my wife got her result in 20 min but after 2 hours and 4 complaints they admitted they had lost mine and I had to repeat it so we boarded 2 1/2 hours late."

"If we must be COVID tested before boarding we should be told when to come be tested."

"There were only about 49 passengers, all of whom were tested and vaccinated. Regarding COVID, they tested (saliva) every day and left small collection tubes each day, which you were to drop off at the main desk every morning."

"Anyway, we were told that COVID testing occurs at dock 10 for all cruise ships. We were given a rather lengthy set of directions and proceeded to get lost."

"The COVID testing was terrible, just mayhem."

"COVID testing was offered to all guests before departure from the ship. Results were immediate."

"The porters seemed strangely disinclined to take our bags, and there was no information about where to go to get the COVID test. Eventually, we saw a long line snaking round the side of the terminal building and having asked a couple of passengers to join it."

There are many studies that indicate that the attributes of entertainment, food and beverages, spa and fitness, pool, childcare area, and casino affect the quality of service on the cruise [9,32,33,35-37,43,61-64]. To reduce the possibility of transmission during the pandemic process, many onboard activities have been restricted. Although the ships sailed at half capacity, in common areas such as spa, pool, Turkish bath, gym, sunbathing area, observation area, cinema, theater, and casino, distance restrictions and masks were imposed, and some services were completely closed to use. In addition, self-service service has been abolished in restaurants and buffets, and table service has been made mandatory. As can be seen in Table 3, although the entertainment theme was included in both periods, the theme associated with the concept of crowds in the pre-COVID period was associated with concepts such as bars, rooms, and

theaters during the COVID period. However, when the passenger comments were examined, it was seen that the restrictions were within the expectations, obligations made passengers feel safe, and even non-compliance with the COVID restrictions created a negative effect on perceived service. Some customer reviews on this subject are shown below:

"Because of COVID, market place was no self service, but that is no problem."

"We know some of the COVID restrictions may seem tiresome, but we are happy to abide by them as it means we are finally able to cruise."

"What stuck out to us was the friendly helpful staff and the COVID restrictions in place, so we all had to wear masks still in inside areas so we all kept safe."

"Thermal pool area is limited to 6 people in 45 min sessions Well organized and very relaxing with super friendly staff."

"COVID restrictions only allowing 10 people a time in the indoor pool the attendant made in fair for everyone to have chance of swimming and using the jacuzzi."

"Entertainment was varied and excellent but due to COVID new regulations the venues had to keep moving around the ship so areas could be sanitized which again I thought was great for the passenger safety."

"Considering all the concessions that the cruise industry had to meet in order to comply with the ever changing cruise restrictions, we thought RCL did an outstanding job!! We felt safe at all times, and on those occasions when we forgot to place our mask over our noses, we were gently reminded."

"Entertainment was positively different, but a few things were curtailed due to weather and COVID.".

"the health and safety procedures to protect us from COVID-the evidence speaks for itself as all three of us caught COVID. We had to stand in long queues in confined spaces, mask wearing was not enforced, and rules such as restricted numbers in lifts or hot tubs were not adhered to or enforced."

While, [65] claimed that cruise itinerary affects service quality, [66] suggested that cruise arrangements such as itinerary, accommodations etc. effects the perceived value of the cruise experience. The cancelation of port of calls, restrictions on solo shore trips, except paid tours and excursions by lines, were noted in passenger reviews. In addition, restrictions applied in paid tours, such as prohibition of exiting tour vehicles, shopping restrictions, social distancing, and mask obligations, have also appeared in narratives. Some customer reviews of these situations are shown below:

"…Not fussed about a cruise to nowhere, just wanted to experience it again albeit expecting a few changes and restrictions due to COVID."

"This cruise only made a stop in Belfast and, as a COVID measure, you were only allowed off the ship through an organized tour via RCL."

"Fortunately, I already had flags from all three of the countries on this itinerary, because independent exploration in the ports was severely limited because of COVID-19 precautions. We enjoy both cruises and land tours; often, our trips combine the two."

"Excursions (obligatory otherwise you're not allowed off-COVID regulations) were really good."

"I can only think that ports and facilities were restricted by the COVID regulations. For me, this resulted in too many days at sea and not enough port excursions."

"Excursions were very limited (due to COVID) and pricey."

"Excursions during COVID are limited and seem to mainly involve sitting on a bus or walking in a group; forbidden to stop and rest, to shop, or even buy an ice cream or coffee on pain of not being allowed to re-board the ship."

"We stayed on the ship because again because of COVID the only excursions were with the ship, I am not complaining about this, we knew this before we boarded and we accepted it."

According to the results of the research, the most frequently used concept to define the COVID factor is "experience". Despite the interruptions, bans, and changes in services during the COVID period, passengers mostly talked about their experiences positively as they felt safe.

"We can honestly say that this cruise exceeded our expectations. I be worried that the COVID restrictions would impact the experience, but on the contrary, they made you feel safe and they were handled brilliantly."

"Many people considering a cruise will ask if COVID precautions will somewhat diminish the experience. "I think the general opinion was not really."

"Wonderful experience from start to finish. The care over our safety at a time when the delta COVID variant was in ascendancy nationally was magnificent and most welcome."

In addition, as shown in Table 3, the ship theme, which included concepts related to family and pricing in the pre-COVID period, started to include concepts such as area, capacity, and cleaning situation of environment during the COVID period. While the staff theme continued to include concepts that create staff-based customer satisfaction, such as helpful and friendly, in both periods, the distance concept was added to the theme in the post-COVID period. The Room/Cabin theme did not differ much, similar to the staff theme, but during the COVID period, the balconies and storage facilities of the cabins were added to the attributes

affecting the perceived service quality as new concepts. Additionally, during the COVID period, the cabin location theme emerged as a new perceived service quality attribute. The themes of area, excursions, and port were associated with similar concepts in both periods, and no significant differences were detected.

7. Conclusion

Forecasting consumer demands and expectations has been an important issue for the manufacturing and service industries at the beginning of the industrial revolution. Especially due to the intangible nature of the service sector, understanding and meeting customer demands and expectations in this field and measuring perceived quality have always been important challenges for the marketing sector. The entire planet is constantly changing. Although companies have plans to estimate and mitigate numerous risks, unexpected, unanticipated, and disastrous occurrences can still occur. Similar to the COVID-19 pandemic, which has developed into an unpredictable occurrence with disastrous consequences, particularly for the cruise industry. Even if the epidemic has impacted the business, today's lessons can help prevent and manage a similar occurrence in the future. Hence, the main motivation of this study was to determine whether the factors affecting customers' perceived service quality changed during the pandemic period in the cruise industry. Therefore, this study aims to determine the factors affecting the perceived service quality of cruise passengers and determine the new factors that occurred during the pandemic.

Because of the study, ten attributes that mostly affect passengers' perceived service quality has been revealed as; ship, staff, COVID, cabin location, public area, entertainment, restaurant, cabin, excursions, and ports. COVID, restaurant, and cabin location revealed three new attributes in this regard. In addition, favorable and unfavorable structures of the COVID attribute have also been examined. Considering all the comments of the passengers, 1887 positive structures were found, while 550 negative structures were used. However, all words describing the COVID attribute are associated with more positive structures than negative structures. This result was interpreted as the fact that the cruise companies' compliance with COVID measures during this period had a positive impact on customer satisfaction.

Another result obtained within the scope of the study that can be described as remarkable is related to demographic findings. According to the findings obtained within the scope of the study, 74% of those who made user comments regarding their cruise travel during the pandemic period were passengers over the age of fifty. However, according to studies in the literature, it is argued that the average age of cruise passengers is around 50 years [67]. In normal times, it is expected that the average age of cruise passengers is high. However, the COVID-19 virus is more lethal in the elderly. Despite this, it is seen that middle-aged and older passenger boarded cruise ships during the pandemic period. This finding was interpreted by the authors in two ways. The first is that people over the age of 50 preferred cruise travel more during the pandemic period, and the second is that people over the age of 50 created more online user comments during the pandemic period. To make a definitive judgment regarding the findings, it is considered that it would be useful to examine the tendencies of individuals over the age of 50 to prefer cruise travel and create online user comments.

This study is important because it analyzes UGC, which although relatively new, is considered a reliable data source for various reasons in different sources. These contents, created almost constantly by people all over the world, create big data sets that are very difficult to analyze and draw meaningful conclusions. However, making this big data meaningful with the help of methods/methodologies based on artificial intelligence and machine learning, such as those used in this study, will greatly benefit both the application and the literature. To the best of our knowledge, this is the second known study to measure cruise passengers' perceived service through artificial intelligence technologies [9]. This study is important because it supports the findings obtained by [9] and it also argues that consumer preferences will be affected in extraordinary situations such as pandemics. Therefore, it is thought that repeating the same method using similar samples in the post-pandemic period and comparing it with the existing results will contribute greatly to the marketing and cruise literature.

Authorship Contributions

Concept design: B. Çullu, N. Özispa, and G. Arabelen, Data Collection or Processing: B. Çullu, Analysis or Interpretation: B. Çullu, Literature Review: N. Özispa, Writing, Reviewing and Editing: B. Çullu, N. Özispa, and G. Arabelen.

Funding: The authors received no financial support for the research, authorship, and/or publication of this article.

References

[1] D. Johnson "Environmentally sustainable cruise tourism: a reality check." *Marine Policy*, vol. 26, pp. 261-270, Jul 2002.

[2] O. Kaya, "A Research on Tourists' Expectations and Performance Levels from Cruise Ships Food and Beverage Services- Turistlerin Kruvaziyer Gemileri Yiyecek ve İçecek Hizmetlerinden Beklenti ve Performans Düzeylerine İlişkin Bir Araştırma." *Journal of Tourism and Gastronomy Studies*, vol. 5, pp. 22-38, 2017.

[3] Statista, Statista research department, *Cruise Industry Worldwide Statistics & Facts*, European Union. https://www.statista.com/topics/1004/cruise-industry/, 2021.

[4] CLIA, Cruise Industry COVID-19 Facts and Resources. Cruise Lines International Association. https://cruising.org/en-gb/cruise-industry-covid-19-facts-and-resources, 2021.

[5] A. Parasuraman, V. A. Zeithaml, and L. L. Berry, "A conceptual model of service quality and its implication for future research." *Journal of Marketing*, vol. 49, pp. 41-50, 1985.

[6] A. Parasuraman, V.A. Zeithaml, and L. L. Berry. "SERVQUAL: a multiple-item scale for measuring consumer perceptions of service quality." *Journal of Retailing*, vol. 64, pp. 12-40, 1988.

[7] D. A. Baker, "Exploring cruise passengers' demographics, experience and satisfaction with cruising the Western Caribbean." *International Journal of Tourism & Hospitality Reviews*, vol. 1, pp. 33-43, Nov 2014.

[8] H. Qu, and E. W. Y. Ping, "A service performance model of Hong Kong cruise travelers' motivation factors and satisfaction." *Tourism Management*, vol. 2020, pp. 237-244, Apr 1999.

[9] H. Araslı, M. B. Saydam, and H. Kilic, "Cruise travelers' service perceptions: a critical content analysis." *Sustainability*, vol. 12, pp. 6702, 2020.

[10] WHO, World Health Organization. *WHO Coronavirus (COVID-19)* Dashboard. https://covid19.who.int/, 2021.

[11] V. A. Zeithaml, L. L. Berry, and A. Parasuraman, "Communication and control processes in the delivery of service quality." *Journal of Marketing,* vol. 52, pp. 35-48, Apr 1988.

[12] N. Seth, S. G. Deshmukh, and P. Vrat, "Service quality models: a review." *International Journal of Quality & Reliability Management,* vol. 22, pp. 913-949, Dec 2005.

[13] V. A. Zeithaml, and M. J. Bitner, "Services marketing: integrating customer focus across the firm." 3rd Edition, Irwin McGraw-Hill, New York, 2003.

[14] C. Grönroos, "A service quality model and its marketing implications." *European Journal of Marketing,* vol. 18, pp. 36-44, Apr 1984.

[15] J. Haywood-Farmer, "A conceptual model of service quality." *International Journal of Operations & Production Management*, vol. 8, pp. 19-29, Jun 1988.

[16] A. A. Brogowicz, L. M. Delene, and D. M. Lyth, "A synthesised service quality model with managerial implications." *International Journal of Service Industry Management,* vol. 1, pp. 27-44, Apr 1990.

[17] J. J. Cronin, and S. A. Taylor, "Measuring service quality: a reexamination and extension." *Journal of Marketing,* vol. 6, pp. 55-68, Jul 1992.

[18] J. Mattsson, "A service quality model based on ideal value standard." *International Journal of Service Industry Management,* vol. 3 pp. 18-33, Sep 1992.

[19] K. R. Teas, "Expectations, performance evaluation, and consumers' perceptions of quality." *Journal of Marketing,* vol. 57, pp. 18-34, Oct 1993.

[20] B. J. Berkley, and A. Gupta, "Improving service quality with information technology." *International Journal of Information Management,* vol. 14, pp. 109-121, Apr 1994.

[21] P. A. Dabholkar, "Consumer evaluations of new technology-based self-service operations: an investigation of alternative models", *International Journal of Research in Marketing,* vol. 13, pp. 29-51, Feb 1996.

[22] R. A. Spreng, and R. D. Mackoy, "An empirical examination of a model of perceived service quality and satisfaction." *Journal of Retailing,* vol. 722, pp. 201-214, Feb 1996.

[23] G. Philip, and S. A. Hazlett, "The measurement of service quality: a new P-C-P attributes model." *International Journal of Quality & Reliability Management,* vol. 14, pp. 260-286, Apr 1997.

[24] J. C. Sweeney, G. N. Soutar, and L. W. Johnson, "Retail service quality and perceived value." *Journal of Consumer Services,* vol. 4, pp. 39-48, Jan 1997.

[25] H. Oh, "Service quality, customer satisfaction and customer value: a holistic perspective." *International Journal of Hospitality Management,* vol. 18, pp. 67-82, Mar 1999.

[26] P. A. Dabholkar, C. D. Shepherd, and D. I. Thorpe, "A comprehensive framework for service quality: an investigation of critical conceptual and measurement issues through a longitudinal study." *Journal of Retailing,* vol. 76, pp. 131-139, 2000.

[27] F. A. Frost, and M. Kumar, "INTSERVQUAL: an internal adaptation of the GAP model in a large service organization." *Journal of Services Marketing,* vol. 14, pp. 358-377, Sep 2000.

[28] A. C. Soteriou, and Y. Stavrinides, "An internal customer service quality data envelopment analysis model for bank branches." *International Journal of Bank Marketing,* vol. 18, pp. 246-252, 2000.

[29] A. J. Broderick, and S. Vachirapornpuk, "Service quality in internet banking: the importance of customer role." *Marketing Intelligence & Planning,* vol. 20, pp. 327-335, Nov 2002.

[30] F. X. Zhu, W. J. Wymer, and I. Chen, "IT-based services and service quality in consumer banking." *International Journal of Service Industry Management,* vol. 13, pp. 69-90, Mar 2002.

[31] J. Santos, "E-service quality: a model of virtual service quality dimensions." *Managing Service Quality,* vol. 13, pp. 233-246, 2003.

[32] Y. Yoon, and K. C. Cha, "A qualitative review of cruise service quality: case studies from Asia." *Sustainability*, vol. 12, pp. 8073, Sep 2020.

[33] S. Yi, J. Day, and L. Cai, "Exploring tourist perceived value: An investigation of Asian cruise tourists' _travel experience." *Journal of Quality Assurance in Hospitality & Tourism,* vol. 15, pp. 63-77, Jan 2014.

[34] J. F. Petrick, "First timers' and repeaters' perceived value." *Journal of Travel Research,* vol. 43, pp. 29-38, Aug 2004.

[35] M. Risitano, A. Sorrentino, and M. Quintano, "Understanding the role of the service experience in the cruise industry." *International Journal of Tourism Policy*, vol. 7, pp. 289-308, Jan 2017.

[36] J. F. Petrick, C. Tonner, and C. Quinn, "The utilization of critical incident technique to examine cruise passengers' repurchase intentions." *Journal of Travel Research,* vol. 44, pp. 273-280, Feb 2006.

[37] B. L. Chua, B. Goh, L. Huffman, C. Jai, and S. Karim, "Cruise passengers' perception of key quality attributes of cruise lines in North America." *Journal of Hospitality Marketing & Management,* vol. 25, pp. 346-371, 2016.

[38] A. Timoshenko, and J. R. Hauser, "Identifying customer needs from user-generated content." *Marketing Science,* vol. 38, pp. 25-38, Jan 2019.

[39] T. K. Naab, and A. Sehl, "Studies of user-generated content: a systematic review." *Journalism,* vol. 18, pp. 1233-1434, 2016.

[40] J. Krumm, N. Davies, and C. Narayanaswami, "User-generated content." *IEEE Pervasive Computing*, vol. 7, pp. 10-11, Oct-Dec 2008.

[41] S. Illum, S. Ivanov, and Y. Liang, "Using virtual communities in tourism research." *Tourism Management*, vol. 31, pp. 335-340, Jun 2010.

[42] C. Haythornthwaite, and A. Gruntz, "*A noun phrase analysis tool for mining online community conversations."* London: Springer, 2007.

[43] P. Brejla, and D. Gilbert, "An exploratory use of web content analysis to understand cruise tourism services." *International Journal of Tourism Research*, vol. 16, pp. 157-168, Sep 2012.

[44] S. Litvin, R. Goldrooneyhuang, and B. Pan, "Electronic word-of-mouth in hospitality and tourism management." *Tourism Management*, 458-468, Jun 2008.

[45] K. Kripendorff, *Content Analysis: An Introduction to Its Methodology*. Sage Publications, 2018.

[46] B. J. Biroscak, J. E. Scott, J. H. Lindenberger, and C. A. Bryant, "Leximancer software as a research tool for social marketers: Application to a content analysis." *Social Marketing Quarterly*, vol. 23, pp. 223-231, Sep 2017.

[47] C. Tseng, B. Wu, A. M. Morrison, J. Zhang, and Y. C. Chen, "Travel blogs on China as a destination image formation agent: a qualitative analysis using leximancer." *Tourism Management*, vol. 46, pp. 347-358, Feb 2015.

[48] N. J. Martin, and J. L. Rice, "Profiling enterprise risks in large computer companies using the Leximancer software tool." *Risk Management*, vol. 9, pp. 188-206, Jun 2007.

[49] W. Ward, et al. "Health services and delivery research: The role of informal networks in creating knowledge among health-care managers: a prospective case study." *Health Services and Delivery Research,* vol. 2, May 2014

[50] A. E. Smith, and M. S. Humpreys, "Evaluation of unsupervised semantic mapping of natural language with Leximancer concept mapping." *Behavior Research Methods,* vol. 38, pp. 262-279, May 2006.

[51] D. Rooney, "Knowledge, economy, technology and society: The politics of discourse." *Telematics and Informatics,* vol. 4, pp. 405-422, Nov 2005.

[52] D. Mahr, S. Stead, and G. Odekerken-Schröder, "Making sense of customer service experiences: a text mining review." *Journal of Services Marketing*, vol. 33, pp. 88-103, Apr 2019

[53] A. Brochado, P. Rodrigues, A. Sousa, A. P. Borges, M. Veloso, and M. Gómez-Suárez, "Resilience and sustainable urban tourism: understanding local communities' perceptions after a crisis." *Sustainability*, vol. 15, pp. 1-21, Sep 2023

[54] S. Huang, and X. Wang, "COVID-19 two years on: a review of COVID-19-related empirical research in major tourism and hospitality journals." *International Journal of Contemporary Hospitality Management*, vol. 35, pp. 743-764, Sep 2022

[55] Leximancer, 2019, November 25. *Leximancer User Guide*. https://static1.squarespace.com/static/5e26633cfcf7d67bbd350a7f/t/60682838c894556d34db2cfb/1617438828923/Leximancer+User+Guide+5.pdf

[56] P. Sotiriadou, J. Brouwers, and T. A. Le, "Choosing a qualitative data analysis tool: A comparison of NVivo and Leximancer." *Annals of Leisure Research*, vol. 17, pp. 218-234, 2014.

[57] M. J. Denny, and A. Spirling, "Text preprocessing for unsupervised learning: Why it matters, when it misleads, and what to do about it." *Political Analysis*, vol. 26, pp. 168-189, Mar 2018. Published online by Cambridge University Press.

[58] D. Buzova, S. Sanz-Blas, and A. Cervera-Taulet, "'Tour me onshore': understanding cruise tourists' evaluation of shore excursions through text mining." *Journal of Tourism and Cultural Change*, vol. 17, pp. 356-373, Dec 2018.

[59] O. M. Stoleriu, A. Brochado, A. Rusu, and C. Lupu, "Analyses of visitors' experiences in a natural world heritage site based on TripAdvisor reviews." *Visitor Studies*, vol. 22, 192-212, Jul 2019.

[60] Z. Zhang, Q. Ye, H. Song, and T. Liu, "The structure of customer satisfaction with cruise-line services: An empirical investigation based on online word of mouth." *Current Issues in Tourism,* vol. 18, pp. 450-464, 2015.

[61] M. Aggett, and W. M. Lim, "Service quality and the cruise industry." *The Business and Management of Ocean Cruises,* pp. 196-205, 2012

[62] S. Hosany, and M. Witham, "Dimensions of cruisers' experiences, satisfaction, and intention to recommend." *Journal of Travel Research*, vol. 49, pp. 351-364, 2010.

[63] O. P. Woodham, J. A. Williams, and K. R. McNeil, "Toward understanding the impact of attributes on satisfaction in different price tiers." *Journal of Consumer Satisfaction, Dissatisfaction and Complaining Behavior,* vol. 29, pp. 91-117, Jan 2017.

[64] Y. Li, and R. Kwortnik, "Categorizing cruise lines by passenger perceived experience." *Journal of Travel Research*, vol. 56, pp. 941-956, 2017.

[65] A. Radić, P. Björk, and H. Kauppinen-Räisänen, "Cruise holidays: how on-board service quality affects passengers' behavior." *Tourism in Marine Environments*, vol. 14, pp. 45-59, 2019.

[66] D. M. A. Baker, and M. Fulford, "Cruise passengers' perceived value and willingness to recommend." *Tourism & Management Studies*, vol. 12, pp. 74-85, 2016.

[67] H. Akpınar, and F. Bitiktaş, Türkiye'deki kruvaziyer limanlarının mevcut durumu, potansiyeli ve gelişimine yönelik öneriler. *III. Ulusal Deniz Turizmi Sempozyumu,* Dokuz Eylül University, İzmir, Türkiye, 2016.

Journal of ETA Maritime Science 2024;12(2):199-212

Calculation of Time-Independent Maneuvering Coefficients of an Underwater Vehicle Based on Single Grid Structure

Oğuzhan Kırıkbaş, Şakir Bal

İstanbul Technical University, Faculty of Naval Architecture and Ocean Engineering, İstanbul, Türkiye

Abstract

A simulation approach relying on a single grid topology has been employed to replicate the motion characteristics of different experimental facilities, including towing tank, rotating arm mechanism, and planar motion mechanism using a single mesh. The control volume and computational mesh setup was built in a way to enable to perform both steady and time dependent simulations to compute entire set of coefficients required by the standard submarine equations of motion. Mesh is consisted of a rectangular prism shaped background and a spherical overset domain which can be rotated, circulated and oscillated depending on the simulation type. To enable the implementation of this approach to the rotating arm simulations, modifications to source code of the open-source computational fluid dynamics software OpenFOAM have been made. Motivation is to change the perspective on the problem by using the knowledge of mathematics behind the solution algorithms and the software structure. In this study extensive set of time-independent coefficients obtained via straight and oblique towing as well as steady rotation simulations are presented for a fully appended generic submarine geometry. Results are then compared with the benchmark experimental data. It is found that the consistency between results are quite satisfactory.

Keywords: DARPA Suboff, Maneuvering coefficient, Rotating arm, OpenFOAM

1. Introduction

Maneuvering for underwater vehicles (UVs) refers to the controlled and intentional alteration of the vehicle's position, orientation or trajectory in a fluid medium. This process involves the precise modulation of hydrodynamic forces and moments in 6-DoF and achieved through the deflection of control surfaces and/or propulsor rotation rate as well as ballast intake or discharge. The prerequisite for solving the maneuvering problem is the expression of these complex motion behavior via a mathematical model known as a maneuvering model. Maneuvering coefficients serve as essential parameters in a maneuvering model, quantifying hydrodynamic forces and moments acting on an UV during various maneuvers. Initially developed by Gertler and Hagen [1], a generalized UV maneuvering model based on the motion equations has undergone revisions by Feldman [2] incorporating crossflow terms.

These coefficients can be roughly categorized based on the time dependency of the computational fluid dynamics (CFD) simulation used in their calculations. Time-independent maneuvering coefficients are fundamental parameters that impact various aspects of UV design, operation, and safety. Their accurate determination contributes to the overall effectiveness and reliability of UVs in a wide range of applications including dynamic stability and control system effectiveness.

Despite recent proposals for more comprehensive approaches to the maneuvering problem of UVs, based on the "synthetic" motion [3] or free running of UV [4-9]; literature commonly employs CFD simulations mimicking experimental setups. A towing tank is imitated in CFD environment as rectangular prism control volume for straight and oblique towing simulations. Whereas rotating arm (RA) mechanism is imitated as a circular segment shaped control volume for mimicking the steady rotational motion. The main difference between CFD simulations and experiments in terms of motion is the object/medium exposed to this motion. For the sake of computational efficiency; the body is

Address for Correspondence: Oğuzhan Kırıkbaş, İstanbul Technical University, Faculty of Naval Architecture and Ocean Engineering, İstanbul, Türkiye
E-mail: kirikbas17@itu.edu.tr
ORCID ID: orcid.org/0000-0002-2504-8727

Received: 26.01.2024
Last Revision Received: 20.04.2024
Accepted: 24.04.2024

To cite this article: O. Kırıkbaş, and Ş. Bal, "Calculation of Time-Independent Maneuvering Coefficients of an Underwater Vehicle Based on Single Grid Structure." *Journal of ETA Maritime Science*, vol. 12(2), pp. 199-212, 2024

at rest and the flow is passing through the body in the CFD simulations of both cases. In order to achieve this for RA simulations and expose the fluid domain to additional forces arose from rotation, governing equations of the flow must be modified. Planar motion mechanism (PMM) simulations are unsteady in nature due to involving the motion of the body with respect to fluid medium as in the experiments.

Unsteady numerical simulations adhere to the availability of high amount of computational resources. Additionally they are subject to certain numerical limitations (i.e. Courant-Friedrichs-Lewy or CFL condition) which strongly effects the potential improvement in their accuracy level with the available computational power. On contrary to the other types of facilities, PMM experiments/simulations can attain an extensive set of coefficients. However their results cannot be used directly to obtain relevant hydrodynamic coefficients. Fourier transform is required for the frequency-time domain transition of the data.

Since motions created by a PMM are time-dependent in nature, PMM simulations are only feasible after achieving adequate computational capacity [10,11]. Phillips et al. [12], Zhang et al. [13] and Pan et al. [14] are among the pioneers in this category. Besides sufficiently accurate methods have been proposed since the beginning of the last century for the UV like shapes [15-18]. As a result of this; researchers initially focused their attention on time independent coefficients.

There's a strong background in understanding oblique flows and cross-flow separation on axisymmetric bodies. Together with the low demand of computational resources and ease of implementation of the problem setup to the CFD environment, working on linear damping coefficients became the initial area of research. Toxopeus [19] investigated the local field variables as well as global measures of the flow around a non-appended submarine hull at incidence.

Motion stability both in horizontal and vertical plane is expressed in terms of stability indices (i.e. G_v and G_h). Ensuring the vehicle has desired level of course-keeping stability in both planes rotational motion coefficients must also be calculated along with the linear damping coefficients. Phillips et al. [20] used time-independent CFD simulations to predict the dynamic stability margin of an autonomous UV by calculating the required coefficients.

Inherently these coefficients are also related with the steady (third phase) turning motion and they can be computed rather than actual rotation of the vehicle with respect to mesh but modification of the flow field to expose UV to Coriolis force and centrifugal acceleration. This is known as multiple rotating reference frame (MRF) approach or frozen rotor method due to its primary are of application is turbomachinery. Although MRF introduce a certain amount of error, the accuracy of the results are generally adequate for an engineering solution.

Common feature of the above mentioned studies is the use of different control volume shapes for mimicking the different experimental facilities. A small number of studies have devised techniques to consolidate different domain types into a single one, enabling the performance of multiple types of analyses. Oblique towing and steady turning simulations are performed by Cao et al. [21] using a single computational domain. They adopt SRF approach to reflect the effects of rotation on the governing equations of the flow.

Differently from [21]; Xiaocui et al. [22] employ MRF approach in a spherical mesh zone located inside a background cuboid control volume. The center of rotation is transferred from the pivot point of the RA mechanism to the body-fixed coordinate system origin. In order to achieve this the authors modified source codes of the CFD software with a user defined function. The source term that represents the Coriolis force and centrifugal acceleration in momentum equation was manipulated. By doing this, using same control volume for both oblique towing and RA simulations becomes possible. In general, these studies demonstrated the adequacy and efficiency of the steady state assumption when solid body motion does not involve. Together with the added mass coefficients, this time-independent coefficients can be used in a maneuvering model to perform trajectory calculations. In terms of definitive maneuvers the trajectories associated with maneuvers steady in nature such as turning circle is essentially governed by time-independent coefficients.

Utilizing the methodology proposed in [10] and [11], the control volume and computational mesh setup used in this study was built in a way to enable to perform both steady (i.e oblique towing and RA) and time independent simulations. By doing so it is possible to compute almost all of the coefficients required by the standard submarine equations of motion [2]. Preliminary results which are limited with the linear damping coefficients presented in [10] and [11] enlarged in this study. An extensive set of hydrodynamic coefficients in relation to time-independent analyses including control surface coefficients are given at this time to show the effectiveness of the single grid topology approach. Independent variable (i.e. drift/attack/control surface deflection angle and rotation radius) intervals, which corresponds to the linear and non-linear variations of dependent variables (i.e. force and moments) are investigated. Results are benchmarked with the RA experiments of Zhao et al. [23,24], PMM experiments of Roddy [25] and wind tunnel experiments of Khan et al. [26] where relevant. This paper organized as follows. Section 2 describes the governing equations including the modifications, as well as the coordinate system, UV geometry, domain, mesh and boundary conditions. Simulation matrix

is given at the end of this section. The computational mesh is validated and the numerical results are given in Section 3. The final remarks are presented in the conclusion section.

2. Materials and Methods

2.1. Geometry and Main Particulars

The model used in the CFD simulations is the fully-appended DARPA Suboff submarine (AFF-8). UV geometry in 3D is depicted in Figure 1. The main particulars of the model were defined in [27] and are provided in Table 1.

2.2. Coordinate System and Standard Convention

The body fixed coordinate system and standard direction convention for forces and moments as well as control surface (rudder and elevator) deflections are shown in Figure 2. Surge, sway and heave forces are identified as X, Y, and Z and the roll, pitch and yaw moments as K, M and N respectively. Prime (') symbol is employed to indicate dimensionless quantities and nondimensionalization is made according to Equations (1) and (2).

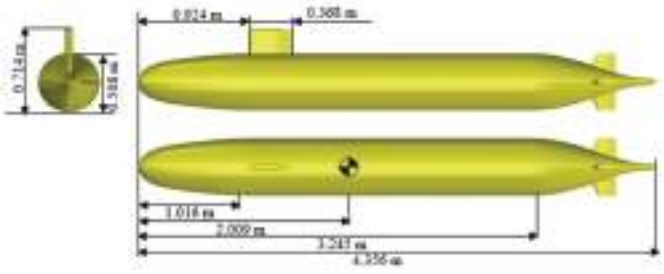

Figure 1. *DARPA Suboff AFF-8 configuration*

Table 1. *Main particulars of DARPA Suboff AFF-8*

L [m]	D [m]	H [m]	S [m²]	∇ [m³]	xg from FP [m]
4.356	0.508	0.714	6.348	0.706	2.009

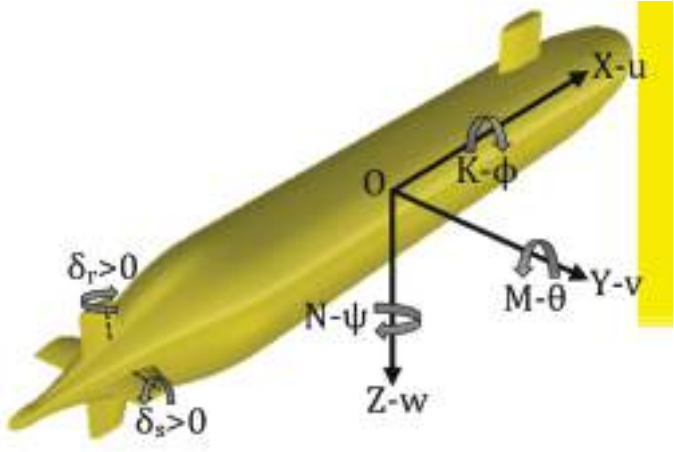

Figure 2. *The standard direction convention for motion parameters*

$$X', Y', Z' = \frac{X,Y,Z}{\frac{1}{2}\rho L^2 U^2}$$
$$K', M' N' = \frac{K,M,N}{\frac{1}{2}\rho L^3 U^2} \quad (1)$$

$$w', v', \delta_r, \delta_s = \alpha, -\beta, \delta_r, \delta_s \text{ (rad.)} \quad (2)$$

2.3. Equations of Motion

Together with the selected turbulence model equation(s); the continuity equation [Equation (3)] and the Unsteady Reynolds-Averaged Navier-Stokes Equations [Equation (4)] are governing the flow field,

$$\frac{\partial \overline{U}_i}{\partial x_i} = 0 \quad (3)$$

$$\frac{\partial \overline{U}_i}{\partial t} + \frac{\partial \overline{U_i U_j}}{\partial x_j} = -\frac{1}{\rho}\frac{\partial P}{\partial x_i} + \frac{\partial}{\partial x_j}\left\{\nu\left(\frac{\partial \overline{U}_i}{\partial x_j} + \frac{\partial \overline{U}_j}{\partial x_i}\right)\right\} - \frac{\partial U_i' U_j'}{\partial x_j} + f_i \quad (4)$$

Where mean velocity is denoted with $\overline{U}_i$, P represents the pressure, summation of the artificial viscosity due to turbulence modelling and molecular viscosity is represented by ν which is the effective viscosity. Density of the fluid is indicated with ρ and f_i represents the external momentum source in the "i" direction. Unsteady term of Equation (4) vanishes for the simulation cases not involving solid body motion. On contrary to the other simulation types, for RA simulations the momentum source term in Equation (4) is non-zero. Representing the steady rotational motion via MRF approach means the Coriolis force and the centrifugal acceleration expressed in Equation (5) acting on the UV.

$$MS = -\rho\left(2\Omega \times U_r + \Omega \times (\Omega \times r)\right) \quad (5)$$

Here, MS represents the momentum source, U_r is the relative velocity, Ω is the angular velocity and r represents the distance from rotation center. Because of change in rotation center, this source term needs to be modified as shown in Figure 3.

The components of the momentum source term with respect to rotation center A and rotation center B are demonstrated in Equation (6) and Equation (7), respectively.

$$MS_{xA} = -\rho\left(2\Omega \times U_r + \Omega \times (\Omega \times (x - x_A))\right)$$
$$MS_{yA} = -\rho\left(2\Omega \times U_r + \Omega \times (\Omega \times (y - y_A))\right) \quad (6)$$
$$MS_{zA} = -\rho\left(2\Omega \times U_r + \Omega \times (\Omega \times (z - z_A))\right)$$

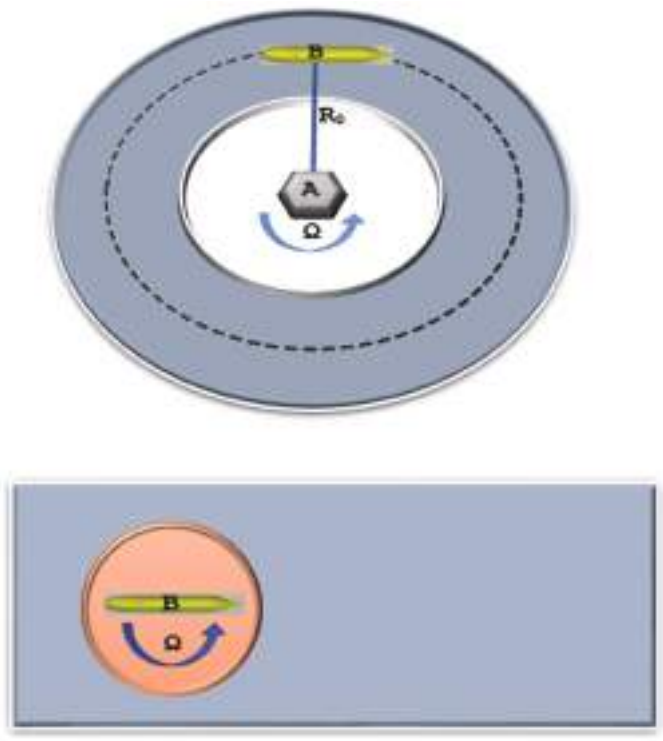

Figure 3. *Rotating reference frame vs. semi-relative reference frame domains*

$$\begin{aligned} MS_{xB} &= -\rho\left(2\Omega \times U_r + \Omega \times \left(\Omega \times (x - x_B)\right)\right) \\ MS_{yB} &= -\rho\left(2\Omega \times U_r + \Omega \times \left(\Omega \times (y - y_B)\right)\right) \\ MS_{zB} &= -\rho\left(2\Omega \times U_r + \Omega \times \left(\Omega \times (z - z_B)\right)\right) \end{aligned} \quad (7)$$

As can be observed in Figure 2; $x_B = x_A$, $|y_B - y_A| = R_0$ and $z_B = z_A$. The momentum source term in Equation (5) can be rexpressed as shown in Equation (8).

$$f_i = MS_{yA} - MS_{yB} = -\rho\Omega \times (\Omega \times R_0) \quad (8)$$

Reynolds Stress Term [i.e. $(\overline{U_i' U_j'})$] in the URANS equations is modelled using a two-equation turbulence model namely k-ω SST for closing the system of governing equations. Being an hybrid turbulence model, the k-ω SST turbulence model has high performance both in low and high Reynolds Number regimes of the flow. Additionally this turbulence model known to have good performance also with the separating flows.

2.4. Numerical Modelling

An overset structural grid, consisting of a rectangular prism background domain and a spherical overset domain, is used for all calculations. The mesh is generated using the native hexagonal mesh generation tool of OpenFOAM, known as snappyHexMesh, around the UV geometry. A combination of O-type and rectangular prism grid is used in overset domain, whereas background domain is consisting of only rectangular prism cells. Overset domain has a radius of 1.2 model length, and its center is arranged to coincide with the moment center of the UV. The background domain dimensions are chosen to be 17 L x 28 D x 28 D. Here, overall length of the model is represented with L, and "D" represents the maximum diameter of the model.

The meshing process consists of five steps: initially, a castellated mesh is generated for the overset domain. Cells are then deformed to snap the model geometry. Next an inflation layer is added adjacent to model surface. Afterwards a background mesh is generated. Merging of two mesh zones is the and final step. This results in a mesh with a total cell count of 24 million, which is used for all of the simulations under consideration. Perspective view of the domain grid and boundary conditions is presented in Figure 4.

Velocity inlet boundary condition is assigned to the front boundary. Where positive x axis is the direction of the velocity vector. Leeward boundary of the control volume is designated as pressure outlet. In order to assure parallel flow for the other boundaries which are positioned at an equal distance (i.e. 28 D) form the UV centerline, the symmetry boundary condition is applied.

All velocity components are enforced to be zero on model surface in order to satisfy the no-slip and no-penetration boundary conditions. Surface of the sphere enclosed the overset zone, is assigned to be an overset boundary. This boundary is used for exchanging information regarding primitive variables between two grids. High resolution spatial discretization is achieved in the low Reynolds number zone in close proximity of the UV. This is done for satisfying the requirement of dimensionless wall distance value of y+≈1 of the selected turbulence model. Non-dimensional wall distance distribution on the model surface is demonstrated in Figure 5.

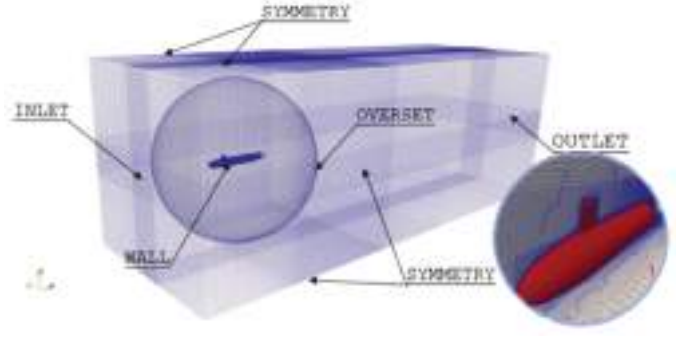

Figure 4. *Perspective view of the domain, grid and boundary conditions*

2.5. Simulation Matrix

Current part of the study involves the towing (straight and oblique) and steady turning simulations of the selected geometry. The simulation matrix of is demonstrated in Table 2. Steady-state simulations are carried out for the entire test matrix. Propulsive forces are not considered in the scope of this study.

3. Results and Discussion

3.1. Mesh Validation and Dependency

The mesh must be validated to ensure the production of accurate results. ITTC provide guidelines [28] for validation of the numerical marine hydrodynamics applications. Computational performance of the mesh is validated through commonly accepted quantities such as pressure and skin friction coefficients and resistance. In this study, validation is performed via a comparison of the above mentioned quantities. Table 3 and Figure 6 summarize the results. The agreement of the results with [29] is satisfactory. The maximum relative difference is less than 3%.

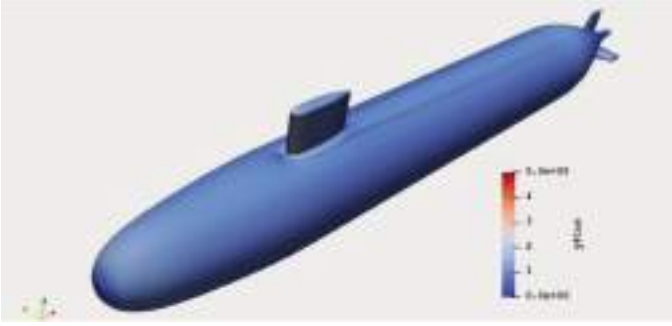

Figure 5. *y^+ Distribution on the surface*

Table 2. *Simulation matrix for the towing and steady turning motions*

Simulation type	U (ms^{-1})	Independent variable
Straight towing	3.046-9.255	3.046-9.255 for U (ms^{-1})
Oblique towing	3.00	-14° - +14° for α and β Δ β= Δ α=2°
Control surfaces	3.3436	-10° - +10° for δ_r and δ_s Δ δ_r = Δ δ_s = 5°
Rotational motion	3.00	10 – 16 m test radius R_0 Δ R=2 m

Table 3. *X-force comparison of the results with Liu and Huang [29]*

U	X-Force [N]		Diff.
[m/s]	CFD	DTRC	[%]
3.046	-105.12	-102.3	2.81
5.144	-278.5	-283.8	1.88
6.091	-382.3	-389.2	1.76
7.161	-516.6	-526.6	1.90
8.231	-670.3	-675.6	0.78
9.255	-835.0	-821.1	1.69

On the upper meridian line of the model; the pressure and skin friction coefficient distributions are measured for the same purpose. Skin friction coefficient (C_f) is presented in Figure 7. Benchmark data is provided by Qiu et al. [30]. Whereas large-eddy simulation (LES) results of Alin et al. [31] are used for benchmarking the pressure coefficient (C_p) distribution presented in Figure 8. Both distributions are in good agreement with the above mentioned benchmark data.

3.2. Oblique Towing

Figure 9 illustrates the variation in sway force (Y) roll (K) and yaw moment (N) with respect to drift angle (β) for drift angle interval of ±4°. Experimental benchmark data of (Zhao et al. [23]) also given for comparison. Coefficient of determination (R^2) is around unity for all three coefficient,

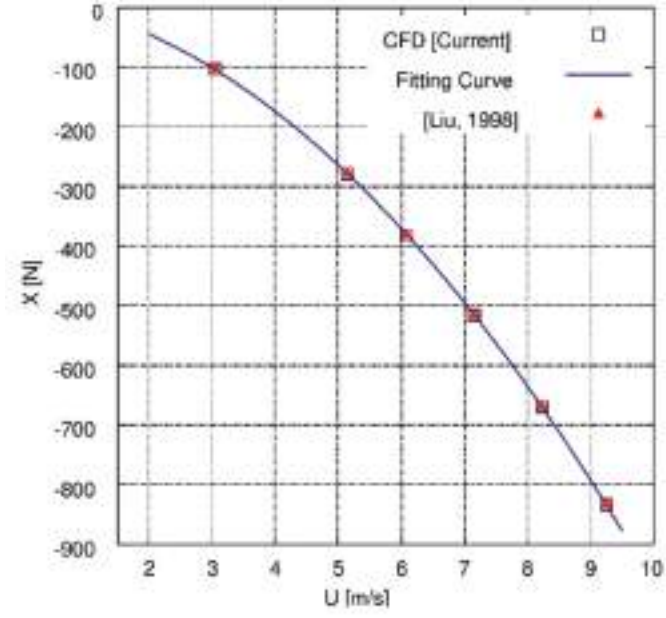

Figure 6. *X-force comparison of the results with Liu and Huang [29]*

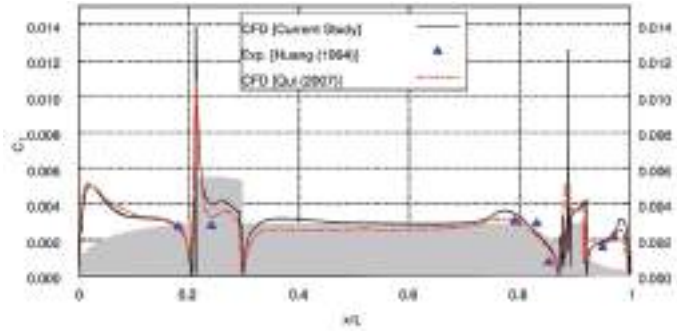

Figure 7. *C_f distribution on the upper meridian line of UV*

which means strong linearity in the data. The dimensionless coefficients of Y'_v, K'_v and N'_v are computed from the slope of the line fit. Results are presented and benchmarked in Table 4. Sway force (Y) and the yaw moment (N) data align well with the benchmark data and relative differences regarding the Y'_v, and N'_v are 6.52% and 0.15 respectively. As for the K'_v coefficient; relative difference is increased to 23%. This relatively high difference is due to limitation of the simulated motion to predict roll motion behavior of the vehicle. Hydrodynamic coefficients order associated with the roll motion known for being challenging to predict and generally requires advanced techniques such as conning motion [32].

In vertical plane; heave force (Z) and pitch moment (M) variation with respect to attack angle (α) are demonstrated in Figure 10 for attack angle interval of ±4°. Experimental benchmark data [23] also given for comparison. Coefficient of determination (R^2) is around unity for both of the coefficients which means strong linearity in the data. The dimensionless coefficients of Z'_w and M'_w are computed from the slope of the fitted line. Results are presented and benchmarked in Table 4. Heave force (Z) and pitch moment (M) data align well with the benchmark data and relative differences regarding the Z'_w and $M'_w$are 0.75% and 6.79 respectively.

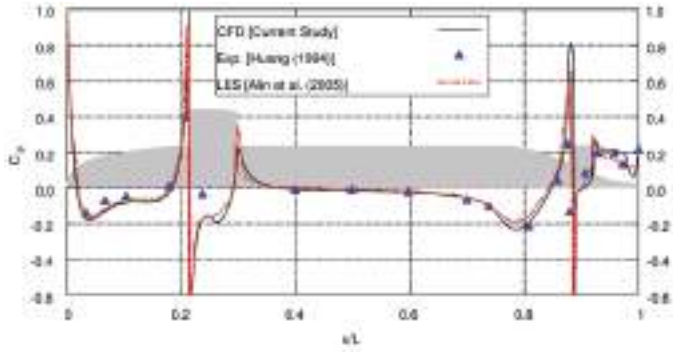

Figure 8. *C_p distribution on the upper meridian line of UV*

Table 4. *Tabulation of hydrodynamic coefficients*

Simulation type	Hydrodynamic coefficient	CFD	Benchmark	Ref	Diff. (%)
Straight towing	X'_{uu}	-0.00090	-0.0012	[24]	25.00
Oblique towing	Y'_v	-0.02925	-0.02746	[24]	6.52
	K'_v	-0.00058	-0.00047		23.40
	N'_v	-0.01375	-0.01377		0.15
	Z'_w	-0.01321	-0.01331		0.75
	M'_w	0.01029	0.01104		6.79
	X'_{vv}	0.01137	0.0130	[26]	12.54
	$Y'_{v\|v\|}$	-0.04932	-0.05775	[24]	14.60
	Z'_{vv}	0.08340	0.08474		1.58
	$K'_{v\|v\|}$	-0.00066	-0.00054		22.22
	M'_{vv}	0.01003	0.00951		5.47
	$N'_{v\|v\|}$	0.01264	0.01058		19.47
	X'_{ww}	0.0043	0.0065	[26]	35.50
	$Z'_{w\|w\|}$	-0.05410	-0.05193	[24]	4.18
	$Z'_{\|w\|}$	2.23-05	0.0000145		53.80
	Z'_{ww}	-0.001161	-0.000704		64.91
	$M'_{w\|w\|}$	0.000193	0.000143		34.96
	M'_{ww}	-0.00060	-0.00046		30.43

Table 4. *Continued*

Simulation type	Hydrodynamic coefficient	CFD	Benchmark	Ref	Diff. (%)
Steady rotational	Y'_r	0.004700	0.00499	[23]	5.81
	K'_r	-0.000110	-0.00013		15.38
	N'_r	-0.003700	-0.00408		9.73
	Z'_q	-0.00697	-0.00808		11.26
	M'_q	-0.00310	0.00392		20.91
	$Y'_{r\|r\|}$	-0.00396	-0.00422	[24]	6.16
	$N'_{r\|r\|}$	-0.0001961	-0.0001966		0.26
	$Z'_{q\|q\|}$	0.00274	0.00279		1.80
	$M'_{q\|q\|}$	0.000700	0.000838		16.47
Control surfaces	$Y'_{\delta r}$	0.0082	0.0069	[26]	19.40
	$N'_{\delta r}$	-0.0033	-0.0032		3.94
	$Z'_{\delta s}$	-0.0082	-0.0070		16.75
	$M'_{\delta s}$	-0.0033	-0.0032		3.30
	$X'_{\delta r\delta r}$	-0.0041	-0.0042		2.38
	$X'_{\delta s\delta s}$	-0.0025	-0.0030		16.67
	$K'_{\delta r}$	2.66E-06	5.00E-6	[25]	46.90
*Table 4 includes two columns					

Variations of forces and moments in 6-DOF with respect to drift angle (β) are demonstrated in Figure 11. Drift angle range is selected as ±14° (with an increment of 2°) in order to observe the non-linear changing behavior of forces and moments. Results of X and Z force as well as M moment are represented with a quadratic curve fit. Whereas Y force K and M moment results are represented with a 3rd degree polynomial. Excluding the Z force and M moment variation R^2 values are around one which means fitted curves can successfully represent the data. Computed coefficients of X'_{vv}, $Y'_{v|v|}$, Z'_{vv} $K'_{v|v|}$, M'_{vv} and $N'_{v|v|}$ from this data is presented and benchmarked in Table 4. If the variation of force/moment is represented by a quadratic curve, the resulting coefficient is the coefficient of the quadratic term. Taylor series expansion is not included terms like$Y'_{v|v|}$. Their inclusion is motivated by physical arguments [33]. For variations represented by a 3rd polynomial, definition of the associated hydrodynamic coefficient is as; $Y'_{v|v|} = \partial^2 Y/\partial|v|\partial v$ at $v = 0$.

The coefficient of X'_{uu} is obtained from the quadratic curve fitted to the data demonstrated in Figure 6. The resulting coefficient deviates from the benchmark data [24] by 25%. This difference is caused by the difference in accuracy level of drag predictions. Current study has a maximal difference of 3% as can be seen in Table 3 compared to 7% relative difference declared by Zhao et al. [23].

Similarly non-linear variations of X and Z force as well as M moment with respect to angle of attack (α) is presented in Figure 12 for the angle of attack range of ±14° (with an increment of 2°). Results of X force as well as M moment are represented with a quadratic curve fit. Whereas Z force results are represented with a 3rd degree polynomial. R^2 values are around one which means fitted curves can successfully represent the data. Computed coefficients of X'_{ww}, $Z'_{w|w|}$, $Z'_{|w|}$, Z'_{ww}, M'_w $M'_{w|w|}$ and M'_{ww} from this data is presented and benchmarked in Table 4.

3.3. Steady Rotational Motion

Sway force, roll and yaw moment variations with respect to yaw angular velocity (r=0.1875~0.3 rad s^{-1}) are demonstrated in Figure 13 for R_0=10 ~16 m. The dimensionless coefficients

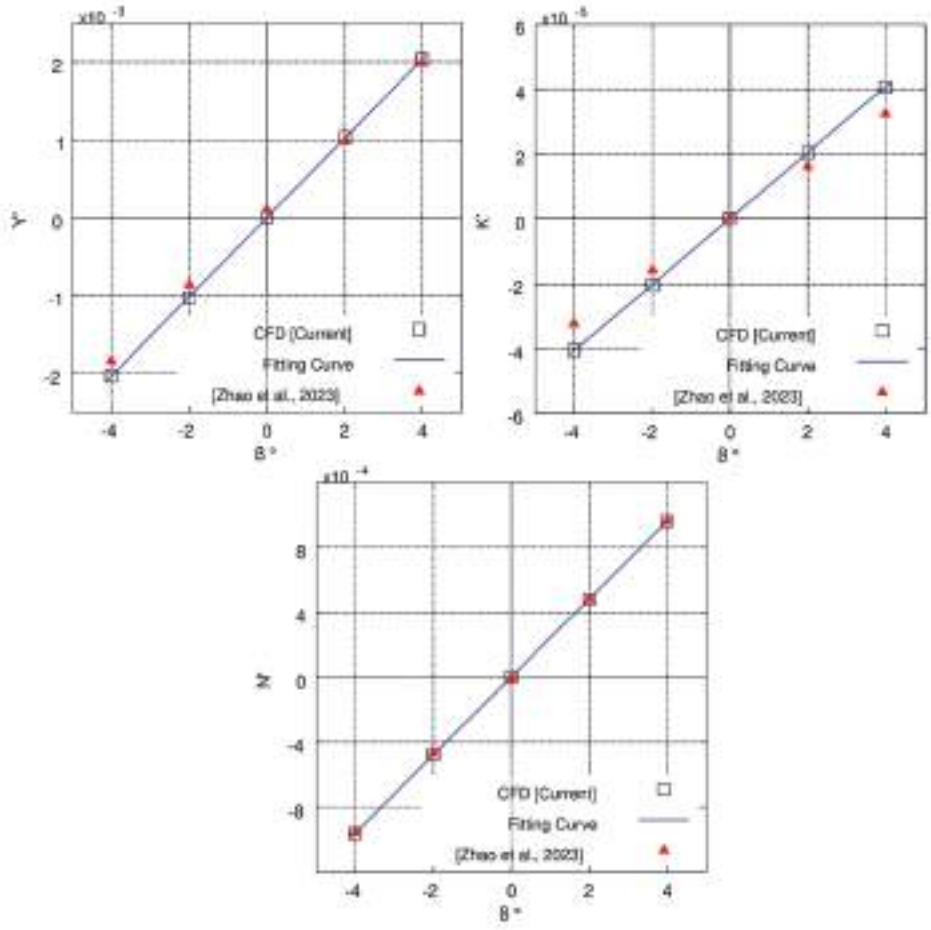

Figure 9. *Oblique towing simulation results in the linear range (horizontal plane)*

**Figure 9 includes two columns*

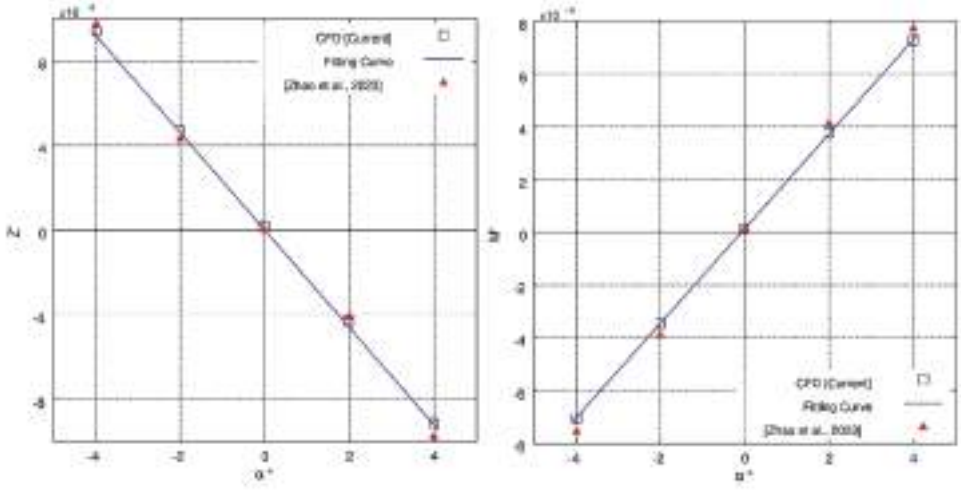

Figure 10. *Oblique towing simulation results in the linear range (vertical plane)*

**Figure 10 includes two columns*

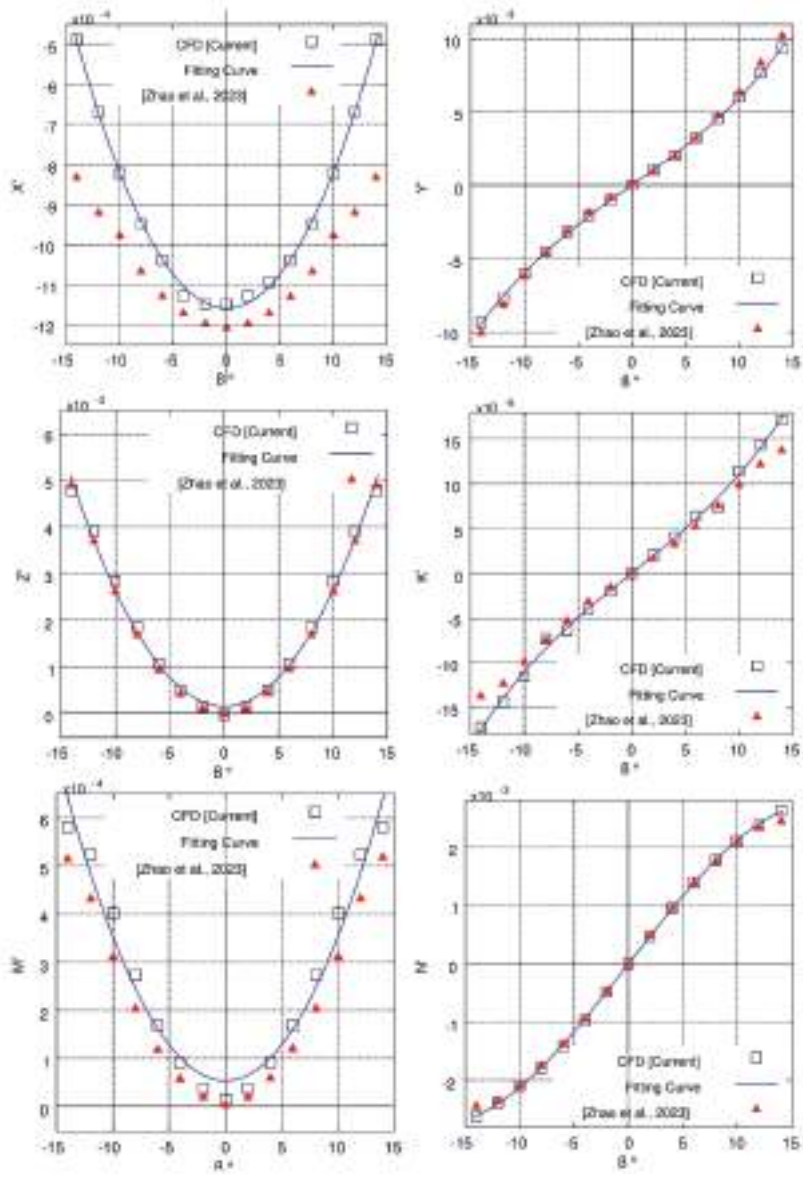

Figure 11. *Oblique towing simulation results in the non-linear range (horizontal plane)*

**Figure 11 includes two columns*

of Y'_r, K'_r and $N'_r$are computed from linear regression. Results are presented and benchmarked in Table 4 In general utilized method for simulation of the steady rotational motion fall short of predicting sway force and yaw moment for the entire test cases. The difference is 35% in average which is associated with two particular reasons. First of all, multiple reference frame (MRF) approach known its severe effects on the flow field and under prediction of the forces and moments. Second reason is originated from the effect of Vortex Induced Vibrations created by the cylindrical strut used in the experiments [23,24]. However MRF method demonstrates a good performance in predicting the rate of change of forces and moments with respect to dimensionless rotation radius where r'=L/R.

For roll moment predictions harmony between simulations and experimental results are quite satisfactory. This phenomenon is also observed by Kim et al. [34] for the rotation motion simulation of bare hull DARPA Suboff modeled via MRF. Y'_r and N'_r are predicted in a 10% relative difference range. Relative difference associated with the prediction of N'_r is slightly greater than the Y'_r. K'_r coefficient is an order of magnitude smaller than the other measured quantities during the simulations. This means steady rotational motion creates very small roll moment due to

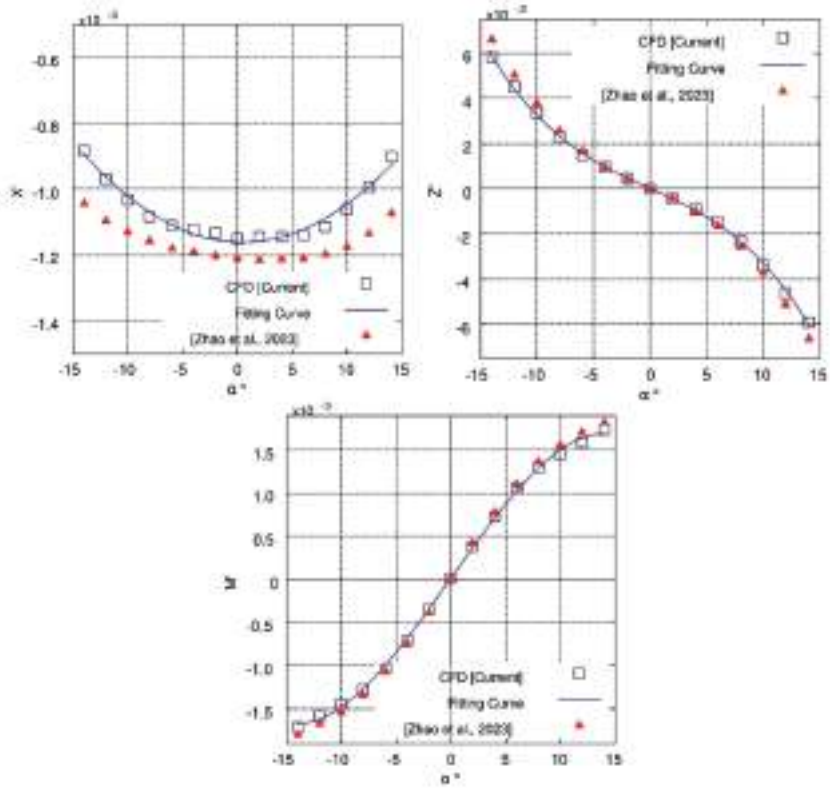

Figure 12. *Oblique towing simulation results in the non-linear range (vertical plane)*

**Figure 12 includes two columns*

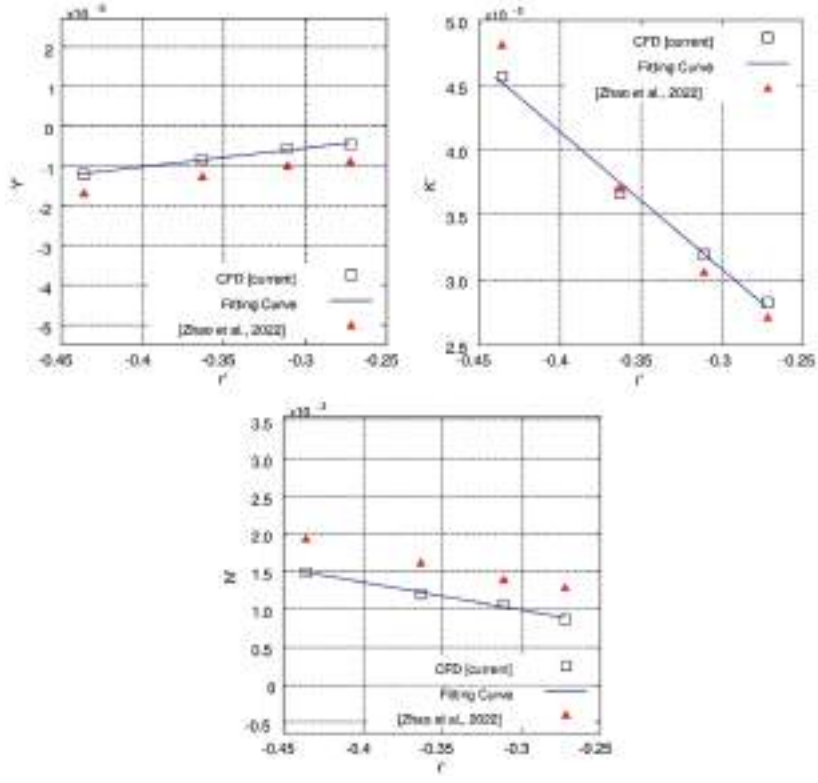

Figure 13. *Steady rotational motion simulation results at 0° incidence (horizontal plane)*

**Figure 13 includes two columns*

the geometric characteristics of the UV. It is hard to achieve an accuracy level for K'_r similar to the other dimensionless quantities. The relative difference associated with the K'_r coefficient is around 15%. The coefficients $Y'_{r|r|}$ and $N'_{r|r|}$ are derived directly from the quadratic curve fitted to the data. The maximum relative difference is 6 % as can be seen in Table 4.

Data related with the steady rotational motion has also noise as in the experiments. Simulations are continued at least 500 additional pseudo time steps after reaching the established convergence criteria of 10^{-5} for primitive variables and turbulence quantities. An oscillatory convergence behavior is observed and the results of integral quantities seems to have small oscillations around an average value.

Steady rotational motion in vertical plane is investigated through its effects on the heave force (Z) and pitch moment (M). Their variation with respect to pitch angular velocity (q=0.1875~0.3 rad/s) are demonstrated in Figure 14 for R_0=10 ~16 m. (with an increment of 2 m). The dimensionless coefficients of Z'_q and M'_q are computed from linear regression. Results are presented and benchmarked in Table 4. As in case of the steady turning motion in horizontal plane; heave force and pitch moment are also under predicted by MRF algorithm. Nevertheless rate of change of heave force and pitch moment with respect to dimensionless rotation radius where q'=L/R can be predicted sufficiently accurate.

Corresponding hydrodynamic coefficients of Z'_q and M'_q are predicted in a 20% difference range. Relative difference associated with the prediction of M'_q is slightly greater than the Z'_q. The coefficients of $Z'_{q|q|}$ and $M'_{q|q|}$ are derived directly from the quadratic curve fitted to the data. The maximum relative difference is around 16%.

3.4. Control Surface Deflection

Variations in surge (X) and sway force (Y) as well as roll (K) and yaw moment (N) as a result of rudder deflection (δ_r) are demonstrated in Figure 15 for rudder angle interval of ±10° (with increment of 5°). Experimental results of Khan et al. [26] and Roddy [25] (in case of roll moment) are also plotted along with the simulation data for comparison purpose. All four quantities exhibit a variation trend which is aligned with the above mentioned benchmark data. Variations of sway force (Y), roll moment (K) and yaw moment (N) are represented with a line fit. On the other hand surge force (X) variation displays quadratic behavior. Computed coefficients of $Y'_{\delta r}$, $K'_{\delta r}$, $N'_{\delta r}$ and $X'_{\delta r\delta r}$ from these regressional analyses are presented and benchmarked in Table 4. Excluding the hydrodynamic coefficient of $K'_{\delta r}$ the maximum relative difference with respect to experimental benchmark data is around 19%. For $K'_{\delta r}$ a relative difference of 47% is calculated. Deviation in this coefficient is attributed to the above mentioned challenges of accurately capturing roll motion behavior for UVs.

In vertical plane elevator deflection is effective on the surge (X) and heave (Z) forces and pitch moment (M). Variations in these quantities with respect to elevator deflection is presented along with the experimental results [26] in Figure 16 for elevator angle interval of ±10° (with increment of 5°). All four quantities exhibit a variation trend which is aligned with the above mentioned benchmark data. Variations of heave force (Z), pitch moment (M) are represented with a line fit whereas surge force (X) variation can be expressed with a quadratic curve. Computed coefficients of $Z'_{\delta s}$, $M_{\delta s}$ and $X'_{\delta s\delta s}$ based on the results of these regression analyses are presented and benchmarked in Table 4. The maximum relative difference is under 17 % for these coefficients.

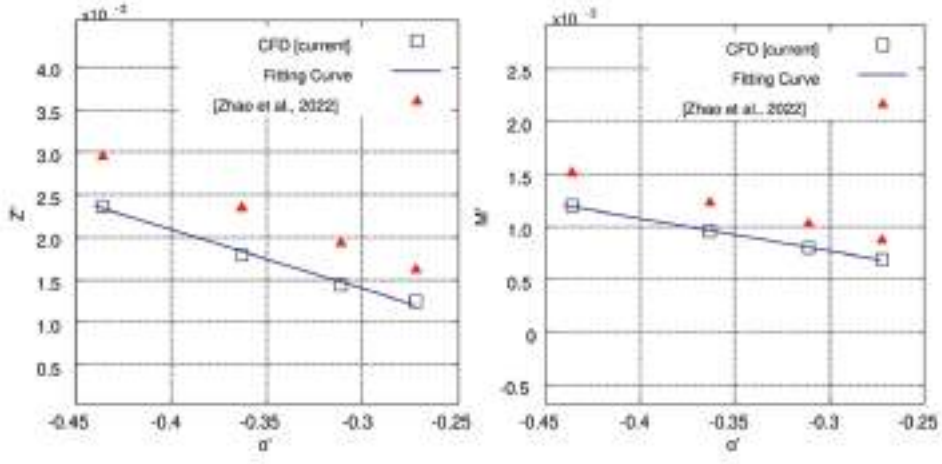

Figure 14. *Steady rotational motion simulation results at 0° incidence (vertical plane)*

**Figure 14 includes two columns*

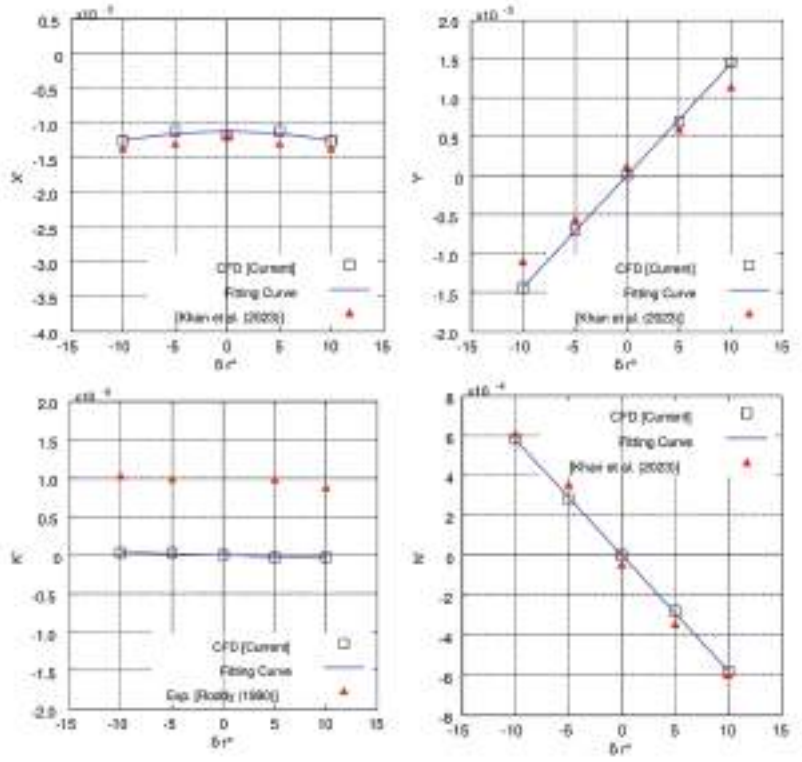

Figure 15. *Control surface simulation results (Rudder)*

**Figure 15 includes two columns*

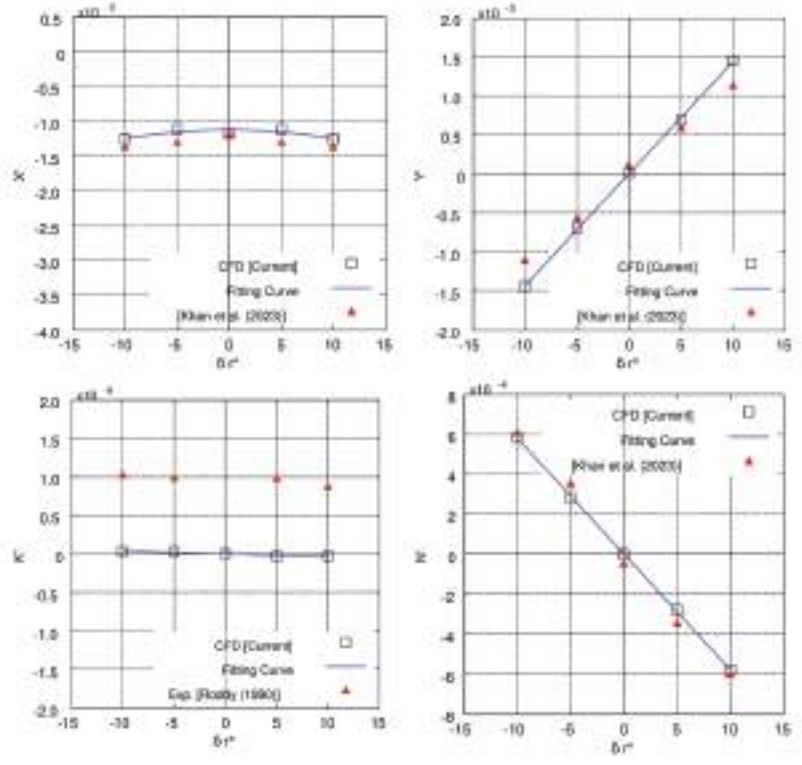

Figure 16. *Control surface simulation results (Elevator)*

**Figure 16 includes two columns*

3.5. Summary and Discussion

Time-independent hydrodynamic coefficients of fully appended DARPA Suboff configuration (AFF-8) are computed, presented and benchmarked in Table 4. For each coefficient reference for the benchmark value is also given. Overall comparable results with the benchmark data are obtained from the numerical analyses. Deviation in the roll moment coefficients is attributed to the inability of the simulated motion to predict roll motion response of the vehicle

For the nonlinear coefficients of the heave force with respect to heave velocity; probable cause of the deviations from the benchmark data is extreme non-linearity due to the existence of sail. As the angle of attack increased, flow field becomes more and more non-linear. Between simulations and experiments it is very challenging to achieve a harmony in the results due to these non-linear effects.

4. Conclusion

A methodology is proposed in this paper for mimicking the motions of the main experimental facilities by using the same grid structure. Independent variable (i.e. drift/attack/control surface deflection angle and rotation radius) intervals, which corresponds to the linear and non-linear variations of dependent variables (i.e. force and moments) are investigated. An extensive set of hydrodynamic coefficients of fully appended DARPA Suboff configuration (AFF-8) associated with the straight/oblique towing and steady turning motions are computed and benchmarked.

The subsequent findings can be outlined as follows:

• Hydrodynamic coefficients of 1st associated with the linear velocities are predicted with a desired level of accuracy. Except roll moment variation with respect to sway velocity. This is attributed to the challenges of capturing roll motion behaviour of the UV with oblique flow simulations.

• In horizontal plane; hydrodynamic coefficients of 2nd order are also well predicted. However in vertical plane, due to the asymmetry of the vehicle, non-linearities become dominant as the angle of attack increased. As a result achieving a harmony between simulations and experiments becomes very challenging. This phenomena can be observed in Table 4.

• Although forces and moments are under predicted by MRF algorithm in steady turning motion, 1st order hydrodynamic coefficients of angular velocities is generally well predicted.

• For 2nd order hydrodynamic coefficients of angular velocities harmony between the simulation results and the benchmark data is satisfactory.

• In general control surface coefficients both in first and second order are aligned with the benchmark experimental data except for the roll motion coefficient with respect to rudder angle. Deviation in this coefficient with respect to experiments is again due to the challenges of capturing roll motion behaviour of the UV.

Overall, this study contributes to the literature by offering a robust methodology for simulating the motions associated with major experimental setups by reducing the amount of pre-processing work significantly. This is achieved by the modification of governing equations which requires a deep understanding of the mathematics behind the solution algorithms and the software structure. The methodology used in the paper and findings provide comprehensive and insights for researchers in the field of marine hydrodynamics for changing their perspective on the maneuvering problem..

Authorship Contributions

Concept design: O. Kırıkbaş, and Ş. Bal, Data Collection or Processing: O. Kırıkbaş, Analysis or Interpretation: O. Kırıkbaş, and Ş. Bal, Literature Review: O. Kırıkbaş, Writing, Reviewing and Editing: O. Kırıkbaş, and Ş. Bal.

Funding: The authors did not receive any financial support for the research, authorship and /or publication of this article.

References

[1] M. Gertler, and G. Hagen, *Standard Equations of Motion for Submarine Simulation.* Technical Report AD653861, June, 1967.

[2] J. Feldman, *DTNSRDC Revised Standard Submarine Equations of Motion.* David Taylor Research Center, Ship Performance Department (June), 1979.

[3] J. A. Foroushani, and M. Sabzpooshani, "Determination of hydrodynamic derivatives of an ocean vehicle using CFD analyses of synthetic standard dynamic tests." *Applied Ocean Research,* vol. 108, 102539, Mar 2021.

[4] B. Overpelt, B. Nienhaus, and B. Anderson, "Free running manoeuvring model tests on a modern generic SSK class submarine (BB2)", *Pacific International Maritime Conference*, 2015.

[5] P. M. Carrica, M. Kerkvliet, F. Quadvlieg, M. Pontarelli, and J. E. Martin, CFD Simulations and Experiments of a Maneuvering Generic Submarine and Prognosis for Simulation of Near Surface Operation, 31st Symposium on Naval Hydrodynamics Monterey, CA, USA, 2016.

[6] G. Dubbioso, R. Broglia, and S. Zaghi, "CFD analysis of turning abilities of a submarine model". *Ocean Engineering,* vol. 129, pp. 459-479, Jan 2017.

[7] H. Kim, D. Ranmuthugala, Z. Q. Leong, and C. Chin, "Six-DOF simulations of an underwater vehicle undergoing straight line and steady turning manoeuvres". *Ocean Engineering,* vol. 150, pp. 102-112, Feb 2018.

[8] Y.x. Wang, J.-f. Liu, T.-j. Liu, Z.-b. Jiang, Y.-g. Tang, and C. Huang, "A numerical and experimental study on the hull-propeller interaction of a long range autonomous underwater vehicle". *China Ocean Engineerin*g, vol. 33, pp. 573-582, Oct 2019.

[9] C. Delen, and O. K. Kinaci, "Direct CFD simulations of standard maneuvering tests for DARPA Suboff". *Ocean Engineering,* vol. 276, pp. 114202, May 2023.

[10] O. Kırıkbaş and Ş. Bal, "Simulation of captive model experiments of an underwater vehicle by CFD based on a single grid structure". In *4th International Symposium on Naval Architecture and Maritime (INT-NAM 2023)*, Istanbul, Turkey, pp. 947-960, Oct 2023.

[11] O. Kırıkbaş and Ş. Bal, *DELOK'23 Calculation of Maneuvering Coefficients of an Underwater Vehicle in CFD Environment Based on the Same Grid Topology,* I. International Maritime and Logistics Congress (MARLOG 2023, Hybrid), Zonguldak Bülent Ecevit University, Maritime Faculty, Zonguldak, Türkiye, September 22-23, 2023, pp. 248-262.

[12] A. Phillips, M. Furlong, and S. Turnock, "Virtual planar motion mechanism tests of the autonomous underwater vehicle autosub," *in STGConference/Lectureday: CFD in Ship Design*, 2007.

[13] H. Zhang, Y. R. Xu, and H. P. Cai, "Using CFD software to calculate hydrodynamic coefficients". *Journal of Marine Science and Application,* vol. 9, pp. 149-155, Jun 2010.

[14] Y. Pan, H. Zhang, and Q. Zhou, "Numerical prediction of submarine hydrodynamic coefficients using CFD simulation". *Journal of Hydrodynamics,* vol. 24, pp. 840-847, Dec 2012.

[15] D. E. Humphreys, and K. W. Watkinson, "*Prediction of acceleration hydrodynamic coefficients for underwater vehicles from geometric parameters".* Naval Coastal Systems Laboratory, Panama City, Florida, 1978.

[16] Z. Lin, and S. Liao, "Calculation of added mass coefficients of 3D complicated underwater bodies by FMBEM". *Communications in Nonlinear Science and Numerical Simulation,* vol. 16, pp. 187-194, 2011.

[17] E. Javanmard, S. Mansoorzadeh, and J. A. Mehr, "A new CFD method for determination of translational added mass coefficients of an underwater vehicle". *Ocean Engineering,* vol. 215, 107857, Nov 2020.

[18] O. Kırıkbaş, and Ş. Bal, "Computation of added mass coefficients of darpa suboff using two different solvers of OpenFOAM", International Conference on Postgraduate Research in Maritime Technology (PostGradMarTech 2023), Hellenic Institute of Maritime Technology (HIMT) Athens, Greece, 8-9 Nov 2023.

[19] S. Toxopeus, "Viscous-flow calculations for bare hull DARPA SUBOFF submarine at incidence". *International Shipbuilding Progress,* vol. 55, pp. 227-251, 2008.

[20] A. Phillips, M. Furlong, and S. R. Turnock, *The use of computational fluid dynamics to determine the dynamic stability of an autonomous underwater vehicle, 10th numerical towing tank symposium (NuTTS'07),* Hamburg, Germany, 2007.

[21] L. Cao, J. Zhu, and G. Zeng, "Viscous-flow calculations of submarine maneuvering hydrodynamic coefficients and flow field based on same grid topology". *Journal of Applied Fluid Mechanics,* vol. 9, pp. 817-826, Feb 2016.

[22] W. Xiaocui, W. Yiwei, W. Chenguang, H. Zhiqiang, and Y. Ruiwen, "An effective CFD approach for marine-vehicle maneuvering simulation based on the hybrid reference frames method". *Ocean Engineering,* vol. 109, pp. 83-92, Nov 2015.

[23] B. Zhao, et al. "Hydrodynamic coefficients of the DARPA SUBOFF AFF-8 in rotating arm maneuver: Part I: Test technology and validation". *Ocean Engineering,* vol. 266, 113148, 2022.

[24] B. Zhao, Y. Yun, F. Hu, J. Sun, D. Wu, and B. Huang, "Hydrodynamic coefficients of the DARPA SUBOFF AFF-8 in rotating arm maneuver - Part II: Test results and discussion." *Ocean Engineering,* vol. 268, 113466, Jan 2023.

[25] R. F. Roddy, *Investigation of the stability and control characteristics of several configurations of the DARPA suboff model (DTRC Model 5470) from captive-model experiments.* David Taylor Research Center, Departmental Report DTRC/SHD- 1298- 08 (September), 1990.

[26] M. K. Khan, M. Korulla, V. Nagarajan, and O. P. Sha, "Measurements of steady manoeuvring forces and moments over an axisymmetric body with appendages in a wind tunnel". *Ship Technology Research*, pp. 1-12, Dec 2023.

[27] N. C. Groves, T. T. Huang, and M. S. Chang, *"Geometric characteristics of DARPA Suboff models: (DTRC Model Nos. 5470 and 5471)*". David Taylor Research Center, 1989.

[28] ITTC, 2011. CFD, General CFD Verification, in ITTC - Recommended Procedures and Guidelines.

[29] H. Liu, and T. T. Huang, "Summary of DARPA suboff experimental program data" Naval Surface Warfare Center Carderock Division (NSWCCD), West Bethesda, MD, USA, Report No. CRDKNSWC/HD-1298-11, 1998.

[30] L. Y. Qiu, Z. K. Shi, G. X. Hou, and F. F. Wei, "Validation of numerical simulation of the flow over submarine geometries with full appendages". *Journal of Ship Mechanics*, vol. 11, pp. 341-350, Jun 2007.

[31] N. Alin, et al. "3D unsteady computations for submarine-like bodies". In *43rd AIAA Aerospace Sciences Meeting and Exhibit,* Jan 2005.

[32] J. Y. Park, et al. "Study on coning motion test for submerged body". *Journal of Ocean Engineering and Technology,* vol. 29, pp. 436-444, Dec 2015.

[33] M. S. Triantafyllou, and F. S. Hover, *Maneuvering and control of surface and underwater vehicles*, 2004, [Online].

[34] T. W. Kim, T. J. Kang, W. G. Park, and C. M. Jung, "Estimation of roll coefficient of underwater vehicle using a calculation of hydrodynamic forces". *Journal of Computational Fluids Engineering,* vol. 20, pp. 81-87, Jun 2015.

Journal of ETA Maritime Science 2024;12(2):213-223

Temporal Analysis of Factors Influencing Countries' Maritime Trade Performance with CRITIC-based VIKOR Method

Emrah Akdamar, Ersin Fırat Akgül, Maruf Gögebakan, Evrim Işık

Bandırma Onyedi Eylül University Maritime Faculty, Department of Maritime Business Administration, Balıkesir, Türkiye

Abstract

Shipping and world trade have grown simultaneously as a result of the increased need for freight transportation capacity brought about by the expansion of world trade. It is important for countries to compare their maritime trade performance in relation to their respective characteristics. It is essential to adhere to the competitive circumstances in order to obtain a larger proportion of the world trade. This study compares maritime trade performance of the 20 countries with the greatest number of ports of call worldwide using multi criteria decision making techniques. Six indicators are weighted by Criteria Importance Through Intercriteria Correlation method and the performances of the countries are ranked by VIšeKriterijumska Optimizacija I Kompromisno Resenje method. Rankings for the years 2018-2022 were constructed independently, and after using the Borda approach to integrate them together, the final ranking was produced. The results provide a perspective for countries to improve their maritime trade performance and the opportunity to make an assessment from macro perspective.

Keywords: Maritime trade, CRITIC, VIKOR, port call

1. Introduction

IInternational trade has grown 140 times in the past 150 years [1]. The growth in world trade has increased the need for cargo transportation capacity, and accordingly, shipping and world trade have developed together. Energy, mining, agriculture and forestry are the largest production industries of the world economy [2]. Transportation solutions are produced according to changing parcels depending on the transportation of raw materials or processed goods, and maritime trade is at the center.

Due to China's and East Asia's economic and industrial growth, this region is now the hub of global trade, forcing major shipping companies to adapt their business models to the conditions of this region and leading to the improvement of global maritime network [3]. Although ship design, technology, customer profile, etc. have changed throughout history, the basic principles of maritime trade have not changed. It can be stated that the analysis of the future in shipping industry, where success is achieved especially in periods when world political dynamics are balanced, is based on the both economic and geopolitical environment.

Comparing the maritime trade performance in terms of their characteristics is significant for countries. In order to get a larger share from the world trade, it is necessary to follow the competitive conditions. As the distance between countries decreases, competition between countries has also intensified due to overlapping hinterlands. The privatization of port operations, especially with the widespread use of container shipping, has an important role in increasing the competition [4-6]. In this context, ports have a vital place in determining the maritime trade performance of countries. Specifically, ports are the areas where the connection between foreland and hinterland is provided, where cargo is collected and consolidated, and where many value-added activities are carried out within industrial and logistics processes [7]. Today, work force is replaced by machinery and equipment at every stage of the work carried out in the ports, and depending on technological development; ports offer safer, modern, faster and more economical

Address for Correspondence: Ersin Fırat Akgül, Bandırma Onyedi Eylül University Maritime Faculty, Department of Maritime Business Administration, Balıkesir, Türkiye
E-mail: eakgul@bandirma.edu.tr
ORCID ID: orcid.org/0000-0002-2208-0502

Received: 09.01.2024
Last Revision Received: 02.04.2024
Accepted: 02.05.2024

To cite this article: E. Akdamar, E. F. Akgül, M. Gögebakan, and E. Işık. "Temporal Analysis of Factors Influencing Countries' Maritime Trade Performance with CRITIC-based VIKOR Method." *Journal of ETA Maritime Science*, vol. 12(2), pp. 213-223, 2024.

services. Accordingly, the following research questions are investigated in this study:

i. What are the importance levels of the factors affecting countries' maritime trade performance and how have they changed over the years?

ii. According to the determined importance levels, what is the performance ranking of the countries and how has it changed over the years?

Among the various initiatives to determine the position of countries in maritime trade, data on port calls shared by the United Nations Conference on Trade and Development (UNCTAD) provide important information on data on port calls and performance that give an overview of the attributes of the ships and the duration they stayed in national ports throughout a given time period. In order to answer the above-mentioned questions, the importance levels of various performance indicators in the UNCTAD database of the 20 countries with the highest number of port calls were determined by Criteria Importance Through Intercriteria Correlation (CRITIC) method, one of the multi-criteria decision-making methods, taking into account the years 2018-2022, and using the VIšeKriterijumska Optimizacija I Kompromisno Resenje (VIKOR) technique, the countries' performances were ranked in relation to the specified importance levels.

The originality of this study has two strands. First, it provides a data-driven perspective for countries' maritime trade performance by answering the research questions considered. Secondly, by taking into account the last 5-year period in which developments such as the COVID-19 pandemic, trade wars between the US and China, the Russia-Ukraine war, the emergence of alternative supply chains, increased regulations on climate change, and the blockage of shipping corridors have been intensively experienced, the time-dependent change of performance indicators and the response of countries to this change have been dynamically revealed in this study.

This paper is structured as follows: The review of the literature on ports and maritime trade is presented in section two. The data set and methods utilized in the study are described in Section 3; the findings and an in-depth overview are presented in Section 4. The conclusion of this study highlights its limitations, implications, and future research recommendations.

2. Literature Review

The success of the global supply chain depends on efficient port operations since they serve as essential bridges between countries. It is critical to comprehend the complex relationship between port call activities and a nation's overall success as the economic landscape changes. The purpose of this literature review is to summarize the state of the art about this intersection, with a particular emphasis on ports and maritime trade performance. A thorough analysis of the body of research indicates that port efficiency and maritime trade performance are the two primary areas of focus. Researchers have carefully examined these elements on their own, offering insightful information about the efficiency of ports' operations and how it affects a nation's economic position. Still, in order to fully understand the complex relationships that exist between port call activities and overall performance of countries, a synthesis of different viewpoints is necessary.

As Owen [8] noted, a port is seen as a country's trading gateway; the more open the gate and the smoother the route, the greater the trade advantage to a country [9]. Supporting this point, various evidence has been presented that there is a linear relationship between the port efficiency and countries' maritime trade performance. From the holistic perspective, Santhi and Setyari [10] investigated the effects of "Trade Facilitation", which means the simplification of countries' international trade activity processes, on the export performance of six ASEAN countries. Among the various indicators used to measure Trade Facilitation, it was suggested port efficiency positively affected countries' export performance. As emphasized by Dick [11], an efficient port infrastructure has a positive impact on increasing the trade volume of countries as well as expanding the range of traded products. It can also contribute to reducing inflationary pressure due to reduced logistics costs and facilitating access to products. Wilson et al. [12] argue that gains in port efficiency have a significant and positive influence on the ability of a country for trade. Among their findings is that a 50% improvement in Trade Facilitation led to an increase of USD 254 billion in intra-APEC trade, half of which was due to an increase in port efficiency.

Similar results are observed when country-based studies are analyzed. Sant' Anna and Kannebley Júnior [13], who examine the relationship between port efficiency and exports in Brazil and consider port time as an indicator of port infrastructure quality, find that every 10% decrease in the port time of ships provides a 1% increase in exports. Similarly, the study by Jordaan [14] emphasized that port efficiency has a positive contribution to exports.

While significant progress has been made on port efficiency and trade performance, there is still a significant gap in combining these perspectives, particularly in light of factors affecting maritime trade, and in cross-country comparative analysis. This study designates the gap as the central focus of our investigation, with the goal of providing quantitative proof and a detailed comparative assessment to enhance

the link about port call and maritime trade performance of countries.

The approach utilized in this study is applied for performance evaluations across several business fields and countries. For instance, CRITIC method was used by Diakoulaki et al. [15] on performance measurement of pharmaceutical companies, Wu et al. [16] on urban rail transit operation safety of Beijing (China) Railways, Jati et al. [17] on components influencing a website's search engine exposure as well as the visibility ranking of the indicators influencing it. Deng et al. [18] applied CRITIC and Entropy to evaluate financial performance of textile companies. VIKOR method also was used by Opricovic and Tzeng [19] on fuel choice for public transport and Paksoy [20] on determining the performance and development levels of Türkiye and European countries. Perçin and Çakır [21] investigated logistics companies by using CRITIC, VIKOR, TOPSIS, SAW, BORDA methods. To the best of our knowledge, since there has never been any prior research on port calls and countries' performance assessments, the major goal of this study is to add something new to the existing collection of knowledge in this field.

3. Data and Methodology

This section introduces the data set and methodology used in the study. In this context, the database from which the data are obtained, the countries analyzed and port call and performance indicators are explained. The CRITIC technique, which establishes the significance levels of performance indicators, and the VIKOR technique, which ranks national performance, and the BORDA Census Technique used to make a holistic assessment covering the years 2018-2022 are discussed.

UNCTAD established in 1964 with the aim of enabling more prosperous member countries to benefit less developed countries supports the sustainable development efforts of developing countries in terms of trade, finance and technology. UNCTAD makes available a free-to-use database called UNCTADstat. The UNCTADstat database contains various datasets on population, economy, trade, technology and transportation. In this study, data on port call and performance statistics were used. The data covers the years between 2018 and 2022. The aim here is to evaluate the countries' port call and performance between 2018 and 2022 separately for each year and ultimately to make a common and single assessment covering all years. Since UNCTADstat publishes data on the 20 countries with the highest number of calls, the measurement and comparison of performance is carried out for these countries that are illustrated in Table 1. In terms of total carrying capacity, the 20 countries considered in this study control 65% of the world merchant fleet according to UNCTADStat. This ratio proves that these countries carry the majority of global merchandise and shape its trade. Also, countries elected to the Council of the World Maritime Organization (IMO) are classified as category (a), which includes the 10 States with the largest interest in providing international shipping services, category (b), which includes 10 States with the largest interest in international seaborne trade, and category (c), which includes 20 States not elected under (a) or (b) above, which have special interests in maritime transport or navigation and whose election to the Council will ensure the representation of all major geographic areas of the world. Since eight of the twenty countries considered in this study are in Category (a), seven in Category (b) and three in Category (c), it can be stated that they have a significant share in world maritime activities and represent the industry in general.

Six indicators as depicted in Table 2 are used in the study to measure the performance of the countries. Although it is possible to include subjective factors consisting of the views of relevant stakeholders in addition to the objective factors discussed in this study when evaluating the performance of countries, subjective factors are not included since this study aims to measure maritime trade performance through analytical methods based on an objective paradigm rather than a subjective one. It is of course possible to evaluate maritime trade performance using different objective

Table 1. *Countries considered in the study*

Germany	Spain
United States of America (USA)	Sweden
Australia	Italy
United Kingdom	Japan
China	Canada
Denmark	Republic of Korea
Indonesia	Norway
France	Russian Federation
Croatia	Türkiye
Kingdom of the Netherlands	Greece

Table 2. *Indicator codes, units of measurement and directions*

Indicator code	Indicator	Unit	Direction
G1	Median time in port	Day	Cost (-)
G2	Average age of vessels	Year	Cost (-)
G3	Average size of vessel	GT	Cost (-)
G4	Average cargo carrying capacity per vessel	Dwt	Cost (-)
G5	Maximum cargo carrying capacity of vessels	Dwt	Benefit (+)
G6	Maximum size of vessels	GT	Benefit (+)

indicators. However, the indicators used in this study are the group of indicators whose data are available for the countries included in the scope of the assessment. The fact that these indicators are worth following by UNCTAD supports the fact that these indicators are objective determinants of fleet performance. In this study, it is aimed to measure the world maritime trade performance through the existing set of variables.

Median time in port (days): It is the average number of days that ships spend within the port borders. The reasons of waiting at ports could be; congestion, strikes or relocation of ships or traffic problems in ports [22]. These problems pose a problem for the carrier and the shipper. The fact that the ship spends less time in port compared to the time it spends at sea can be characterized as a cost factor. Among these cost factors, minimizing the costs of services such as maintenance-repair, accommodation and terminal can be expressed as a goal of carriers [23].

Average age of vessels (years): Ship age is one of the most important characteristics of ships. The age of a ship is calculated as of the date of delivery to the shipowner by the shipyard where it was built. Insurance, flag and classification society certificates should be issued according to that date [24]. As the ship ages, structural elements should also be updated. Another significant factor influencing the frequency of ship collision is ship age. An old ship is more likely to be involved in a collision due to structural failure [25]. In this study, the average age of the ships calling at the country's ports during the period was taken into consideration.

Average size (GT) of vessels: It shows the total volume of indoor spaces of the ships calling at the country's ports during the period.

Average cargo carrying capacity (dwt) per vessel: It is the value found as a result of subtracting the empty ship weight from the loaded displacement of the ship. This weight includes cargo, fuel, fresh water and ballast water etc.

Maximum cargo carrying capacity (dwt) of vessels: This indicator includes the deadweight tonnage of the ship with the highest deadweight tonnage that called at any of the country's ports at least once during the period.

Maximum size (GT) of vessels: This indicator includes the value of the ship with the highest gross tonnage that called at any of the country's ports at least once during the period.

UNCTAD only considers arrivals to measure the total number of ships calling at a port, and passenger ships and Ro/Ro ships are not included in the calculations [26]. In performance measurement, it should be decided whether the indicators considered in the study are cost-oriented or benefit-oriented. Accordingly, if an upturn in an indicator's value corresponds to better performance, that indicator is determined as benefit-oriented. If an indicator's value declines and performance increases as a result, that indicator is determined as cost-side. In this context, the abbreviations, measurement units and directions of the indicators used in the study are shown in Table 2.

3.1. The CRITIC Method

CRITIC as an objective weighting method developed by Diakoulaki et al. [15] in 1995 is frequently used by the analysts [27].

The method provides an objective calculation by using the values of the indicators in the initial decision matrix instead of the subjective evaluation of the decision makers. When calculating the importance weights of indicators, each indicator's standard deviation and correlation coefficients with other indicators serve as the foundation [28]. Thus, the variability of the indicators, the degree and direction of the relationship between the indicators determine the indicator weights used in the problem.

Calculation of the CRITIC method consists of 4 steps [15]:

Step 1: The initial decision matrix is developed. In the X_{ij} element in the matrix, it corresponds to the values of i alternatives and j indicators. When the decision matrix is being developed, the first decision matrix with n possibilities and m indicators is formulized as follows:

$$X = [X_{ij}]_{nxm} = \begin{bmatrix} X_{11} & X_{12} & \cdots & X_{1m} \\ X_{21} & X_{22} & \cdots & X_{2m} \\ \vdots & \vdots & \vdots & \vdots \\ X_{n1} & X_{n2} & \cdots & X_{nm} \end{bmatrix} \quad (1)$$

Step 2: With the normalization process from the initial decision matrix, the benefit and cost values of the indicators were obtained by Equations (2) and (3), respectively, as follows.

$$r_{ij} = \frac{X_{ij} - X_j^{min}}{X_j^{max} - X_j^{min}} \quad (2)$$

$$r_{ij} = \frac{X_j^{max} - X_{ij}}{X_j^{max} - X_j^{min}} \quad (3)$$

Where, the indicator's normalized value j belonging to alternative I is shown as r_{ij}. X_j^{max} and X_j^{min} denotes, respectively, the highest and lowest values of indicator j.

Step 3: Relationship coefficients are obtained from normalized matrices. The correlation coefficient between two indicators is calculated as p_{jk} as in (4).

$$p_{jk} = \frac{\sum_{i=1}^{n}(X_{ij}-\bar{X}_j)(X_{ik}-\bar{X}_k)}{\sqrt{\sum_{i=1}^{n}(X_{ij}-\bar{X}_j)^2 \sum_{i=1}^{n}(X_{ik}-\bar{X}_k)^2}} \quad j,k = 1,2,3,\dots m \tag{4}$$

The standard deviation of j indicators is shown in Equation (5). To determine the contrast between indicators, the total amount of information carried by indicator j was calculated with C_j in Equation (6).

$$\sigma_j = \sqrt{\frac{\sum_{i=1}^{n}(r_{ij}-\bar{r}_j)^2}{n}} \tag{5}$$

$$C_j = \sigma_j \sum_{k=1}^{m}(1-p_{jk}) \tag{6}$$

Step 4: In this step, the indicator weights denoted by w_j are obtained from the degree of information and the correlation coefficient calculated for each indicator as follows:

$$w_j = \frac{C_j}{\sum_{j=1}^{m} C_j} \tag{7}$$

The order of importance of the indicators is determined according to the height of the w_j value obtained.

3.2. The VIKOR Method

VIKOR technique is developed for multi-criteria decision optimization of multi-criteria complex systems based on finding the closest reasonable solution to the ideal solution by focusing on sorting and choosing between alternatives with different weights [19,29]. In this method, the initial weight, benefit and cost aspects of the indicators must be known. The VIKOR method is calculated in 7 steps as follows [19,30].

Step 1: In the decision matrix X, the indices I and j refer to the alternatives and indicators, respectively.

$$X = \begin{bmatrix} X_{11} & X_{12} & \cdots & X_{1m} \\ X_{21} & X_{22} & \cdots & X_{2m} \\ \vdots & \vdots & \vdots & \vdots \\ X_{n1} & X_{n2} & \cdots & X_{nm} \end{bmatrix} \tag{8}$$

Step 2: Using the elements in the decision matrix, j to show the (f_j^*) best and (f_j^-) worst values for each indicator. Benefit-oriented values from the indicator are calculated with Equations (9) and cost-oriented values (10).

$$f_j^* = \max_i X_{ij}$$
$$f_j^- = \min_i X_{ij} \tag{9}$$

$$f_j^* = \min_i X_{ij}$$
$$f_j^- = \max_i X_{ij} \tag{10}$$

Step 3: Normalization operations are carried out using the benefit-cost values of the decision matrix. The values normalized of r_{ij} are acquired from (11) as following.

$$r_{ij} = \frac{f_j^* - X_{ij}}{f_j^* - f_j^-} \tag{11}$$

The R normalized matrix from r_{ij} values, where i=1,2,3,..., n and j=1,2,3,..., m, is shown as follows:

$$R = \begin{bmatrix} r_{11} & r_{12} & \cdots & r_{1m} \\ r_{21} & r_{22} & \cdots & r_{2m} \\ \vdots & \vdots & \vdots & \vdots \\ r_{n1} & r_{n2} & \cdots & r_{nm} \end{bmatrix} \tag{12}$$

Step 4: V decision matrix; The weighted normalized matrix's elements are employed to calculate it, as demonstrated in the equation as follows.

$v_{ij} = r_{ij} w_{ij}$, where $\sum w_{ij} = 1$ represents the relative weights of the indicators.

$$V = \begin{bmatrix} v_{11} & v_{12} & \cdots & v_{1m} \\ v_{21} & v_{22} & \cdots & v_{2m} \\ \vdots & \vdots & \vdots & \vdots \\ v_{n1} & v_{n2} & \cdots & v_{nm} \end{bmatrix} \tag{13}$$

Step 5: S_i; *i*. The total indicator value of the alternative and R_j ; *j*. To show the value of the maximum indicator, the largest value of the weighted normalized matrix $\max_j v_{ij}$ is calculated as follows.

$$S_i = \sum_{j=1}^{m} v_{ij}$$
$$R_j = \max_j v_{ij} \tag{14}$$

Step 6: The min and max values of S_i and R_j are obtained respectively as follows.

$$S^* = \min_i S_i$$
$$S^- = \max_i S_i$$
$$R^* = \min_j R_j$$
$$R^* = \max_j R_j \tag{15}$$

Q_i values for the ranking of alternatives are calculated as follows:

$$Q_i = \frac{q.(S_i - S^*)}{(S^- - S^*)} + \frac{(1-q).(R_j - R^*)}{(R^- - R^*)} \tag{16}$$

The q value in (16) shows the weight of the option that maximizes group advantage. (1-q) is defined as the strategy weight that ensures regret in opposing views. When the q value is selected (>0.5), it indicates that the majority tends to have a positive attitude towards the Q_i index, and when (<0.5) is selected, it indicates that the majority shows a negative attitude towards the Q_i index. In studies, q=0.5 is generally chosen. In other words, it is assumed that the

experts receiving the evaluation display a conciliatory attitude [31].

Step 7: The obtained Q_i, S_i *and* R_j values are sorted from smallest to largest. The optimum option is identified as the one with the lowest Q_i value. But in order for this outcome to be legitimate, two requirements need to be fulfilled. These conditions are;

Condition 1 (Acceptable advantage): This requirement entails demonstrating that the best and options that are most similar to the best differ significantly from one another. While $Q(P1)$ is the lowest first alternative; $Q(P1)$ is the second lowest alternative. The DQ value is obtained as follows.

$$Q(P2) - Q(P1) \geq DQ$$
$$DQ = \frac{1}{(i-1)} \quad (17)$$

Condition 2 (Acceptable stability): A high score for at least one of the S and R values of the option with the best Q value is required to demonstrate the stability of the compromise solution. If one of the two specified conditions is not met, the compromise solution set is proposed as follows:

- If the 2nd condition is not met, P1 and P2 alternatives,
- If condition 1 is not met, the inequality is reviewed as follows, taking into account the alternatives P1, P2,... PN.

$$Q(PN) - Q(P1) < DQ \quad (18)$$

The compromise solution set is sorted according to Q values. One of the options with the lowest Q value is the best option, as determined by Q values.

3.3. BORDA Counting Method

BORDA Counting Method, one of the most used voting techniques in social election theory, emerged in 1784 with the work of Jeans-Charles de Borda. It is a method that does not ensure that units are ranked according to their preference scores in social selection problems [32]. Units are ranked according to the board score calculated from the rankings determined by the decision makers. In addition, since BORDA Counting Methods are known as a data fusion technique, it allows creating a more realistic ranking result by combining two or more ranking lists.

In this method, which is based on selecting the decision units most suitable for the purpose, The most desired option among n choices receives (n-1) points, the second most preferred receives (n-2) points, and the least preferred receives 0 points in the calculation of board scores. With these obtained scores, the best unit is determined by ranking them from largest to smallest [33]. In the calculation of the BORDA Counting Method; The formula used to represent B_i^k, k value represents the classifier, and the i value determined by the classifier represents the rank given to the unit [33].

$$B(i) = \sum_{k=1}^{n} B_i^k \quad (19)$$

4. Findings

In this section, firstly, performance indicators are weighted for each year between 2018 and 2022 employing CRITIC method and the importance weights (weight coefficients) of the indicators are determined. Secondly, using the weights obtained from the CRITIC method, countries are ranked and compared according to their performance using the VIKOR method.

4.1. Determination of Importance Weights with CRITIC Method

The importance weights of the performance indicators were determined by following the previously given steps of the CRITIC technique. In Table 3, the standard deviation, amount of information and weight coefficient of each indicator values for the time period considered are calculated. The indicator with the highest importance weight for 2018 is the Maximum size (GT) of vessels (22.42%) indicated by G6, while the indicator with the lowest importance weight is the Average cargo carrying capacity (dwt) per vessel (13.34%) indicated by G4. In 2019, the most important indicator and the least important indicator are the same as in 2018. Maximum size (GT) of vessels (20.75%), denoted by G6, has the highest importance weight, Average cargo carrying capacity (dwt) per vessel (12.61%), denoted by G4, has the lowest importance weight among the indicators. The most striking change was in the indicator Maximum cargo carrying capacity (dwt) of vessels denoted by G5. This indicator was ranked 5th in terms of importance in 2018 and 2nd in 2019. The difference in 2020 results from 2019 is that the importance rankings of the Average age of vessels (years) indicator denoted by G2 and the Average size (GT) of vessels indicator denoted by G3 have changed places. In 2020, as in the previous two years, Maximum size (GT) of vessels (20.75%), denoted by G6, has the highest importance weight, while Average cargo carrying capacity (dwt) per vessel (12.61%), denoted by G4, has the lowest importance weight among the indicators. Looking at the 2021 fleet performance indicators' weight coefficient values, different rankings are observed in importance weights compared to previous years. While the indicator Maximum size (GT) of vessels denoted by G6 was the indicator with the highest importance weight in all of the previous three years, this indicator was replaced by the indicator Maximum cargo carrying capacity (dwt) of vessels denoted by G5 (19.83%)

in 2021. As in the previous three years, the Average cargo carrying capacity (dwt) per vessel indicator denoted by G4 is the indicator with the least importance weight (12.32%) among the other indicators in 2021.

The position of the indicator with the lowest importance weight, Average cargo carrying capacity (dwt) per vessel (12.78%), denoted by G4, has not changed in 2022. However, the indicator Maximum cargo carrying capacity (dwt) of vessels, denoted by G5, which had the highest importance weight in the previous year, ranked fourth in terms of importance in 2022. Unlike previous years, the indicator with the greatest weight of significance in 2022 was the Average age of vessels (years) (21.40%) denoted by G2.

Table 3. *Standard deviation of indicators, amount of information (C_j) and weight coefficient (w_j) values for the year 2022*

Indicator	Year	σ	C_j	w_j	$\%w_j$	Ranking
Median time in port (G1)	2018	0.306	1.026	0.148	14.88%	4
	2019	0.316	1.097	0.149	14.94%	5
	2020	0.281	1.007	0.129	12.92%	5
	2021	0.292	0.97	0.135	13.57%	5
	2022	0.305	0.975	0.134	13.40%	5
Average age of vessels (G2)	2018	0.258	1.096	0.158	15.89%	3
	2019	0.272	1.172	0.159	15.97%	4
	2020	0.318	1.373	0.176	17.61%	3
	2021	0.301	1.237	0.173	17.32%	4
	2022	0.317	1.536	0.214	21.40%	1
Average size of the vessel (G3)	2018	0.249	1.302	0.188	18.87%	2
	2019	0.245	1.3	0.177	17.72%	3
	2020	0.248	1.303	0.167	16.72%	4
	2021	0.255	1.262	0.176	17.67%	3
	2022	0.267	1.277	0.183	18.31%	2
Average cargo carrying capacity per vessel (G4)	2018	0.24	0.92	0.133	13.34%	6
	2019	0.239	0.925	0.126	12.61%	6
	2020	0.239	0.919	0.118	11.80%	6
	2021	0.238	0.88	0.123	12.32%	6
	2022	0.236	0.894	0.127	12.78%	6
Maximum cargo carrying capacity of vessels (G5)	2018	0.23	1.006	0.145	14.59%	5
	2019	0.272	1.32	0.179	17.98%	2
	2020	0.265	1.437	0.184	18.44%	2
	2021	0.279	1.417	0.198	19.83%	1
	2022	0.259	1.126	0.159	15.91%	4
Maximum size of vessels (G6)	2018	0.349	1.546	0.224	22.42%	1
	2019	0.354	1.523	0.207	20.75%	1
	2020	0.359	1.753	0.224	22.49%	1
	2021	0.33	1.376	0.192	19.26%	2
	2022	0.304	1.275	0.181	18.17%	3

When the changes in the importance levels of the indicators over the years are analyzed, it is seen that the least important indicator is the Average cargo carrying capacity (dwt) per vessel for all years. The importance of the Maximum size (GT) of vessels indicator has decreased over the years. In addition, the importance of the Maximum cargo carrying capacity (dwt) of vessels indicator increased in 2019, 2020 and 2021, and the Average age of vessels (years) became the most important indicator in 2022.

4.2. Ranking of Countries with VIKOR Method

Applying the importance weights that the CRITIC technique provided, the performance of the countries between 2018-2022 was ranked and compared with the VIKOR method. As mentioned before, there are two conditions necessary for the VIKOR method results to be valid. The option with the highest Q value ranking is suggested as an acceptable compromise if the requirements are achieved [34].

For all years, it was observed that the conditions detailed in the methodology section were met. It was also observed that a compromise solution was reached when the "q" value was taken as 0.5. Therefore, interpretations and rankings are based on q=0.5. Table 4 illustrates the calculated Q_i values for the countries considered. A low Q_i value indicates high performance. Table 4 shows that Japan, the Netherlands, and Germany are generally among the best performers on a consistent basis, while Australia, Russian Federation and Croatia are among the worst performers. The rankings for each year are shown in Table 5.

4.3. Ranking of Countries by Borda Counting Method

The Borda counting method is the last stage of the study and was used to obtain a single ranking by combining the values obtained for the five years of the CRITIC-based VIKOR method analyzed. The findings are shown in Table 5.

The integrated ranking was calculated by obtaining the VIKOR method rankings and Borda scores of the countries in Table 5 for the years 2018-2022. In this ranking, Japan ranked first, Netherlands second and Germany third. Considering that the factors that cause the importance of indicators to change are the developments in the world, the change in country rankings over the years should be read from this perspective. Within the context of this study, both the performances of the countries and the indicators affecting their performances are comparatively shown in Table 6. Thus, it is revealed how country performances are affected by changes in the importance of indicators.

The importance levels of indicators change from year to year due to the international conjuncture and shocks such as pandemics. In this case, countries need to achieve an agile structure in terms of all indicators. For example, in the transition from 2021 to 2022, when the maximum cargo

Table 4. *Time dependent variation of values of countries*

	Q_i values				
Country	**2018**	**2019**	**2020**	**2021**	**2022**
Japan	0	0	0.099663	0	0.039967
Netherlands	0.100274	0.094595	0.031141	0.057888	0.010035
Germany	0.130046	0.162475	0.115662	0.158235	0.273513
Denmark	0.145359	0.623183	0.580787	0.70822	0.498661
Greece	0.195612	0.29214	0.553602	0.71398	0.389771
Spain	0.202752	0.207294	0.416274	0.53489	0.12997
United Kingdom	0.273869	0.278804	0.153919	0.20725	0.187671
Republic of Korea	0.311406	0.282615	0.216903	0.239464	0.14806
France	0.398051	0.42579	0.257965	0.344361	0.29172
Norway	0.450015	0.469943	0.493658	0.15876	0.069681
Sweden	0.520954	0.68173	0.332439	0.365805	0.542618
Italy	0.531819	0.586731	0.577297	0.710261	0.750567
USA	0.540871	0.621283	0.498077	0.626477	0.789911
China	0.603413	0.564735	0.44689	0.567589	0.536055
Croatia	0.660743	0.845586	0.816843	0.713887	0.589903
Canada	0.660791	0.674271	0.681384	0.656198	0.653487
Russian Federation	0.696667	0.775659	0.791723	0.947166	0.944444
Türkiye	0.697671	0.596991	0.520783	0.385308	0.582929
Australia	0.850066	0.87809	0.870261	0.866053	0.844496
Indonesia	0.89129	0.631204	0.619282	0.545238	0.40753

Table 5. *VIKOR and BORDA ranking for 2018-2022*

	VIKOR ranking					BORDA total points	BORDA ranking
	2018	**2019**	**2020**	**2021**	**2022**		
Germany	3	3	3	3	7	81	3
USA	13	13	11	13	18	32	14
Australia	19	20	20	19	19	3	20
United Kingdom	7	5	4	5	6	73	4
China	14	10	9	12	12	43	11
Denmark	4	14	15	15	11	40	12
Indonesia	20	15	16	11	10	28	16
France	9	8	6	7	8	62	8
Croatia	15	19	19	17	15	15	18
Netherlands	2	2	1	2	1	92	2
Spain	6	4	8	10	4	68	6
Sweden	11	17	7	8	13	44	10
Italy	12	11	14	16	17	30	15
Japan	1	1	2	1	2	93	1
Canada	16	16	17	14	16	21	17
Republic of Korea	8	6	5	6	5	70	5
Norway	10	9	10	4	3	64	7
Russian Federation	17	18	18	20	20	7	19
Türkiye	18	12	12	9	14	34	13
Greece	5	7	13	18	9	50	9

carrying capacity lost its importance in performance and the average age of vessels gained importance, countries with older ships experienced a decline in performance. In this respect, in order to determine the extent to which countries have been able to achieve stability in their rankings over the years, standard deviation values for their five-year rankings were calculated and given in Table 7.

According to Table 7, where a standard deviation of 3 and above is considered as high variability, the countries that failed to achieve stability are Greece, Denmark, Indonesia, Sweden, Norway, Norway and Türkiye, respectively.

The countries whose ranking has changed the least over the years and whose standard deviation value is below 1 point are Japan, Netherlands and Australia, respectively. It should be noted here that Japan and Netherlands have achieved stability at the top, while Australia has always been at the bottom.

5. Conclusion

For much of the last 50 years, globalization has been the wind in the sails of multinational corporations and investors, with China's gradual opening up to western trade, the collapse of the Iron Curtain, the rise of the BRICS (Brazil, Russia, India, China, South Africa, Iran, Egypt, Ethiopia, and the United Arab Emirates) countries, and the liberal policies adopted in free trade. In a highly integrated trade scene, the ability of countries to realize their ambitions of becoming the main actor and getting a bigger piece of the pie is undoubtedly highly dependent on their ability to allocate sea power or to maintain or strengthen their existing positions.

The weighting of indicators with analytical decision-making methods provides descriptive information in terms of evaluating the port call and performance of countries. The CRITIC method used for this purpose is preferred because it does not include subjective approaches in the weighting of indicators. When the indicators are ranked in terms of their importance levels for the years 2018-2022, it is observed that a different indicator stands out in terms of

Table 7. *Standard deviation values for five-year rankings of countries*

Country	Std. Dev.	Country	Std. Dev.
Germany	1.79	Spain	2.61
USA	2.61	Sweden	4.02
Australia	0.55	Italy	2.55
United Kingdom	1.14	Japan	0.55
China	1.95	Canada	1.10
Denmark	4.66	Republic of Korea	1.22
Indonesia	4.04	Norway	3.42
France	1.14	Russian Federation	1.34
Croatia	2.00	Türkiye	3.32
Netherlands	0.55	Greece	5.18
Std. Dev.: Standard deviation			

Table 6. *Analyzing country performances based on indicators*

Change in indicators	Change in country rankings
Maximum cargo carrying capacity becomes important in the transition from 2018 to 2019	**Underperformers:** Australia, Denmark, Croatia, Greece, Russia, Sweden, Sweden, Russia **High performers:** China, Indonesia, France, France, Italy, Italy, Republic of Korea, Norway, Norway, Türkiye, Spain, United Kingdom **Constant performers:** Germany, USA, Netherlands, Japan, Canada
From 2019 to 2020, average age of vessels rises to 3rd place, average size of vessels falls to 4th place.	**Underperformers:** Australia, Denmark, Indonesia, Canada, Indonesia, Italy, Japan, Norway, Spain, Sweden, Sweden **High performers:** China, France, France, Republic of Korea, Greece, Netherlands, United Kingdom, USA **Constant performers:** Germany, Australia, Croatia, Russia, Türkiye
In the transition from 2020 to 2021, the average age of vessels fell back to 4th place, while the average size of vessels rose to 3rd place. In addition, maximum cargo carrying capacity became the most important indicator.	**Underperformers:** USA, United Kingdom, China, France, Netherlands, Spain, Sweden, Italy, Republic of Korea, Russian Federation, Greece **High performers:** Australia, Indonesia, Croatia, Japan, Canada, Norway, Türkiye **Constant performers:** Germany, Denmark
In the transition from 2021 to 2022, the average age of vessels rose from 4th to 1st place in terms of importance. Maximum cargo carrying capacity decreased from 1st to 4th place.	**Underperformers:** Germany, USA, United Kingdom, France, Sweden, Italy, Japan, Canada, Türkiye **High performers:** Denmark, Indonesia, Croatia, Netherlands, Spain, Republic of Korea, Norway, Greece **Constant performers:** Australia, China, Russian Federation

importance each year. This variability in the importance of indicators shows that the determinants of countries' performance are affected by time-dependent economic, social and environmental factors. Therefore, countries need to be prepared in terms of all indicators in order to demonstrate an effective performance and to be prepared for these factors.

Country performance scores were obtained according to the weighted indicators of the countries with the VIKOR method and the rankings obtained with the BORDA method for the years 2018-2022 were combined. In the last five years, Japan, Netherlands, Germany, the United Kingdom and Republic of Korea have been the five countries with the best performance in the ranking of countries based on weighted indicators. Port call and performance of the countries is directly proportional to their share in world trade.

The analyses show how the changes in the importance levels of the indicators affect the performance of the countries, to what extent the five-year performance rankings of the countries vary, and which countries have changed their rankings in the same direction and in the opposite direction due to the changes in the importance levels of the indicators. It can be said that the maritime trade structures of the countries affected in the same direction in terms of ranking are similar, while the maritime trade structure of the countries affected in the opposite direction are different. It can be stated that countries that have low standard deviation in terms of five-year performance rankings and have achieved stability are resistant to changes in the importance levels of indicators, that is, to economic, social and environmental events occur over the years. In other words, these changes did not affect the performance ranking of these countries. Among these countries, Japan and Netherlands performed well in the face of all kinds of changes, while Australia continued to perform poorly even though the importance levels of indicators changed.

On the other hand, countries such as Greece, Denmark, Indonesia, Sweden, Norway and Türkiye, whose performance varies greatly as the importance levels of indicators change, can be said to have strong or weak performance in terms of certain indicators. These countries should focus on improving their weaknesses in order to become more resilient to economic, social and environmental developments related to their port call and performance.

This study is anticipated to contribute to the body of literature. on the evaluation of port call and performance. As a matter of fact, the number of studies on the subject with multi criteria decision making techniques is quite low. The Critic method used for weighting indicators is a method of objective weighting, and methods of subjective weighting are likely to produce different results. This may be considered as a limitation of this study. Moreover, different time spans could yield different results.

In future studies, first, it would be more appropriate to conduct country-specific studies on countries that are small but have an important place in maritime trade. Second, the fact that the impact of emerging technologies (such as blockchain and autonomous ships) and new regulations (such as those targeting emissions) on maritime trade performance can also be investigated. Third, exploring dynamic weighting of indicators over time could offer insights into changing priorities and factors influencing maritime trade performance. Fourth, the use of different sets of indicators in the evaluation of maritime trade performance can be considered. Lastly, comparative analyses can be made on the weighting of indicators and ranking of countries with different methods..

Authorship Contributions

Concept design: E. Akdamar, E. F. Akgül, and E. Işık, Data Collection or Processing: E. Akdamar, M. Gögebakan, and E. Işık, Analysis or Interpretation: E. Akdamar, E. F. Akgül, M. Gögebakan, and E. Işık, Literature Review: E. Akdamar, E. F. Akgül, and M. Gögebakan, Writing, Reviewing and Editing: E. Akdamar, E. F. Akgül, and M. Gögebakan.

Funding: The authors declare that no funds, grants, or other support was received during the preparation of this manuscript.

References

[1] J. Ojala, and S. Tenold, "Maritime trade and merchant shipping: The shipping/trade ratio since the 1870s". *International Journal of Maritime History,* vol. 29, pp. 838-854, Nov 2017.

[2] M. Stopford, *Maritime Economics*, 3rd edition. London; New York: Routledge, 2009.

[3] R. Kerbiriou, "Modernisation of container ship fleets: state of play and consequences for the Baltic Sea". *TransNav, The International Journal on Marine Navigation and Safety of Sea Transportation,* vol. 18, pp. 211-217, 2024.

[4] K. Cullinane, and D.-W. Song, "Estimating the relative efficiency of European container ports: A stochastic frontier analysis". *Research in Transportation Economics,* vol. 16, pp. 85-115, Jan 2006.

[5] M. Luo, and T. Grigalunas, "A spatial-economic multimodal transportation simulation model For US coastal container ports". *Maritime Economics & Logistics,* vol. 5, pp. 158-178, Jun 2003.

[6] M. R. Brooks, "The governance structure of ports". *Review of Network Economics,* vol. 3, pp. 168-183, Jan 2004.

[7] W. K. Talley, *Port Economics*, New York: Routledge, 2009.

[8] D. Owen, *Ocean trade and shipping*, Cambridge, MA: University Press, 1914.

[9] T. Heaver, "The evolution and challenges of port economics". *Research in Transportation Economics,* vol. 16, pp. 11-41, Jan 2006.

[10] L. P. G. Santhi, and N. P. W. Setyari, "The Impact of trade facilitation on export performance in six ASEAN countries period 2005-2016". *International Journal of Applied Economics, Finance and Accounting,* vol. 5, pp. 89-100, 2019.

[11] H. Dick, "The 2008 shipping law: Deregulation or re-regulation?". *Bulletin of Indonesian Economic Studies,* vol. 44, pp. 383-406, Dec 2008.

[12] J. Wilson, C. Mann, and T. Otsuki, "Trade facilitation and economic development: Measuring the impact". *Policy Research Working Papers,* Mar 2003.

[13] V. P. Sant' Anna, and S. Kannebley Júnior, "Port efficiency and Brazilian exports: A quantitative assessment of the impact of turnaround time". *The World Economy*, vol. 41, pp. 2528-2551, Sep 2018.

[14] A. C. Jordaan, "The impact of trade facilitation factors on South Africa's exports to a selection of African countries". *Development Southern Africa,* vol. 31, pp. 591-605, Jul 2014.

[15] D. Diakoulaki, G. Mavrotas, and L. Papayannakis, "Determining objective weights in multiple criteria problems: The critic method". *Computers & Operations Research,* vol. 22, pp. 763-770, Aug 1995.

[16] H.-W. Wu, J. Zhen, and J. Zhang, "Urban rail transit operation safety evaluation based on an improved CRITIC method and cloud model". *Journal of Rail Transport Planning & Management,* vol. 16, pp. 100206, Dec 2020.

[17] H. Jati, Nurkhamid, and R. Wardani, "Visibility ranking of university e-learning websites -CRITIC method approach". *Journal of Physics: Conference Series,* vol. 1737, 012030, Jan 2021.

[18] H. Deng, C.-H. Yeh, and R. J. Willis, "Inter-company comparison using modifed TOPSIS with objective weights". *Computers & Operations Research,* vol. 27, pp. 963-973, Sep 2000.

[19] S. Opricovic, and G.-H. Tzeng, "Compromise solution by MCDM methods: A comparative analysis of VIKOR and TOPSIS". *European Journal of Operational Research,* vol. 156, pp. 445-455, Jul 2004.

[20] S. Paksoy, "Assessment of country indicators with VIKOR method". *The International Journal of Economic and Social Research,* vol. 11, pp. 153-169, 2015.

[21] S. Perçin, and S. Çakır, "Performance measurement of logistics firms with multi-criteria decision making methods". *Ege Academic Review,* vol. 13, pp. 449-459, Oct 2013.

[22] B. Slack, C. Comtois, B. Wiegmans, and P. Witte, "Ships time in port". *International Journal of Shipping and Transport Logistics,* vol. 10, pp. 45-62, Jan 2018.

[23] T. E. Notteboom, "The time factor in liner shipping services". *Maritime Economics & Logistics,* vol. 8, pp. 19-39, Mar 2006.

[24] A. Apostolidis, J. Kokarakis, and A. Merikas, "Modeling the dry-docking cost - The case of tankers". *Journal of Ship Production and Design,* vol. 28, pp. 134-143, Aug 2012.

[25] E. Cakir, C. Sevgili, and R. Fiskin, "An analysis of severity of oil spill caused by vessel accidents". *Transportation Research Part D: Transport and Environment,* vol. 90, 102662, Jan 2021.

[26] UNCTADstat, "Port call and performance statistics: time spent in ports, vessel age and size, annual". Accessed: Jan. 03, 2024. [Online]. Available: https://unctadstat.unctad.org/datacentre/reportInfo/US.PortCalls

[27] M. Ozcalici, "Asset allocation with multi criteria decision making techniques". *Decision Making: Applications in Management and Engineering,* vol. 5, pp. 78-119, Oct 2022.

[28] F. Ecer, *Çok kriterli karar verme: Geçmişten günümüze kapsamlı bir yaklaşım*. Ankara: Seçkin, 2020.

[29] S. Opricovic, and G.-H. Tzeng, "Extended VIKOR method in comparison with outranking methods". *European Journal of Operational Research,* vol. 178, pp. 514-529, Apr 2007.

[30] F. Sari, "Forest fire susceptibility mapping via multi-criteria decision analysis techniques for Mugla, Turkey: A comparative analysis of VIKOR and TOPSIS". *Forest Ecology and Management,* vol. 480, 118644, Jan 2021.

[31] J. Wei, and X. Lin, "The multiple attribute decision-making VIKOR method and its application". In *2008 4th International Conference on Wireless Communications, Networking and Mobile Computing*, Dalian, China: IEEE, pp. 1-4, Oct 2008.

[32] N. Aktaş, and N. Demirel, "A hybrid framework for evaluating corporate sustainability using multi-criteria decision making". *Environment, Development and Sustainability*, vol. 23, pp. 15591-15618, Oct 2021.

[33] A. C. Gök Kisa and S. Perçin, 'Bulanık çok kriterli karar verme yaklaşımı ile Türkiye İmalat Sanayii'nde performans ölçümü', *Uluslararası İktisadi ve İdari İncelemeler Dergisi*, Prof. Dr. Talha Ustasüleyman Special Issue, pp. 31-56, Feb 2020.

[34] S. Hezer, E. Gelmez, and E. Özceylan, "Comparative analysis of TOPSIS, VIKOR and COPRAS methods for the COVID-19 regional safety assessment". *Journal of Infection and Public Health,* vol. 14, pp. 775-786, Jun 2021.

Journal of ETA Maritime Science 2024;12(2):224-236

Fire Safety Analysis Onboard Passenger Ships by using Fire Dynamics Simulations: Case Study of a Turkish Domestic Passenger Ship

Tolga Aycı[1], Barış Barlas[1], Aykut Ölçer[2]

[1]İstanbul Technical University Faculty of Naval Architecture and Ocean Engineering, Department of Naval Architecture and Marine Engineering, İstanbul, Türkiye
[2]World Maritime University, Department of Maritime Energy Management, Malmö, Sweden

Abstract

Fire hazards onboard are a significant cause of accidents, leading to loss of life and property. According to the Global Integrated Shipping Information System database, 6.82 out of every 1000 passenger/Ro-Ro/Ferry ships have reported fire casualties within the category of "serious to very serious", a rate higher than that of other ship types. This study analyzes fire safety on passenger ships through fire dynamics simulations. A Turkish domestic passenger ferry with a capacity of 600 passengers was selected as the case study. The model analyzed fire extinguishing and structural fire protection systems under five scenarios. The heat release rate, total energy, and temperature parameters were also scrutinized. In addition to fire extinguishing systems like sprinklers, structural fire protection systems such as fire-rated bulkheads and decks significantly impact fire safety on passenger ships. During maintenance and operation processes, these components should undergo regular inspections by the crew and technical teams. The key findings of this study are that temperatures in the engine room increase extremely to around 500 °C in the early stages and application of neither structural nor active (extinguishing etc.) fire protection systems together led to fatal consequences onboard passenger ships.

Keywords: Passenger ships, Fire safety, Fire dynamics simulation, Field modeling

1. Introduction

No ship can operate with 100% safety or be completely error-free. Hazard classification and risk evaluation are primarily focused on assessing risk levels and identifying the greatest fire hazards on board. Properly conducted analyses can reduce failure risk to an acceptable level and enhance ship reliability under critical conditions. Therefore, risk assessment applications are of great importance to safeguard system reliability in ships. A thorough analysis of historical ship incident data can inform amendments to regulations and decrease theoretical accident risk. Maritime safety is not only of primary environmental importance but also has a considerable commercial aspect. An obvious safety level is a critical component of the package offered by operators to their customers [1].

onboard fires are among the main ship accidents, leading to loss of life and property. If a fire on board is not extinguished, it can lead to catastrophic consequences, total actual loss, and severe victimization. The data was collected from the Global Integrated Shipping Information System (GISIS), a database provided by the International Maritime Organization (IMO), containing casualty and incident data reported by IMO member states. We analyzed various types of ships reporting serious and very serious fire casualties from January 2000 to December 2022 [2]. In GISIS, fire casualty reports are classified into four categories: very serious, serious, less serious, and unspecified. Total loss of the ship and/or loss of life can be defined as very serious fire casualties. Serious fire casualties are fatalities to ships that do not qualify as "dreadful fire casualties" and which involve a fire and/or explosion, resulting in immobilization

Address for Correspondence: Tolga Aycı, İstanbul Technical University Faculty of Naval Architecture and Ocean Engineering, Department of Naval Architecture and Marine Engineering, İstanbul, Türkiye
E-mail: aycit@itu.edu.tr
ORCID ID: orcid.org/0000-0002-0186-1510

Received: 18.04.2024
Last Revision Received: 29.04.2024
Accepted: 07.05.2024

To cite this article: T. Aycı, B. Barlas, and A. Ölçer. "Fire Safety Analysis Onboard Passenger Ships by using Fire Dynamics Simulations: Case Study of a Turkish Domestic Passenger Ship." *Journal of ETA Maritime Science*, vol. 12(2), pp. 224-236, 2024.

of main engines, extensive accommodation damage, severe structural damage, etc. In this study, only very serious and serious reported casualties were investigated. The serious and very serious fire incidents of different types of ships between January 2000 and December 2022 are listed in Table 1.

Table 1. *Reported serious and very serious fire casualties between 2000 and 2022 for different ship types [2]*

Ship types	Total	Percentage
Tanker	78	24.1%
Ro-Ro/Ferry/Pass.	54	16.7%
General cargo	45	13.9%
Fishing vessel	43	13.3%
Bulk/Ore carrier	34	10.5%
Others	30	9.3%
Container	30	9.3%
Tug/Supply vessel	9	2.8%

Ro-Ro/Ferry/Passenger ships accounted for 16.7% of marine casualties globally from 2000 to 2022. However, one must consider not only the number of incidents but also the incidence rate. The average occurrence rates of ship types that recorded serious and very serious fire fatalities between 2000 and 2022 are shown in Table 2. The average rate describes the number of fire casualties per 1,000 ship over 22 years. It is calculated by dividing the casualty numbers by the average number of ships. The average incidence rate of fire casualties for Ro-Ro/Ferry/Passenger ships from 2000 to 2022 is 6.82, meaning that, on average, 6.82 out of every 1000 such ships reported serious or very serious fire fatalities. During the same period, the average incidence rate for all other ship groups was 3.58. Therefore, the incidence rate of Ro-Ro/Ferry/Passenger ships is almost twice that of all other ship types.

Table 2. *The incidence rates and numbers of different ship types reporting serious and very serious fire casualties between 2000 and 2022*

Ship types	Average incidence rate	Average number of ships
Ro-Ro/Ferry/Pass.	6.82	7907
Tanker	5.42	14380
General cargo	2.53	17784
Fishing vessel	1.86	23000
Bulk/Ore carrier	2.63	12941
Container	5.38	5574
Tug/Supply vessel	0.43	20804

Given the high frequency of fire incidents on passenger ships, this study analyzes passenger ship fire safety from the perspective of fire dynamics simulations. As a case study, we meticulously examine a Turkish Domestic Passenger Ferry, namely SH SUTLUCE (IMO: 9564009), with a capacity of 600 passengers belonging to the Sehir Hatlari passenger ship fleet. Sehir Hatlari operates public sea transportation services in İstanbul, 933 daily trips, and transports 40 million passengers annually, offering a crucial alternative for transportation [3].

Although the literature review section investigates the fire safety onboard passenger ships in terms of regulations, modeling, risk assessment, evacuation, and performance-based design perspectives, the fire safety measurement of the Sehir Hatlari fleet reveals a research gap in the literature. In this study, fire dynamics simulation tools are used to assess the fire safety of one passenger vessel from the Sehir Hatlari fleet.

Fire safety onboard passenger ships is profoundly affected not only by fire extinguishing systems such as sprinklers but also by the presence of structural fire protection systems such as fire-rated bulkheads and decks. To reduce fire hazard risk, fire compartmentation and extinguishing systems significantly affect temperature spread in crucial compartments such as engine rooms. It is of paramount importance to ensure the proper installation of these systems with appropriate materials, paying special attention to their stability. During the maintenance and operation of passenger ships, regular inspections of the fire protection systems by both the crew and technical teams are imperative.

The aims of this study are as follows:

- Outline strategies for mitigating fire risk, particularly on passenger ships, with a case study on Sehir Hatlari.
- Simulate fire dynamics, including fire protection active and structural systems, in a passenger ship and analyze engine room fires due to the fatality and risk of these fires.
- Observe the outcomes of fire protection systems, for instance, extinguishing and structural systems, in the fire dynamics simulation,
- Develop a risk framework for onboard fire casualties, especially on passenger ships, to minimize their occurrence.
- Determine the variables that contribute to onboard fire casualties, particularly on passenger ships, thereby expanding our understanding of these phenomena and supporting new approaches to preventing onboard fires.

2. Literature Review

The literature review is analyzed in detail in terms of fire safety regulation onboard ships, fire modeling, fire

protection systems such as extinguishing systems, and performance-based design depending on fire dynamics simulations and evacuations in the literature review section.

Ships are protected against fire hazards through the regulations of the IMO's International Convention for the Safety of Life at Sea (SOLAS) [4,5]. The well-known SOLAS convention was first established in 1914 after the Titanic disaster. Its main purpose was to set the minimum safety requirements onboard. Then, the SOLAS convention was constantly amended after the major accidents that highlighted new safety aspects onboard. Chapter II-2 of SOLAS governs fire safety onboard. The regulations provide all fire safety provisions, starting with division and separation by thermal and structural boundaries, and then continuing with restrictions on combustible materials and fire detection systems at the origin of fires. In the event of a fire incident, the regulations cover containment and extinction procedures at the fire's origin. The regulations also ensure the availability of fire-extinguishing appliances and minimize ignition possibilities, thus protecting the means of escape and firefighting through special provisions [4].

Fires that occur in restricted spaces, such as compartments within buildings, ships, and airplanes, are referred to as "compartment fires". This typically starts slight and then expands to involve a significant fuel source, becoming influenced by the compartment's boundaries [6]. Various fire models have been developed and are continually being refined and validated to predict compartment fire consequences [7]. There are two types of models available: deterministic and probabilistic. Deterministic models allow for a "single possible development", while probabilistic models attempt to investigate a range of potential developments. Over the years, deterministic models have gained popularity among fire safety engineers primarily because they provide numbers that are readily usable, often taking a conservative approach [8]. Initial semi-empirical and basic analytical models, or hand-calculation models, laid the foundation for deterministic fire models. Zone models, the earliest generation and most widely used types of fire models, were developed as a result of this evolution. The ability to solve the fundamental conservation equations of mass, energy, and momentum has facilitated advances in Computational Fluid Dynamics (CFD) modeling to enable the simulation of fire phenomena from first principles. Field or CFD modeling is an approach that has shown efficacy in addressing a range of fire safety issues [9].

An innovative simulation method to examine the propagation rule of ship cabin fire and smoke, with model validation performed using a miniature model, is presented [10]. The fire smoke flow characteristics in closed ship cabins, which lay a theoretical basis for firefighting in ship cabins, were analyzed and verified [11]. The Fire Dynamics Simulator (FDS) tool, equipped with a Large Eddy Simulation (LES) turbulence model, was used to model a full-scale cabin fire experiment designed by the U.S. Coast Guard [12]. FDS could calculate the precise temperature distribution in the cabin sections. Fire scenarios are considered rather than a formal risk modeling process. The machinery room of the target ship was used for the fire simulation [13]. Fire suppression models are studied using reinforcement-learning techniques to aim at fire extinguishing nozzles [14]. A general overview of machine learning and specific techniques being explored for performing low-cost, high-fidelity fire predictions are offered [15]. A comprehensive study [16] delves into the structural strength of fire protection installation systems, providing valuable guidelines for the appropriate implementation of fire-related systems in ship compartments. The fire safety of multilayer and monolayer engine rooms using three-dimensional numerical simulations has been investigated [17]. Fire incidents in the ship engine room were numerically analyzed in terms of temperature and smoke based on OpenFOAM, and the main factors such as fire position, fire area, and ventilation situation factors were investigated to determine the temperature distribution and smoke propagation in the engine room [18]. From the perspective of passenger evacuation, [19] displays a non-monotonic relationship between the peak heat release rate (HRR) and the required safe egress time by combining fire dynamics and evacuation simulations. Wang et al. [20] studied the ship evacuation route assignment approach and added new parameters to simulate human performance under special circumstances, such as lifting, trimming, and ship motions. The suppression of a pool fire in an engine room under different ventilation conditions has been studied depending on the fire extinguishing situation of the spray equipment [21].

3. Materials and Methods

3.1. Fire Modeling

Generally, there are two types of deterministic models: zone and field models. The former rely mostly on empirical correlations between specific variables derived from laboratory-scale experiments. Zone models are subdivided into one-layer, two-layer, and HVAC models, depending on the type of problem they are attempting to solve. Field models assume fewer empirical relations and attempt to solve the governing conservation equations (mass, momentum, and enthalpy) using numerical techniques.

One-layer models attempt to calculate smoke movement in regions remote from the fire and can handle large, complex buildings with numerous floors and rooms. On the other hand, two-layer models are limited to fires in small enclosures (with no vertical shafts) and consider smoke movement in the immediate vicinity of the fire. The HVAC models calculate smoke spread by HVAC systems and are theoretically similar to the one-layer models. Various types of computer fire models are illustrated in Figure 1 [8].

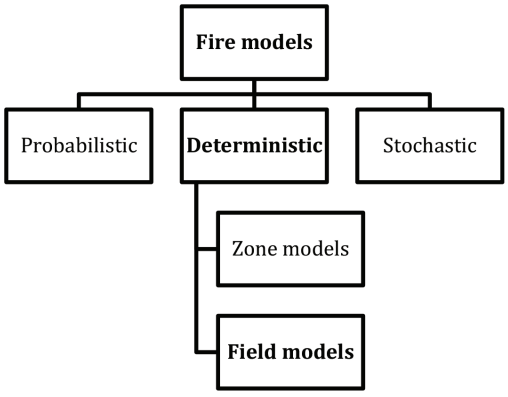

Figure 1. *Types of computer fire models*

This study employs a field model for fire modeling. Field (or CFD) models split the domain into multiple smaller control volumes to calculate the flow. With advancements in computer science, field models have become increasingly common and are now extensively used [8]. The conservation laws of mass, momentum, energy, and species concentrations are applied to each of these control volumes. Solving the equations, along with the equation of state, provides predictions of fluid flow properties with an accuracy level that is dependent on the size and number of control volumes considered. Figure 2 depicts the two layers and plumes in a room fire, divided by field models into small control volumes [22]. Fire scenario outcomes onboard passenger ships were numerically predicted by comparing the zone and field models and concluded that the role of the zone model is significant in the early design phase of passenger ships [23].

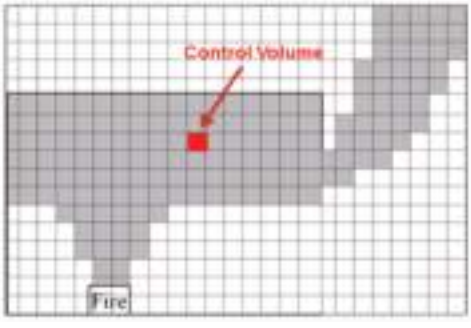

Figure 2. *The two layers and plumes in a room fire as divided by field models into small control volumes*

The transport equations for mass, momentum, and energy are given as [24]:

$$\frac{\partial \rho}{\partial t} + \frac{\partial}{\partial t}(\rho u_i) = 0 \quad (1)$$

Is the continuity Equation,

$$\frac{\partial}{\partial t}(\rho u_i) + \frac{\partial}{\partial x_i}(\rho u_i u_j) = -\frac{\partial P}{\partial x_i} + \frac{\partial \tau_{ij}}{\partial x_i} + F_i \quad (2)$$

is the momentum equation, where u_i is the velocity and ρ is the variable density, noting that the density in a combusting flow is dependent on pressure, temperature, and species concentration, p is the pressure, F_i represents the body forces including gravity and τ_{ij} is the viscous stress tensor defined as follows:

$$\tau_{ij} = \mu\left(\frac{\partial u_i}{\partial x_j} + \frac{\partial u_j}{\partial x_i} - \frac{2}{3}\delta_{ij}\frac{\partial u_k}{\partial x_k}\right) \quad (3)$$

The transport equations for species k can be written as:

$$\frac{\partial}{\partial t}(\rho Y_k) + \frac{\partial}{\partial x_i}(\rho u_i Y_k) = \frac{\partial}{\partial x_i}\left(\rho D_k \frac{\partial Y_k}{\partial x_i}\right) + \dot{\omega}_k \quad (4)$$

where Y_k is the mass fraction of a species k, D_k is the species diffusion coefficient in (m^2/s) which is usually considered a single value for all the involved species and $\dot{\omega}_k$ is the source or sink term representing the generation or destruction of a species due to chemical reactions. The energy equations in their simplified form can be written as:

$$\frac{\partial}{\partial t}(\rho h) + \frac{\partial}{\partial x_i}(\rho u_i h) = \frac{\partial}{\partial x_i}\left[\frac{\mu}{\sigma_h}\frac{\partial h}{x_i}\right] + \frac{\partial P}{\partial t} + S_{rad} \quad (5)$$

The HRR (also known as energy release rate) is a crucial time-varying parameter that provides a quantitative description of a design fire. The major fire properties, including smoke layer height, gas temperature, and plume velocity, are all within its control. HRR, measured in kW and plotted against time, represents the size of the fire and its potential damage. The fuel mass loss rate (MLR in kg/s) and the effective heat of combustion for the burning fuel (Δhc in kJ/kg) can be multiplied to obtain the HRR of combustion (HRR in kW); HRR = MLR · Δhc [25].

3.2. Case Study of a Turkish Domestic Passenger Ship

Sehir Hatlari provides vital public sea transportation services in İstanbul, offering a crucial alternative to public transportation. The Sehir Hatlari fleet comprises 28 passenger vessels, categorized on the basis of passenger

capacity into five classes: 2100, 1800, 1500, 700, and 600 passengers. A review of the fleet reveals that the vessels were built between 1973 and 2005, and the newer vessels have a smaller capacity than the older ones. According to [26], the change in capacity is related to the operational expenses of the vessels and the occupancy rate of the lines. The propulsion system alternatives of passenger ships used in public transportation, such as Sehir Hatlari, are analyzed in terms of fuel consumption and investment costs [27]. In addition to passenger vessels, Sehir Hatlari has invested in Sea Taxis, which offer private sea transportation with a capacity of 6-10 passengers.

In this study SH SUTLUCE passenger vessel from İstanbul's Sehir Hatlari fleet, which has the lowest passenger capacity, was chosen for research. The specifications are provided in Table 3 and a photograph of SH SUTLUCE is depicted in Figure 3 [28].

Table 3. *Technical specifications of the SH SUTLUCE (IMO: 9564009)*

Building year	2009
Passenger capacity	600
Gross tonnage (ton)	175.4
Net tonnage (ton)	69.2
Length overall (m)	41.97
Beam (m)	8.5
Depth (m)	2.8
Freeboard (m)	0.754
Main engine type	D16C-BMH VOLVO PENTA
Power	2X641BHP

Figure 3. *Six hundred passenger capacity vessels SH SUTLUCE (IMO: 9564009)*

In general, the structure of a whole passenger ship is very complex for modeling all details in a model. In the first step, this study focuses on the lower deck of selected passenger vessels depending on [29] that evaluates 20 common risks in ship engine rooms, and fire risk appears among the five most significant hazards. The detailed shapes of each piece of equipment in this deck are irregular. Therefore, since the FDS tool is used for investigating the fire within the vessel and cuboid meshes are used for building the physical model, the structure information of the actual deck should be simplified as follows:

a) The intricate layout of the deck: most of these small pieces of equipment are disregarded while creating the numerical model because they may not have a significant impact on the spread of the fire.

b) Explosibility: Because the deck contains a lot of small equipment, such as gas bombs, oil tanks, and high-pressure containers, an explosive phenomenon might easily occur when a fire starts. This could make the fire more destructive. To simplify the calculation, this would be disregarded because of the complexity of explosibility.

c) The impact of human activity on the spread of the fire: during the early stages of the fire's development within the deck, people's movements have very little bearing on the distribution of flow. Human action can therefore be disregarded. However, because of human interference, the fire's course will be unpredictable in its later stages. The consequences of human behavior are not discussed in this study.

d) The ignitability of the fuel system is disregarded in order to streamline the model computation.

3.3. Boundary and Initial Conditions for the Simulations of the Case Study

In this case, the simplified structure and the final model are shown in Figure 4. The overall length of the model is 41.1 m, width is 8.5 m, and height is 2.8 m. The entire deck is separated by fire-rated bulkheads into four main zones: helm station, engine room, mechanical and electrical workshop, and warehouses. The length between each fire-rated bulkhead is 4.3 m. Two diesel engines are in the center of the engine room. In each fire, the rated bulkheads have three door openings. In addition, ladder and service openings are modeled on the basis of the current situation of the passenger ship. The study assumes that the openings are stable and do not change during the life of the vessel. In this control volume, the boundary conditions and mesh figure for the case of fire dynamics simulation are depicted in Figure 5.

The fire source is located in the center of the engine room and its cuboid dimension is 1 m*1 m*0.25 m. Therefore, the maximum heat release rate is 3460 kW [30]. The fire during its growth stage and during its decay period can be described by a t2 curve. The methane reaction is used in fire modeling, and the specific heat of combustion is determined as 50 MJ/kg [31,32]. The well-known very LES is used based on the

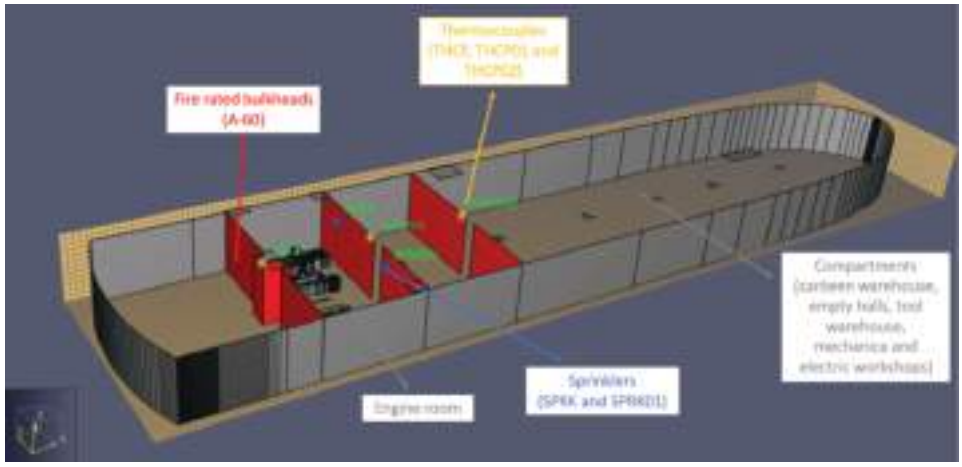

Figure 4. *Geometric model structure of the lower deck of SH SUTLUCE*

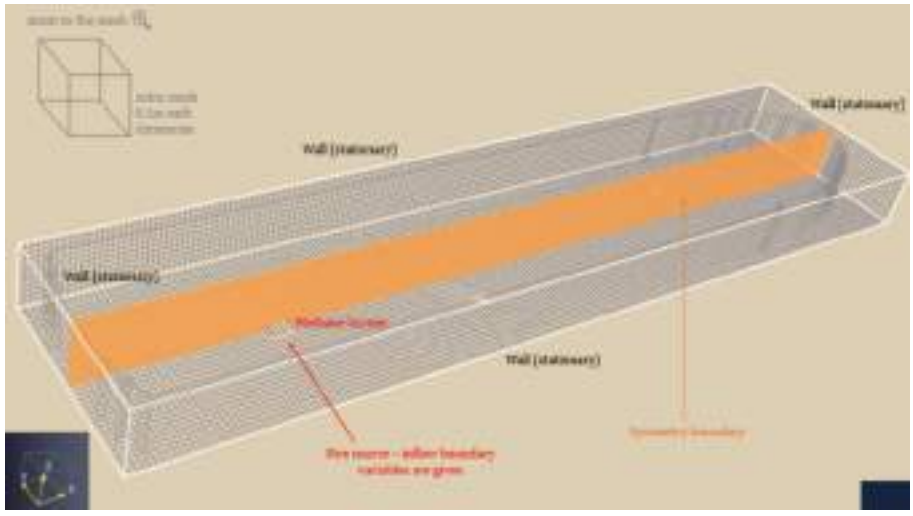

Figure 5. *Boundary conditions and mesh figure for the case of fire simulation*

concept of filtering a larger part of turbulent fluctuations compared with the standard LES [33]. It can be concluded that the VLES model has better predictions of the swirling flow field for both the mean and root mean results than the LES model [34].

From the perspective of fire protection systems, extinguisher systems such as sprinklers and structural systems such as fire-rated bulkheads & decks are concentrated in this study. On the other hand, fire detection and alarm systems are ignored to simulate. The sprinklers are of generic industrial type, and the activation temperature is 93.33 °C. To determine the arrangement of sprinklers, the geometrical shape method is used. The geometrical shape method is the simplest and most widely used spacing method because it provides the highest uniformity for the system [35]. In conclusion, the main parameters of the fire simulation are given in Table 4.

3.4. Experimental Validation and Mesh Dependency

Before running the fire dynamics simulations of the case study, the parameters mentioned in the previous section must be validated and verified by an experimental study. Steckler et al. [36] conducted several fire tests inside a compartment to study fire-induced flows. The experimental data gathered from these fire tests were used as part of the validation for fire dynamics simulations. The data indicate non-spreading fires in small compartments. A series of 45 experiments were conducted to investigate fire-induced flows in a compartment 2.8 m * 2.8 m in plane and 2.18 m in height. The 0.3 m diameter burner was supplied with commercial grade methane at fixed rates, producing a constant fire strength of 62.9 kW. The model of the Steckler et al. [36] experiment is depicted in Figure 6. Depending on the burner type and geometry of the case study, experiments are performed as a validation study [36].

Table 4. *The main parameters of fire simulations*

	Reaction	Methane
Fire source	Maximum heat release rate	3460 kW
	Specific heat of combustion	50 MJ/kg
	Original volume of the fire	1 m*1 m*0.25 m
Fire rated bulkheads	Material	Steel
	Thickness	0.01 m
Fire extinguishing system	Type	Generic industrial
	Arrangement method	Geometric shape method
	Quantity	1, 2 or 4 (depends on scenarios)
	Activation temperature	93.33 °C

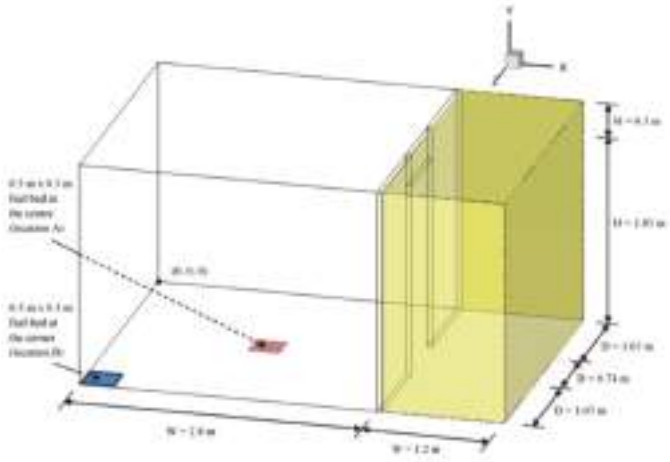

Figure 6. *Model of Steckler experiment*

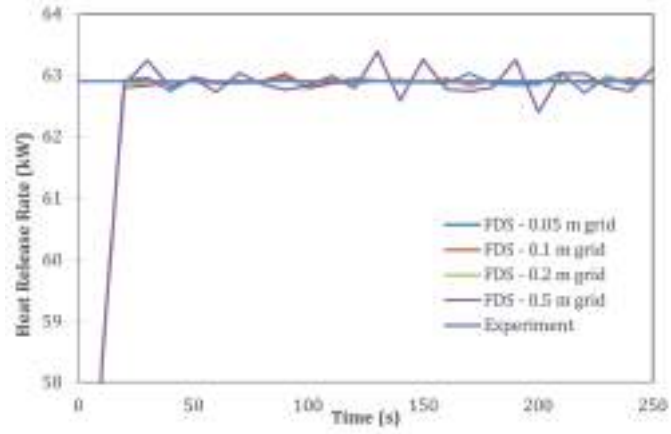

Figure 7. *Heat release rate results of the experiment and fire dynamic simulations*

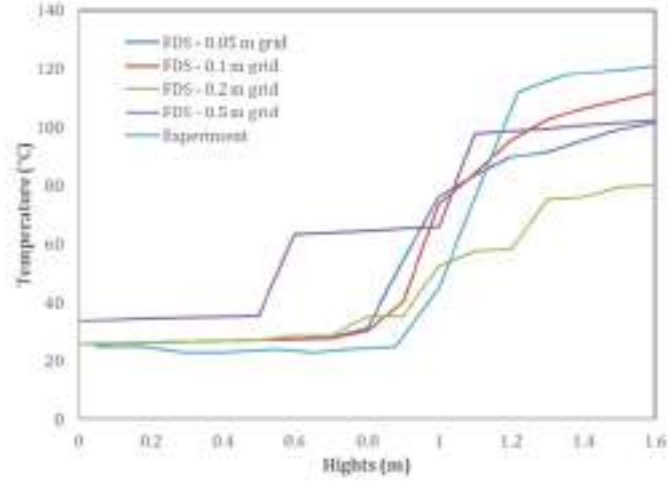

Figure 8. *Temperatures of thermocouples in experiments and fire dynamics simulations with different mesh sizes*

Initially, comparison of heat release rate between fire dynamics simulations with 4 different mesh sizes and experiment are given in Figure 7. In fire dynamics simulations, heat release rate is zero at time zero and significantly increases to around 60 kW at approximately 20 seconds. Experiment and FDS results are validated in terms of heat release rate and mesh sizes at heat release rate are not affected mainly.

In the model, 19 thermocouples are placed at heights from 0 to 1.8 m from bottom to top. To validate the model and running mesh dependencies, temperatures on these thermocouples for experiments and fire dynamics simulations are illustrated in Figure 8. Differences in temperatures between the experiment and FDS results are approximately 10%. Because of the grid resolution, the grid size was selected as 0.1 m according to Figure 8.

The simulation results match well with the experimental data; despite some initial differences, these are reasonable because of the response time of the temperature sensor used in the experiment. The recorded values are delayed from the true temperature during the early stages of the fire because of the extremely high rate of temperature increase. As the temperature increase rate decreases, the variations disappear.

In addition to the grid resolution of Steckler experiments, the characteristic fire diameter (D^*) is calculated according to Equation 6 [37]:

$$D^* = \left(\frac{\dot{Q}}{\rho_\infty c_p T_\infty \sqrt{g}}\right)^{\frac{2}{5}} \quad (6)$$

where $\dot{Q}$ is the total heat release rate of the fire, ρ_∞ is the air density (kg/m^3), c_p is the air specific heat (kJ/kg·K), g is the gravitational constant (m/s^2) and T_∞ is the ambient temperature (K). Depending on the calculation, D^* is calculated as a 0.1 m grid size that is aligned with the Steckler experiment results.

4. Results of Fire Dynamics Simulations

In order to analyze fire safety onboard passenger ships in the case of SH SUTLUCE, several scenarios are derived in terms of fire fatality level. Table 5 shows the details of the fire simulation scenarios. Scenario 1 is divided into three main categories depending on the quantity and arrangement of sprinklers. To determine the end time of the simulation, each scenario was run up to the stabilization point; therefore, the end time was specified as 280, 480, and 300 s for Scenarios 1, 2, and 3, respectively. In each scenario, simulations were run until the heat release rate, temperature, and pressure parameters stabilized.s

Heat release rate - time graphs for each scenario are illustrated in Figure 9. In the first few seconds, the heat release rates increase dramatically for all scenarios and continue fluctuating at roughly the same level as the determined maximum heat release rate in the simulation; 3460 kW.

The total energy of the control volume is another crucial factor in fire dynamics simulations. In Figure 10, the total energy and time charts are analyzed for each scenario. Similar to the heat release rate, the total energy dramatically increases with the ignition of the fire in the compartment. After almost 50 s for all scenarios, the average total energy converges to zero. In the worst scenario, this convergence starts mainly after 100 s, and the total energy is approximately doubled compared to other scenarios at 50 s.

In the scenarios, thermocouples were placed into the mid-top of each fire-rated bulkhead in the lower deck. Figure 11 demonstrates the location of thermocouples in the lower deck. The measured temperatures on the thermocouples are given in Figure 12. THCP1 is the most critical one that reaches more than 500 °C for all scenarios except the worst one. Fire-rated bulkheads cause closed compartments, which leads to a temperature increase in THCP1. At the end of the simulation, THCP1 stabilizes at approximately 400 °C for each scenario. THCP2 reaches at 250 °C in only scenario 2 and in other cases; THCP2 fluctuates below 150 °C. Lastly, same graph characteristic is shown for TCHP3 with fluctuating at almost 120 °C.

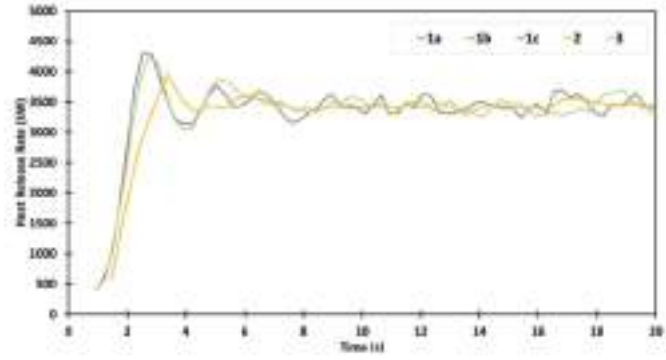

Figure 9. *Heat release rates of three different scenarios*

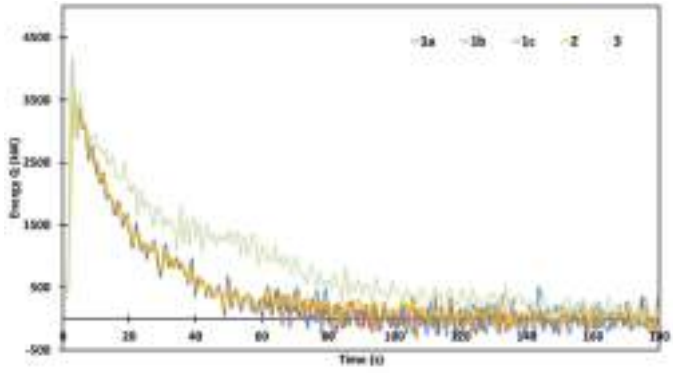

Figure 10. *Total energy (Q) of three different scenarios*

Table 5. *Scenarios of the fire simulations*

Scenarios	Fire extinguishing system (sprinklers)	Fire-rated bulkheads & decks	Number of sprinklers nozzles	Simulation time (s)	Scenario fatality
Scenario 1a	Yes	Yes	1	280	Best
Scenario 1b	Yes	Yes	2	280	Best
Scenario 1c	Yes	Yes	4	280	Best
Scenario 2	No	Yes	-	480	Medium
Scenario 3	No	No	-	300	Worst

In the three best scenarios, the arrangement and number of sprinklers are derived from each scenario. Figure 13 presents the arrangements of the sprinklers in the engine room. The arrangement of sprinklers is determined according to the geometrical shape method, and Scenarios 1a, 1b, and 1c have one, two, and four sprinklers, respectively. In Figure 14, the temperature change of sprinkler nozzles for the scenarios is illustrated. In Scenarios 1b and 1c, the temperature can reach 160 °C even though Scenario 1a has a maximum nozzle temperature of 180 °C. The characteristics of the graphs are the same due to the selection of the same fire source and sprinkler type as generic industrial. For this case, Scenario 1b, which includes two sprinkler nozzles, can be selected as the best fire-extinguishing sprinkler arrangement.

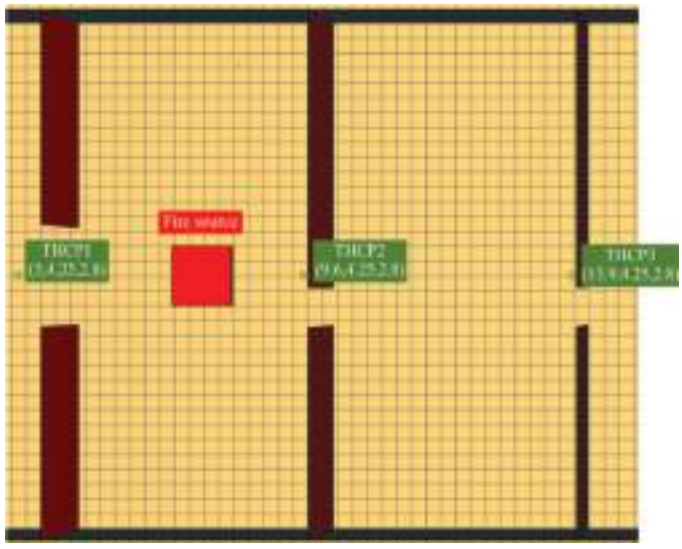

Figure 11. *Arrangement of thermocouples in the lower deck*

The temperature distribution on y=4.25 m at t=50 s for all scenarios is depicted in Figure 15. Time is selected depending on the activation of the sprinklers. In the scenarios, sprinklers break out after the 50s. In only Scenario 3, temperature along the ship length is distributed, and other zones such as workshop areas and warehouses in the lower deck are affected by the fire in the engine room. This indicates that fire-rated bulkheads play a crucial role in compartmentation even though only 50 s last. Figure 16 represents the temperature distribution at y=4.25 and t=150 s along the lower deck for the scenarios. This figure states that even though the time goes to 100 s, the temperature of the sprinkler included scenarios is almost the same as in Figure 12. However, the temperature of other zones increases dramatically to almost 300 °C in Scenario 3, which lacks fire-rated bulkheads. In addition, differences between scenario 3 and others last the same until the end of the simulation.

In Figures 17 and 18, the temperature distribution on the fire-rated bulkhead located at x=5.4 m is given at time 100 s and 250 s, respectively. This bulkhead is crucial in terms of fire safety because it separates the engine room from the helm station. In these figures, the positive effect of sprinklers is shown when comparing Scenarios 1c and 2.

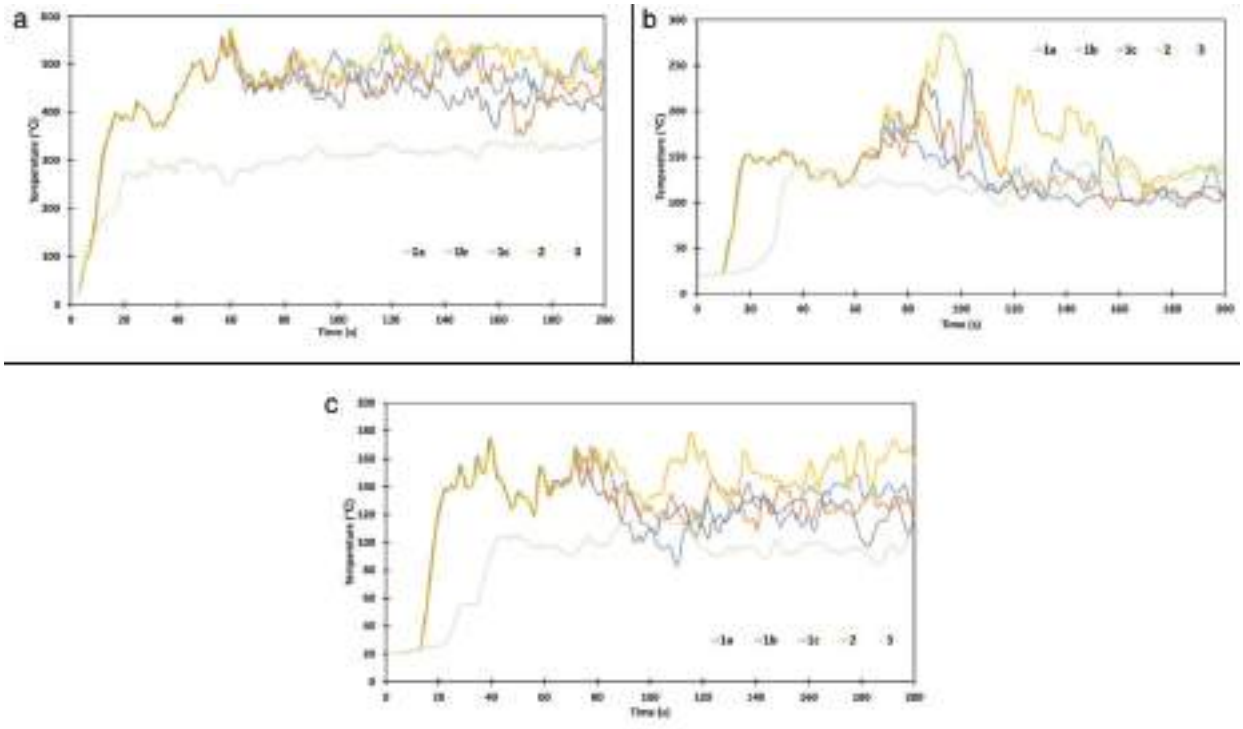

Figure 12. *Temperature change of the thermocouples in each scenario: a) THCP1, b) THCP2, and c) THCP3*

Lastly, the fire-rated deck is placed at z=2.8 m along the vessel. Figure 19 represents the temperature change on the z=2.8 m plane at 100 and 200 s, respectively. This plane in the z direction is a significant obstacle for spreading fire along the ship vertically. If this fire-rated deck collapses because of the temperature increase, passenger compartments would be in danger in terms of fire safety.

In conclusion, similar studies were compared with the results of this study. Azzi [38] investigated cabin, large space, and corridor fire scenarios onboard passenger ships using a CFD tool called a field model. The models for the scenarios provided in the study are considered to examine results similar to those of this study in terms of temperature [38]. Kang et al. [13] used computational fire simulations in the early stage of ship design, including fire suppression systems in the engine room and field model. Similar to our study, this work shows the effect of the extinguishing system on the temperature [13]. Wang et al. [39] investigated the vertical distribution profile of the temperature in a sealed ship engine room and found that the temperature gradient in the vertical direction is slightly smaller than that in a compartment with openings similar to our study. In summary, the CFD results in this study are aligned with similar studies and contribute to the literature by simulating the entire deck, including the engine room and other technical compartments together, and using both extinguishing and structural fire protection systems in the simulation.

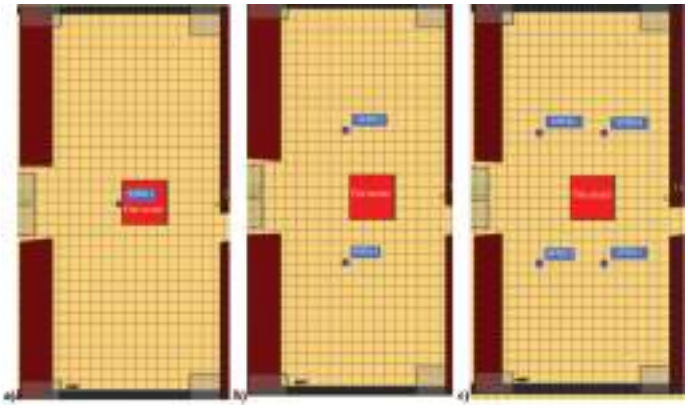

Figure 13. *Arrangement of the sprinklers in the engine room scenarios a) 1a, b) 1b, c) 1c*

5. Conclusion and Recommendations

In this study, fire safety onboard passenger ships was examined using a fire-specific CFD tool called fire dynamics simulation. The case study specifically focuses on analyzing the engine room fire of a 600-passenger passenger ship operated by Sehir Hatlari, a governmental organization responsible for public marine transportation in İstanbul, which transports 40 million passengers annually. Simulation scenarios are called best, medium, and worst according to fire incident severity, and the scenarios vary depending on active and structural fire protection systems. Active fire protection systems are selected as generic industrial sprinklers, and structural fire protection systems are selected as fire-rated bulkheads and decks. Additionally,

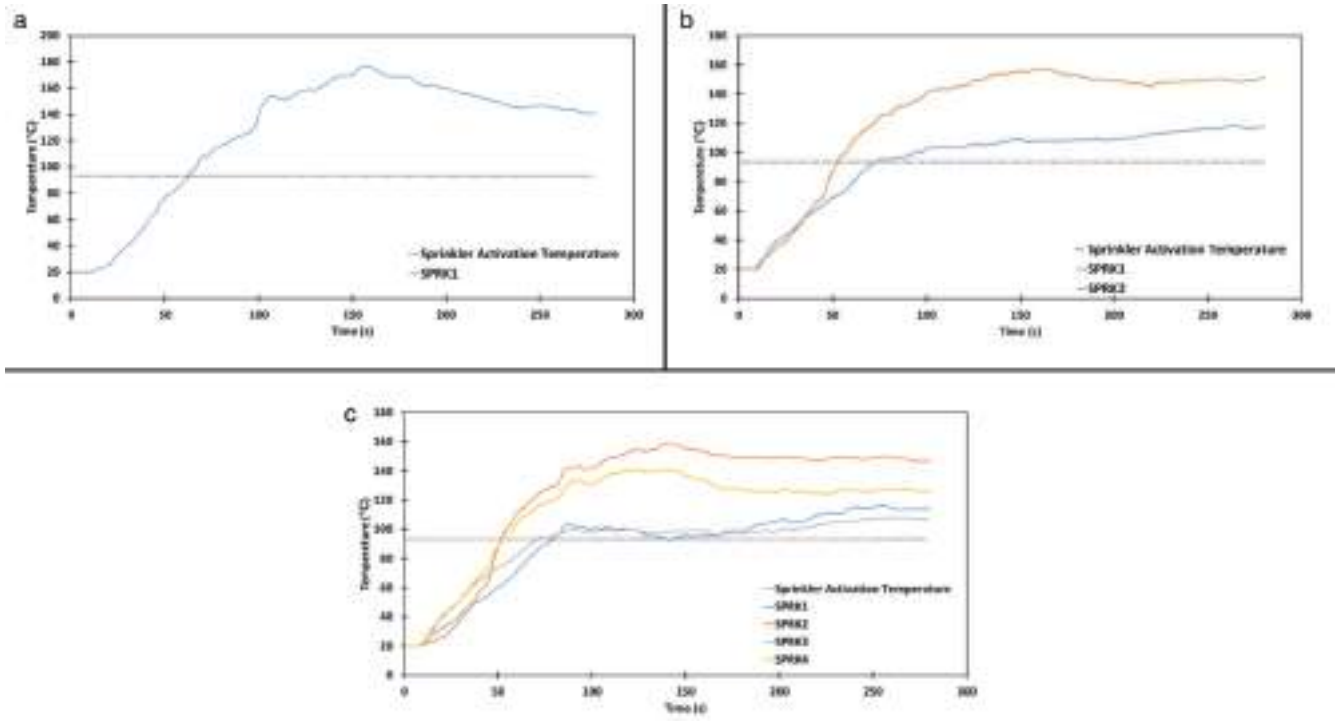

Figure 14. *Temperature change of sprinklers in the scenarios a) 1a, b) 1b, c) 1c*

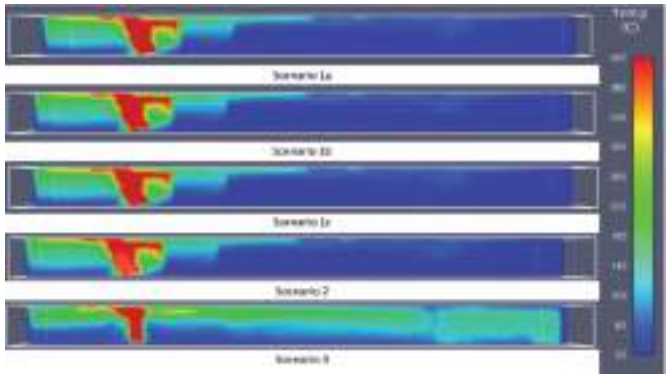

Figure 15. *Temperature distribution at y=4.25 m at t=50 s for all scenarios*

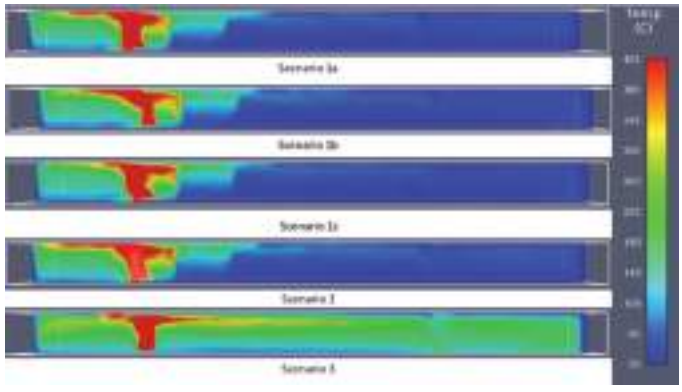

Figure 16. *Temperature distribution on y=4.25 m at t=150 s for all scenarios*

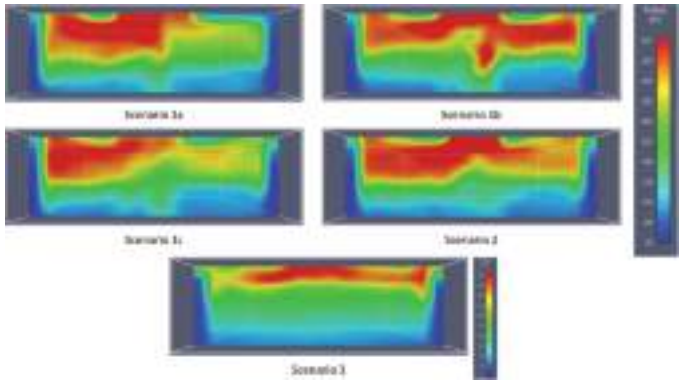

Figure 17. *Temperature distribution on x=5.4m at t=100s for all scenarios*

in the best scenario, the number and arrangement of sprinklers diversify into three sub-cases with one, two, and four sprinklers in the engine room. The cubic grids were selected as 0.1 m in each dimension.

The findings derived from the fire dynamics simulations underscore the critical role played by the protection systems in impeding the spread of fire across passenger ships. Also, this study provides a novelty to the marine safety literature by applying fire dynamics simulation to a

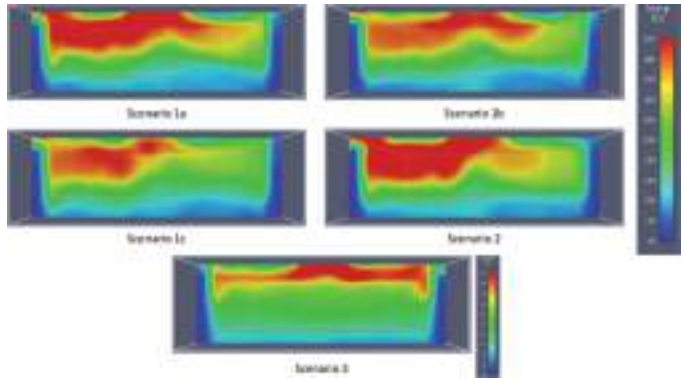

Figure 18. *Temperature distribution on x=5.4 m at t=250 s for all scenarios*

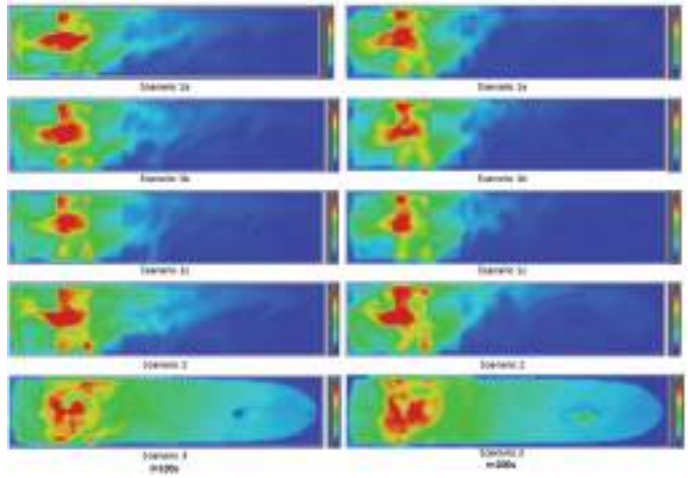

Figure 19. *Temperature distribution on z=2.8 m at t=100 s and t=200 s for all scenarios*

domestic passenger ship. The key findings of this study are that temperatures in the engine room increase extremely to around 500 ℃ in the early stages and application of neither structural nor active (extinguishing etc.) fire protection systems together led to fatal consequences onboard passenger ships.

For future research, the following are recommended:

• The inclusion of other compartments to the fire dynamics simulation, such as atriums, upper decks, galleries, etc., is suggested.

• The selection of different types of fire origin within the control volume can give more diversified results.

• Exploration of diverse sprinkler types and activation temperatures should be included in scenarios involving malfunctioning systems.

In addition to the above recommendations, human factor analysis can be added to the study for future research. The evacuation model and fire detection system design are affected directly by human factors. For the evacuation

modeling, a simulation tool dedicated to the fire safety industry called PathFinder is advised to be integrated. In addition, performance-based fire safety analysis onboard passenger ships is a developing research area, and fire dynamics simulations can be applied to other ship types such as Ro-Ro, container, and tanker. Lastly, smoke propagation can be added to the study, including the materials that led to the smoke in the control volume. For instance, antiskid coatings can be considered for smoke concentration and implicit evacuation.

The authors believe that undertaking these suggested investigations can yield valuable insights and contribute to the enhancement of fire safety measures on passenger ships.

Acknowledgements

This work is a part of the first author's PhD study at İstanbul Technical University, Department of Naval Architecture and Marine Engineering. We would like to express our deepest appreciation to the stakeholders of this study; Sehir Hatlari, Turkish Lloyd, Endaze Engineering, and Thunder Engineering (Pyrosim software provider).

Authorship Contributions

Concept design: T. Aycı, B. Barlas, and A. Ölçer, Data Collection or Processing: T. Aycı, B. Barlas, and A. Ölçer, Analysis or Interpretation: T. Aycı, Literature Review: T. Aycı, B. Barlas, and A. Ölçer, Writing, Reviewing and Editing: T. Aycı, B. Barlas, and A. Ölçer.

Funding: The authors declare that no funds, grants, or other support was received during the preparation of this manuscript.

References

[1] B. Barlas, R. Ozsoysal, E. Bayraktarkatal, and O. A. Ozsoysal. "A study on the identification of fire hazards on board: A case study". *Brodogradnja* vol. 68, pp. 71-87, Dec 2017.

[2] *GISIS*, 2023. Maritime casualty and incidents, global integrated shipping information system. http://gisis.imo.org. Accessed: 1st January 2023.

[3] *Sehir Hatlari*, 2023. https://www.sehirhatlari.istanbul/en/corporate/sehir-hatlari-616. Accessed: 28th September 2023.

[4] SOLAS, 2004. The international convention for the safety of life at sea (SOLAS), International Maritime Organization (IMO) Chapter II-2.

[5] J. Cowley, "Fire safety at sea". *Institute of Marine Engineering, Science and Technology,* 2002.

[6] D. Drysdale, *An introduction to fire dynamics*. 2nd ed. Wiley, USA, 1999.

[7] SFPE, *Handbook of fire protection engineering*. 5th ed. Springer, USA, 2016.

[8] D. Rasbash, G. Ramachandran, B. Kandola, J. Watts, and M. Law, *Evaluation of fire.* John Wiley & Sons, England, 2004.

[9] V. Novozhilov, "Computational fluid dynamics modelling of compartment fires". *Progress in Energy and Combustion Science*, vol. 27, pp. 611-666, 2001.

[10] Y. Jiao, J. Wang, M. Xiao, T. Xu, and W. Chen, "Development of field-zone-net model for fire smoke propagation simulation in ships". *In: 2014 7th International Conference on Intelligent Computation Technology and Automation,* pp. 190-193, 2015.

[11] J. Li, J. Pu, K. Ren, K. Zhang, and L. Ding, "Fire smoke characteristics in closed ship cabin: A fire model study". *International Journal of System Assurance Engineering and Management,* vol. 7, pp. 257-261, Apr 2016.

[12] X. Zhu, Z. Chenhua, and Y. Zhiqing, "Research of temperature prediction in steel cabin fire with large eddy simulation and experiment". *International Conference on Computational and Information Sciences ICCIS,* pp. 889-892, Oct 2011.

[13] H. J. Kang, C. Jin, L. Dongkon, and J. P. Beom, "A framework for using computational fire simulations in the early phases of ship design". *Ocean Engineering,* vol. 129, pp. 335-342, Jan 2017.

[14] E. J. Lee, W. S. Ruy, and J. Seo, "Application of reinforcement learning to fire suppression system of an autonomous ship in irregular waves". *International Journal of Naval Architecture and Ocean Engineering,* vol. 12, pp. 910-917, 2020.

[15] B. Y. Lattimer, J. L. Hodges, and A. M. Lattimer, "Using machine learning in physics-based simulation of fire". *Fire Safety Journal,* vol. 114, 102991, Jun 2020.

[16] D. K. Park, J. H. Kim, J. S. Park, Y. C. Ha, and J. K. Seo, "Effects of the structural strength of fire protection insulation systems in offshore installations". *International Journal of Naval Architecture and Ocean Engineering,* vol. 13, pp. 493-510, 2021.

[17] L. Wang, and S. Su, "Three-dimensional numerical simulation of smoke motion in fire of the ship engine room with multilayer structure". *Brodogradnja*, vol. 62, pp. 366-372, Dec 2011.

[18] Y. Zhao, H. Zhao, Z. Miao, D. Ai, and Q. Wang, "A numerical study on the smoke dispersion and temperature distribution of a ship engine room fire based on OpenFOAM". *Sustainability,* vol. 15, 15093, Oct 2023.

[19] Q. Xie, S. Guo, Y. Zhang, C. Wang, C. Ma, and Q. Li, "An integrated method for assessing passenger evacuation performance in ship fires". *Ocean Engineering,* vol. 262, 112256, Oct 2022.

[20] W. L. Wang, S. B. Liu, S. M. Lo, and L. J. Gao, "Passenger ship evacuation simulation and validation by experimental data sets". *Journal of Procedia Engineering,* vol. 71, pp. 427-432, 2014.

[21] C. Li, J. Mao, Z. Kang, S. Zhao, and H. Ren, "Influence of firefighting intervention on fire spread characteristics in ship engine room". *Journal of Marine Science and Engineering,* vol. 11, pp. 877, Apr 2023.

[22] C. Azzi, and D. Vassalos, "Performance-based design for fire safety onboard passenger ships". In: *11th International Symposium on Practical Design of Ships and Other Floating Structures PRADS,* vol. 1, pp. 644-651, 2010.

[23] A. Salem, F. Mauro, and D. Vassalos, "The role of zone models in the numerical prediction of fire scenario outcomes onboard passenger ships". *Journal of Marine Science and Engineering,* vol. 12, pp. 1-18, Dec 2023.

[24] H. K. Versteeg, and W. Malalasekera, "An introduction to computational fluid dynamics 2nd edition". Pearson Education Limited, England, 2007.

[25] J. Quintiere, and B. Rhodes, "Fire growth models for materials". *MSc Thesis University of Maryland*, College Park, USA, 1994.

[26] T. Ayci, and B. Barlas, "İstanbul Şehir Hatları'nın gemi ve hat analizi". *GIDB Journal*, vol. 2, pp. 17-30, 2015.

[27] Z. Roland, Z. Máté, and S. Győző, "Comparison of alternative propulsion systems - a case study of a passenger ship used in public transport". *Brodogradnja*, vol. 72, pp. 1-18, Jun 2021.

[28] Şehir Hatları, 2023. SUTLUCE ferry https://sehirhatlari.istanbul/en/ferries/sutluce-109. Accessed: 24th May 2023.

[29] V. Bashan, H. Demirel, and M. Gul, "A novel risk evaluation approach for frequently encountered risks in ship engine rooms". *Brodogradnja*, vol. 71, pp. 31-54, Jun 2020.

[30] S. Su, and L. Wang, "Three-dimensional reconstruction of the fire in a ship engine room with multilayer structures". *Ocean Engineering,* vol. 70, pp. 201-207, Sep 2013.

[31] S. Ergin, and A. Sulus, "The effects of openings on the fire development in an engine room of a chemical tanker". In: *13th Congress of International Maritime Association of Mediterranean,* Istanbul, Turkey, 2009.

[32] S. Ergin, and A. Bolek, "A large eddy simulation of LNG pool fire on board a chemical/oil tanker". *Journal of Physics: Conference Series*, vol. 1107, 042006, 2018.

[33] M. Labois, and L. Djamel, "Very-large eddy simulation (V-LES) of the flow across a tube bundle". *Nuclear Engineering and Design,* vol. 241, pp. 2075-2085, 2011.

[34] P. Tiwari, Z. Xia, and X. Han, "Comparison of VLES and LES turbulence modeling for swirling turbulent flow". *Journal of Applied Fluid Mechanics,* vol. 13, pp. 1107-1016, Jul 2020.

[35] F. Dwomoh, "Computation model of sprinkler spacing and layout". *International Journal of Engineering Sciences & Emerging Technologies,* vol. 7, pp. 481-489, Aug 2014.

[36] K. D. Steckler, J. G. Quintiere, and W. J. Rinkinen, "Flow induced by fire in a compartment". *Symposium (International) on Combustion,* 19, 913-920, 1982.

[37] K. McGrattan, S. Hostikka, R. McDermott, J. Floyd, C. Weinschenk, and K. Overholt, "*Fire dynamics simulator, user's guide sixth edition*". National Institute of Standards and Technology, Gaithersburg, Maryland, USA and VTT Technical Research Centre of Finland, Espoo, Finland, 2013.

[38] C. Azzi, "*Design for fire safety onboard passenger ships*". PhD Thesis, Universities of Strathclyde, United Kingdom, 2010.

[39] J. Wang, et al. "An experimental and non-dimensional study on the vertical temperature distribution of a sealed ship engine room fire". *Ocean Engineering,* vol. 165, pp. 22-33, Oct 2018.

Reviewer List of Volume 12 Issue 2 (2024)

Achraf Touil	Hassan First University	Morocco
Ali Doğrul	National Defense University	Türkiye
Arda Toygar	Ordu University	Türkiye
Asım Sinan Karakurt	Yıldız Technical University	Türkiye
Ayfer Ergin	İstanbul University	Türkiye
Buğra Çelebi	Yıldız Technical University	Türkiye
Deniz Bayraktar Bural	İstanbul Technical University	Türkiye
Emin Deniz Özkan	Dokuz Eylül University	Türkiye
Emre Kahramanoğlu	İstanbul Technical University	Türkiye
Fatih Cüneyt Korkmaz	Yıldız Technical University	Türkiye
Fatih Yılmaz	Ministry of Transport and Infrastructure	Türkiye
Guo-Niu Zhu	Fudan University	Türkiye
Güven Gonca	Yıldız Technical University	Türkiye
Hasan Gökhan Güler	Middle East Technical University	Türkiye
Hasan Ölmez	Karadeniz Technical University	Türkiye
Hasan Uğurlu	Ordu University	Türkiye
Hüseyin Gençer	Piri Reis University	Türkiye
Koray Şahin	İzmir Katip Çelebi University	Türkiye
Mihaela Greti Manea	Mircea cel Batran Naval Academy	Romania
Momoko Kitada	World Maritime University	Sweden
Olgun Konur	Dokuz Eylül University	Türkiye
Onur Yüksel	Zonguldak Bülent Ecevit University	Türkiye
Ömer Arslan	Çanakkale Onsekiz Mart University	Türkiye
Özkan Uğurlu	Ordu University	Türkiye
Refik Özyurt	Ordu University	Türkiye
Sedat Baştuğ	Bandırma Onyedi Eylül University	Türkiye
Tahsin Görmüş	Gebze Technical University	Türkiye
Taner Çoşgun	Yıldız Technical University	Türkiye
Umut Yıldırım	Karadeniz Technical University	Türkiye
Volkan Efecan	Mersin University	Türkiye
Yasemin Arıkan Özden	Yıldız Technical University	Türkiye
Yasemin Nemlioğlu Koca	İstanbul University	Türkiye
Zdeslav Juric	University of Split	Croatia

Volume 12 Issue 2 (2024) is indexed in

TRID

the TRIS and ITRD database

TÜBİTAK

ULAKBİM

Scopus

JEMS's Sponsors

INCE SHIPPING GROUP

GEMLIK PILOTS

DENIZ ÇALIŞANLARI DAYANIŞMA DERNEĞI

EGE GAZ INC.

SEFİNE SHIPYARD

GÜRDESAN SHIP MACHINERY CORP.

ER SHIPPING

ONURSAN

ONURSAN

40 YEARS

Istanbul / Türkiye

onursan@onursan.net

SAFETY FIRST

GEPA

Istanbul / Türkiye

info@gepafiberglass.com

AMERICAN MARINE SAFETY

Houston / Texas

sales@americanmarinesafety.com

ONURSAN Europe

Rotterdam / Netherlands

rotterdam@onursan.net

RINA · DNV · KR · ClassNK · CCS

GEMLIK PILOTS

Gemlik Pilotage and Tugboat Services Inc.

GEMLIK Pilotage and Tugboat Services Inc., provides the highest level of navigation and maneuvering safety, which aims to continuous training and development, in Gemlik Bay.

GEMLIK PILOTS
GEMLIK Pilotage and Tugboat Services Inc.

Adress : Ata Mh. Sanayi Cd. No:4 İç Kapı No:9
Gemlik / BURSA Phone : 0224 524 77 35 - 0224 524 77 36
Fax : 0224 524 77 64
e-mail : pilotage@geptco.com


UCTEA CHAMBER OF MARINE ENGINEERS
1960